CHARACTERIZATION OF GROUNDWATER IN THE COASTAL AQUIFERS OF PONDICHERRY REGION USING CHEMICAL, ISOTOPIC AND GEOCHEMICAL MODELING APPROACHES

By

K.TIRUMALESH

Enrolment number: CHEM01200604019

Bhabha Atomic Research Centre

Mumbai, India

A thesis submitted to the
Board of Studies in Chemical Sciences
In partial fulfillment of requirements
for the Degree of

DOCTOR OF PHILOSOPHY

of

HOMI BHABHA NATIONAL INSTITUTE

June, 2012

CHARACTERIZATION OF GROUNDWATER IN THE COASTAL AQUIFERS OF PONDICHERRY REGION USING CHEMICAL, ISOTOPIC AND GEOCHEMICAL MODELING APPROACHES

A thesis submitted to the
Board of Studies in Chemical Sciences
In partial fulfillment of requirements
for the Degree of

DOCTOR OF PHILOSOPHY
in
CHEMICAL SCIENCES

By

K.TIRUMALESH
Enrolment number: CHEM01200604019
Bhabha Atomic Research Centre
Mumbai, India

Research Supervisor

Prof. Dr. K.L. Ramakumar (DS)
Director, Radiochemistry and Isotope Group
Bhabha Atomic Research Centre
Mumbai, India

Homi Bhabha National Institute

Recommendations of the Viva Voce Board

As members of viva voce board we certify that we have read the dissertation prepared by Mr. K. Tirumalesh entitled "Characterization of Groundwater in the Coastal Aquifers of Pondicherry Region using Chemical, Isotopic and Geochemical Modeling Approaches" and recommend that it may be accepted as fulfilling the dissertation requirement for the Degree of Doctor of Philosophy.

________________________ Date: 12-09-2012

Chairman - Prof. Gursharan Singh

________________________ Date: 12-9-2012

Supervisor/ Convener – Prof. K.L. Ramakumar

R. Rang________________________ Date: 12/09/2012

External Examiner – Prof. R. Rangarajan, NGRI, Hyderabad

S.K Agga________________________ Date: 12/9/2012

Member – Prof. S. K. Aggarwal

RmTripathi________________________ Date: 12/09/2012

Member – Prof. R.M. Tripathi

Final approval and acceptance of this dissertation is contingent upon the candidate's submission of the final copies of the dissertation to HBNI.

I here by certify that I have read this dissertation prepared under my direction and recommend that it may be accepted as fulfilling the dissertation requirement.

Date: 12-9.2012

Place: Mumbai

प्रो.के.एल. रामकुमार/Prof. K.L. Ramakumar
संयोजक/CONVENER
अध्ययन बोर्ड-रासायनिक विज्ञान
BOARD OF STUDIES-CHEMICAL SCIENCES
होमी भाभा राष्ट्रीय संस्थान
HOMI BHABHA NATIONAL INSTITUTE
भाभा परमाणु अनुसंधान केंद्र/B.A.R.C.
मुंबई/MUMBAI-400 085, भारत/INDIA

Statement by Author

This dissertation has been submitted in partial fulfillment of requirements for an advanced degree at Homi Bhabha National Institute (HBNI) and is deposited in the library to be made to borrowers under the rules of the HBNI.

Brief quotations from this dissertation are allowable without special permission provided that accurate acknowledgement of source is made. Requests for permission for extended quotation from or reproduction of this manuscript in whole or in part may be granted by the Competent Authority of HBNI when in his or her judgment the proposed use of the material is in the interest of scholarship. In all other instances, permission must be obtained from the author.

K. Tirumalesh

Declaration

I, hereby declare that the thesis entitled "Characterization of Groundwater in the Coastal Aquifers of Pondicherry Region using Chemical, Isotopic and Geochemical Modeling Approaches" submitted to Homi Bhabha National Institute (HBNI), Mumbai, India, for the award of **Doctor of Philosophy** in **Chemical Sciences** is the record work carried out by me under the guidance of Prof. Dr. K.L. Ramakumar, Director, Radiochemistry and Isotope Group (RC & I G), BARC. The work is original and has not been submitted earlier as a whole or in part for a degree, diploma, associateship, fellowship at this or any other institute/university of higher learning.

K. Tirumalesh

Dedications

I dedicate this dissertation to

My Mother,

Smt. K. Laxmamma

Acknowledgement

I wish to express my sincere respect and gratitude to Prof. Dr. K. L. Ramakumar, Director, Radiochemistry and Isotope Group, Bhabha Atomic Research Centre, for his wholehearted support, encouragement and guidance during the whole research work. His excitement in science and trust in me are instrumental to accomplish this work. Undoubtedly this is by far the most significant work in my scientific career. I am also grateful to him for his painstaking effort to go through the manuscript of research papers and the thesis in spite of his extremely busy schedule.

I would also like to thank Prof. Dr. Gursharan Singh, Associate Director (I), RC & I Group, without his encouragement and support this work would not have been possible. I am indebted to his undwindling faith in me and for boosting my spirits during tough phases of my life. My sincere thanks to doctoral committee members, Prof. Dr. S. K. Aggarwal and Prof. Dr. R. M. Tripathi for their constructive remarks that helped significantly in improving the focus of thesis.

My sincere thanks to Prof. S. Chidambaram, Earth Science department, Annamalai University, and Dr. Pethaperumal, Scientist, Agricultural department, Puducherry and research scholars of Earth Science department Annamalai University for their kind cooperation in sampling and providing literature on geological and hydrogeological aspects of study area.

I sincerely thank all my colleagues of Isotope Hydrology Section, esp. Mr. U.P. Kulkarni, Mr. Mohokar, Mr. U.K. Sinha and Dr. U.S. Kumar for their kind support. I also thank Department of microbiology (Pune), National Institute of Hydrology (Roorkee) and IIT (Kharagpur) for getting samples analyzed for microbial parameters and environmental isotopes.

My sincere thanks to Dr. A. Venkata Ramana Reddy, Head, Analytical Chemistry Division for his constant support and guidance. I wish you express my wholehearted thanks to Dr. R.K. Singhal, Dr. Kallol Swain, Dr. Sanjukta, Mrs. Minal, Mrs. Manisha, Mrs. Arushi and Dr. Sangeetha of Analytical Chemistry Division, Dr. Acharya (RCD), Dr. Jaison, Mr. Manoj Sharma and Dr. Sangeetha Dhara of Fuel Chemistry Division, Dr. Kedarnath (ChD), Dr. S. Anjaneyulu and Mr. Nagar and Mr. Sumit Kumar of RACD, Dr. Maitre (NABTD), Dr. Shashidhar (FTD), Mr. P. Ramakrishna (RTD), Dr. Maitre (NA & BTD) and Dr. Hareendran (UED) for their unconditional support at various stages of my thesis work. I sincerely thank my friends Dr. Pramod and Dr. Dubey for their kind support and encouragement.

My dear friends Sudarshan, Ramakrishna, Chary, Narsimha, Venkat reddy, Ravivardhan, Ramesh and other navodayans were always with me for good and bad, I owe a lot to them. I thank my childhood teachers Mr. Thirumal Rao, Mr. V.B.K. Murthy, Mr. Umachandra Shekar, Mr. Veerabhadram, Mr. Nagireddy, Mrs. Vandana Kulshreshta and Mrs. Pushpa Rajan who nurtured my personality and helped me grow as a researcher.

I would like to thank my sister, brother in law and their family, and my Pappa, my in laws for their love and support.

Finally I thank my dearest wife Vinisha and lovely kids, Anish and Nishtha who have been a great source of happiness and pillar of my sustenance, their emotional sacrifices can’t be forgotten.

Table of Contents

DESCRIPTION PAGE NO.

CHAPTER 1: INTRODUCTION

CHAPTER 2: METHODOLOGY

CHAPTER 3: ASSESSMENT OF GROUNDWATER QUALITY

CHAPTER 4: ISOTOPE AND GEOCHEMICAL EVALUATION OF FACTORS AFFECTING GROUNDWATER CHARACTERISTICS

CHAPTER 5: IDENTIFICATION OF SOURCE, WEATHERING AND DEPOSITION CHARACTERISTICS OF SEDIMENTS

CHAPTER 6: ROLE OF GROUNDWATER PARTICLES IN TRACE METAL MIGRATION

SYNOPSIS

PREAMBLE

With the rapid population growth and rising expectation for better life, the natural resources of our earth are subjected to increasing pressure. It is paramount that basic resources for human survival, viz., air, water and land must be properly managed. Groundwater which occupies 80% of total freshwater resources on earth is the worst affected resource. The growing dependence on groundwater is mainly due to population growth, frequent failure of monsoons and degrading quality of surface waters. Intensive use of groundwater resources and contamination by anthropogenic activities pose a great threat to groundwater in terms of quantity and quality. This scenario is widely witnessed in coastal aquifers especially in high population zones. Coastal aquifers are typically characterized by variations in groundwater quality in space and time, and are vulnerable directly and indirectly to anthropogenic activities. The coastal zones, in general, have been a major focus for the development of human society and continue to be areas of rich potential for our modern society. Thus understanding groundwater characteristics in coastal aquifers of urban regions is of utmost importance due to their vulnerability to seawater intrusion, upconing of deep seated salt water and other anthropogenic contamination.

Pondicherry, a coastal area in south India, enclosed three sides by Tamil Nadu, is endowed with substantial water resources due to wide network of tanks, two rivers (Gingee and Pennaiyar) that flow into Bay of Bengal through this region and good rainfall. About 90 per cent of the Pondicherry region comprises alluvial aquifers with fairly good quality and shallow water levels in the wells ranging between 12 and 14 meters below ground level. Nearly 80% of groundwater usage is meant for agriculture which is supplied by as many as 6500 tube wells tapping both shallow and deep aquifers and resulting in drastic depletion of groundwater levels at many areas. In addition, there are many industries located in this region which also pose threat to groundwater resources. A proper evaluation of groundwater quality and factors affecting their characteristics in different aquifers is needed to ensure optimal utilization of groundwater and to suggest appropriate remedial measures.

Geochemistry has played an important role in understanding the quality of groundwater. Not only has geochemistry addressed questions of water quality but it has also played a significant role in defining certain physical properties of aquifers such as recharge rates, residence times and flow paths. The advances in geochemical methods and approaches aided to interpret hydrochemical processes in groundwater systems, provided improved understanding of how structural, geological and mineralogical, and hydrological features affect flow and chemistry in groundwater systems. Significant advances have been made through computer programs which have provided increasingly sophisticated interpretations of geochemical data to predict driving forces affecting groundwater characteristics. Geochemistry and environmental isotopes in conjunction with modeling tools have proven to be potential tools in assessing processes and factors governing groundwater chemistry and benefiting various water managers and agencies in designing the effective groundwater usage and managing groundwater resources.

The work described in this thesis deals with the assessment of groundwater quality and its suitability for potable and irrigational purposes as a first step towards understanding the groundwater characteristics. Subsequently the chemical results along with microbiological, environmental isotope and modeling data were interpreted to identify the factors and processes governing the groundwater characteristics in different sedimentary formations of coastal Pondicherry region especially in potential aquifers (Alluvium, Cuddalore and Vanur sandstone aquifers). Results demonstrate that the groundwater is fresh in most of the locations and suitable for drinking and agriculture. Major processes influencing groundwater chemistry were found to be dissolution of Carbonate, Gypsum and Silicate minerals in addition to contribution from soil zone in the case of shallow waters. Utility of trace, rare earth elements and carbon isotope was also explored in this thesis for evaluating the nature of sediment, its weathering and deposition characteristics. An attempt has been made to assess the arsenic distribution in groundwater as well as in sediments of this regions and data was interpreted in light of available theories of As release into groundwater which was further discussed with geochemical and microbiological inferences.

Environmental particles have received world attention in recent past for their association with trace metals and contaminant transport in groundwater. Two size fractions, small (1 – 14 nm) and large (0.45 – 8 µm) size particles, were separated and studied in selected groundwater samples of this region to evaluate their chemistry and association with trace metals. The study

has identified preferential association of Sr^{2+} with colloidal size particles over large particles and its subsequent migration. The work embodied in this thesis has been divided into seven chapters.

1. *Introduction*
2. *Methodology*
3. *Assessment of groundwater quality*
4. *Isotope and geochemical evaluation of factors affecting groundwater characteristics*
5. *identification of source, weathering and deposition characteristics of sediments*
6. *Role of groundwater particles in trace metal migration*

   Summary

CHAPTER 1: INTRODUCTION

The Chapter 1 describes coastal aquifer system, a very dynamic groundwater system with high vulnerability, and introduces various factors influencing the groundwater characteristics. It outlines the importance of chemistry, environmental isotopes, geochemical modeling and statistical analysis in understanding groundwater characteristics for future management of these resources in a sustainable manner. Geological, hydrogeological features of the groundwater system in Pondicherry region are given and the uniqueness of this groundwater system is highlighted. Literature pertaining to quality degradation and depleting groundwater levels in Pondicherry as well as nearby coastal regions of Tamilnadu is summarized. The basic groundwater issues pertaining to quality and quantity in this region are highlighted and major objectives are formulated in accordance with the problems. The broad objectives are i) assessment of groundwater quality and its suitability to potable and irrigation purposes, ii) understanding the processes and identification of sources affecting the groundwater characteristics, iii) identification of source, weathering characteristics and deposition conditions of sediments iv) Role of groundwater particles in trace metal migration.

CHAPTER 2: METHODOLOGY

Chapter 2 deals with strategy adopted to address the stated objectives for which three components were studied viz., *groundwater*, *sediment* and *particles*. Different sampling techniques were adopted for collecting representative groundwater samples, sediments from deep geological formations and particles from groundwater. Water samples were mainly collected from major water bearing formations of this region, namely, Alluvium, Tertiary formation (Cuddalore sandstone) and Cretaceous formation (Vanur sandstone). The sampling was done during post monsoon season (Feb 2009) but a few samples were also collected during pre monsoon season (June 2008). Depth-wise sediment samples representing various formations of this region were collected during construction of a bore hole in Andiarpalayam village located west of Pondicherry. Particle separation from groundwater was carried out by both sequential filtration (large particles) and ultra filtration (small particles) methods.

Most of the chemical analysis was carried out using ion chromatography (major anions and cations), ICP-MS and ICP-AES (trace metals and silica). The working principle and operating conditions of ion chromatography technique is described. Some of the analytes such as boron, total carbon and sulphur were measured using different techniques. Analytical equipments used for characterizing groundwater, sediments and particles have been given in this chapter. In addition to chemical analysis, microbial assay was also carried out for groundwater for *total viable bacteria*, *e coli* and *sulphate reducing bacteria*, the details of assay are given. As (III) is more toxic than As (V), therefore determination of arsenite in nanomolar concentrations in selected groundwater that showed total arsenic about 10-40 ppb was carried out using a modified Differential Pulse Anodic Stripping Voltammetry technique, a brief description of this technique was included. Environmental stable isotopes (^{2}H, ^{18}O and ^{13}C) were measured using isotope ratio mass spectrometer (IRMS) after adopting appropriate sample preparation method and environmental radio isotope tritium (^{3}H) was measured using liquid scintillation counter (LSC) after electrolytic enrichment. A brief description of IRMS and LSC is given in this chapter. Various geochemical models and multivariate methods commonly used for groundwater studies are mentioned in this chapter. A detailed description to inverse geochemical model (NETPATH) and factor analysis employed in this work is mentioned.

CHAPTER 3: ASSESSMENT OF GROUNDWATER QUALITY

One of the main objectives of the groundwater quality monitoring is to assess the suitability to drinking purpose. Contaminants including inorganic (chloride, fluoride, nitrate, iron and arsenic etc.) and microbial (faecal contamination) are important in determining the suitability of groundwater for drinking purpose. Bureau of Indian Standards and World Health Organization prescribed values were taken as reference for checking drinking water suitability. Since 80% of the agriculture needs are met by groundwater resources, it is also important to check the suitability of groundwater for irrigation purpose, for which Na%, RSC (residual sodium carbonate), SAR (sodium absorption ratio) indicators were used as indicators.

Results suggest that sodium & calcium are dominant cations and chloride & bicarbonate are dominant anions in the groundwater. Contour maps are prepared collectively for all aquifers to view broad variation in major ions. Cl^- and Cl^-/HCO_3^- ratio contour maps indicate that there is no increase towards coast which would be case in case of seawater intrusion, but in Quaternary aquifer, an increase is noted in southern part of the study area (EC ~ 800 to 2000 µS/cm) indicating contribution from backwater. Na^+ contour also shows similar variations. Ca^{2+} and SO_4^{2-} contours show similar trends and found to be high in North central part, which can be attributed to presence of Gypsum in Cretaceous sediments. On the other hand HCO_3^- and Mg^{2+} contours are similar and indicate high values in Northern region. Other chemical species (K^+, Sr^{2+} and iron) show complex variations due to multiple sources and sinks.

Among different hydrochemical parameters only pH and Na^+ fall outside the drinking water permissible limits in 10-20 % of the samples whereas all other parameters are well within the limits. Based on TDS, 29 % and 61 % of the samples fall under desirable and permissible categories respectively and remaining 10 % is unfit for drinking purpose. No nitrate and fluoride contamination is observed in groundwater, but arsenic concentration up to 40 ppb is noted in some deep groundwater. Indicators such as SAR, RSC and Na% that qualify the water for irrigation suitability are found to fall under 'excellent' and 'permissible'categories. SAR values range from 0.43 to 6.9 which fall under low sodium hazard class. As per Na% criteria, 20% of samples fall under unfit category. Presence of high Na% along with high EC in groundwater reduces the osmotic activity of plants and thus interferes with the absorption of water and nutrients from the soil. RSC values range from -9.1 to 3.2 and only 5% samples fall under unfit category. There are also cases of water samples falling under doubtful to unfit category due to presence of high bicarbonate concentrations.

Microbial assay in groundwater of different formations demonstrates a wide variety of micro-organisms with loads varying from 1.8×10^3 to 3.3×10^4 cfu/100 ml. Even though all the microbes don't fall under faecal origin, half of the samples analyzed indicated the presence of E.

coli. The E. coli has shown positive correlations with DO and TOC while an inverse trend was found with well depth. The anaerobic bacteria, SRB, are found in a few locations in deeper Tertiary and Cretaceous aquifers where DO levels are very low. Presence of SRB is indicative of reducing condition of the groundwater.

CHAPTER 4: ISOTOPE AND GEOCHEMICAL EVALUATION OF FACTORS AFFECTING GROUNDWATER CHARACTERISTICS

Chemical constituents dissolved in groundwater of an aquifer system reflect the evolution and interaction of various processes within the flow system, e.g., nature and source of recharge water, water-rock interaction, residence time, length of groundwater flow path, and mixing of groundwater from adjacent hydrogeologic units. In this chapter major and few minor inorganic chemical constituents and environmental isotopes results are interpreted using various graphical and modeling techniques to evaluate the geochemical processes.

Groundwater in Quaternary aquifer is mainly Na-Mg-HCO_3-Cl and Na-Ca-HCO_3-Cl water types. Characteristic ionic ratios such as $SiO_2/(Na^+ + K^+ - Cl^-)$, $Na^+/(Na^+ + Cl^-)$, $Ca^{2+}/(Ca^{2+} + SO_4^{2-})$ and $Mg^{2+}/(Mg^{2+} + Ca^{2+})$ indicate ion exchange and weathering of carbonate rocks as dominant processes. An increase in TDS is noted in few samples towards seaside in southern part of the study area. In Tertiary aquifers the groundwater is mainly distributed into Na-Ca-HCO_3-Cl type and Ca-Mg-HCO_3 type. Characteristic ion ratios indicate that samples North of river Gingee demonstrate silicate dissolution from the source rock whereas samples South of the river indicate dominance of carbonate weathering. These ratios also indicate processes like Dolomite weathering, Calcite precipitation and cation exchange. In the case of Cretaceous aquifer, the groundwater is dominantly Ca-Mg-HCO_3 type except at a few locations close to coast which show Na-Mg-HCO_3-Cl and Na-Ca-HCO_3-Cl water types. In this aquifer low TDS waters are found to be Ca-Mg-HCO_3 type which changes their facies with increasing TDS in two different geochemical pathways;

i) Ca-Mg-HCO3-Cl alters to Ca-Na-SO_4-Cl type
ii) Na-Mg-SO_4-Cl alters to Na-Cl-HCO_3 type.

From characteristic ion ratios the basic reactions governing the geochemical reactions are deduced to be dissolution of calcite followed by cation exchange and dissolution of clay minerals. The facies variations in different aquifers are clearly depicted in piper trilinear plots. Seasonal variation in groundwater chemistry was monitored in selected samples mostly from Tertiary and Cretaceous aquifers during pre and post monsoon seasons. The facies remain same in all the samples except at two locations indicating negligible/delayed impact of local precipitation.

Modeling is used to determine the type of reactions occurring between the aquifer matrix and the media, and the degree to which reactions occur and the conditions under which the reactions occur. This information can help us in understanding the dissolution and precipitation process of different minerals and also in predicting the behavior of water in the event of some change to the system. PHREEQCi and NETPATH geochemical codes are used in this thesis work.

Mineral saturation indices for groundwater are calculated for common minerals found in these sedimentary formations. Minerals such as Gypsum, Anhydrite, Albite and Fluorite are found to be unsaturated whereas Goethite, K-Mica, Kaolinite, Illite, Montmollinite are supersaturated in all the groundwater. Other minerals like, Chalcedony, Christobalite, Aragonite, Calcite and Dolomite vary in degree of saturation in different aquifers. Complex aluminosilicate minerals such as Feldspar minerals dissolve incongruently and form residual clay minerals. The stability of aluminosilicate minerals is commonly evaluated by thermodynamic stability diagrams using cation and silicate chemistry. In K-system all the Tertiary and Cretaceous sample data fall in Kaolinite stability field, whereas for Quaternary samples Kaolinite and K-Feldspar are stable solid phases. Kaolinite was found to be stable solid phase along with Na-Montmorllionite in Na-system and Ca-Montmorllionite in Ca-system and Chlorite in Mg-system. The factor analysis of the groundwater is carried out to identify important components/sources that explain the variations in water quality in each formation. Albite weathering, backwater influence and denitrification are found to be dominant controls in Quaternary aquifer, whereas silicate and calcite weathering play major role in controlling Tertiary and Cretaceous aquifers.

One of the objectives of the modeling is speciation of chemical species. Among undissociated forms, most of the alkaline earth metals were found to be present as $MHCO_3^+$ followed by MSO_4 and MCO_3 which together make up to 30 %. Strontium was found to be associated more with undissociated forms compared to Mg^{2+} and Ca^{2+}. For calculating mole transfer values of minerals, pairs of samples are selected from each of Quaternary, Tertiary and Cretaceous aquifers along the flow path. The conditions in initial waters are considered to be open or partially open to atmosphere, whereas closed to atmosphere in the case of final waters. The mole transfer values were found to be positive for Aragonite, Dolomite, Goethite, Albite and Gypsum indicating dissolution and negative for Pyrite, Calcite with varying magnitudes representing the process of precipitation. Modeling studies indicate that high strontium concentration in final waters is due to incongruent dissolution of Aragonite.

Pyrite oxidation and reductive dissolution of iron oxyhydroxide (Goethite) are the two main processes identified as responsible for the release of arsenic into groundwater. The reductive dissolution theory is found to hold good in the present case as the organic matter present in the formation can reduce Goethite and release sorbed arsenic into groundwater. This is further supported by presence of Goethite in sediments, low DO & sulfates, H_2S odor at the sampling sites and presence of SRB.

Environmental isotopes are used in order to assess the groundwater of recharge and its dynamics. An attempt has also been made for the first time to establish local meteoric water line (LMWL) for north east monsoon ($\delta^2H = 7.7\delta^{18}O + 4.2$) which is a major contributor of rainfall to this region. The results indicate enriched isotopic composition of Quaternary samples ($\delta^{18}O$: -5.1 to -1.3‰) indicating that the recharge is mostly from evaporated surface water bodies, while Tertiary ($\delta^{18}O$: -6.5 to -3.0‰) and Cretaceous ($\delta^{18}O$: -6.3 to –4.5 ‰) samples mostly fall along the LMWL indicating contribution from precipitation without significant evaporation. Mineralization by dissolution of minerals, evaporative enrichment and saline water mixing are three processes easily distinguished by Cl^- versus $\delta^{18}O$ plots. Quaternary groundwater demonstrates all the three processes mentioned above, which is in agreement with the geochemical trends. In the case of Tertiary aquifer, a few samples showed enriched isotopic composition which can be attributed to contribution from shallow Quaternary aquifer, whereas dissolution of aquifer material is the main process governing the chemistry of Cretaceous aquifer. No seasonal variation is observed in stable isotope values of Tertiary and Cretaceous groundwater samples indicating direct recharge from precipitation is not significant. $\delta^{13}C$ values range from -22 to -9 ‰ in groundwater indicating contribution from root respiration and dissolution of carbonate minerals.

Environmental tritium values of the groundwater are in the range of 4.5 - 6.5 T.U. indicating modern recharge to groundwater. A few deep samples from Tertiary and Cretaceous aquifers show tritium <2 T.U. indicating old groundwater. From environmental isotope results and hydrogeology of the region, it can be concluded that Quaternary aquifer is mostly recharged by local precipitation and surface sources whereas Tertiary and Cretaceous formations derive most of the recharge from precipitation occurring in western part of the study area.

CHAPTER 5: IDENTIFICATION OF SOURCE, WEATHERING AND DEPOSITION CHARACTERISTICS OF SEDIMENTS

Compositional characteristics of source rocks are generally well recorded in sedimentary deposits and provide valuable information about nature of source rocks, weathering conditions and deposition environment. This chapter deals with the application of major, trace and REE geochemistry to identify the nature of source rock, weathering characteristics and deposition conditions in different sedimentary formations of the Pondicherry region. The bulk XRD pattern of the sediment samples indicates Quartz and Feldspar as the major minerals whereas Mg-Calcite, Aragonite, Calcite and clay minerals as minor ones. Based on the vertical trends of the geochemical parameters in the sediments different geological formations were demarcated at the study site. The trace elemental ratios suggest that sediments are mainly derived from felsic source rocks and ternary plots indicate contribution of intrusive rock such as Tonalites. The major and trace elements show depleted values compared to upper continental crust (UCC) suggesting that source rocks are weathered and diagenetically altered to remove lithic fragments and increase in the proportion of Quartz relative to source rock. The ratios of redox sensitive elements (Th/U) infer oxic weathering in shallow sediments. Variable Chondrite normalized ratios of La/Lu and low TREE also support moderate to intense weathering of source rocks. Positive Eu anomaly is observed in NASC normalized REE patterns which is in agreement with earlier studies carried out in Cauvery basin. Since sporadic occurrences of arsenic are noted in groundwater of Tertiary and Cretaceous formations, arsenic distribution and its correlation with other elements is studied in detail.

The arsenic content in the sediments of this site ranges between BDL to 30 ppm and represents background value of crustal abundance. There is only single instance of high arsenic content in the case of sediment collected from 129-131 m depth. An increasing trend is noted along the depth in arsenic and other measured elements except iron. Sediments from lower Cretaceous formation show comparatively higher arsenic concentration. The presence of As is further confirmed by TXRF study. Arsenic correlates positively with iron and sulfur concentrations while iron and sulfur contents don't show good correlations suggesting other minerals for iron in addition to iron sulfide. Both positive and inverse trends are noted between arsenic and organic matter. A positive correlation between total organic carbon and As content in shallow sediments indicates that arsenic is present in association with organic sources, whereas inverse trend in the case of deep sediments point to bacterial mediated reduction of organic carbon.

CHAPTER 6: ROLE OF GROUNDWAER PARTICLES IN METAL MIGRATION

The particles in ground and surface waters have received increased attention in recent years, as it has been recognized that these entities are important in the transport of contaminants and radionuclides. For proper risk assessment and remediation measurements, the role of particles in pollutant transport assumes greater importance, for which size, chemical and mineralogical aspects of particles need to be studied in detail.

A study on particles in groundwater of selected wells in this region is carried out to assess the nature and abundance of particles, morphological feature of particles and their implication on trace metal migration. It is found that the total particle loads are in the range of 4.5×10^5 to 3.3×10^6 /L and the average particle load is found to be in the range of 0.64 to 2.6 mg/L. A systematic decrease in particle number is observed with increasing in particle size and well depth. The β value, which signify the relative abundance of smaller particles is calculated from particle size distribution curves and is found vary between 2.54 and 4.03. Samples collected from Cretaceous formation show higher β values compared to Tertiary formation indicating abundance of smaller particles. The Cretaceous formations are composed of abundant clay layers which retard the groundwater flow and increase residence time, facilitating the filtering out of larger particles generated at the recharge or unsaturated zones leading to increased smaller particle number. Longer residence time for Cretaceous groundwater is also supported by low tritium values (<2 T.U.). The particle number in this region is mainly influenced by organic carbon and ionic strength whereas pH and temperature of the groundwater show negligible effect. The reason for increase in finer particles along groundwater flow path in Quaternary and Tertiary formations can be attributed to differential settling velocities.

The morphological and mineralogical examinations suggest that the particles are of spherical, elongated and tubular shapes and belong to clay minerals and iron oxides. Chemical analysis of the particles indicate presence of Na^+, K^+, Ca^{2+}, Mg^{2+} and iron elements. The source can be Feldspar, Carbonate and Ferromagnesian minerals present in these sedimentary formations. Also, the mineralogy of the particles is found to be consistent with the make-up of the host rock composition. Distribution of major elements doesn't not indicate that mineral composition of smaller particles is different from larger ones.

Association of Sr^{2+} with particles is studied using Sr^{2+}/Ca^{2+} (percent ratio) in this work. It is observed that Sr^{2+}/Ca^{2+} ratio ranges between 0.7 and 2.5 % in particulate matter whereas in colloidal fractions it ranges from 1 to 9 %. This clearly demonstrates that Sr^{2+} preferentially partitions into colloidal over particulate matter as compared to Ca^{2+}. The saturation index values for common minerals of Sr^{2+} (Celestite or Strontionite) don't favor formation of mineral precipitates, so it can be implied that Sr^{2+} is associated as sorbed ion on clay minerals.

SUMMARY

The research work undertaken pertains to the study of groundwater characteristics in different sedimentary aquifers of Pondicherry region, factors and processes affecting the groundwater characteristics, source of sediments and the role of groundwater particles in trace metal migration.

The groundwater is mostly fresh and potable as per BIS standards. Among different hydrochemical parameters only pH and Na^+ are found to be beyond drinking water permissible limits in 10-20 % of the samples. No nitrate or fluoride contamination is observed and indicators (SAR, RSC and Na %) that qualify the water for irrigation suitability are found to fall under excellent to permissible category. Microbial assay demonstrates a wide variety of micro-organisms with loads in the order of 10^3 - 10^4 cfu/100 ml and 50% of the samples analyzed contain E. coli. Sulphate reducing bacteria (SRB) is found in a few locations in deeper Tertiary and Cretaceous aquifers which is indicative of anoxic condition.

Quaternary groundwater is mainly Na-Mg-HCO_3-Cl and Na-Ca-HCO_3-Cl water types and their characteristic ionic ratios indicate contribution of weathered carbonate rocks and ion exchange for the observed changes in groundwater characteristics. An increase in TDS is noted from inland to coast in the southern part which could be attributed to contribution of backwater, which is further verified by stable isotope signatures. In Tertiary aquifers the groundwater mainly belongs to Na-Ca-HCO_3-Cl and Ca-Mg-HCO_3 types. Samples collected from North of river Gingee display dominance of silicate dissolution whereas samples from South represent indicate carbonate contribution. Geochemical variations in Cretaceous groundwater show two evolutionary pathways, i) Ca-Mg-HCO_3 to Ca-Mg-HCO3-Cl to Ca-Na-SO_4-Cl and ii) Ca-Mg-HCO_3 to Na-Mg-SO_4-Cl to Na-Cl-HCO_3. The governing reactions are found to be dolomite weathering followed by leaching from sediments in the former case and dissolution of dolomite followed by calcite precipitation and cation exchange and sulphate reduction in the later case. These observations were further supported by $\delta^{18}O$, $\delta^{13}C$ inferences.

Inverse modeling results indicate that the mole transfer values are positive for Aragonite, Dolomite, Goethite, Albite and Gypsum indicating dissolution and negative for Pyrite, Calcite representing the process of precipitation with varying magnitudes in different aquifers. Modeling studies also indicate incongruent dissolution of Aragonite as the source for strontium in groundwater. From speciation calculations, it is found that most of the alkali elements are present as free ions, whereas alkaline earth metals are found to be present as $M^{2+} > MHCO_3^+ > MSO_4 > MCO_3$ and the total undissociated species amounting to 30%. Factor analysis of the chemical data also indicates three major processes that affect groundwater chemistry viz., carbonate/gypsum dissolution, surface water contribution and inputs from soluble fertilizers and livestock excrement.

Local meteoric water line (LMWL) for north east monsoon ($\delta^2H = 7.7\delta^{18}O + 4.2$) which is a major contributor of rainfall to this region is established in this work. Quaternary samples fall on evaporation line indicating contribution of evaporated surface water sources whereas Tertiary and Cretaceous aquifer samples fall on LMWL indicating dominance of precipitation recharge. Chloride variation with $\delta^{18}O$ indicated dissolution of minerals, evaporative enrichment and saline water mixing as reasons for observed increase in chloride concentration of Quaternary aquifer samples, whereas dissolution of aquifer material is the main process governing for the observed chloride variation in Tertiary and Cretaceous aquifer. Environmental tritium results

indicate that most of the groundwater is modern but a few deep samples from Tertiary and Cretaceous aquifers show tritium <2 T.U. indicating old groundwater.

Based on the vertical trends of the geochemical parameters in the sediments, different geological formations are demarcated at the study site. Results conclude that sediments are mainly derived from felsic source rocks which are moderately to intensely weathered and diagenetically altered. The arsenic content in the sediments varies from BDL to 30 ppm and increases with depth. Arsenic correlates positively with iron and sulfur concentrations while both positive and inverse trends are observed between arsenic and organic matter pointing to bacterial mediated reduction of organic carbon.

Particle measurements in groundwater indicate particle loads in the range of 0.64 to 2.6 mg/L. A systematic decrease in particle number is observed with increasing in particle size and well depth. The particle number is mainly influenced by organic carbon and ionic strength while pH and temperature of the groundwater show negligible effect. It is found that Sr^{2+} preferentially associates with colloidal particles over larger particles as compared to Ca^{2+} and modeling studies suggest Sr^{2+} migration as sorbed ion on clay particles rather than its mineral precipitate.

LIST OF FIGURES

LIST OF TABLES

LIST OF APPENDICES

LIST OF PLATE

LIST OF ABBREVATIONS

AFM	Atomic Force Microscopy	PSD	Particle Size Distribution
ASDPV	Anodic Stripping Differential Pulse Voltammetry	PVC	Poly Vinyl Chloride
BGL	Below Ground Level	REE	Rare Earth Elements
BIS	Bureau of Indian Standards	RSC	Residual Sodium Carbonate
CBE	Charge Balance Error	SAR	Sodium Absorption Ratio
CGWB	Central Ground Water Board	SEM	scanning electron microscopy
DO	Dissolved Oxygen	SPC	Single Particle Counter
E. coli	Escherichia Coliform	SRB	Sulphate Reducing Bacteria
EC	Electrical Conductivity	SWM	South West Monsoon
EDS	Energy Dispersive Spectroscopy	T.U.	Tritium Units
EDXRF	Energy Dispersive X Ray Fluorescence	TC	Total Carbon
ESEM	Environmental Scanning Electron Microscopy	TDV	Total Data Variability
GFAAS	Graphite Furnace Atomic Absorbance Spectroscopy	TEM	Transmission Electron Microscopy
GMWL	Global Meteoric Water Line	TH	Total Hardness
HREE	High Rare Earth Elements	TIC	Total Inorganic Carbon
LMWL	Local Meteoric Water Line	TOC	Total Organic Carbon
LPM	Liters per Minute	TVC	Total Viable Counts
LREE	Low Rare Earth Elements	TXRF	Total X Ray Fluorescence
MSL	Mean Sea Level	UCC	Upper Continental Crust
NASC	North American Shale Composite	VPDB	Vienna Pee Dee Belemnite
NEM	North East Monsoon	VRBA	Violet Red Blue Agar
ONGC	Oil and Natural Gas Corporation	VSMOW	Vienna Standard Mean Ocean Water
PAAS	Post Archean Australian Shale	WHO	World Health Organization
PPB	Parts Per Billion	XRD	X Ray Diffraction
PPM	Parts Per Million		

CHAPTER - 1
INTRODUCTION

1.1 Background

With the rapid population growth and rising expectation for better life, the natural resources of our earth are subjected to increasing pressure. It is paramount that basic resources for human survival, viz., air, water and land must be properly managed. Groundwater which occupies 80% of total freshwater resources and 96% of the unfrozen freshwater on earth is the worst affected resource [1]. The developing global water crisis has evolved in little over half a century and affected most severely the arid and semi-arid regions of the world where groundwater is relied upon for water supply [2]. Groundwater is found in aquifers, which have capability of both storing and transmitting groundwater. Commonly, the large volume of water stored in aquifers provides a reliable source during periods of drought lasting months or years. Groundwater extraction accounts for 32% of the total Indian water production distributed for agriculture and livestock (89%), drinking (9%), and industry (2%) [3]. Growing dependence on groundwater is mainly due to population growth, frequent failure of monsoons and degrading quality of surface water. This crisis is further aggravated due to engineering advancement, which led to creation of large well-fields. Viewed in the international perspective of '<1700 m^3/person/year, as water stressed' and '<1000 m^3/person/year, as water scarce', India is stressed today and likely to be water scarce by 2050 [4]. Already many parts of the country are water scarce. Recent study by Rodell et al (2009) reported that groundwater depletion was equivalent to a net loss of 109 km^3 of water, which is double the capacity of India's largest surface-water reservoir [6]. Natural recharge measurements carried out in about 20 river basins across India suggest that about 15–20% of seasonal rainfall contributes to groundwater recharge in the Indo-Gangetic plains and only 5–10% in the peninsular hardrock regions [5]. With changing land use patterns, infiltration rates of rainfall into soil decreased drastically and diminished the natural recharging of aquifers. Intensive use of groundwater resources and contamination by anthropogenic activities further aggravated the situation by affecting the groundwater quality. The dependency on groundwater is likely to increase for both domestic and agricultural needs.

The scenario of groundwater over exploitation is widely witnessed in coastal aquifers especially in high population zones. Coastal aquifers are typically characterized by variations in groundwater quality in space and time, and are vulnerable directly and indirectly to anthropogenic activities and climate change induced sea water intrusion. Indian coastal aquifers constitute the second richest groundwater reservoirs after the Indo-Gangetic alluvial plain, which is one of the world's largest fresh groundwater reservoirs. Stretching over a length of more than 7000 km, the Indian coastline offers an excellent opportunity for agriculture, particularly on the east coast which has vast stretches of fertile alluvial soils. The coastal zones, in general, have been a major focus for the development of human society and continue to be areas of rich potential for our modern society. Thus understanding groundwater characteristics in coastal aquifers of urban regions is of utmost importance due to their vulnerability to seawater intrusion, upconing of deep seated salt water and other anthropogenic contamination. The hydrogeology of the coastal aquifers has been studied intensively during the past decades, stimulated by both scientific interest and societal relevance. Most of these studies are connected to contamination of fresh water resources by seawater. But, there are many other potential sources of groundwater contamination in coastal aquifers including natural and anthropogenic which needs thorough investigation. Proper management of available groundwater reserves is difficult without knowledge of spatial distribution of its quality and the processes that determine the evolution. It is, therefore, necessary to have most relevant information for arriving at rational decisions that will result in maximum benefit to most people. Accurate and reliable information on the water system can therefore be a vital aid to strategic management of the resource.

1.2 Overview of geochemistry

Geochemistry has played an important role in understanding the quality of groundwater. Not only has geochemistry addressed questions of water quality but it has also played a significant role in defining certain physical properties of aquifers such as recharge rates, residence times and flow paths [7, 8]. The advances in geochemical methods and approaches aided to interpret hydrochemical processes in groundwater systems, provided improved understanding of how structural, geological and mineralogical, and hydrological features affect flow and chemistry in groundwater systems. Significant advances have been made through computer programs which have provided increasingly sophisticated interpretations of geochemical data to predict driving forces affecting groundwater characteristics. Geochemistry and environmental isotopes in conjunction with modeling tools have proven to be potential tools in assessing processes and factors governing groundwater chemistry and benefiting various water managers and agencies in designing the effective groundwater usage and managing groundwater resources.

1.2.1 Influence of rocks

The nature of rock influences the groundwater chemistry, independently of climatic, ecological and topographical influence. Siliceous rocks such as sand and sandstone contain few soluble substances; hence water passing through them has characteristically low total dissolved salts (TDS: 20-300 ppm) with a low Cl^- and SO_4^{2-} content [9]. Carbonate rocks on the other hand contain large fissures and channels rendering rapid water circulation and evapotranspiration has a small influence on the total dissolved salts. Water passing through these kinds of massive limestone has low salt content. The predominant ions are Ca^{2+} and HCO_3^- with relatively little SO_4^{2-}, Cl^- or Na^+. The Mg^{2+} content in groundwater depends on the amount of Mg^{2+} in the carbonate. But when the limestone is porous (containing fine fissures), the water circulates slowly and the contact area between the water and the rocks, and interaction time are more. Groundwater passing through sulphate or halite bearing rocks (evaporites) contains large quantities of $CaSO_4$ and NaCl even to the point of saturation. However, water with all possible degrees of concentration may occur, depending on the rate of circulation, the groundwater travel time and the evaporate content of the aquifer fabric [10, 11]. Water in clays and shales may be more or less salty depending on the degree of leaching. Clay also absorbs some ions, and facilitates ion exchange reactions in water. When water circulates very slowly, it may gain Ca^{2+}, Mg^{2+}, Na^+, Cl^- and SO_4^{2-}. This leads to formation of Ca-Cl and Mg-Cl water facies. In crystalline rocks, such as granites water circulates through fissures and has low TDS.

1.2.2 Influence of hydrogeological conditions

A large portion of the infiltrated rain water is removed through evapotranspiration from the soil, leading to concentration of salts in the infiltrating water. Further changes occur in groundwater while in transit through the rocks. During the flow there may be considerable secondary concentration of constituents, particularly when the aquifer has not been strongly leached. Especially in confined aquifer there may be a general increase in the TDS, if groundwater circulates slowly through the rocks, with consequent changes in the chemical composition. The deeper the groundwater lies, the more slowly it circulates and the more difficult it is for it to be replaced by other water. As a result, the dissolved salt concentration in the water tends to increase with depth. The modification of the chemical composition with depth is given by Chebotarev, 1955 [12];

$HCO_3^- \rightarrow HCO_3^- + SO_4^{2-} \rightarrow SO_4^{2-} + Cl^- \rightarrow Cl^- + SO_4^{2-} \rightarrow Cl^-$

When a freshwater aquifer is connected to a surface water body of salt water, such as the sea or a salt lake, the denser salt water will tend to penetrate some distance into the aquifer until a state of balance with out-flowing fresh water is established. The freshwater – saline water interface will advance or recede in accordance with variations in head caused by changes in the rate of pumping, or changes in atmospheric pressures or under the influence of tidal fluctuations in the surface water body [6]. Streams also affect groundwater chemistry by penetrating into the groundwater through permeable sections of the river bed and banks. Groundwater fluctuations may also affect its chemistry. When the water levels are shallow, close to the root zone, a larger number of plant roots may draw water from it, in which case transpiration and possibly evaporation losses will be greater, and the salt content will increase. Conversely, a lowering of the water table may induce lateral inflow from nearby areas with a consequent change in salinity.

Climate influence on the groundwater chemistry happens by facilitating evaporation and transpiration processes. The effect of evaporation will be greatest where the air is warmer, drier and more mobile. On the other hand, transpiration losses depend on the density of vegetative cover, which in turn is dependent on the rainfall. Intensity of the rainfall also plays a role in controlling groundwater chemistry. Downward percolation of salts from infrequent but heavy downpours is much greater than from prolonged but light showers. In subtropical climate the temperature is higher and the production of CO_2 in soil zone is more abundant. The TDS vary from 100 to 1000 ppm depending on the nature of rocks. Close to the equator, in a hotter and arid climate, the rainfall is less than the evapotranspiration [13]. The Cl^- and SO_4^{2-} being less subject to leaching will get concentrated in the soil by evaporation and subsequently flushed downward into the groundwater after rains. In some regions the heavy tropical rainfall may be greater than evapotranspiration losses, in which case the groundwater salinity will be low, the main anion often being HCO_3^-. The chemical composition of the groundwater also depends on paleohydrogeology [14].

1.3 Geochemical processes

The main processes influencing groundwater composition can be subdivided into physical, geochemical and biochemical. Mixing, dispersion and filtration are the important physical processes which modify the chemical composition of groundwater. In assessing the significance of the physical processes it is important to consider the relative importance of solute transport mechanisms and secondly the particle size of the components of the groundwater in relation to the primary (intergranular space) and secondary porosity (fissures and fractures). Majority of the sedimentary aquifers have fissures as small fraction of total storage. The rate of solute transport in the intergranular pore spaces is much slower than in fissures. Thus a compositional disequilibrium exists between water transiting via fissures and that moving through inter-granular spaces. The heterogeneity may be detectable as a difference in elemental composition between fissure water and intergranular water [15] and in some cases dissimilarities in elemental composition may not exist and the differences could only in the age of water in two components.

Solution-precipitation reactions, complex formation, acid-base reactions, oxidation-reduction reactions and ion exchange - surface reactions are the major geochemical processes that govern groundwater chemistry in addition to geochemical abundance of elements [16]. Oxidation-reduction reactions are common reactions that control the pH of the water. Oxidation will lead to a decrease in pH while reduction contributes to increasing of pH levels [17]. The solubility of almost all minerals is dependent on pH, therefore very small pH changes can drastically affect the predicted aqueous levels of ions in solution. Oxidation reduction reactions involve iron and related transition metals and subsurface biochemical reactions involving the C, N, O and S cycles. In moderately oxidising groundwater the redox potential is controlled primarily by the DO content of water. As the DO decreases along the flow path reducing conditions dominate [17].

Many rock forming minerals are capable of exchanging cations or in some cases anions at their surfaces. It is well documented that many clay minerals can have large cation exchange capacities [18]. For a mineral to have ion exchange properties, it is necessary for there to be a charge imbalance in the crystal structure or at its surface. Similarly clays and similar geological materials also act as semi-permeable membranes which will restrict or retard the flow of charged solutes. This membrane filtration is a significant process in some deep sedimentary formations where large enough head differences exist.

1.4 Groundwater modeling

Groundwater modeling is carried out broadly for two reasons, viz., i) to understand the flow conditions of an aquifer and ii) to understand the behaviour of chemical species in an aquifer. Flow modeling is generally attempted by solving a set of mathematical equations governed by Darcy's law. In general most of the widely used groundwater flow models assume porous media flow, which is the flow associated with granular aquifer and fractured rock aquifer. Flow modeling of groundwater aquifer system was done by several people [19, 20] for understanding the dynamic behaviour of groundwater flow, basin-wise water balance, spatial distribution of hydrologic components of water balance and predictive simulation.

A geochemical model is an attempt to explain the chemical characteristics of the system in terms of water/rock/gas interactions active in the system. In chemical modeling the available chemical and isotope data is used to determine chemical processes occurring in subsurface, extent to which these reactions have proceeded, the conditions in which these reactions are taking place (close or open to CO_2 gas etc.), impact of natural perturbations on chemical quality. The models that were developed as an outgrowth of these efforts can be grouped as forward and inverse models. In forward modeling, reaction progress is governed by thermodynamic expressions; hence, the result is an equilibrium prediction [21]. In inverse modeling, probable reactions are calculated based on the information supplied at initial and final points along a flow path, and as such, do not necessarily represent equilibrium. Forward modeling may be preferred when only the final outcome of the interaction of groundwater with soils or sediments is desired, i.e., groundwater composition and mineral saturation index. Inverse modeling provides hydrologic information about an aquifer, such as net mass transfer and mixing, and can be used to determine relative rates of reactions. Another comparison may be made in which forward modeling tests the validity of suspected reactions based on thermodynamic considerations while inverse modeling tests their feasibility based on mass balance considerations. Inverse modeling is especially useful after bench-scale column tests reveal the levels of various water quality parameters in the initial water and final water. Reaction-transport modeling is different from the above two modeling methodologies, it can be used to simulate real transport processes, such as advection and dispersion, in addition to predicting groundwater chemistry [22]. These reaction-transport models are especially useful for predicting the flow path of both conservative and non-conservative species. A few forward modeling programs are EQ3NR, MINEQL, MINTEQA2, PHREEQC, SOILCHEM, SOLMNEQ.88 and WATEQ4F which deal with the speciation, geochemical reactions and soil, agricultural applications. Commonly used inverse models are BALANCE, EQ6 and NETPATH, these codes generally deal with interpreting the net geochemical mass reactions between initial and final waters along a hydrologic flow path. NETPATH modeling is applied in the present work.

The objective of inverse modeling is to find sets of phases (minerals and gases that are consistent with supporting observations) that, when reacted in appropriate amounts, quantitatively account for the differences in composition between initial and final solutions (constraints). NETPATH code solves a set of linear equations that account for conservation of mass to find every subset of the selected phases and the computed mass transfer that satisfies the chosen constraints. It is assumed that initial groundwater changes composition only by chemical reactions and not by dispersion, evaporation and mixing etc. For every set of conditions (constraints and phases) NETPATH checks for different combinations of minerals and their mass transfer that can lead to final water composition and displays only those models that are suitable.

Geochemical modeling rarely leads to unique solutions. But this modeling process is best suited for eliminating reaction models from further consideration. A mass-balance model could be eliminated if it requires net precipitation of a phase that is known to be undersaturation (from its saturation index value) and similarly if the predicted isotopic composition of the final water significantly differs from the observed one. Apart from thermodynamic criteria, further validation of model output can be done based on parameters such as detailed petrographic, mineralogic and isotope information. The validity of mass-balance models depends significantly on the geochemical insight of the modeler in selecting appropriate phases and constraints and the geochemical models can be no better than the data on which they are based. Mass-balance for waters along flow path doesn’t include compositional mixing effects due to hydrodynamic dispersion (Plummer et al., 1990). Although this effect is less significant in the case of regional flow systems, in local systems such as point source injection this could lead to serious error.

1.5 Statistical approach

Multivariate statistical analyses such as cluster, factor and discriminant analysis, aim to interpret the governing processes through data reduction and classification. Multivariate statistical techniques are unbiased methods and help in identifying natural associations between samples and/or variables thus highlighting information not available at first glance [23]. The application of different multivariate approaches for the interpretation of these complex data matrices offers a better understanding of water quality and ecological status of the studied systems, allows the identification of the possible factors/sources that influence the water systems and offers a valuable tool for reliable management of water resources as well as rapid solutions on pollution problems [24].

1.5.1 Correlation matrix

A correlation matrix is established using Pearson's correlation coefficient between ion pairs. It is known as the best method of measuring the correlation, because it is based on the method of covariance [25]. The correlation coefficient gives information about the degree of correlation and the direction of correlation. The Pearson's correlation coefficient value lies between +1 to -1 and the degree of correlation is said to be perfect correlation if the correlation coefficient value is near ± 1. For values ranging between ± 0.75 and ± 1 it is said to be a high degree of correlation, similarly moderate degree of correlation for values between ± 0.25 and ± 0.75 and low degree of correlation for values between 0 and ± 0.25.

1.5.2 Factor analysis

The usual procedures of interpretation of chemical quality of groundwater with the help of plots of different ions and pairs of ions do not define simultaneously the similarities or otherwise between all ions or samples. Factor analysis offers a powerful means of detecting such similarities among the variables or samples [26]. The purpose of factor analysis is to interpret the structure within the variance covariance matrix of a multivariate data collection. This technique extracts the eigen values and eigen vectors from the matrix of correlation or covariance. The factors are constructed to reduce the overall complexity of the data by taking advantage of inherent inter-dependencies. As a result, a small number of factors will usually account for approximately the same amount of information as do the much larger set of original observations. The interpretation is based on rotated factors, rotated loadings and rotated eigen values. Factor analysis does not require a priori knowledge of the number of types of sources influencing the samples, nor does it require knowledge of the source composition.

1.6 Environmental isotope indicators

Among different methods used to understand hydrological processes, application of tracers in particular isotope tracers has been the most useful in terms of providing new insights. Stable isotopes of H and O (i.e. ^{2}H and^{18}O) being integral parts of water molecules are ideal tracers to follow the movement of water. Identification of water sources for precipitation, assessment of post precipitation processes during groundwater recharge have been possible because stable water isotopes are influenced directly by the atmospheric processes (e.g. water vapor advection, condensation or evaporation) and groundwater recharge mechanism (evaporation, mixing and dispersion). The hydrological application of isotope measurements is mainly based upon the variations in the concentrations of ^{2}H, ^{3}H and ^{18}O, along with ^{13}C and ^{14}C in dissolved carbon, in natural waters [27 – 29]. The most important objectives of isotopic studies are determining i) hydrological and hydrogeological relations, ii) residence times of groundwater and iii) estimating pollutant transfer.

1.6.1 ^{2}H and ^{18}O isotopes

Precipitation is the primary source for the earth's surface runoff, groundwater recharge and evapo-transpiration moisture. In spite of great complexity in different components of the hydrological cycle, δ^{2}H and δ^{18}O in majority of waters of meteoric origin correlate on a global scale. This linear relation is the outcome of covariations of relative vapor pressures of $H^{2}H^{16}O$ versus $H_2{}^{16}O$ and $H_2{}^{18}O$ versus $H_2{}^{16}O$ that prevail during the various processes which characterize the cloud dynamics. A Global Meteoric Water Line (GMWL) was established by Craig, 1961 [30] which given as;

$$\delta^2 H \ = 8 \ \times \delta^{18} O + 10 \qquad (1.1)$$

This equation represents the modern day GMWL and is further modified by Rozanski et al., 1993 [31] covering a large set of data from many rain stations.

$$\delta^2 H = 8.17\ (\pm 0.07) \times \delta^{18} O + 11.27\ (\pm 0.65) \qquad (1.2)$$

There are several factors that control the isotopic composition of precipitation. Precipitation becomes isotopically lighter as the parent air masses move farther from their sources and over the continents because they undergo multiple cycles of precipitation (*continental effect*). Depletion in heavy isotopes also occurs with increasing latitude because the degree of rainout of air masses increases and temperatures decrease with latitude (*latitude effect*). The isotopic composition of water becomes lighter with increasing altitude, again because it is colder at higher altitudes fractionation increases (*altitude effect*). The depletion in $\delta^{18}O$ content is around -0.2 to -0.5 ‰ per 100m elevation. The isotopic values of the rain falling at a given station are high in months with little rain and depleted during rainy season (*amount effect*). Seasonal changes in temperature clearly affect the isotopic composition of precipitation, except in the tropics where temperature is effectively constant throughout the year. Isotopic values are depleted in winter rains compared to summer rains (*seasonal effect*).

Despite the fact that ocean water is the ultimate source of all meteoric water, the data for ocean water doesn't lie on the GMWL. This is attributed to non-equilibrium processes such as evaporation. A parameter d- excess (equation 1.3) is used to signify the kinetic effects associated with the evaporation of water at the surface of the oceans or inland [27, 29, 32]. The primary evaporation from the sea surface fixes the d-excess value which remains unaltered as the air moves across the continents and loses moisture by rainout. However the d-excess of the air masses is impacted by the secondary process that returns moisture to the air, such as evaporation from an open surface water body (recycling of water). The inherited d-excess value can be altered as the air mass moves inland. The d-excess of the evaporating water body will progressively decrease and that of the resulting vapor will progressively increase [31]. Hence this parameter helps in estimating the kinetic fractionation process undergoing under humidity less than 100%.

$$d - excess = 8 \times \delta^{18} O - \delta^2 H \qquad (1.3)$$

1.6.2 Carbon-13 isotope

Identifying the sources and sinks of dissolved inorganic carbon species is an important step in understanding the geochemistry of groundwater systems. This is particularly important for sedimentary aquifers because bicarbonate is frequently the major anion. Stable carbon isotopes are useful indicators of dissolved carbon sources in groundwater systems. This is due to different isotopic signatures of different geologic materials. Marine carbonate shell material, which is important lithologic material in many aquifers (esp. coastal aquifers), typically has a $\delta^{13}C$ value of about 0.0 ± 0.3 ‰ [33].

The carbon isotope content of the groundwater is generally controlled by the carbon isotope composition of recharging water. Precipitation is considered as the principal recharge mechanism in most of the aquifers, hence, the dissolved CO_2 source responsible for the dissolved inorganic carbon in groundwater is expected to be primarily the atmosphere. Atmospheric CO_2 has been reported to range from -6.4 to -7.6 ‰. Although CO_2 may be primarily of atmospheric origin, the subsurface interactions involve dissolution of root respired CO_2 from native vegetation. P_{CO_2} in root zone (-0.3 kPa) is much greater than atmosphere (-0.03 kPa), therefore shallow zone groundwater shows slightly more negative $\delta^{13}C$ than atmospheric CO_2. This depletion results from diffusion of soil gas having a $\delta^{13}C$ of about -18 ‰ (in case of C_4 plants) or -25 ‰ (in case of C_3 plants) in to the groundwater [27, 29, 34].

1.6.3 Environmental tritium

The determination of aquifer recharge is one of the most important steps in quantitative and qualitative hydrogeological characterization. The recharge corresponds to the renewal of groundwater resources of aquifers. If the aquifer is properly exploited, its natural recharge compensates its extractions. Thus it avoids the progressive depletion in groundwater levels, which may lead to complete exhaustion. Tritium (^3H), a radioactive isotope of hydrogen is a best suited isotopic tool which can indicate modern recharge occurring during last 40 odd years. Owing to its variation in input concentration spatially and temporally, ^3H is used as qualitative tool.

Tritium is produced from a nuclear reaction between atmospheric nitrogen and thermal neutrons ($^{14}N + n \rightarrow {}^{12}C + {}^{3}H$) in the upper atmosphere [35]. The ^3H thus formed enters the hydrologic cycle after oxidation to $^1H^3HO$ and it decays according to following equation;

$^{3}H \rightarrow {}^{3}He + ß^{-}$ ($E_{\beta max}$ = 18 keV) (1.4)

Tritium has a half-life of 12.43 years and owing to short residence time of ^{3}H in the atmosphere, the natural ^{3}H concentration in the air is very low. Low level tritium concentration is expressed in Tritium Unit (TU). One TU corresponds to one tritium atom per 10^{18} atoms of hydrogen ($^{3}H/^{1}H = 10^{-18}$). A concentration of 1 TU is equivalent to a specific activity of 0.118 Bq/L of water. Tritium concentration in precipitation rose rapidly following the atmospheric bomb test during 1963. Tritium data is interpreted primarily in two ways, that is, ^{3}H-free groundwater contains only precipitation water from the "pre-bomb period" and is more than 40 years old, and ^{3}H-rich water contains much precipitation water since 1960s.

1.7 Sediment Geochemistry

The nature of sedimentary rocks is determined by geological processes that occur in the four main earth surface environments encountered over the sediment's history from source to final sink. They are, i) the site of sediment production (provenance), where interactions among bedrock geology, tectonic uplift and climate control weathering & erosion processes, ii) the transport path, where the medium of transport, gradient and distance to the depositional basin may modify the texture and composition of weathered material, iii) the site of deposition, where a suite of physical, chemical, and biological processes control the nature of sediment accumulation and early burial modification and iv) the conditions of later burial, where diagenetic processes may further alter the texture and composition of buried sediments. Many of these geological processes leave characteristic geochemical signature making sedimentary rocks one of the most important archives of geochemical data available for reconstructions of ancient earth surface environments [36-38].

Major and trace element geochemistry is used in many studies for deducing nature of source rock [39] and reconstructing the paleogeography and paleotectonics of sedimentary basins [40]. In recent times rare earth elements (REE) abundance in the continental crust has also received much attention as their distribution provides reliable information on the origin of source rocks [41]. Researcher also opined that REEs contribute more than major and trace elements to decipher the provenance, since their concentrations are not affected during erosion, sedimentation and diagenesis, and thus represent average source rock composition [42]. In addition to geochemical parameters, environmental isotopes have also been used to provide a stratigraphic tool on both local and global scales [28]. Lithological profiles can be well correlated on the basis of physical and petrographic features as well as isotope signals. Isotope data of rocks/sediments, especially ^{13}C of carbonates, is being used to provide palaeoecological and palaeoclimatological information [43].

A geologic source in the aquifer system is the most fundamental risk factor for the potential mobilization of trace elements. The greater the concentration in the geologic source material, the smaller the overall fraction that needs to be mobilized before groundwater concentration exceeds permissible limits. Studies on arsenic in groundwater have observed that arsenic has definite correlation with the nature of sediment and condition of aquifer [44, 45]. Therefore, in order to understand arsenic behavior in groundwater, it is important to quantify arsenic content in sediments and evaluate its associations with other elements. Sporadic occurrences of arsenic are found in groundwater of Tertiary and Cretaceous formations, therefore it is of very important to quantify the arsenic content in sediments of this region. The coastal aquifers of Pondicherry region are not similar deltaic/fluvial plain as many other arsenic regions, and are millions of years older, consolidated and marine-influenced units. Thus managing groundwater here could/should be different than other arsenic-prone regions.

1.8 Role of groundwater particles

Traditionally the transport of pollutants in groundwater has been predicted by evaluating their distribution between two phases: i) a dissolved, mobile phase and ii) a stationary phase, aquifer solids. But, the unexpected transport of radionuclides in the subsurface during 1980s started the discussion on how far mobile colloidal particles (humic acids, mineral particles and bio-colloids) may contribute to transport processes. This led to an extension of the two-phase (soil-solution) model to a three-phase (solid-colloid-solution) model [46]. Now, after more than 25 years of research, it is generally accepted that natural colloids play a significant role in the transport of trace metals in all environmental compartments [47]. Particulate matter has the potential to concentrate pollutants by sorption and enhance metal mobility if the particles are sufficiently small to migrate with groundwater [48].

Particles are termed as any entity with a size larger than 1 nm, but for most of the earth science disciplines including limnology, oceanography and hydrology, this term in principle is used to refer to living or nonliving entities larger than 0.45 µm. Based on the dimension of entities following terms are given; solutes (<1 nm), colloids or macromolecules (1 nm to 0.45 µm) and particles (> 0.45 µm). These classifications are mostly based on experimental reasons and are arbitrary [49]. It is said that colloids are blamed or claimed for everything that can't be explained [47], often without adequate colloid characterization for proving most of the claims. During the last 3 decades, numerous studies concerning the characterization of natural inorganic colloids in water have been reported. However, most of these studies deal with surface water such as lakes, rivers, ponds, etc. whereas data on groundwater is relatively limited [50]. The role of aquifer geology and groundwater chemistry on the behavior of colloids is not completely understood and still is an emerging subject. All these factors underline the need for detailed study on particles in groundwater related to chemical and physical characterization.

1.9 Study area description

Extensive studies were carried out by many authors on the geological, physiological, hydrogeological and tectonic aspects of the study area [51 - 53]. A brief description of these aspects is given below.

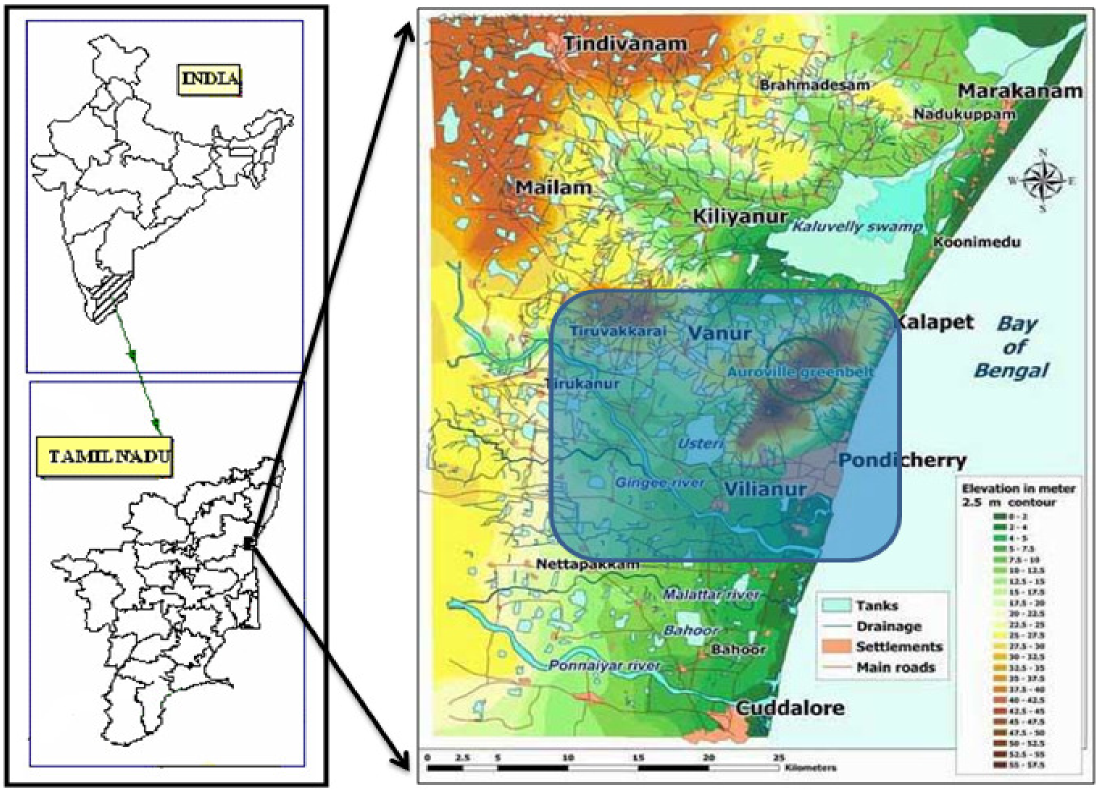

Fig.1. 1 Location map of the study area (shaded region)

1.9.1 Location, Physiography and Land use

Pondicherry is 160 km. South of Chennai and is located on the East coast, bounded by Bay of Bengal and surrounded by Cuddalore district of Tamilnadu. The study area is intersected by the deltaic channels of River Gingee and Pennaiyar. It is also endowed with lakes and tanks. The thick alluvium near Pondicherry is indicative of the place having been part of an extensive lagoon. The geographical coordinates of the study area are 11° 45’ and 12° 03' N latitudes and 79° 37' and 79° 53' E longitudes and forms parts of Survey of India topographical maps Nos.58 M/9, M/13 and 57 P/12 and P/16. Pondicherry region encompasses an area of 293 km^2 with seven communes consisting of a total of 179 villages. The location map is shown in Fig. 1.1. In general this region is a flat peneplain with an average elevation of 15m above msl (mean sea level). The terrain becomes a little undulating with prominent high grounds varying from 30 to 45m above msl towards interior Northwest and Northeastern part of the study area. The three major physiographic units are generally observed viz., i) Coastal plain, ii) Alluvial plain and iii) Uplands. The coastal plain extends as a narrow stretch of four to six hundred meters width on the eastern part of the region along Bay of Bengal. The major part of coastal plain comprises gently sloping land with a chain of sand dunes extending all along the coast.

Other characteristic physiographic units of the coastal plains are spit bars, mud flats, lagoons and tidal inlets. Alluvial plains were formed by two major rivers namely Gingee and Pennaiyar that traverse through this region and occupy major portion of region covering Bahour, Nettapakkam, Ariyankuppam, Southern half of Mannadipet, Villianur and part of Ozukarai communes. These alluvial plains are more or less monotonous with slope ranging from 1m to 3m. Intensive cultivation is being carried out throughout the year in these alluvial plains. Besides the rivers and major canals, there are many depressions acting as storage tanks that are spread all over the terrain to serve as surface water reservoirs. Towards the Northwest and Northeast of Pondicherry region an undulating high ground occurs with elevations of about 30 to 45m above msl. These are known as uplands and are intersected by a number of gullies and deep ravines giving rise to badland topography. A patch of gently sloping fossiliferous limestone terrain also exists in the Northwestern portion.

Major drainage network in this region is covered by Rivers Gingee and Pennaiyar. River Gingee traverses diagonally from Northwest to Southeast, while River Pennaiyar forms the Southern border of Pondicherry region (Fig. 1.2). River Gingee branches off into River Ariyankuppam in the North and Chunnambar in the South, in eastern part of the region and finally joining Bay of Bengal. The Vikravandi, the Pambaiyar and the Kuduvaiyar are the tributaries of River Gingee. The Malattar is the distributary of the River Pennaiyar that drains in the Southern part.

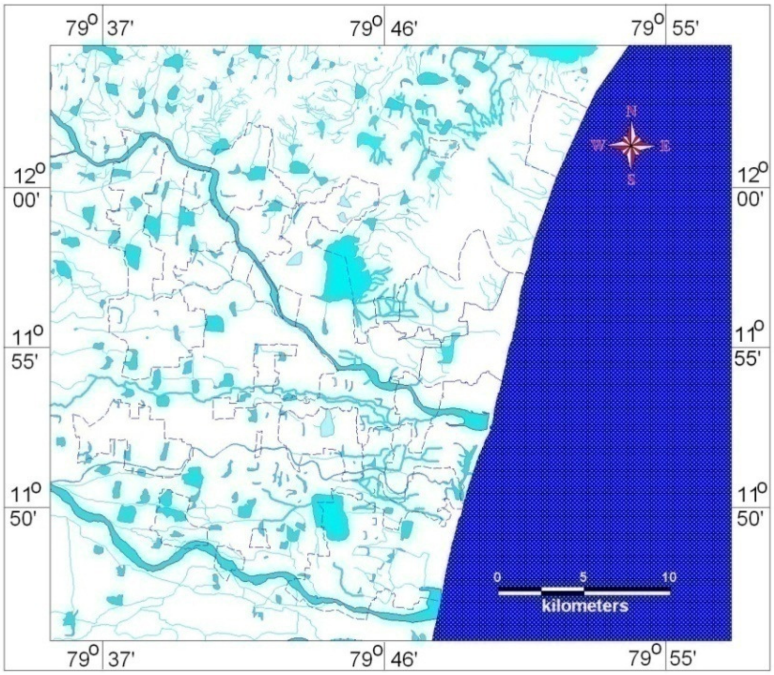

Fig.1.2 Drainage pattern of the study area

The climate of Pondicherry region is humid and tropical. The mean monthly temperature ranges between 22^0C and 33^0C and the temperature is maximum during the months of May and June. The relative humidity varies between 70 % and 85 % and highest during the months of December and January and is lowest in June. The average annual rainfall in Pondicherry is 1254 mm. The region receives rainfall from both the monsoons with annual rainfall spread over a period of eight months. The Southwest monsoon precipitation occurs from June to September and accounts for 29 % of the annual rainfall and the Northeast monsoon rainfall occurring during October to December constitutes 63 % of the annual rainfall. Rest of the rainfall is contributed by dry spells.

The agricultural area is about 56%, but consequent to urbanization and industrialization the land put to non-agricultural purposes is on the increase with time and as a result the net area sown and net area irrigated is gradually declining. Groundwater forms the major source of irrigation in the region and is developed mainly through tube wells even though there are 84 numbers of surface water storage irrigation tanks exist with a total command area of 6,765 hectares and a water holding capacity of 46.4 MCM. These tanks do not receive water on time due to vagaries of monsoon and uncertainty in the release of the impounded water from the rivers. Agriculture in Pondicherry region is well diversified and almost all the crops with different types of cropping pattern are cultivated here. The lands are cultivated with crops all through the year and are rarely kept fallow. The major food crop raised is paddy and the minor crops are ragi, cumbu and maize. The cash crops raised are groundnut and sugarcane.

1.9.2 Geology and Structure

Except for a meager part of the Northeastern corner of Pondicherry region, the entire area is covered by sedimentary formations ranging in age from Cretaceous to Recent. To establish the stratigraphy of the area, the Oil and Natural Gas Commission (ONGC) had carried out detailed geological, geophysical surveys and drilled 9 shallow boreholes. The general stratigraphic succession established by the ONGC is presented in table 1.1. Geological set up of this region is shown in Fig. 1.3 a.

Cretaceous Sediments

The oldest sedimentary formations belong to Cretaceous period and are exposed in the Northwestern part of the region and North of River Gingee. The trend of these formations is NE-SW. Four stratigraphic units were identified namely the Ramanathapuram, Vanur, Ottai and Turuvai formation.

The *Ramanathapuram formation* representing the Lower Cretaceous age is not exposed anywhere. They were encountered only in boreholes drilled to the North of River Gingee and also between Rivers Pennaiyar and Gingee on the Western part of the region. At Ramanathapuram, they are unconformably overlain by younger Cuddalore formation, whereas in the rest of the area they are overlain by Vanur sandstones. They comprise alternate layers of grey sandstone and carbonaceous-clay stone with thin seams of lignite. The thickness of this formation ranges between 55 m - 250 m.

The *Vanur formation* represents the oldest unit of Upper Cretaceous formation. This formation comprises coarse-grained, friable, greyish white, pebbly sandstones, feldspethic at places with veins of Aragonite and with thin intercalations of dark grey to greenish grey shales. Garnet is the major heavy mineral.

Table 1. 1 Geological stratigraphy of the area (after ref. [51])

Era	**Period (approximate age in million years)**	**Formation**	**Lithology**
Quaternary	Recent (up to 0.01)	Alluvium	Sands, Clays, Silts, Kankar and gravels
		Laterite	laterite
Tertiary	Mio-Pliocene (1.8 to 23.8)	Cuddalore Sandstone	pebbly and gravelly and coarse grained sandstones with minor clays and siltstone
			with thin seams of lignite
unconformity			
	Paleocene (54.8 to 65)	Manaveli Claystone	Yellow and brown, grey calcareous siltstone and claystone and shale with thin
			bands of limestone
		Kadaperrikuppam limestone	yellowish and white to dirty white sandy, hard, fossilliferous limestone calcareous
			sandstone and clays
unconformity			
Mesozoic	Upper Cretaceous (65 to 99)	Turuvai limestone	Highly fossilliferous limestone, conglomerate at places, calcareous sandstone and clays
		Ottai Claystone	Greyish to green claystones, silts with thin bands of sandy limestone and
			fine grained calcareous sandstone
		Vanur Sandstone	quartzite sandstones, hard, coarse grained, occasionally feldspethic or calcareous with minor clays
	Lower Cretaceous (99 to 144)	Ramanathapuram Sandstone	black carbonaceous silty clays and fine to medium grained sands with bands of lignite and medium to coarse grained sandstones
unconformity			
Archean	Eastern ghat complex		Charnockite and biotite-hornblende gneiss

These are found exposed in the open well-sections at Vanur, Katterikuppam and Thailapuram. These sandstones are also encountered in the boreholes drilled to the North of River Gingee in the Eastern part of the study area between Rivers Pennaiyar and Gingee. The thickness of this formation is 152 m at Vanur, whereas it is only 52 m at Katterikuppam.

The *Ottai formation* consists of black to greenish grey clay stone with few bands of limestone and calcareous and micaceous silts and siltstones. These are exposed in comparatively larger area of the Cretaceous sediments covering part of Valudhavur, Ottai and Pulichappallam villages and North of River Gingee. The thickness of this formation is about 139 m at Karasur (just close to the outcrop), over 231 m at Lake Estate and about 88 m at Kalapet. This formation thins out towards Northeast at Auroville and Kalapet. The uppermost of the Upper Cretaceous formation known as *Turuvai limestone* is exposed as a narrow strip in NE-SW direction, extending from Mettuveli in the South to Apprempattu of Tamil Nadu in the North. The Turuvai formation consists of fossilliferous, cement grey limestone with few bands of sandstone. These are highly conglomeratic with pebbles of Quartz at places as seen in the dug well section at Royapudupakkam. This formation is encountered in the boreholes drilled at Karasur, Alankuppam and Koluvari.

Tertiary Sediments

The Tertiary formations are represented by the Kadaperrikuppam, Manaveli and Cuddalore formations. The *Kadaperrikuppam formation* is exposed near Pillaiyarkuppam, Sedarapet, Kadaperrikuppam and Alankuppam. These formations are predominantly calcareous sandstone, yellowish grey to dirty white in color with thin lenses of clay and shale and bands of shell limestone. The thickness of these formations varies widely which may be due to the unevenness of the Cretaceous basement. The *Manaveli formation* belongs to Upper Paleocene age. These formations comprise yellowish brown calcareous sandy clay and shale with thin shell and limestone bands. The upper contact with Cuddalore sandstone is unconformable and is marked by laterite. These formations occur in a small stretch covering the villages Manaveli, Thiruchitrambalam, Kottakkarai and east of Alankuppam. The *Cuddalore formation* is composed of thick succession of pebbly and gravelly, coarse-grained sandstones with minor clays, rarely with thin seams of lignite. Silicified wood has been noticed at places in the outcrops and well sections. In the Northwestern margin, the Cuddalore formation overlies the Ramanathapuram formation by completely concealing them and overlapping the Vanur sandstones. In the Northeastern portion they overlie the Manaveli formation. The thickness of these formations varies from 30 m to 130 m at outcrop area and maximum thickness of 450 m is observed at Manapet along the coast in the Southeastern side.

Quaternary sediments

The *Quaternary (Recent) formations* in the region are represented by laterites and alluvium. Laterite occurs as thin cap over the Cuddalore formations. Thick alluvial deposits are formed along the course of Rivers Pennaiyar and Gingee covering three-fourth of Pondicherry region. It occurs in the inter-stream area and also North of River Gingee extending from Pondicherry town to the West. The alluvium in the area is composed of sands, clays, silts, gravels and kankar. The thickness of alluvium varies from 10 m to 55 m with a maximum of 55 m at Sathamangalam.

1.9.3 Facies changes and structure

The various formations when followed down the dip direction are often difficult to identify based purely on lithological considerations. To obtain a comprehensive picture of the disposition of the various geological formations in the area, a panel diagram is prepared based on the data of selective boreholes drilled in the area [52]. The fence diagram is shown in Fig. 1.3.b. The Cretaceous and Tertiary formations exhibit wide variations both vertically and laterally. The Ramanathapuram and Vanur formations which are coarser and clastic in the Northwest, closer to the provenance becoming finer clastics and limestone bands in the down dip direction. The Kadaperrikuppam formation showed wide variation along the strike, even in the outcrop area.

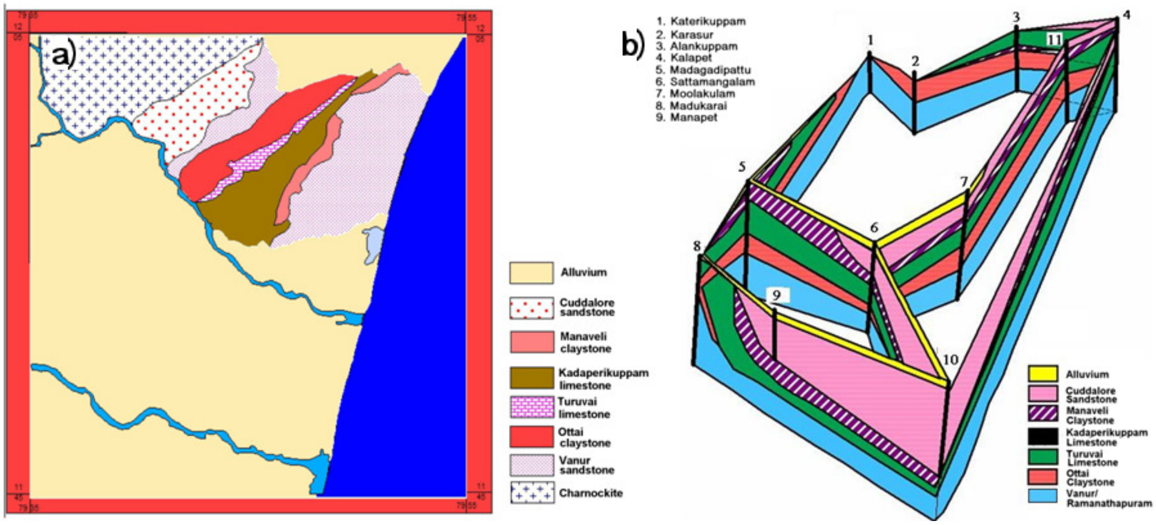

Fig. 1. 3 a) Geological map and b) Fence diagram of the study area

The general strike of the Cretaceous and Tertiary formations trends NE-SW with gentle dip. The abrupt termination of the outcrops of Cretaceous and Paleocene formations to the Northeast is rather remarkable. Further the boreholes in the Northeast of River Gingee encountered basement at shallow depth as in the boreholes at Karasur, Katterikkuppam and Alankuppam, whereas the boreholes drilled in the same strike direction to the Southwest at Madagadipet and Madukarai did not encounter the basement even at 600 m depth. The lateritised high ground bordering from the NNW of Muthirapalayam to West of Kanagachettikulam is due to fault [53]. The structural dislocation is inferred as the reason for the loss of circulation of mud in boreholes around Muthirapalayam and Gorimedu. A fault to the West of coast line indicated by a straight scarp running almost parallel to Pondicherry – Marakanam road is inferred.

1.9.4 Hydrogeology

Groundwater occurs in these sedimentary formations occurs in both confined and unconfined conditions and is being developed by means of dug wells, dug-cum-bore wells and tube wells.

Cretaceous aquifers

Among the various water bearing formations of Cretaceous age, the Ramanathapuram and Vanur formations form potential aquifers. They occur in the Northwestern part of Pondicherry region, and are encountered in boreholes drilled in the major part of the region. The aquifers of this formation include sands and calcareous sandstones. They are coarse grained in the Western part and graded finer facies towards East and Northeast. The thickness of these aquifers ranges between 38 m and 92 m. Groundwater occurs under confined conditions and the piezometric head at present is about 20 m to 60 m bgl. The depth of the tube wells tapping these aquifers ranges between 65 m in the NW and 300m in the NE of Pondicherry region. The yield of the tube wells tapping these aquifers ranges between 120 liters per minute (lpm) and 700 lpm. The investigation carried out reveals that the transmissivity value of these aquifers ranges between 92 m^2/day and 1925 m^2/day. The storage coefficient value ranges between 2.93×10^{-5} and 1.36×10^{-4}.

The water-bearing property of Ottai aquifers is chiefly dependent on the few bands of fine grained sandstone and limestone occurring locally at deeper depths and as a result, it yields meager to moderate quantity of water. The thickness of this aquifer varies from 42 m to 56 m and yield of the wells ranges between 120 lpm and 600 lpm with drawdown varying from 6.6 m to 25m.

Tertiary aquifers

The Manaveli formation of Paleocene is mainly an aquitard and the localized granular zones do not provide any appreciable yield. The aquifers of *Kadaperrikuppam formation* are constituted by fine-grained sandstones and give moderate to good yield. The thickness of aquifer ranges between 52 m and 90 m in the areas to South of River Gingee, whereas in the areas to the North of River Gingee, it is between 13 m and 37 m. Groundwater occurs under un-confined condition. The field permeability is 3 m/day in the areas to the South of River Gingee and 0.8 m/day towards North of River Gingee.

The *Cuddalore aquifers* comprising sandstones and gravels occupy an extensive area in the region and have a maximum thickness of 245 m in Southern part of the region. Groundwater occurs in this aquifer mainly under confined condition and is developed by means of tube wells ranging in depth between 27 m and 200 m bgl. The yield of the tube wells tapping this aquifer ranges between 200 lpm and 3000 lpm. The average transmissivity values of these aquifers are about 2000 m^2/day [52, 53].

Quaternary aquifer

Alluvial deposits occupy nearly 75 % of the study area. These aquifers form the most potential shallow aquifer system of the study area with thickness ranging between 5 m and 34 m. Groundwater occurs in this aquifer under un-confined to semi-confined condition. The depth of the tube wells tapping this aquifer ranges between 25 m and 50 m bgl. The average annual fluctuation is around 7.50 m. The transmissivity value of the aquifers in the West is 275 m^2/d at Madukarai and 770 m^2/d at Thirukanji in the East [52, 53].

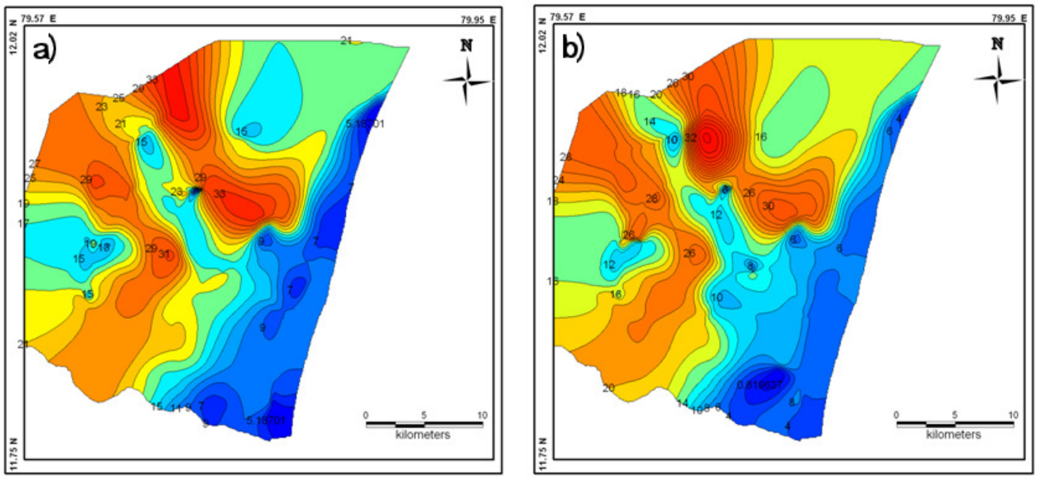

Fig.1. 4 Water table fluctuations a) pre-monsoon b) post-monsoon during 2008

1.9.5 Groundwater availability

The Pondicherry region is supposed to have plentiful water resources because of good rainfall received from both the Southwest and Northeast monsoons. It is also well watered by two Rivers, Gingee and Pennaiyar, which flow into the Bay of Bengal. There are also 84 tanks which have the considerable capacity to store water for irrigation. The utilizable groundwater resource (at 85% of the gross recharge potential) is assessed as 151 MCM. There are about 6500 tube wells in the Pondicherry region which extract water for agriculture, industrial, and domestic purposes (State Groundwater Unit of Agriculture Department, 1996).

The water level contour map prepared based on the water level data collected from various observatory tube wells in the study area during Pre-monsoon (Fig 1.4 a) shows that the water level ranges between 5.18 m bgl and 33 m bgl and deeper water levels are noticed in the Central, Northwest and Southwestern parts of the study area. Similar trend is also noticed during the Post-Monsoon (Fig 1.4 b).

1.10 Previous studies carried in the study area and adjoining regions

Groundwater contamination has been a serious problem in this region due to increasing population coupled with unplanned development, which led to the lowering of living standards (http://www.pon.nic.in). There are several reports on seawater intrusion and adverse impacts of anthropogenic activities in groundwater along the east coast of Pondicherry and Tamil Nadu. Groundwater contamination in coastal Chennai by anthropogenic activities (municipal and industrial activities) was reported during late nineties by Somasundaram et al., 1993 [54]. Contamination of coastal groundwater by upward leakage of highly mineralized water was reported in Kazhuveli basin by Nathalie Gassama et al., 2003 [55]. Several other studies also pointed out groundwater contamination in major aquifers of Southern India especially in coastal regions by various contaminants originating from irrigational practices and industrial effluents [56 - 58]. Studies also revealed presence of high levels of trace elements in groundwater [59 - 61], where the contamination was found to be local and sporadic due to diverse nature of source and biogeochemical processes occurring at local scales. Microbial contamination of groundwater was also noticed by many researchers in coastal aquifers of Tamil Nadu [62]. With continuing outbreaks of water-borne diseases in India [63, 64] and abroad [65, 66] assay of faecal contamination has become imperative for water supplying agencies so that the risk of water-borne diseases is minimized.

Not many studies were carried out with regard to environmental isotopes of groundwater in Pondicherry region. There were some studies on groundwater isotopic composition to evaluate the recharge conditions to the aquifer, palaeoclimatic conditions and assess seawater intrusion [67 - 72]. The isotopic study on South West Monsoon (SWM) was carried out by Chidambaram et al., 2010 [73] wherein the local meteoric water line for TN for SWM was established. However these studies did not furnish any information on the isotopic signatures of NEM which contributes to 60 - 75% of total rainfall in Pondicherry and coastal Tamil Nadu region. There was no systematic isotope study carried out on groundwater of Pondicherry region.

Geochemistry of sediments in this region was mostly concentrated on the surface or shallow sediments [74 - 76]. A study by Altrin et al., 2004 [74] pointed out that detrital sediments present in the limestone are derived from felsic sources in Miocene formations of Kudankulam area and deposited under oxygen-rich environment. Studies also reported that the sediments from Upper Cretaceous Sillakkudi formation and floodplains of Cauvery basin are of felsic origin [76, 77]. Influence of Deccan volcanism in the sedimentary rocks of Late Cretaceous period in Cauvery basin was inferred in studies by Madavaraju and Lee, 2010 [78]. Whilst there is abundant background information on the Cretaceous and Tertiary successions, which are mainly confined to biostratigraphy, there is only a limited on the sedimentary successions in Pondicherry region.

There are many reports on As occurrence in water as well as sediments in many parts of India [79 – 81]. Despite the large amount of information on As geochemistry in groundwater and sediments, to the best of our knowledge there is no data on the As occurrence and distribution in sedimentary formations of South India. Data characterizing deeper aquifer materials are particularly sparse, and little work has been done on the Cretaceous sedimentary deposits which are used extensively in many parts of the Southern India due to their capacity to yield good quality groundwater and provide a reliable source of drinking water in coastal communities. The presence of elevated levels of As in these formations may present a serious consequence to a huge population dependent on these aquifers for drinking water supplies.

Very few studies were carried out on colloid/particle distribution in surface/groundwater in Indian context. Distribution of Pb and As in the bed sediments as particulates from Ganges, Brahmaputra, Krishna, Godavari and Cauvery was studied by Subramanian et al., 1987 [82] which concluded that Pb in the particulate is about 5-40 times abundant compared to bed load. The fine silt-clay fraction (< 20 µm) tend to have higher Pb and As relative to sand-silt fraction (20-100 µm). Size fractionation of transition metals in seawater was studied by Singhal et al., 2006 [83] wherein it was found that iron is associated with smaller particles while reverse trend is noted in the case of other transition elements (Zn, Cu, Ni and Mn). Along the coast of Tamil

Nadu, the Pb, Cd and Hg were found to be high and associated with particulate matter [84, 85]. Enrichment of total trace metals in bulk sediments of coastal Nagapattinam region in relation to sediment texture, carbonates and organic carbon was reported [86]. This study concluded that the sediments are mostly sandy silt inorganic carbonates and trace elements (Fe and Mn) are concentrated in the finer particles and organic carbon fraction that was derived from river inputs. Recent studies near Kalpakkam site also reported colloidal concentrations up to 6 mg/L in the groundwater [87].

Despite a number of scientific researches in this region, groundwater evolution in different sedimentary formations, possible controls on geochemistry, flow paths and dynamics are not fully understood. This could be attributed to dependency on single techniques and lack of combination of multiple techniques. An approach is used here that combines different techniques to provide a comprehensive understanding on the groundwater characteristics in different zones of sedimentary formations of Pondicherry region and also understand the role of groundwater particles in trace metal migration. The techniques employed are;

- Hydrochemistry and isotope hydrology to understand the groundwater characteristics and dynamics
- Geochemical modeling and statistical analysis to assess driving factors affecting groundwater quality and to estimate the mole transfer values for common minerals
- Sediment geochemistry to identify source rock
- Characterization of groundwater particles to assess trace metal migration in aquifers

1.11 Objectives of the thesis

The main objectives are;

i. Assessment of groundwater quality and its suitability to potable and irrigational purposes
ii. Understanding the processes and identification of sources affecting the groundwater characteristics
iii. Identification of source rock, weathering and deposition conditions of sediments
iv. Study on role of groundwater particles in trace metal migration

1.12 Thesis outline

The remainder of the thesis is organized as follows. Chapter 2 deals with protocols adopted for sampling and analyses of groundwater, sediment and particles. In addition, optimization of the analytical method for the determination of trace levels of arsenite in groundwater is also included. Basic groundwater quality in different aquifers of this region is presented in chapter 3, with special emphasis on suitability to drinking and irrigational purposes. The spatial distribution of major ions is examined using contour maps indicate that there is no increase in Na^+ and Cl^- ion towards coast, but an increase is noted in these ions in Southern part of the study area indicating contribution from backwater. In addition, microbial contamination is also studied and it is observed that half of the groundwater samples showed presence of faecal contamination.

Chapter 4 discusses the major, minor chemical species and environmental isotopes results obtained for groundwater for understanding the geochemical processes taking place in subsurface. Characteristic ionic ratios indicate that ion exchange and weathering of carbonate rocks as dominant processes in Quaternary aquifer, whereas in Tertiary aquifers silicate and carbonate weathering is noticed and in Cretaceous aquifer ion exchange and leaching of clay minerals are found to be dominant. Geochemical modeling and statistical techniques also confirm above findings. Model output showed presence of undissociated species for alkaline earth metals up to 30%. It also indicates that high strontium concentration in final waters is due to incongruent dissolution of Aragonite. A few groundwater samples showed marginally high As (10 to 40 ppb), the probable mechanism seems to be reductive dissolution of iron oxyhydroxide, which is supported by low DO and low sulfate concentrations in groundwater as well as H_2S odor at the sampling sites. Microbial analysis showed the presence of SRB in groundwater, which also confirms reducing condition of the aquifer.

Environmental isotope results indicate that the recharge for Quaternary aquifer is mostly from evaporated surface water bodies while Tertiary and Cretaceous aquifers receive contribution from precipitation without significant evaporation. Mineralization of the groundwater in different aquifers is discerned using chloride and isotope covariations. $\delta^{13}C$ isotope data also suggests contribution of root zone CO_2 and dissolution of carbonate minerals. Environmental tritium indicates that most of the groundwater is modern excepting a few deep samples from Tertiary and Cretaceous aquifers.

Chapter 5 presents the vertical distribution of different ions and highlights the importance of rare earth element trends in deciphering deposition and weathering condition of the formation. Source rock is identified using ionic ratios and found to be in line with the findings obtained in nearby areas of similar geology. Arsenic distribution and its correlation with other elements are elaborated in this chapter. Chapter 6 focuses on the chemistry of groundwater particles collected from selected wells. Particle number density and loads in groundwater are determined. Elemental and morphological features indicate contribution of clay minerals and iron oxides. Preferential association of Sr^{2+} to colloidal over particulate matter as compared to Ca^{2+} is observed. From modeling results it can be deduced that Sr^{2+} is associated as sorbed ion on clay minerals.

CHAPTER – 2
METHODOLOGY

This chapter deals with the strategy adopted to address the stated objectives for which three components are studied viz., groundwater, sediment and particles. Different sampling techniques are employed for collecting representative groundwater samples, sediments from deep geological formations and particle from groundwater. The samples are characterized using multiple analytical techniques.

2.1 Groundwater characterization

2.1.1 Sampling

Water samples are mainly collected from major water bearing formations of this region, namely, Quaternary aquifer (Alluvium), Tertiary aquifer (Cuddalore sandstone) and Cretaceous aquifer (Vanur sandstone). The sampling is done during post-monsoon season (February 2009) but a few samples are also collected during pre-monsoon season (June 2008). A total of 41 samples are collected during post-monsoon and 9 samples during pre-monsoon period from municipal supply wells, private domestic and irrigation wells and hand pumps. Sample site coordinates and altitudes are determined in the field using the Differential Global Positioning System. The geographical coordinates, location name, aquifer and well depth are listed in Table (appendix 2.1). The sample location map is shown in Fig. 2.1.

Samples collected are filtered using 0.45 µm pore size membrane filters and stored in polyethylene bottles that were initially washed with concentrated HNO_3 and rinsed with distilled water. A duplicate set is collected and acidified to $pH < 2$ by adding ultra pure concentrated HNO_3 for cation and trace metal determinations.

Rainwater: Ten precipitation samples were collected during North East Monsoon from different locations along the coast from Pondicherry to Nagapattinam in order to characterize the rain water isotopically. Rainwater was allowed to fall in a bucket that was left out for the duration of the rain event and sampled in a 100 mL bottle. Samples belonging to a single month were mixed to get monthly integrated precipitation sample.

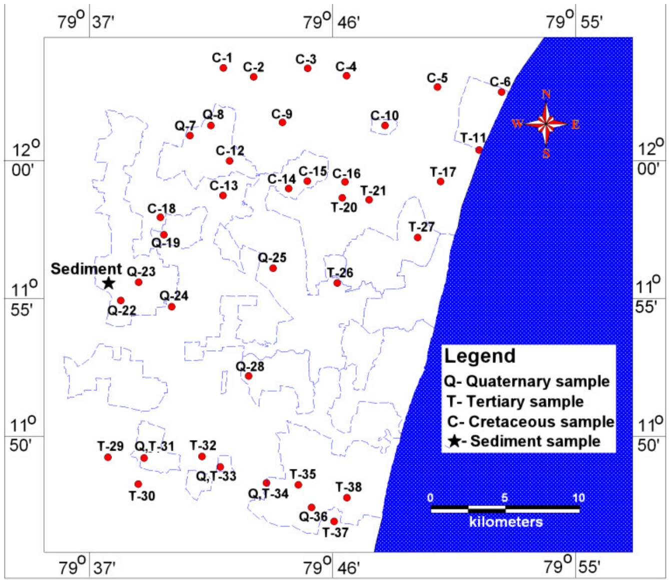

Fig. 2.1 Sample location map for groundwater and sediment

2.1.2 Analytical techniques

In situ analysis

Physical parameters like temperature, pH and DO are measured in situ using portable pH/Temp – DO meter (Corning, model 313) with a precision of 0.02 units and 0.1% for pH and DO respectively. Electrical conductivity is measured using conductivity meter (Orion model 130) with a precision of ±0.5%. Alkalinity (mg $CaCO_3$/L) is measured in the field by titration method, in which, 10 mL of the water sample is titrated using 0.02N H_2SO_4 and a mixed indicator is used to check the end point. Since the grounder pH is normally found between 6.5 and 8, the

Plate 2. 1 Ion chromatography system (DX-500)

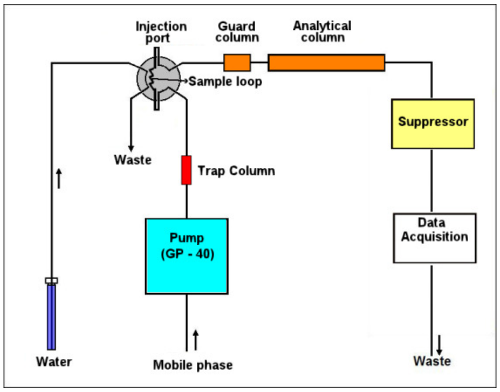

Fig. 2. 2 Schematic map of ion chromatography setup

bicarbonate content of the water is calculated from alkalinity value. The data is presented in table (appendix 2.1).

Chemical species

Depending on the element of interest and matrix present multiple techniques are needed for quantification. Most of the chemical measurements were done using Ion Chromatograph shown in Plate 2.1.

In this technique ions are separated on an ion exchange column (stationary phase) by eluting with a suitable buffer solution (mobile phase). The ions are identified based on their retention time in the chromatogram which is governed by the interaction of ion with column material. For ion detection, conductivity detector is used after suppressing the background conductivity of mobile phase. A schematic diagram is shown in Fig. 2.2. Sample volume of 25 µL is used for injection. Calibration and quantification is done using PeakNet Software and the measurement precision is better than 5%. Internal standard checks were inserted into the sample sequence after every fifth sample for quality control.

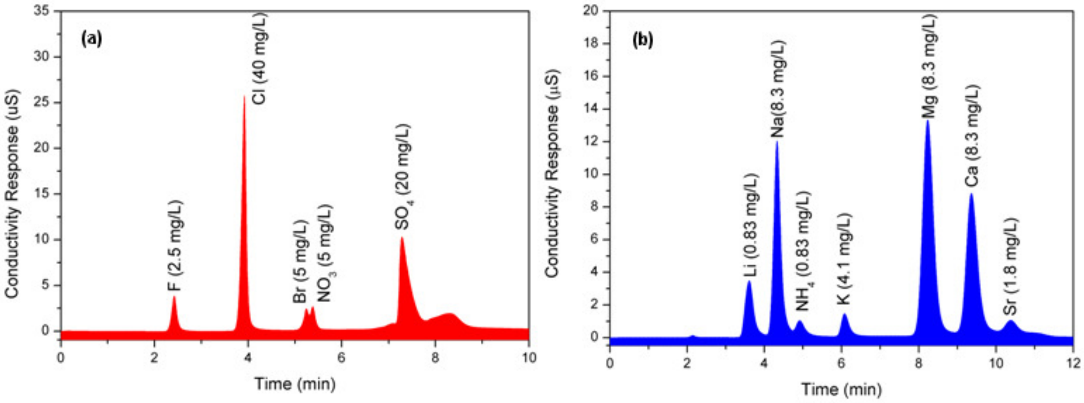

Fig. 2. 3 Chromatograms of (a) anions and (b) cations

For anions (F^-, Cl^-, Br^-, NO_3^-, SO_4^{2-} and PO_4^{3-}), AS-11 column coupled with AG-11 guard column is used for separation. This column consists of macroporous copolymer of divinylbenzene and ethylvinyl benzene which is functionalized with very low hydrophobic quaternary ammonium group. NaOH solution is used as mobile phase in gradient mode (5 - 35 mN). For suppression of mobile phase conductivity, Anion Self Regenerating Suppressor (ASRS-II ultra) is used in external water mode operation. The background conductivity is usually better than 1 µS/cm. A typical chromatogram of anions is shown in Fig. 2.3 a.

For cations (Li^+, Na^+, NH_4^+, K^+, Mg^{2+}, Ca^{2+} and Sr^{2+}) CS-12A column coupled with CG-12A is used for separation. This column consists of macroporous copolymer of divinylbenzene and ethylvinyl benzene which is functionalized with medium to low hydrophobic carboxylic/phosphonic acid group. 21mN H_2SO_4 solution is used as mobile phase in isocratic mode. For suppression of mobile phase conductivity, Cation Self Regenerating Suppressor (CSRS-II ultra) is used in external water mode operation. The background conductivity is usually better than 1 µS/cm. A typical chromatogram of cations is shown in Fig. 2.3 b.

Elements such as Si, Al, Fe, Mn, Zn, Ba, Cu and Ni are determined using Inductively Coupled Plasma-Optical Emission Spectroscopy (JY 2000) whereas As is determined using Inductively Coupled Plasma Mass Spectrometer (Model VG PQ ExCell, VG Elemental, UK). A few samples are rechecked for As using HG-AAS. Boron analysis is done by measuring the absorbance of boron-curcumin complex by spectrophotometer [88]. The typical analytical precision for trace element determination is 10%.

For total organic carbon (TOC) measurements samples are acidified with HCl to pH 3 immediately upon collection and stored at 4°C in the dark until analysis. The measurements are performed with a SGE TOC analyzer (ANATOC II series). This is a closed loop technique that employs the principle of photo catalytic oxidation process occurring at room temperature in near UV region at 400 nm using atmospheric oxygen. The carbon dioxide thus formed is measured by non-dispersive infrared detection. The precision and the detection limit of the measurement are 2% and 0.025 mg/L respectively.

Overall accuracy of the chemical data is generally checked by charge balance error (CBE), which is expressed as,

$$\text{CBE (\%)} = \frac{\text{meq}(\text{cations}) - \text{meq}(\text{anions})}{\text{meq}(\text{cations}) + \text{meq}(\text{anions})} \times 100 \qquad (2.1)$$

The major, minor and trace ion chemical data along with CBE has been given in Tables (appendix 2.2 and 2.3). The CBE of the chemical data was within ±5%, which is acceptable for meaningful interpretation of geochemical processes [89].

Arsenite determination

A few groundwater samples showed the presence of arsenic up to 40 µg/L. In order to determine the arsenite (As^{3+}) which is more toxic than arsenate (As^{5+}) an electrochemical method, Anodic Stripping Differential Pulse Voltammetry (ASDPV), is optimized. This method is first used by Andrew et al., 2005 [90], but it suffers from poor sensitivity. In this work deposition potential and its duration, preconditioning potential and its duration are optimized for achieving a better sensitivity.

Voltametric measurements are carried out using electrochemical analyzer (CH instruments). A three electrode cell setup at room temperature is used for conducting experiments. The solutions are purged with high pure nitrogen gas before each measurement. A silver electrode of surface area 0.0315 cm^2 is used for the experiments. The counter and reference electrodes are platinum wire and Ag-AgCl respectively. The electrode is renewed by polishing with 0.05 µm alumina paste on soft lapping pads.

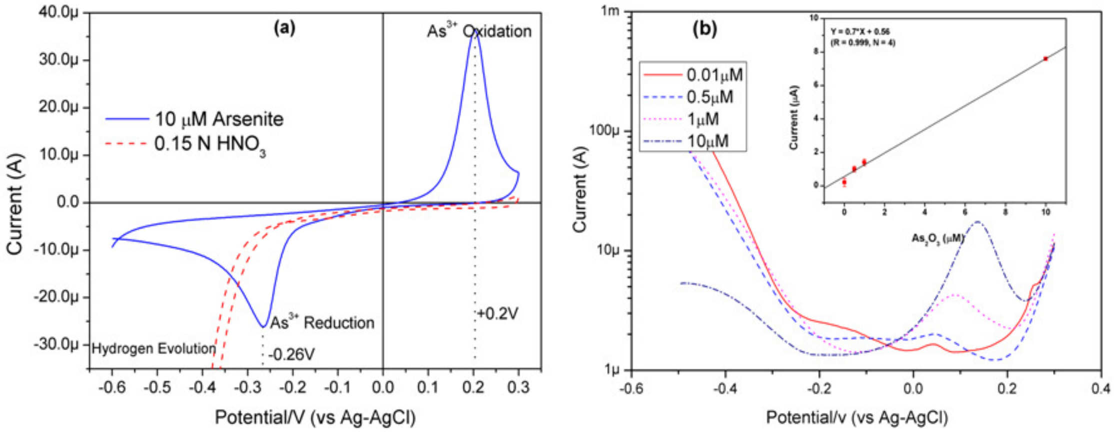

Fig. 2. 4 (a) Cyclic Voltagram of Arsenite (10µM) and blank (0.15N HNO3), (b) Working range of the method and calibration plot (inset)

The cyclic voltagram (Fig. 2.4 a) shows the performance of silver electrode in 0.15 N HNO_3 solution containing 10 µM arsenite standard solution. It is found that As (III) reduction peak is at - 0.26 V and stripping peak at + 0.2 V. Silver oxidation occurs above + 0.4 V so the scan is halted at + 0.3 V. The deposition potential is varied from 0 to -1 V using standard conditions of 10 µM arsenite solution in 0.15 N HNO_3 and it is found that at a potential of -0.6 V arsenic deposition is maximum, low deposition at more negative potentials (below - 0.7 V) can be attributed to hydrogen evolution. With the optimized conditions (appendix 2.4), ASDPV is carried out varying the deposition time from 30 to 300 sec, which indicated only a marginal increase in current after 180 seconds. Therefore in further experiments deposition period is set at 180 seconds. The limit of detection is found out by standard addition method. From ten additions of 0.1 µM arsenite solution a limit of detection is found to be 5 nM (1.5 µg/L) and the precision of the method is found to be 8.4 % at 10 µM arsenite. The linear working range is found to be from 10 nM to 10 µM (3 to 3000 µg/L) with a linear regression of 0.999 (Fig 2.4 b). The measured values for As^{3+} and As^{5+} are given in Table (appendix 2.5).

Microbiological parameters

The water sample for microbiological analyses is collected in a sterile glass bottle, kept in airtight ice-cold containers and transported to laboratory within 6-8 hrs of their collection for the further processing. For determination of reducing bacteria, sample bottles are flushed with nitrogen and sealed using Teflon to prevent contact with atmospheric oxygen.

Total viable bacteria detection

The enumeration of microbial populations is accomplished by using Total Viable Count (TVC) method [91]. TVC was performed on nutrient agar media by means of spread plate method. Dilution of the sample is made in the order of 10^{-3} and 10^{-4} using sterile saline, and one milliliter of diluted sample is transferred in petriplates containing molten agar medium (45°C). The plates were incubated at 37°C for 24 hrs to obtain viable colonies. Each test is duplicated and comparable results are averaged, to reduce any errors related to measurement. The viable colonies are counted and converted to represent as colony forming units per mL (cfu/mL). Bacterial colonies are shown in Plate 2.2 a.

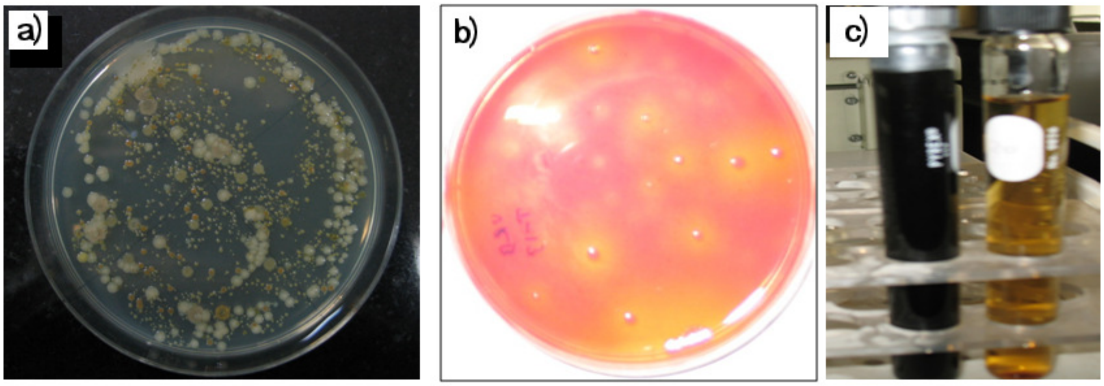

Plate 2. 2 (a) bacterial colonies, (b) E.coli colonies and (c) SRB presence indicated by black color of FeS

Escherichia coli detection

A medium containing violet red bile agar (VRBA) is used to detect the coliforms in which one ml aliquot of sample is transferred on VRBA by pour plate method and incubated at 35°C for 24 hrs.

The positive colonies (purple red colonies with diameter 0.5mm or more) are counted and expressed as cfu / 100 mL. The presence of E. coli is also confirmed by Indole test. E. coli colonies (pink color) are shown in Plate 2.2 b.

SRB detection and Enumeration

Sulfate reducing bacteria are grown in long necked bottles with the medium composition of tryptone (30 g), sodium sulfate (5 g), sodium sulfite (5 g) and ferric citrate (2 g) in one liter distilled water [92]. The growth of a sulfate reducer is recognized by the appearance of the black color of ferrous sulfide (Plate 2.2 c).

Medium used for the growth of SRB is prepared with the following composition (g/L): Yeast Extract (1), Ascorbic acid (1), $MgSO_4$ (0.2), K_2HPO_4 (0.01), Ferrous Ammonium Sulfate (0.1), NaCl (10), Agar-agar (25), Sodium Lactate (4 ml). The pH of the medium was maintained at 7.0 by 1 N NaOH. The above medium is autoclaved at 15 lbs for 15 min. The medium is cooled to 40°C and the samples were diluted ten times. Pour plate method is employed and the plates are allowed to solidify. Once the medium is set, the plates are stacked in an anaerobic jar and the jar is subjected to vacuum to remove the residual oxygen (-15 lbs). The jar is then filled with a mixture of gases (10% CO_2, 5% O_2 and 85% N_2) till the gauge read zero. The jar is incubated at 37°C for 5 days. Black colonies displaying sulfur reduction are further sub cultured on the medium mentioned above in slants and incubated in a similar manner. Plates where the count is prevalent but did not exhibit any black colonies are not considered. The microbial data is presented in appendix 2.2.

Environmental isotopes

For environmental isotopes deuterium (δ^2H) and oxygen-18 ($\delta^{18}O$) analyses, water samples are collected in a 60 mL capacity polyethylene bottles after pumping out the stagnant water, in order to get representative samples. The sample bottles are filled completely and preserved airtight in order to avoid evaporation. Deuterium and oxygen-18 are measured by mass spectrometer (Geo 20-20, Europa) using gas equilibration method [93] with a precision of ± 0.5 ‰ and ± 0.1 ‰ (2σ criterion) respectively. Stable isotope results are expressed with respect to VSMOW (Vienna Standard Mean Ocean Water) in δ units (‰), where

$$\delta^2\text{H or }\delta^{18}\text{O}(‰) = \frac{\text{Rsample} - \text{Rstandard}}{\text{Rstandard}} \times 10^3 \qquad (2.2)$$

Carbon stable isotope (^{13}C) analysis was performed on CO_2 samples generated by converting dissolved inorganic carbon to CO_2 through acid hydrolysis with phosphoric acid. Carbon isotope ($\delta^{13}C$) values are reported in permil (‰) notation against VPDB. Na_2CO_3 salt calibrated against Vienna Pee Dee Belemnite (VPDB) standard is used for calibration. Measurement precision is ± 0.30 ‰ (2σ precision). Plate 2.3 shows the mass spectrometer (Geo 20-20, Europa) used in this study.

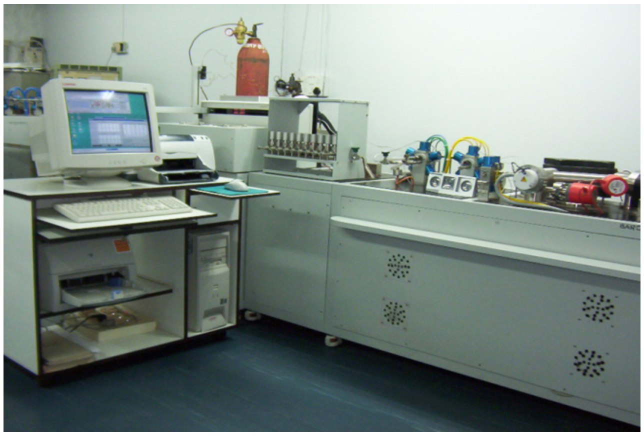

Plate 2. 3 Isotope Ratio Mass Spectrometer (GEO 20 20)

Tritium analyses were performed using a Quantulus 1220 spectrophotometer in low level counting laboratory [94]. As some degree of enrichment is essential to obtain measurable count rate for the natural tritium, electrolytic enrichment is used. For this, 250 g of distilled water sample is transferred into cell comprising mild steel perforated cathodes and stainless steel anode and 0.5 g of Na_2O_2 is added. The electrolysis is expressed by following equation.

$$2\ Na_2O_2 + 2\ H_2O \rightarrow 4\ NaOH + O_2 \qquad (2.3)$$

These cells containing spike, distilled tap water and samples are put into freezer unit. Constant current is passed continuously through DC power supply and ampere-hour meter to the cells, which are connected in series. Temperature of the cells is maintained at $5 \pm 2^{o}C$ throughout the electrolysis which takes about a week. Electrolyzed samples are alkaline in nature due to use of alkali electrolyte. Therefore lead chloride is added to for neutralization and then samples are distilled and counted.

Suitable scintillator is mixed with processed water samples in high density polythene vial and counted in low level liquid scintillation counter. Results are reported in Tritium Units (TU) and the detection limit is 0.5 TU. The isotope data for groundwater and precipitation is given in appendix 2.6. Pre-monsoon chemical and isotope data is given in appendix 2.7.

2.1.3 Geochemical Modeling

A code Net geochemical Pathways (NETPATH) developed by Plummer et al., 1994 [95] is used in this work to model mass-balance changes in chemical composition of groundwater along flow paths from an initial well/recharging well to a final well/discharging well. This geochemical mass-balance reaction consists of the masses of plausible minerals and gases that must enter or leave the initial water along the flow path to produce the composition of the selected set of a chemical and isotopic observation in the final water. Every possible mass-balance reaction is examined between two waters of single hydrologic flow regime for a set of chemical and isotopic parameters and a set of feasible minerals or gases. The calculations are useful in deducing geochemical reactions, mixing ratios, concentration or dilution of waters and mineral mass transfers.

Essential files in NETPATH

This modeling software uses two basic codes which were initially developed using FORTRAN: DB.WIN and NETPATH.WIN. Data input for a set of water analysis is given using DB.WIN, which is processed for activity coefficients, ionic strengths and mineral saturation indices using WATEQ, WATEQF and WATEQ4F programs [96, 97]. NETPATH.WIN allows the input data to be used to create mass-balance models between waters of same flow path. In order to derive suitable models, phases, elements, isotopes and processes needs to be specified. This file can be modified to limit number of models. Isotope computations can be carried out by initializing Rayleigh calculation in model data option. Choosing NETPATH.WIN executes the code and displays model output.

Terminology in NETPATH

Constraint: A constraint is typically a chemical element, or redox state (summation of operational valencies of the constraints) or a particular isotope of an element. A constraint is included in the model to constrain the masses of selected phases (minerals and gases) that can enter or leave the aqueous solution. The constraints selected for the model will determine the number and types of phases that need to be selected to solve the modeling problem.

Phase: A phase is any mineral or gas that can enter or leave the aqueous solution along the evolutionary path. Selected phases should be known to occur in the system. Some of the phases only be precipitated or dissolved, but not both along the flow path. NETPATH allows phases to be marked as precipitation or dissolution only, this helps in limiting the model outputs.

Model: A model is defined according to the masses (per kilogram H_2O) of minerals and gases that must enter or leave the initial water solution to produce the composition observed in the final solution. A model is a subset of the selected phases (and the computed mass transfer) that satisfies all the selected constraints. The model is of the form,

$$\text{Initial water + Reactant Phases} \rightarrow \text{Final water + Product Phases} \tag{2.4}$$

2.1.4 Statistical Methods - Factor analysis

Multivariate analyses are widely applied mainly to spatial data in geochemistry, hydrochemistry, mineralogy and other fields [98, 99]. The use of these methods to water quality monitoring and assessment has increased in the last decade, mainly due to the need to obtain appreciable data reduction for analysis and decision [100]. Multivariate treatment of environmental data is also useful for evidencing temporal and spatial variations caused by natural and human factors linked to seasonality. In this work, factor analysis is applied to decipher the hidden correlations between various hydrochemical parameters so that the source or process responsible could be identified.

Factor analysis is a very powerful technique applied to reduce the dimensionality of a data set consisting of a large number of inter-related variables [101]. This reduction is achieved by transforming the data set into a new set of variables, the principal components (PCs), which are orthogonal (non-correlated) and are arranged in decreasing order of importance. Mathematically, the PCs are computed from covariance or other cross-product matrix, which describes the dispersion of the multiple measured parameters to obtain eigen values and eigen vectors. Varimax rotation distributes the PC loadings such that their dispersion is maximized by minimizing the number of large and small coefficients (Richman, 1986). Besides considerable data reduction, entire data set variability is described through few varimax rotated factors without losing much information. Each factor signifies a particular geochemical process or source.

2.2 Sediment Characterization

Depth-wise sediment samples are collected from Andiarpalayam located west of Pondicherry at 11°55′30″N latitude and 79°37′14″E longitude. This site is characterized by flat peneplain physiographically with an average elevation of 15 m above mean sea level. Location of the site is shown in Fig. 2.1.

2.2.1 Sampling

Sediment samples representing various formations of this region are collected during construction of the bore hole. Samples are immediately sealed in polythene bags and numbered in the field. Later the sediments are dried in an oven at 60°C and ground to fine powder for mineralogical and chemical assay. Representative samples are chosen based on their in situ nature of the sediment and local subsurface geology for further analysis.

2.2.2 Analytical techniques

Chemical analysis

About 50 mg of the sediment samples is sealed doubly in aluminum foil and irradiated in D8 position at Apsara reactor under a neutron flux of 10^{13} cm^{-1} s^{-1} for 6 hrs. A total of fifteen elements (As, Fe, Na, K, Ca, Co, Sc, Cr, Zn, Hf, Th, U, La, Ce, Eu, Yb and Lu) are determined. Certified Reference Materials Sl-1 and 7 are used as standards. After appropriate cooling time gamma-ray measurements are performed using Ge detector coupled with a computer assisted multichannel analyzer. The details of target nuclei, gamma energies are given in appendix 2.8. The deviations of the measured values for different elements in CRM Sl-7 are given in appendix 2.9. In this study calcium is determined based on gamma ray activity of ^{47}Sc which is produced by ^{46}Ca (n, γ; β^-) ^{47}Sc, because of comparable half lives (^{47}Ca and ^{47}Sc have 4.54 and 3.34 days respectively). The decay correction is made based on Mitsuru and Tsutomu, 1996 [102]. Results are given in appendix 2.10.

Total organic carbon (TOC) is measured using wet digestion with concentrated sulfuric acid and titrating against ferrous ammonium sulfate (Walkey and Black, 1934). The minimum detection limit was 0.005 %. Total carbon (TC) and sulphur measurements are done using elemental analyzer (Leco CS6). Total inorganic carbon (TIC) is taken as the difference between TC and TOC. The analytical results are given in appendix 2.10.

Mineralogical and morphological analysis

The X-ray diffraction analyses (XRD) of the powdered sediment samples were performed using Philips PW-1820 diffractometer equipped with a diffracted beam monochromator and multi channel detector. The analysis conditions were as follows: CuKα radiation, 40kV, 30mA, step scanning at 0.02° /250s in the range of 3-70° 2θ. The qualitative analysis was done by PCPDF and XTAL software. For TXRF measurements, an ITAL Structures TXRF spectrometer TX 2000 equipped with a Si (Li) detector was used.

For morphological studies freshly cut grain surfaces are examined under environmental scanning electron microscopy (FEI Quanta 200) equipped with an energy dispersive spectrometer (EDS).

Carbon-13 determination

For environmental carbon-13 isotope measurement, 2 gms of dried sediment is acidified with concentrated H_3PO_4 and the generated CO_2 gas was fed into mass analyzer. Rest of the analysis is explained in section 2.1.2. Results are given in appendix 2.10.

2.3 Particle characterization

2.3.1 Sampling

The particle concentration is a function of the history of the aquifer prior to sampling as the newly constructed wells may demonstrate different nature of particles compared to that of naturally occurring ones due to filling material or drilling induced turbidity or colloid formation by metal casings [104]. Therefore in this study wells are chosen in such that the wells are 2 - 10 years old and PVC is used as the casing material (mild steel casing wells are discarded during sampling for particles) so that formation of drilling induced turbidity and colloidal formation by the casing can be avoided. Each well is purged in case of unused well and sample is collected after achieving a stable temperature reading to get a representative sample and avoid artifacts due to initial turbulence and stored water. Depth of the wells is also taken into account for sample collection, so that comparisons can be made between shallow younger water and deeper older water.

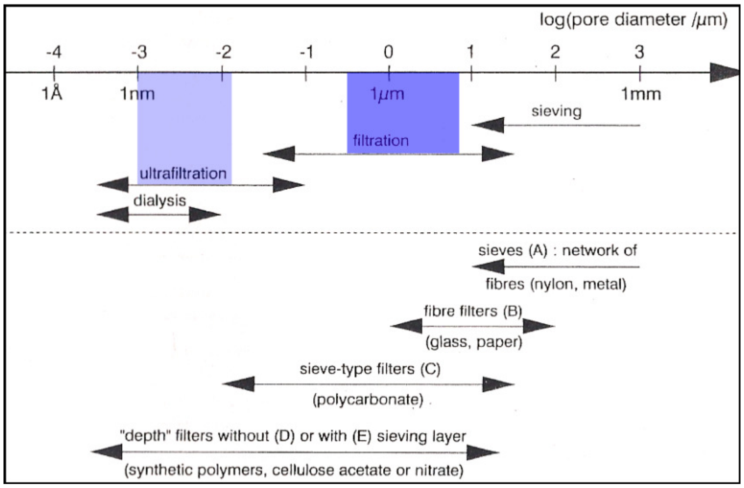

Fig. 2. 5 Nature of filters used for different particle size ranges (adopted from ref 178), boxes represent particle size ranges studied in this work

Although a large number of techniques can be used for particle size measurements, only a few categories of techniques can be used to separate particles in groundwater with minimum perturbation. These are primarily; i) sieving, ii) filtration, iii) ultrafiltration and iv) dialysis. The various techniques differ from each other by the size range of particles they can separate, the nature of filters used and experimental conditions (Fig. 2.5). Re-suspension of colloids after stoppage of rotor limits the applicability in the case of ultracentrifugation, whereas sieving is most suitable for larger particles. Dialysis is currently used for preconditioning colloids from surface water and it is necessary to consider large water samples up to 5000 litre which is difficult to apply in situ. In this work, sequential filtration and ultra filtration are used to separate the particles in the range 0.45 to 8μm and 1-14nm respectively (studied particle size ranges are shown by boxes in Fig. 2.5).

Sequential filtration

For separating the particles from 0.45 μm - 8 μm, online filtration unit was fabricated in house using polypropylene tube. The design of the filtration assembly and photograph of complete filtration set up are shown in plate 2.4 (a & b). Particulate matter is separated using different pore size filter circles (8, 5, 3, 1.2, 0.8, 0.45, 0.22, 0.10 μm) by passing the groundwater through the filtration unit. Filter circles used were of 47 mm diameter and made up of cellulose nitrate and cellulose acetate composition (Sartorius make). The filter circles were soaked in Milli-Q water over night prior to application. Before filtering the groundwater, the filtration unit is conditioned by passing 500 mL of Milli-Q water. Then groundwater is allowed to pass through the filters with the help of peristaltic pump with constant RPM to get a flow rate of about 100 mL/min. Once the flow reduces to half of the initial value (~50 mL/min) the filtration is stopped and Milli-Q water of about 100 mL is allowed to pass through the unit. This procedure allows washing the filters and avoids salt preparation in the last step when drying the filter circles. After stopping the pump, the filter circles are quickly removed and placed into a clean and dry polyethylene bags. The filters are subsequently dried under IR lamp and weighed.

Weighing the filters accurately in normal microbalance is very difficult as the moisture in air causes errors in the order of milligrams whereas the particle loads on the filter circles are in the order of hundreds of micrograms to a few milligrams. Therefore a different instrument is employed in this study to weigh the microgram levels of particle loads on the filter circles without being affected by the moisture. The initial and final weights of the filter circles are taken on infra red moisture determination balance (FD-720). The temperature is set at 60°C to attain a constant weight of the filter circle so that variations due to moisture are nullified. The minimum amount that can be weighed using this balance is 10 µg. The photographs of the filter circles after filtration are shown in plate 2.4c.

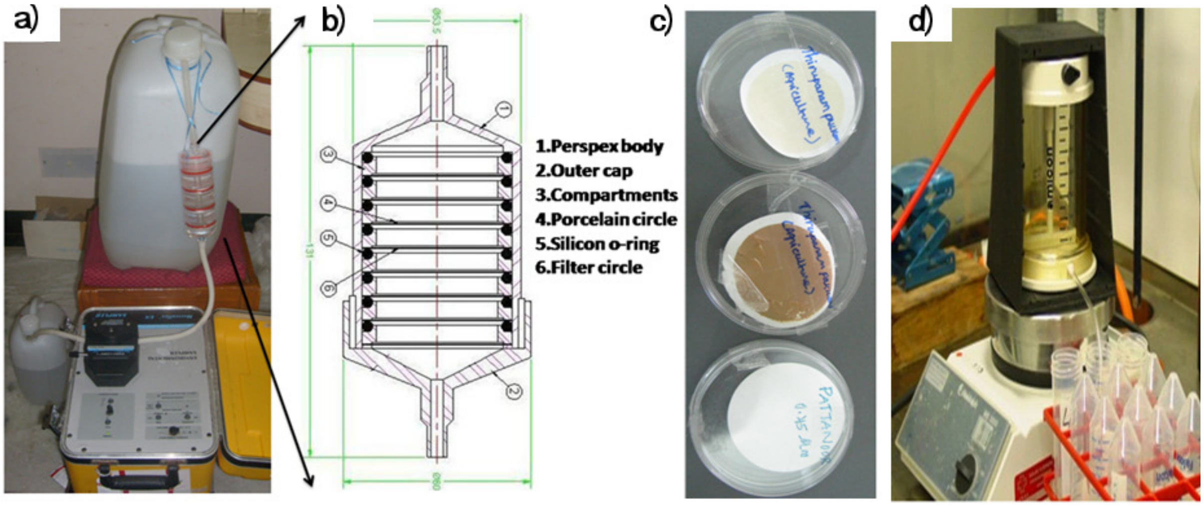

Plate 2. 4 a) sequential filtration set up, b) diagram of filter unit, c)exposed filter circles and d) ultrafiltration set up

Ultrafiltration

In groundwater abundance of finer particles (colloids) is generally very low therefore separation of colloids from water is needed. For separating the colloidal fractions, ultrafiltration is applied. The water sample obtained from filtration through 0.45 µm is passed through the ultra-filtration membrane of cellulose acetate by using stirred ultrafiltration cells (Model 8200, Millipore), set up is shown in plate 2.4 c. The cell is used in concentration operation mode wherein argon gas is applied with pressure (0.5 kg/cm^2) directly to the ultra-filtration cell. Colloids above the membrane molecular weight cut-off are retained in the cell while water and solute below the cut-off pass through the filter and drain out of the cell. The filtrate is again loaded in to the cell with a lower cut-off membrane and this sequence of steps is repeated for all the filter membranes. The characteristics of filtering membranes are given in appendix 2.11. Constant stirring above the membrane surface is used to avoid the accumulation of solute molecules at the membrane surface in an attempt to minimize localized concentration effects. Before using, the membranes were soaked in 0.1 M nitric acid for one day and then in distilled water for 3 days. Before loading the sample, 500 mL of deionised water is passed through these membranes and this solution is used for blank sample preparation. During each filtration, about 10 mL of a sample is removed at the final stage of filtration from the stirred cell. After the completion of each stage of filtration, the membranes are washed with 20 mL of 0.1 M HNO_3 and mixed with that stage solution and the necessary dilution corrections are applied.

2.3.2 Analytical techniques

Particle concentration (number) is estimated by multifunctional particle counting system for liquids. Morphological characterization of the particles is done by SEM, ESEM-EDS. Elemental determination is carried out using EDXRF and chemical analysis of ultrafiltration aliquots (for colloids) and acid leached fractions (for particles). Zeta potential is also determined to evaluate the stability of the colloids.

Particle size distribution (PSD)

In this study, non-perturbing particle size measurement was carried out by single particle counter (SPC) in the range 1 – 100 µm. The instrument multifunctional particle counting system for liquids (PAMAS3108FM) consists of a high sensitive liquid in situ monitor (HCB-LD – 15/25) which measures colloids in the range 1 – 100 µm up to 32 free adjustable size channels and coupled with PMA software for displaying averaged data. The maximum particle concentration that can be measured with this equipment is 200,000 p/mL at 10 mL/min flow rate. This instrument works based on the principle of light scattering by single particles [106]. The sample has to be diluted before being measured in order to ensure that only one particle crosses the laser beam at a time. Error in number particle concentration is < 5 %.

PSD is measured in the collected groundwater samples along with pre-filtered Milli Q water (0.22 µm). The obtained data is background subtracted to get the actual particle counts in the water samples. All the samples showed particle counts much less than the maximum allowed levels of the equipment, therefore no sample dilution is carried out. Data is given in appendix 2.12.

Morphological and elemental studies

Classical bulk techniques used for mineralogical determination, such as X-ray diffraction [107] or infrared methods have severe limitations when applied to particles. However, electronic microscopy techniques are better suited to the characterization of the particulate and colloidal fractions in natural water provided that a well adopted sample preparation method is used [108]. In this work, most of the samples are studied by Environmental Scanning Electron Microscopy (ESEM FEI Quanta 200) for morphological features as there is no need for modifying the filter surfaces for conduction, however a few selected samples are characterized by Scanning Electron Microscopy (SEM Vega TESCAN) coupled with energy dispersive spectroscopy (EDS) after the filter circles are coated with gold under vacuum vaporizer. In addition, the elemental identification for the particles deposited on the filter circles is also done using EDXRF (Jordan Valley Make). In addition to EDS and EDXRF, Neutron Activation Analysis is also performed on one set of filter circles for understanding behavior of elemental concentrations with respect to particle sizes (appendix 2.13).

Zeta potential

Zeta potential measurements are carried out for the colloidal fractions by zeta analyzer (Malvern, Zetasizer Nano ZS). Samples were taken in a clear disposable zeta cell and measurements are carried out in triplicate. The instrument calculates the electrophoretic mobility of the particle and converts it to zeta potential using the Smoluchowski equation. The Smoluchowski equation (Eq. 2.4) gives the direct relationship between zeta potential and electrophoretic mobility.

$$\zeta = 4\,\pi\,\eta\,\mu\,/\varepsilon \qquad (2.4)$$

where μ is electrophoretic mobility, η is viscosity of the suspending liquid in centipoise, ε is the dielectric constant, and ζ is the zeta potential in mV. A few selected samples are measured for zeta potential.

Chemical analysis

The major and trace ion concentration of the colloidal and particle fractions is determined by ion-chromatography (DX-500) and Graphite Furnace Atomic Absorption Spectrometry (GFAAS). In the case of particles, the filter circles are leached using 0.1N HNO_3 in three steps each step containing 5 mL of the acid for 24 hrs, an unused filter is also treated in the same way for blank correction. The final dilution is made to 20 mL. For colloidal fractions, the separated fractions are measured without any modification. Rest of the analysis is same as explained in the case of groundwater analysis (section 2.1.2).

CHAPTER - 3
ASSESSMENT OF GROUNDWATER QUALITY

3.1 Introduction

Study of quantity of water alone is not sufficient to solve water management problems because their use for various purposes mainly depends on the quality of water. Groundwater is utilized significantly to meet the water demands not only for agriculture sector but also for industrial and domestic sectors in this region. The average population density in Pondicherry region is about 6.8 times higher than the national average (Dept. Statistics and Economics, Govt. Pondicherry, 2010). Despite several laws and regulations endorsed by agencies like Pollution Control Board, Central & State Groundwater Boards, several municipal agencies, sewer outflows and discharge of the partially treated and untreated wastes from septic systems and storm water runoffs from urban and rural areas are still major sources of pollution for drinking water in this region.

In order to comprehend the current water quality situation in this region, physicochemical, chemical and microbial parameters data is used to i) evaluate the distribution of physico-chemical, major, minor and trace elements in groundwater from major water bearing zones, ii) assess the suitability to drinking and irrigational purposes and iii) assess microbial contamination. Potability of the groundwater is checked based on parameters such as major ions, common inorganic contaminants and microbial contamination, while EC (electrical conductivity), sodium percent (Na%), residual sodium carbonate (RSC), sodium absorption ratio (SAR) and TH (total harness) are used for assessing irrigational suitability of groundwater. Bureau of Indian Standards and World Health Organization prescribed values are taken as reference for checking drinking water. Classifications based on Wilcox, Richard and USSL were adopted for verifying irrigational suitability.

3.2 Physico-chemical parameters and organic carbon

Temperature is extremely important as it governs biological activity, the rate of chemical reactions and the solubility of gases [109]. In the study area the temperature of groundwater varies from 29.3°C to 32.9°C (Table 3.1) and no systematic spatial trend is observed (appendix 2.1). Natural uncontaminated groundwater shows pH values in the range of 6.0 - 9.0 [110] and it is influenced by carbon dioxide input from the atmosphere, microbial activity and plant photosynthesis. The pH observed in groundwater of this area range from 5.8 to 8.8 (Table 3.1). Higher pH of 8.8 is observed in two samples, which are collected from shallow wells with a depth of about 15 m bgl, this could be due to man-made activities (untreated industrial effluents). In contrast, a few deep-zone samples showed slightly acidic nature (pH 6.0 – 6.5) possibly resulted from subsurface chemical processes like oxidation of sulfide minerals or biological processes. Electrical conductivity is one of the important indices of water quality, which gives the measure of the dissolved salts and salinity. High EC of the water samples reflects leaching or dissolution of the aquifer material or mixing of saline water [89]. The groundwater samples of this region have EC values ranging between 256 and 2194 µS/cm and are mostly fresh in quality (Table 3.1).

Table 3.1 Summary of Physical and Chemical data

Parameter	Minimum	Maximum	Parameter	Minimum	Maximum
Temp (°C)	29.3	32.9	**Li^+**	0.01	0.05
pH	5.82	8.83	**Sr^{2+}**	0.08	3.8
DO	1	6.9	**Al^{3+}**	0.01	0.26
Cl^-	15.9	550	**B**	0.02	0.54
NO_3^-	0.01	35	**TOC**	0.146	3.243
SO_4^{2-}	3.81	570	**Fe(total)**	0.008	0.059
HCO_3^-	73.2	664.9	**As (total)**	0.0005	0.0419
Na^+	10.7	275	**Mn^{2+}**	0.001	0.1027
K^+	0.6	12.8	**Zn^{2+}**	0.0082	0.18
Mg^{2+}	7.8	72.6	**Ba^{2+}**	0.0162	0.5148
Ca^{2+}	8.4	264	**Cu^{2+}**	0.002	0.0287
Si	8.48	58.82	**Ni^{2+}**	0.0025	0.0519
F^-	0.02	1.62	**TDS**	164	1404
Br^-	0.11	1.3	**TVB (cfu/mL)**	1800	33000
PO_4^{3-}	0.06	1	**E. coli (cfu/100 mL)**	5	300
			SRB (cfu/mL)	250	3100

All concentrations in ppm otherwise given in parenthesis

The dissolved oxygen concentration of water in equilibrium with air at 25°C at 1 atm. is 8.3 ppm [111]. In uncontaminated surface water and freshly recharged groundwater the DO values are close to 8.3 ppm. However lot of biological and inorganic processes taking place in the subsurface may consume dissolved oxygen and deplete the DO levels in deep horizons. The water samples collected in the study area have DO values between 1 and 6 ppm (Table 3.1). It is observed that even shallow wells which are supposed to be in equilibrium with atmosphere contain DO levels between 3 and 6 ppm. This lowering of DO can be attributed to the presence of ferruginous / lateritic soil in this region. Oxygen is consumed during the conversion of ferrous to ferric ion in soil zone and the equilibrium reaction can be shown as;

$$Fe^{2+} + \frac{1}{2} O_2 + H^+ \leftrightarrow Fe^{3+} + \frac{1}{2}H_2O \qquad (3.1)$$

Most of the deep wells showed depleted DO levels that can be attributed to biological or/and inorganic processes. As per the classification given by Tyson and Pearson, 1991 [112], most of the groundwater tapping deep zones with DO levels close to 2.0 ppm can be considered to be under sub-oxic condition. Although H_2S gas odor is very prominently felt during the field sampling, none of the samples showed complete depletion of DO (i.e. DO = 0 ppm). This might be mostly due to the air leakage during sampling. The spatial distribution of DO values represents high levels in Northern and Southwestern regions, which reduces towards the Central and Eastern parts (Fig. 3.1 a). This trend indicates preferential groundwater recharge from Northern, Southwestern and Western parts and DO gets consumed subsequently during the course of groundwater flow.

Organic carbon is generally used as an indicator of susceptibility of groundwater for bacterial contamination, since it serves as a nutrient source for microbes. Organic substances dissolved in groundwater originate either from active soil zone or from aquifer material and lead to growth of fungi and algae, which is not desired for groundwater used for drinking purposes. These substances include humic acids, hydrocarbons, fatty acids, etc. The dissolved organic matter is also contributed by anthropogenic sources such as petroleum products or industrial wastes. The groundwater mostly from shallow depths shows TOC between 0.1 and 3.2 ppm (Table 3.1). The low amount indicates consumption of the organic carbon by microbial processes. Contour map of TOC shows higher concentration close to urban areas (Fig. 3.1 b).

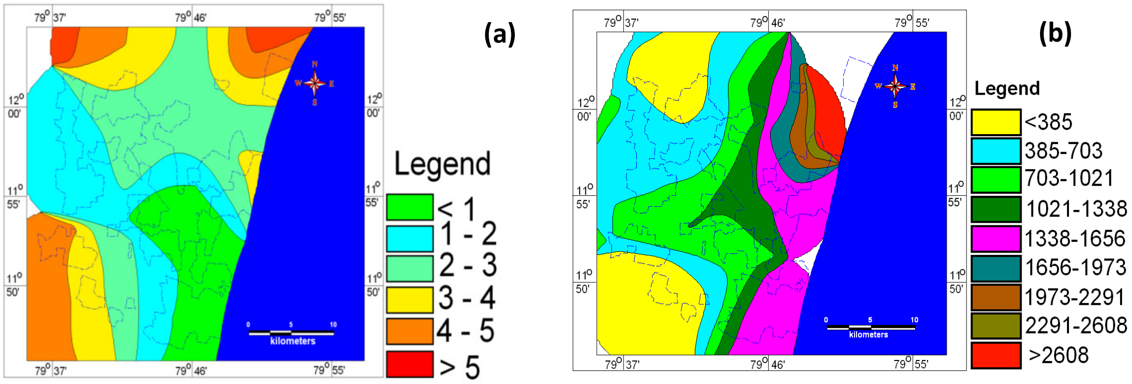

Fig. 3. 1 Contour diagram of a) DO (ppm) and b) TOC (ppb)

3.3 Major chemical species

Sodium (Na^+) is one of the most commonly found cation in water. Hydrochemical alteration of rock materials, ion exchange processes, sewage contamination and infiltration from agricultural runoff and mining activities render groundwater with high sodium concentration. Repeated use of water in irrigated areas also contributes high sodium concentration in groundwater. In the study area, the sodium concentration in groundwater ranges from 10.7 - 275 ppm (Table 3.1). The sodium content in groundwater of this region has been mapped on Fig. 3.2 a. High levels are noticed in Southeastern part of the study area, which could be due to contribution from backwaters. The region North of River Gingee show low levels of sodium in groundwater, which is possibly due to limited availability of sodium rich minerals. Potassium (K^+) is an essential nutrient but if ingested in excess may behave as a laxative. Orthoclase, microcline and clay minerals are the chief sources for this element. Potassium concentration in groundwater of this region varies from 0.6 to 12.8 ppm (Table 3.1). Unlike sodium, potassium exhibits opposite trend (Fig. 3.2 b), high levels in North of river Gingee and low in Southern parts of the study area. The high concentrations can probably be explained by dissolution of potash feldspars and/or contribution from fertilizers.

Calcium (Ca^{2+}) is another abundant cation in natural water which is mainly contributed by carbonate (Calcite and Dolomite) and plagioclase minerals. Calcium concentration in groundwater of this region ranges from 8.4 - 264 ppm (Table 3.1). Groundwater rich in carbon dioxide dissolves carbonate minerals easily leading to increased Ca^{2+} concentration. Similarly weathering of silicates is also enhanced in presence of dissolved CO_2.

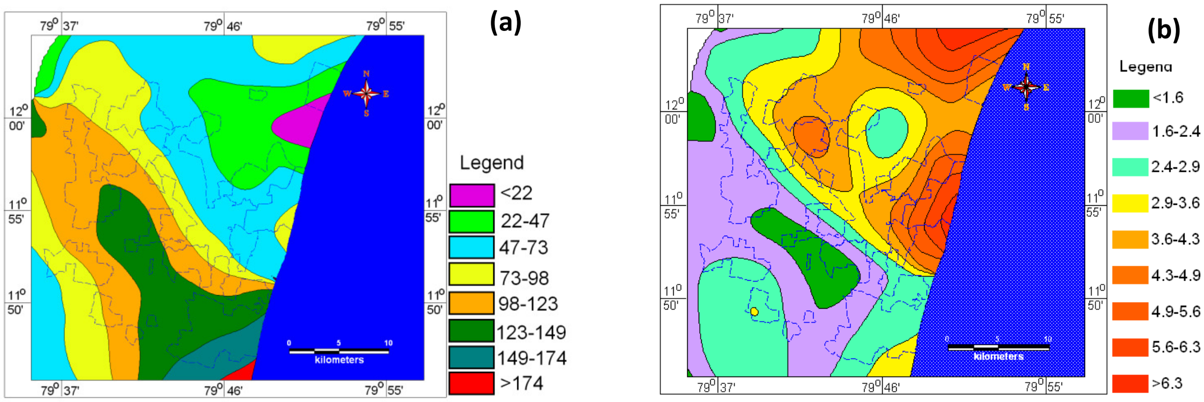

Fig. 3. 2 Contour diagrams of a) Na^+ and b) K^+ concentrations in groundwater (ppm)

A common calcium silicate mineral weathering can be shown as follows;

$$CaAl_2Si_2O_8 + 3\ H_2O + 2\ CO_2 \leftrightarrow Al_2Si_2O_5(OH)_4 + Ca^{2+} + 2HCO_3^- \tag{3.2}$$

The calcium concentration in groundwater has been mapped on Fig. 3.3 a, which indicates that high levels of Ca^{2+} are found in North central parts of the study area and shows a decreasing trend along the groundwater flow. The decrease in Ca^{2+} can be attributed to ion exchange or Calcite precipitation. These geochemical processes are discussed in detailed in Chapter 4. Magnesium (Mg^{2+}) is essential as an activator of many enzyme systems but it is cathartic and diuretic. The source of Mg^{2+} is mainly Mg-calcite, dolomitic rocks and sulphate minerals. Some silicate minerals also contribute to Mg^{2+} in groundwater. The concentration of Mg^{2+} in groundwater of this region varies from 7.8 to 72.6 ppm (Table 3.1). High level of Mg^{2+} is found in the Northern part which reduces towards Eastern direction (Fig. 3.3 b).

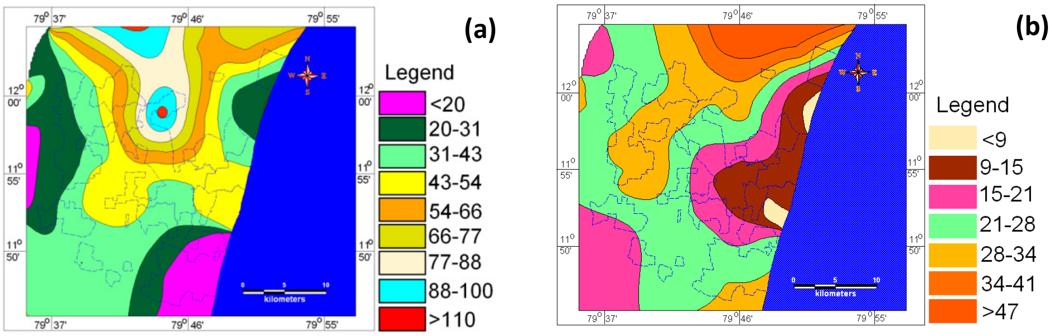

Fig. 3. 3 Contour diagrams of a) Ca^{2+} and b) Mg^{2+} concentrations (ppm) in groundwater

The presence of bicarbonate (HCO_3^-) is mostly responsible for alkalinity of groundwater. The HCO_3^- content in groundwater ranges from 73 – 665 ppm (Table 3.1). Bicarbonate in groundwater generally decreases from West to East (Fig. 3.4 a) which is very similar to Ca^{2+}

variations. The predominance of Ca^{2+} and HCO_3^- ions in groundwater suggest that bicarbonate is largely due to Calcite/Dolomite dissolution.

$$Ca\ (Mg)\ CO_3 + H_2O + CO_2 \leftrightarrow Ca\ (Mg) + HCO_3^- \tag{3.3}$$

Chloride is the one of the main anions present in natural waters. The processes responsible for chloride in groundwater are erosion and weathering of crystalline rocks. High concentrations of chloride in natural water may result from contamination by sewage, seawater and saline residues in the soil [9]. In study area chloride in groundwater ranges from 16 - 550 ppm (Table 3.1) and chloride content above 500 ppm is observed in only one sample. Because of the easy solubility of most chloride salts, chloride content in groundwater increases as water moves through the flow system. The chloride content in groundwater in this region has been mapped on Fig. 3.4 b. From the map it can be seen that concentration of chloride in most of the region is generally unchanged, but a small pocket of high Cl^- level is noticed in Southeastern part which is very similar to Na^+ variation. This could be due to backwater contribution. Similarly a low Cl^- pocket is noted near coast (also in the case of Na^+ contour), which could be due to presence of sand dune.

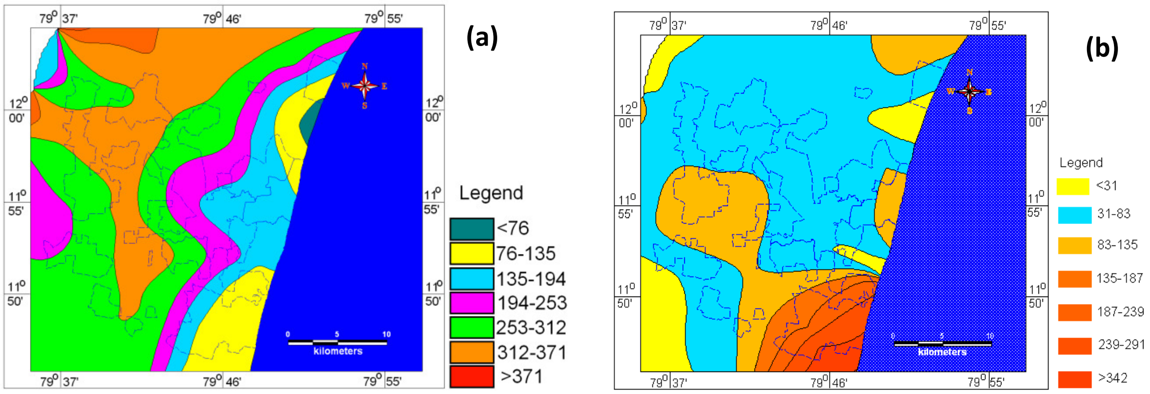

Fig. 3. 4 Contour diagrams of a) HCO_3^- and b) Cl^- in groundwater (in ppm)

Dissolved sulphate (SO_4^{2-}) is derived from the dissolution of Gypsum or the oxidation of sulphide minerals such as Pyrite. Wastes resulting from domestic activities, feedlots and agricultural runoff (fertilizers) add excess sulphate to groundwater. Sulphate concentration in study area ranges from 3.8 - 576 ppm (Table 3.1) and most of the samples show sulphate concentration < 200 ppm. The sulfate content in water has been mapped on Fig. 3.5 a. The map shows that concentration of sulfate is high in North central part of the study area, which is very similar to

Ca^{2+} profile, and decreases South wards. The high value of Ca^{2+} and SO_4^{2-} noted in North central region indicate presence of Gypseous rocks in subsurface.

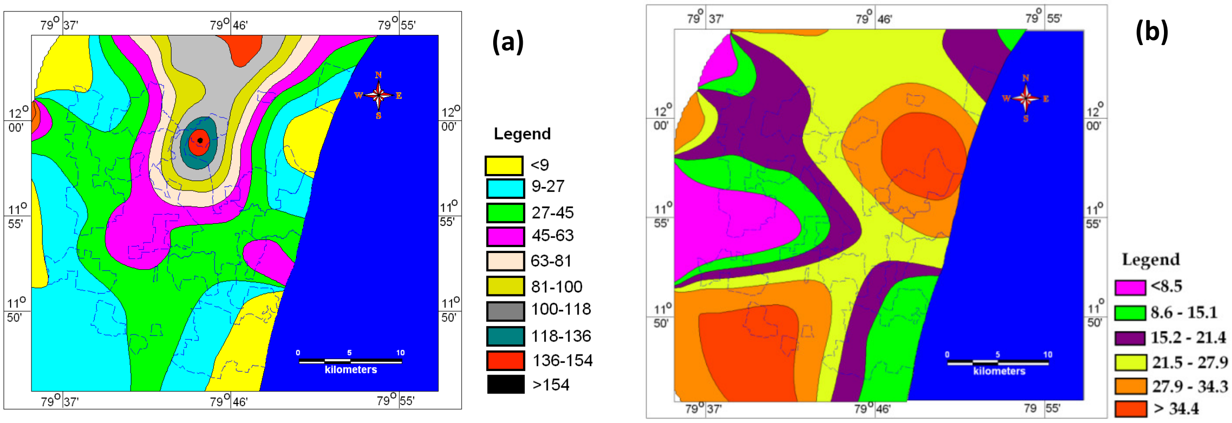

Fig. 3. 5 Contour diagrams of a) SO_4^{2-} and b) SiO_2 in groundwater (in ppm)

Silicon is one of the most abundant elements in igneous and some sedimentary rocks, commonly combined with oxygen in the form of silicates. The amount of silica in groundwater is governed by abundance of Chalcedony or amorphous SiO_2 or Cristobalite. The silica content in groundwater in Pondicherry region has been mapped on Fig. 3.5 b. The map shows that concentration of silica generally increases from highlands toward the coastal regions in the northern parts. Some exceptions to this general trend are seen in Southern parts of River Gingee, where it is high in the central part and reduces towards coast. This can be due to dilution by the greater volume of vertical leakage that has lower silica content.

3.4 Minor and trace elements

Fluoride contamination is widespread in India and recorded in 17 states. Generally fluoride concentration in surface and groundwater sources is low, therefore it is sometimes added to drinking water to help prevent tooth decay in children. High fluoride concentration in groundwater beyond the permissible limit of 1.5 ppm is one of the most worrying toxicological problems that India is facing [113, 114]. Due to its strong electronegativity, F^- is attracted by positively charged calcium ions in teeth and bones, and hence excessive intake can results in pathological changes in teeth and bones. In the present study, the fluoride concentration in groundwater is found to vary from BDL to 1.6 ppm (Table 3.1) and no cases of fluorosis have been reported in the habitants in this region.

Nitrate (NO_3^-) is considered to be the most widespread contaminant in groundwater in India. Decaying organic matter, wastes generated from domestic and agricultural activities are major sources of nitrate in groundwater [115]. The nitrate concentration in groundwater of this area ranges from 0.01 - 35 ppm (Table 3.1). Bromide and phosphate are also found in few groundwater samples and range from 0.11 to 1.3 ppm and 0.06 to 0.1 ppm respectively (Table 3.1). Bromide mainly contributed by marine or organic sources whereas phosphate is derived from fertilizers. There is no clear trend observed in spatial or vertical distribution of these elements. Boron is noticed in most of the groundwater and it varies from 0.03 to 0.56 ppm (Table 3.1). Industrial waste and marine deposits are the main sources for boron in this area.

Table 3.2 Percentage of the water samples suitable for drinking purposes

Water quality parameter	WHO (1993)		BIS (1991)		% samples exceeding WHO (1993)	% samples exceeding IS (1991)	Undesirable effect produced beyond the MPL
	DL	MPL	DL	MPL			
TDS	500	1500	500	2000	Nil	Nil	Taste, gastrointestinal irritation
pH	6.5-8.5		6.5-8.5		20	20	Taste effects, mucus membrane and water supply system
TH	100	500	300	600	7	7	Encrustation in water supply and adverse effect on domestic use
Ca	75	200	75	200	2	2	
Mg	50	150	30	100	Nil	Nil	
Na		200		200	12	12	
K		12			2	Nil	
AS	0.01		0.05		12.5l	Nil	
F	1.5		1.0	1.5	2.5	2.5	Skeletal and dental fluorosis
NO_3	45		45	45	Nil	Nil	Blue-baby syndrome in infants
Cl	200	600	250	1000	Nil	Nil	salty taste indicates pollution
SO_4	200	400	200	400*	2	2	cause gastrointestinal irritation

Units in mg/L, except pH; * up to 400 mg/L if Mg^{2+} concentration doesn't exceed 30 mg/L; DL – desirable limits; MPL – maximum permissible limits

Strontium is found commonly in the groundwater with a concentration range from 0.08 to 3.8 ppm (Table 3.1). In most sedimentary aquifers, the strontium levels are primarily controlled by the reaction of groundwater with carbonate or sulphate minerals present. A marked enrichment of strontium is observed in this groundwater. Dissolution of minerals like Aragonite or Gypsum, or evaporite deposits or mixing of meteoric water with the interstitial water (pore water) are the main sources of strontium. An excess in Sr^{2+} concentration in groundwater can be attributed to recrystallisation of Aragonite, this aspect is discussed in chapter 4.

Iron concentrations are generally low in groundwater of this region varying from 8 to 59 µg/L (Table 3.1). Low concentration of iron in groundwater could be due to oxidation and subsequent precipitation of iron in recharge areas. This observation is further verified by low DO values in shallow zone (section 3.2). Relatively higher iron concentrations are noted in deeper formations which could be due to the weathering of iron-bearing minerals. Other trace elements found in groundwater include Mn^{2+}, Zn^{2+}, Ba^{2+}, Al^{3+}, Cu^{2+}, Ni^{2+} and As. The ranges of these metals are given in Table 3.1. Among these elements, Ba^{2+} is found to be abundant probably due to its association with alkaline earth elements. Arsenic in groundwater is mostly found to be within 10 ppb, but marginally higher values up to 42 ppb are also encountered in a few groundwater samples. The probable As release mechanism is discussed in chapter 4.

3.5 Suitability to drinking purposes

The analytical results have been examined for their suitability to drinking purpose based on World Health Organization [116] and Bureau of Indian Standards [117]. The permissible limits as per WHO and BIS, percentage of outliers and undesirable effects produced beyond permissible levels are given in Table 3.2. Chemical and microbial quality aspects are discussed in the following sections.

3.5.1 Chemical quality

Measurement of conductivity is often used as an indirect method of estimating the dissolved solids content of a solution. In the present study TDS was calculated as follows [118];

$$TDS = 0.64 \times EC \tag{3.4}$$

where units for TDS and EC are ppm and µS/cm respectively. Calculated TDS in groundwater of this region ranges between 164 and 1404 ppm and falls within the drinking water limits set by BIS [117]. Two deep well samples (depths 90 &185 m bgl) and one shallow well sample (depth 20 m bgl) showed TDS values more than 1000 ppm. This might be due to leaching of salts from the formation in the case of deep wells and influence of backwaters in the shallow well. Classification of groundwater based on TDS [119] is presented in Table 3.3. As per this classification, 29% of the samples are desirable, 61% of samples are permissible and rest is unfit for drinking purpose.

Potability of water also depends on its hardness expressed as TH (total hardness), which is caused by dissolved salts of calcium, magnesium or iron and expressed as ppm of $CaCO_3$. The total hardness is determined by the following equation [120];

$$TH = 2.497 \times Ca^{2+} + 4.115 \times Mg^{2+} \quad (3.5)$$

where Mg^{2+} and Ca^{2+} concentrations are expressed in equivalents per million and TH in ppm of $CaCO_3$. In the study area the TH levels measured in groundwater samples are in the range of 78 – 701 ppm. Water classification based on TH [121] is given in Table 3.3. About 15% of the samples fall in moderately hard and hard types where as remaining 70% samples fall under very hard type of water. pH values prescribed for potable water should range between 6.5 and 8.5 [117] and most of the samples (80%) fall in this range (Table 3.3). About 12% of the samples show sodium and arsenic higher than permissible limits. No permissible limits are suggested for K^+ in groundwater by BIS [117], however WHO prescribes levels up to 12 ppm and 2% of the samples fall above this value. None of the samples show contamination by nitrate and fluoride.

Table 3.3 Classification of groundwater based on TDS and hardness

TDS	Water Classification	% Samples	Total Hardness (as $CaCO_3$ as mg/L)	Water Classification	% Samples
up to 500	Desirable for drinking	29	<60	Soft	nil
500-1000	Permissible for drinking	61	60-120	Moderately hard	14
1000-3000	Useful for irrigation	10	120-180	Hard	15
> 3000	Unfit for irrigation and drinking	nil	>180	very hard	71

3.5.2 Microbial quality

Microbial assay of groundwater in this region demonstrates a wide variety of micro-organisms. Identification of the colonies is carried out based on their culture characteristics and microscopic observations. Five to ten different species of bacterial communities with different morphology are observed. Total viable bacteria (TVC) are found in the range of 1.8×10^3 to 3.3×10^4 cfu/mL (appendix 2.2). Presence of E.coli in groundwater is an indication of contamination from sewage. According to the WHO guidelines for drinking water quality, there should be no fecal coliforms present in 100 mL of water. Based on this criterion, half of the groundwater samples measured can be considered unfit for drinking. A few samples show higher values (between 100 and 300 cfu/100 mL), which are considered to be severely contaminated. The presence of E. coli can be attributed to pollution sources such as waste dumps and sewage and it is observed that more E. coli contamination is found more frequently in rural areas, which can be mainly attributed to unlined sewages and open pits for municipal dumping. The anaerobic bacteria, sulfate reducing bacteria (SRB), are also found in a few locations in deeper formations where DO levels are very low (< 1 ppm). Presence of SRB is indicative of reducing condition of the aquifer. The correlations of E. coli and SRB with other parameters and the inferences are discussed in chapter 4.

3.6 Suitability to irrigation

Irrigation suitability of groundwater is mainly evaluated based on EC, SAR, RSC, Na %, USSL classification and Wilcox diagram. According to Richards, [122] the irrigation water is classified into four groups based on EC as given in Table 3.4. High EC in water leads to formation of saline soil. It can be found that none of the samples fall in either excellent category or unfit category. About 27% of the samples fall in good category and remaining 73% in permissible category.

The irrigation water containing high proportions of sodium will increase the exchange of sodium content of the soil, affecting the soil permeability and the texture which makes the soil hard to plough and unsuitable for seedling emergence [123]. The sodium/alkali hazard is typically expressed as sodium adsorption ratio. This index quantifies the proportion of Na^+ to Ca^{2+} and Mg^{2+} in a given water sample. When the concentration of Na^+ is high in irrigation water, it tends to be absorbed by clay particles displacing to Ca^{2+} and Mg^{2+}. This exchange process of Na^+ in water for Ca^{2+} and Mg^{2+} in soil reduces the permeability and eventually results in soil with poor internal drainage [124]. The SAR values for each water sample are calculated by using following equation [122];

$$SAR = \frac{Na^+}{\sqrt{\frac{Ca^{+2} + Mg^{+2}}{2}}} \tag{3.6}$$

where the concentrations are reported in equivalents per million. SAR value of groundwater in the study area varies from 0.43 to 6.9 and all samples fall in low sodium hazard class (Table 3.4).

In addition to SAR, Na % is also a common parameter for assessing suitability of water for agricultural purpose [125]. Sodium in presence of inorganic carbon (HCO_3^- and CO_3^{2-}) forms alkaline soils while it combines with chloride to form saline soils. Both these soils are not favorable for plant growth. Na % in epm (milliequivalents per litre) can be calculated using following equation;

$$Na\% = \frac{(Na^+ + K^+) \times 100}{Ca^{2+} + Mg^{2+} + Na^+ + K^+} \tag{3.7}$$

A maximum allowed Na% in groundwater used for agricultural purpose is 60 % [126]. Na % in groundwater of this study area ranges from 11.6 to 73.3 %. It is found that most of the samples fall in excellent to permissible class and only about 20 % samples are found to be unsuitable (Table 3.4). Presence of high Na % in water along with high EC reduces the osmotic activity of plants and thus interferes with the absorption of water and nutrients from the soil. The combined effect of EC and Na% can be visualized using Wilcox diagram [127]. Fig. 3.6 a shows 78 % of the groundwater are suitable for irrigation purposes, whereas only 20 % samples fall under permissible to doubtful category. A more detailed analysis with respect to irrigational suitability of the groundwater is done using United States Salinity Laboratory diagram [130]. According to this classification, low-salinity water (< 250 µS/cm) can be used for all types of soils (Fig. 3.6 b). The groundwater of the study area falls into three zones, C2S1, C3S1 and C3S2. Overall 90% of the samples indicate medium to high salinity and low alkalinity water, which can be used for irrigation on almost all types of soil with little danger of exchangeable sodium.

Groundwater with high percentage of inorganic carbon (HCO_3^- and CO_3^{2-}) has a tendency to form precipitates with calcium and magnesium. To quantify this effect Eaton [128] has proposed a term known as residual sodium carbonate (RSC). This parameter is calculated using the following equation;

$$RSC = (HCO_3^- + CO_3^{2-}) - (Ca^{2+} + Mg^{2+}) \tag{3.8}$$

Based on the classification given by Lloyd and Heathcote [129] water with RSC less than 1.25 are suitable for irrigation, whereas marginally suitable up to 2.5 and not suitable for irrigation above 2.5. In the study area the RSC value ranges from -9.1 to 3.2 (Table 3.4). Majority of the samples falls under good category (73 %) and some in doubtful category (22 %) and only 5 % samples fall under unsuitable category.

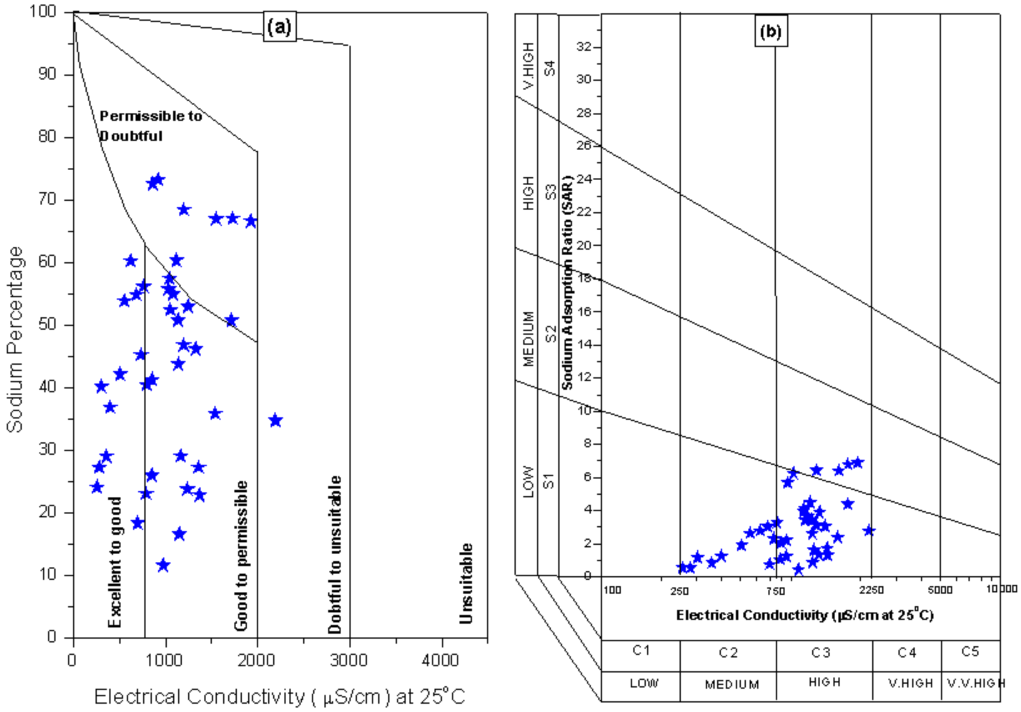

Fig. 3. 6 Irrigational suitability of groundwater based on a) Wilcox and b) USSL classification

3.7 Conclusions

Results suggest that calcium and sodium are major cations, and bicarbonate and chloride are major anions in the groundwater. Among different hydrochemical parameters only pH is found to be beyond drinking water permissible limits in 20% of the samples and other parameters are within the limits. Based on TDS, 29% and 61% of the samples fall under desirable and permissible categories respectively and remaining 10 % is unfit for drinking. No nitrate or fluoride contamination is observed in groundwater, but arsenic concentration up to 40 µg/L is observed in some samples of deeper aquifers.

A wide variety of micro-organisms with TVC ranging from 1.8 X 10^3 to 3.3 X 10^4 cfu/ mL are found in groundwater. Even though all the microbes don’t fall under faecal origin, half of the samples analyzed indicate the presence of E. coli, which is harmful. SRB is found in a few locations in deeper groundwater indicating reducing condition of the aquifer, which is further supported by low levels of DO in groundwater.

Indicators such as SAR, RSC and Na % that qualify the water for irrigation suitability are found to fall under ‘excellent’ and ‘permissible‘categories. SAR value ranges from 0.43 to 6.9, which fall under low sodium hazard class. As per Na% criteria, 20% of samples fall under unfit category. Based on RSC values, about 5% samples fall under unfit category. There are also cases of water samples falling under doubtful to unfit category due to presence of high bicarbonate concentration. Overall groundwater quality is good and suitable to irrigation, however microbial decontamination is necessary before using for potable purposes.

The geochemical reactions taking place in subsurface that are driving the variation of the chemical species in groundwater from different zones need to be understood for predicting the future variability in groundwater quality. A detailed account of geochemistry of the groundwater of this region is elaborated in the next chapter.

CHAPTER - 4
ISOTOPE AND GEOCHEMICAL EVALUATION OF FACTORS AFFECTING GROUNDWATER CHARACTERISTICS

4.1 Introduction

This chapter deals with the application of hydrochemical, environmental isotope and geochemical modeling techniques to determine major chemical processes governing the groundwater characteristics in this region. Variations of groundwater composition in different aquifers and factors or processes responsible for these variations are also evaluated.

4.2 Hydrochemical trends

Hydrochemical facies are useful tools for describing the chemical character of groundwater. The format for hydrochemical facies diagram used in this thesis was developed by Piper [131]. This diagram allows the plotting of relative concentrations of major anions and cations, and also the chemical character of multiple water samples at a time. The two triangles at the base of the plot demonstrate the cation (Na^++K^+, Ca^{2+} and Mg^{2+}) and anion (Cl^-, SO_4^{2-}, HCO_3^-) dominance, whereas the central diamond field illustrates various sources and processes associated with the groundwater system.

The groundwater of Quaternary aquifer shows Na^+ dominant character and hydrochemical facies are mainly Na-Mg-HCO_3-Cl and Na-Ca-HCO_3-Cl (Table 4.1). Weathering of silicate minerals followed by ion exchange is the chemical reaction largely responsible for the above facies of groundwater in this aquifer. Presence of Kankar is noted in Quaternary formation which can be source for Ca^{2+} and Mg^{2+}, as CaO and MgO are common constituents of Kankar. In most natural waters an affinity is observed where an ion with a larger hydrated radius is displaced from the mineral lattice/ surface by an ion with smaller hydrated radius. The order of affinity is Cs^+ > Rb^+ >

$K^+ > Na^+ > Li^+$ for monovalent ions and $Ba^{2+} > Sr^{2+} > Ca^{2+} > Mg^{2+}$ for divalent ions [132]. Therefore Ca^{2+} gets replaced easily by monovalent ions as compared to Mg^{2+}, It is for this reason, Mg^{2+} representation is also found in the facies.

Table 4. 1 Hydrochemical facies and characteristic ionic ratios of groundwater

sample	Facies	SiO	HCO3	Na/(Na+Cl	Mg/(Ca+Mg)	Ca/(Ca+SO4	K/Cl
Quaternary aquifer							
Q-7	Na-Ca-Mg-HCO3-	0.1	21.02	0.60	0.49	0.91	0.04
Q-8	Na-Mg-HCO3-Cl	0.1	42.05	0.63	0.68	0.80	0.03
Q-19	Na-Mg-HCO3-Cl	0.1	34.84	0.72	0.84	0.51	0.02
Q-22	Na-Mg-HCO3-Cl	0.1	20.12	0.56	0.68	0.80	0.02
Q-23	Na-Mg-HCO3-Cl	0.1	35.44	0.59	0.72	0.75	0.02
Q-24	Na-Ca-HCO3-Cl	0.1	45.05	0.58	0.37	0.66	0.01
Q-25	Na-Mg-Ca-HCO3-	0.4	8.19	0.58	0.52	0.72	0.03
Q-28	Na-Ca-HCO3-Cl	0.5	12.00	0.71	0.45	0.70	0.02
Q-32	Na-Mg-HCO3-Cl	0.8	5.50	0.70	0.82	0.41	0.06
Q-35	Na-Mg-Cl-HCO3	0.9	5.81	0.57	0.66	0.50	0.00
Q-36	Na-Ca-Mg-HCO3	0.4	15.13	0.67	0.43	0.67	0.06
Q-39	Na-Mg-Cl	0.7	3.05	0.44	0.71	0.79	0.01
Tertiary aquifer							
T-11	Na-Ca-Mg-Cl-HCO	0.4	2.73	0.46	0.40	0.82	0.06
T-17	Ca-Mg-Na-HCO3-	0.5	2.08	0.41	0.41	0.91	0.18
T-20	Mg-Ca-HCO3-Cl	0.9	8.79	0.37	0.60	0.93	0.00
T-21	Ca-Mg-Na-HCO3	0.9	2.05	0.54	0.37	0.94	0.20
T-26	Na-Ca-HCO3-Cl-	0.5	6.09	0.60	0.27	0.66	0.06
T-27	Na-Ca-Cl-HCO3	0.5	7.00	0.46	0.33	0.77	0.03
T-29	Na-Ca-Mg-HCO3	0.6	9.79	0.67	0.40	0.83	0.03
T-30	Na-Ca-Mg-HCO3-	0.6	8.27	0.63	0.44	0.84	0.03
T-31	Na-Ca-Mg-HCO3-	0.6	9.89	0.66	0.45	0.74	0.04
T-33	Na-Ca-Mg-HCO3-	0.6	11.20	0.60	0.43	0.80	0.01
T-34	Na-Ca-Mg-HCO3-	0.7	10.32	0.63	0.44	0.74	0.01
T-37	Na-Ca-HCO3-Cl	0.3	13.38	0.81	0.48	0.69	0.01
T-38	Na-Ca-HCO3-Cl	0.1	15.59	0.70	0.45	0.66	0.06
T-40	Ca-Mg-Na-HCO3	0.1	15.07	0.59	0.43	0.85	0.08
T-41	Ca-Na-Mg-HCO3-	0.1	17.67	0.51	0.42	0.89	0.04
Cretaceous aquifer							
C-1	Ca-Mg-Na-HCO3	0.7	15.19	0.74	0.31	0.95	0.04
C-13	Ca-Mg-Na-HCO3-	0.3	7.90	0.47	0.28	0.54	0.02
C-2	Ca-Na-Mg-SO4-Cl	0.5	12.51	0.33	0.55	0.75	0.03
C-3	Mg-Ca-Na-HCO3-	0.5	11.69	0.83	0.56	0.40	0.14
C-4	Na-Mg-Ca-HCO3-	0.4	16.67	0.47	0.50	0.74	0.04
C-5	Na-Ca-Mg-HCO3-	0.2	20.94	0.55	0.48	0.55	0.01
C-6	Na-Cl-HCO3	0.4	16.70	0.50	0.45	0.92	0.17
C-9	Ca-Mg-HCO3	0.3	20.89	0.64	0.58	0.51	0.10
C-10	Na-Mg-Ca-HCO3-	0.5	11.74	0.70	0.55	0.87	0.17
C-12	Mg-Ca-HCO3	0.7	9.92	0.45	0.43	0.81	0.07
C-14	Ca-Na-SO4-Cl	0.4	9.22	0.51	0.06	0.53	0.02
C-15	Mg-Ca-Na-HCO3	0.8	7.52	0.55	0.58	0.80	0.04
C-16	Mg-Ca-Na-HCO3	0.9	7.72	0.75	0.54	0.84	0.02
C-18	Na-Mg-Ca-HCO3-	0.6	11.75	0.62	0.51	0.57	0.01

From Piper plot, it can be found that most of the samples fall in no cation-no anion dominant field shown by circle (Fig. 4.1). This suggests that there is no single dominant reaction that governs the major ion composition of groundwater in this aquifer. There can be multiple sources/processes influencing the groundwater chemistry such as weathering, ion exchange, dissolution, contribution of evaporated surface water and anthropogenic inputs etc. An increasing EC is noted in the Quaternary aquifer along with changing chemical facies in the Southern part of the study area (Q-31 to Q-33 to Q-36). The chemical facies changes from Na-Mg-HCO_3-Cl to Na-Mg-Cl-HCO_3 to Na-Mg-Cl as indicated by arrow in the Piper plot (Fig. 4.1). The changing hydrochemical facies can be attributed to the contribution from backwater present in the area. The sample Q-36 (Mel Parikkalpet) is located in the vicinity of backwater canal, so its EC is relatively high and the facies is Na-Mg-Cl.

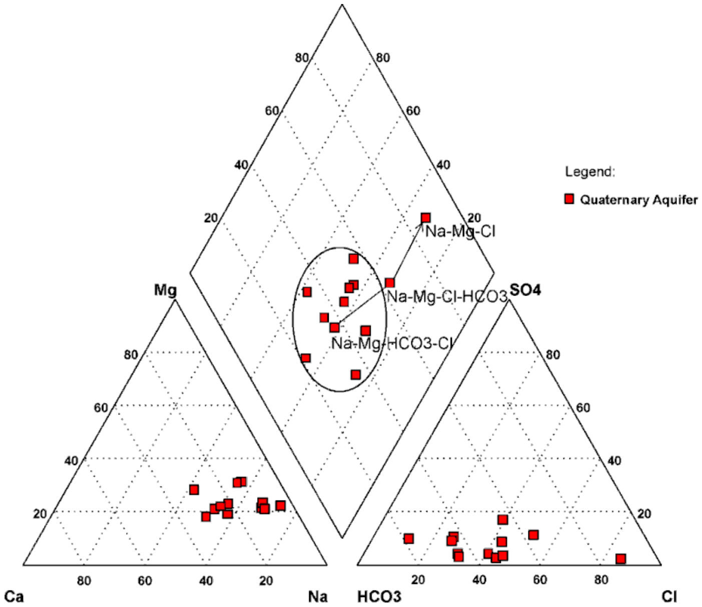

Fig. 4. 1 Piper plot of Quaternary aquifer samples, arrow indicates change in facies along flow path

In the case of Tertiary aquifer, many facies are found viz., Na-Ca-Cl-HCO_3, Ca-Mg-HCO_3-Cl, Na-Mg-HCO_3-Cl, Na-Mg-Cl-HCO_3, Ca-Na-HCO_3-Cl and Na-Ca-HCO_3-Cl. However, Piper plot clearly demonstrates two broad groups of groundwater (Fig. 4.2). Samples falling above the line in the diamond field belong to region North of River Gingee. Samples below this line belong to region South of River Gingee. Among North bound samples, both Ca^{2+} and Na^{+} dominant facies are seen. A close analysis of this behavior indicate that Ca^{2+} dominant facies is seen in the case of samples tapping shallow depths ranging from 30 - 80 m bgl (T-17, T-20 & T-21), whereas Na^{+} dominant facies is noted in deeper depths ranging from 95 - 130 m bgl (T-11, T-26 & T-27).

South bound samples invariably show Na^+ dominant facies, except two deep zone samples, Manapattu and Periyakanganankuppam, near the coast with a depth 140 and 215 m bgl.

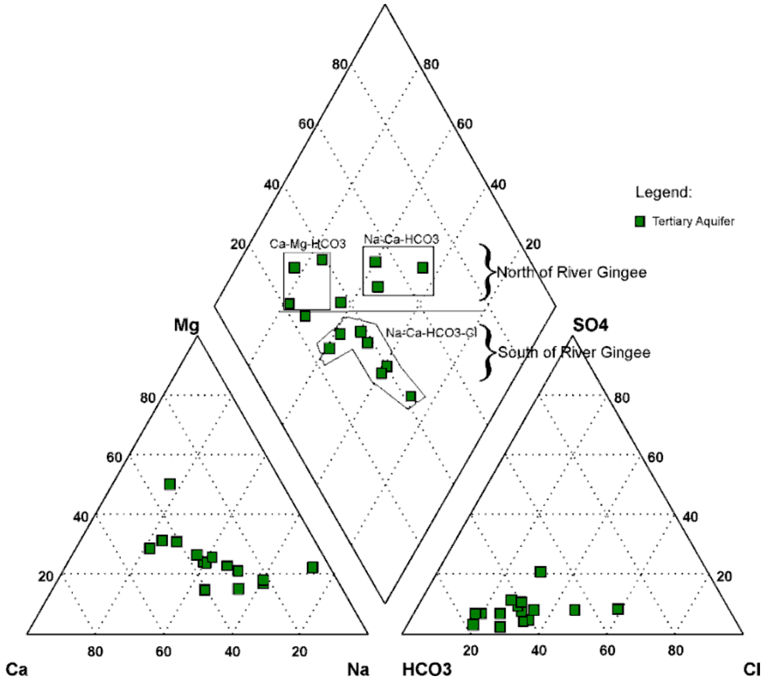

Fig. 4. 2 Piper plot of hydrochemical data of Tertiary aquifer, solid line in diamond field divides samples from North and South of River Gingee

Ca^{2+}, Mg^{2+} and HCO_3^- are chief constituents in carbonate minerals, whereas Na^+ and Cl^- might have derived from common sources, like saline backwater or evaporites from the unsaturated zones. It is also possible that Na^+ can be derived from silicate weathering and Cl^- might be leached from clay layers [133]. Based on these observations, it can be understood that samples collected from region North of River Gingee basically belong to Upper Tertiary formation, whereas in the case of samples collected South of River Gingee belong to Lower Tertiary. Both these formations have distinct lithology (Table 1.1). These groups also demonstrate distinguishing ionic ratios and isotope compositions as discussed in the later sections.

Groundwater from Cretaceous aquifer show mainly four hydrochemical facies, viz., Na-Mg-HCO_3-Cl, Na-Mg-HCO_3-SO_4, Ca-Mg-HCO_3 and Ca-Na-SO_4-Cl. From Piper plot (Fig. 4.3) it is evident that Cretaceous aquifer exhibit two path ways of facies changes, shown by arrows in the figure. Groundwater with low TDS is mostly Ca-Mg-HCO_3 type, which along the flow direction mineralizes (increased TDS) and changes the facies in two different evolutionary pathways;

Pathway –I: Ca-Mg-HCO_3 → Ca-Mg-HCO_3-Cl → Ca-Na-SO_4-Cl

Pathway-II: Ca-Mg-HCO_3 → Na-Mg-HCO_3-Cl → Na-Cl-HCO_3

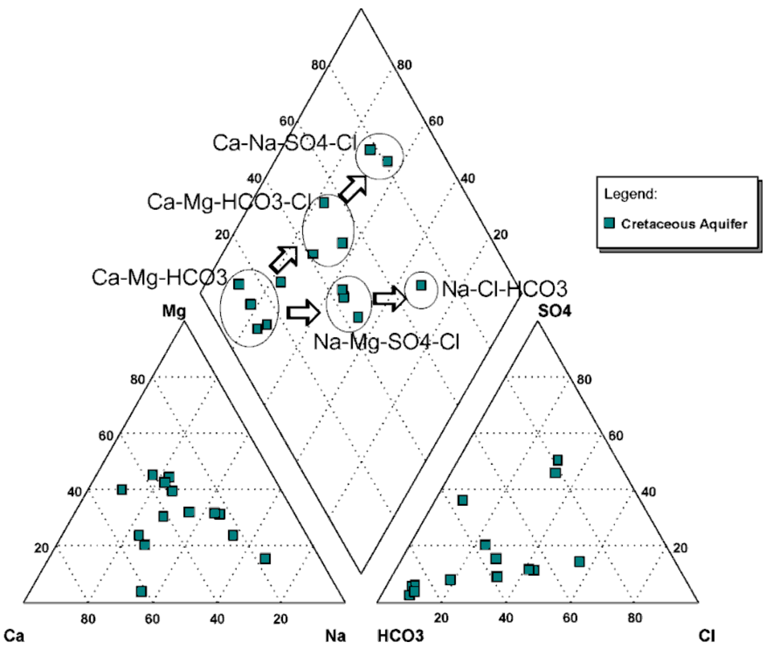

Fig. 4. 3 Piper plot of hydrochemical data of Cretaceous aquifer, arrows indicate pathway-I and pathway-II

Pathway – I demonstrates Ca-Mg facies followed by Ca-Na facies which can be attributed to high solubility of ions representing Halite mineral composition. Ion exchange is another mechanism which can also lead to changes in cationic facies. This is, however, explained by characteristic ionic ratios (Section - 4.3). In the case of anionic species, variations are basically governed by dissolution and precipitation reactions. Variation of anions along the flow path from recharge area to discharge area due to the dissolution-precipitation reactions is discussed by many researchers [10]. Low TDS with high Ca^{2+}/Mg^{2+} ratio, low SO_4^{2-} and high HCO_3^- signify recharging waters [134]. These features are observed in samples C-1 and C-9, indicating groundwater is at the initial stage of geochemical evolution. The subsequent facies Ca (Na)-Mg-HCO_3-Cl is resultant of dissolution of salts from the formation. This facies is observed in samples C-5 & C-13. Finally this pathway attains Ca-Na-SO_4-Cl type of water. This is possible with the contribution of Gypseous rocks and interaction with clay layers, which seems feasible as Cretaceous formation comprises abundant clay layers. This facies is observed in samples C-2 & C-14. Sample C-2 falls in the boundary between Vanur and Ramanathapuram formation which contain abundant Gypseous rocks (Table 1.1).

Pathway – II demonstrates facies variations that are generally observed in metamorphic formations [12]. Initial stage signifies the ion exchange where Ca^{2+} is replaced by Na^+ ion, which is termed as natural softening [89] in which case, Ca-Mg-HCO_3 modifies to Na-Mg-HCO_3-Cl. This facies change is noted in samples C-10 & C-18. Ion exchange can be possible if significant clay bands/layers are present in the aquifer, which is the case with Cretaceous formation. This facies further modifies to Na-Cl-HCO_3, which typically signifies the dissolution reaction. This facies is found in sample C-6. Dissolved sulphate species is not found in this pathway which could be due to low abundance of Gypsum/Anhydrite or removal of sulfates by reduction process.

In this pathway, most of the waters showed Na^+ dominant facies, this can be possible, if the recharge area is devoid of a well-developed soil horizon or vegetative cover and little or no oxygen is available [135]. In such cases carbonic acid is not generated and silicate hydrolysis would be the dominant dissolution mechanism. With increased aquifer-residence time and more chemical interaction with the aquifer matrix, the cation composition of the groundwater evolves to a predominant sodium (Na^+) character. The evolution of the groundwater to Na-HCO_3-Cl chemical water type is attributed to a number of geochemical processes, including; i) Calcite precipitation, ii) cation-exchange processes and iii) Na^+ increase by dissolution reactions. Feasibility of these reactions can be assessed by characteristic ionic ratios [135].

At a few selected sites, Mg^{2+} dominant facies is also noticed (C-3, C-12, C15, C-16 and T-20). This could be possible by dedolomitization, where the dissolution of Gypsum or Anhydrite causes increased Dolomite solubility as Calcite becomes supersaturated [16]. The strongly held hydration shell of the smaller Mg^{2+} ion contrasts that of the larger Ca^{2+} ion and makes it more soluble in water. Calcite precipitation in the presence of Dolomite dissolution has been studied extensively [136, 137]. The chemical equilibrium for dedolomitization is given as follows;

$$CaMg(CO_3)_2 + Ca^{2+} \leftrightarrow 2CaCO_3 + Mg^{2+} \qquad (4.1)$$

The sources and sinks for the major ions can be evaluated using ion versus chloride plots. Chloride is a conservative ion and it does not react or enter into precipitation processes except at brine concentrations and rarely enters into redox or adsorption reactions [138]. Its conservative nature makes it suitable candidate for comparing the relative loss or gain of other ions. Concentration of dissolved chemical species is plotted against chloride and shown in Fig.4.4 (a-f). In the plot Na^+ versus Cl^- (Fig. 4.4 a) best fit line indicates that a good positive correlation is found in all the three aquifers. The correlation coefficient is close to 0.8 for all the best fit lines. These trends indicate a common source of Na^+ and Cl^- ions. This inference strengthens the assumption that dissolution of evaporites/ contribution of saline sources govern the chemistry of groundwater. In the case of Ca^{2+} versus Cl^{-} plot (Fig. 4.4 b) samples from Quaternary and Cretaceous aquifers show scattered nature indicating source and processes affecting the Ca^{2+} distribution is independent of chloride. But, in the case of Tertiary aquifer a positive correlation is noted between these two ions, which indicate dissolution of salts is contributing both Ca^{2+} and Cl^{-} ions.

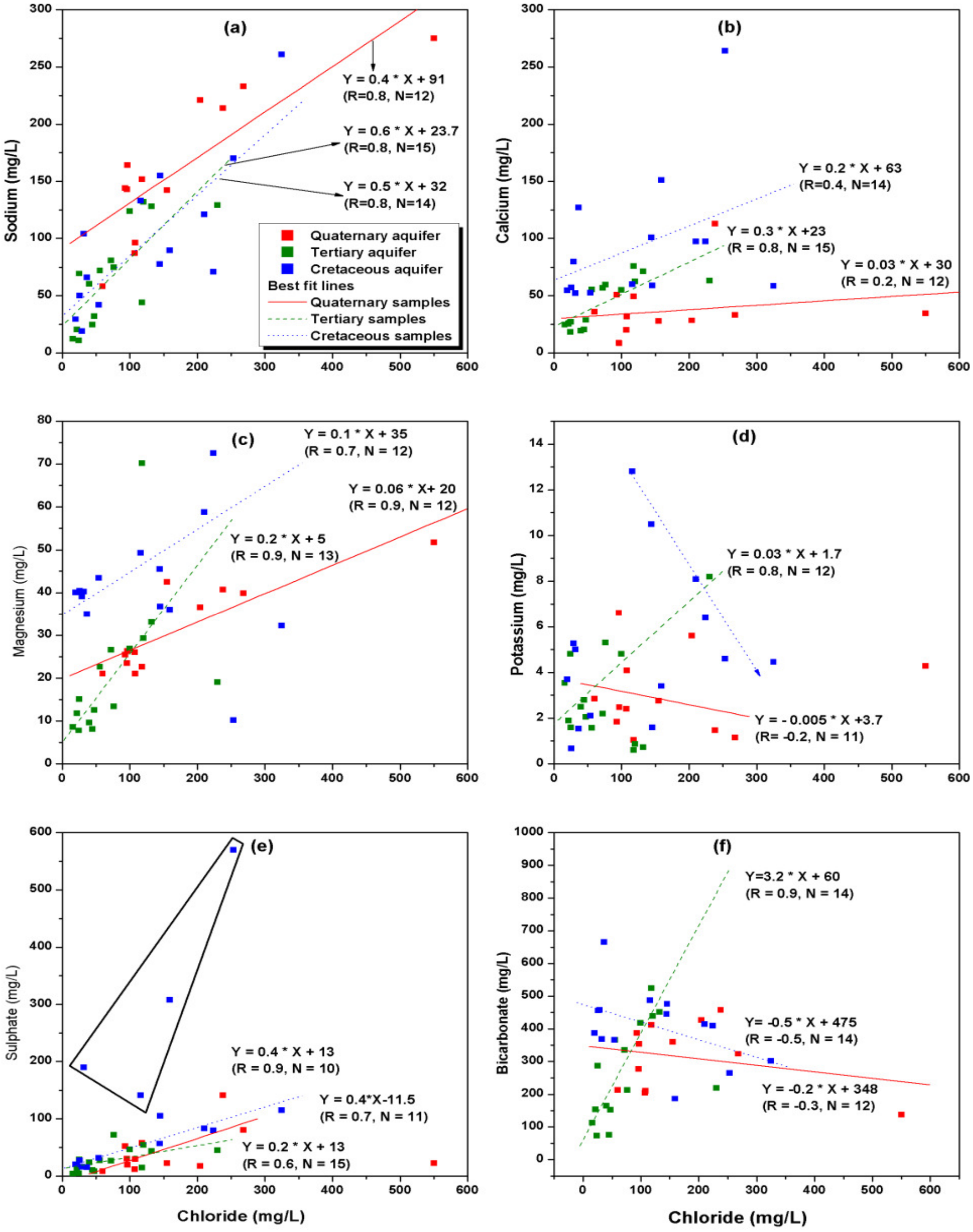

Fig. 4. 4 Ions versus chloride plots of groundwater

In the case of Mg^{2+} versus Cl^- (Fig. 4.4 c), groundwater from all the aquifers shows a positive correlation with correlation coefficients > 0.7, except for T-20 & T-27 in Tertiary and C-6 & C-14 in Cretaceous aquifers. This trend is similar to Ca^{2+} - Cl^- correlation for groundwater in Tertiary aquifer. Lower values of Mg^{2+} represent ion exchange or precipitation, whereas enriched values indicate additional sources of Mg^{2+} such as Pyroxene or Ferromagnesian minerals. In the case of K^+, (Fig. 4.4 d) groundwater shows decreasing trend in the case of Quaternary aquifer which could be due to K^+ removal by ion exchange or K^+ is devoid in the formation. A positive correlation is found in the case of groundwater from Tertiary aquifer with a correlation coefficient 0.8 indicating contribution of K-feldspar from the formation. Cretaceous aquifer shows scattered trend indicating few samples exhibiting positive trend and others negative trend (shown by dotted arrow in the Fig. 4.4 d). This indicates both addition and removal of K^+ is occurring in the formation based up on the availability of K-feldspar and clay layers. However a few samples from Cretaceous aquifer indicate reduction in K^+ content with Cl^- indicating ion exchange as the governing processes for the chemical characteristics of these waters. These samples also fall in the evolutionary path way –II which emphasizes ion exchange process.

In the case of anions, SO_4^{2-} shows positive correlations with Cl^- (Fig. 4.4 e) in all the aquifers excepting a few samples with high SO_4^{2-} in Cretaceous formation (C-2, C-4, C-6, C-10 & C-14). High SO_4^{2-} in Cretaceous aquifer clearly demonstrates contribution of Gypsum. In the case of HCO_3^- (Fig. 4.4 f) groundwater from Quaternary and Cretaceous indicate negative correlation indicating with increasing Cl^- values, HCO_3^- tend to deplete, possibly by carbonate precipitation. In contrary, Tertiary formation indicates a positive correlation between Cl^- and HCO_3^- contents. This trend is very similar to the one observed in the case of Ca^{2+} and Mg^{2+} versus Cl^- plot, (Fig. 4.4 b & c) indicating Ca^{2+}, Mg^{2+} and HCO_3^- are closely associated in Tertiary aquifer.

4.3 Characteristic ion ratios

Waters present in sedimentary formations generally contain relatively low TDS. In very dilute groundwater systems, atmospheric input may contribute significantly to the overall chemistry. Also in these formations, water chemistry may be substantially influenced by even small quantities of Calcite due to the substantially higher dissolution rate of Calcite compared to silicate minerals. Ionic ratios of major ions are widely used by researchers to deduce source-rock and geochemical processes [89]. A few selected ratios (milliequivalents) are calculated for the groundwater of all the three formations and given in Table 4.2.

Two basic weathering processes that affect the groundwater chemistry are silicate and carbonate weathering and these processes are differentiated using HCO_3^-/SiO_2 ratio. A value > 10 signifies carbonate weathering whereas < 5 signify silicate weathering. From table 4.1, it can be found that all the samples from Quaternary formation demonstrate carbonate weathering except in Q-36 in which this ratio indicates silicate weathering. This finding is in agreement with hydrochemical facies of the groundwater. All the groundwater indicates Ca^{2+}, Mg^{2+} and HCO_3^- in the facies except for Q-36. In the case of Tertiary aquifer, samples with high value of this ratio (> 10) are mostly observed in samples collected from South of Gingee River whereas North bound samples show values < 10. This indicates carbonate weathering in Southern region and silicate weathering in Northern region. This observation matches well with the hydrochemical trends observed in Piper's plot (Fig. 4.2). In the case of Cretaceous aquifer, none of the sample shows ratio < 5 indicating lesser possibility of silicate weathering.

Carbonate weathering includes, Dolomite weathering, Limestone weathering or Dolomite dissolution and Calcite precipitation. $Mg^{2+}/(Mg^{2+}+Ca^{2+})$ ratio is helpful in differentiating these processes. This ratio is equal to unity in the case of Dolomite weathering, < 0.5 for Limestone weathering and > 0.5 for Dolomite dissolution with Calcite precipitation. Seawater contribution yields a value > 0.5 for this ratio. In the case of Quaternary samples, only three samples (Q-7, Q-24 and Q-34) show this ratio < 0.5, whereas rest of the samples show value > 0.5. This indicates Dolomite dissolution and Calcite precipitation are governing processes in the groundwater. In Tertiary aquifer, all the samples (T-32 to T-35, T-37 and T-38) with HCO_3^-/SiO_2 ratio < 10 also show $Mg^{2+}/(Mg^{2+}+Ca^{2+})$ ratio < 0.5 indicating Dolomite dissolution and Calcite precipitation processes. Rest of the samples which indicate silicate weathering exhibit $Mg^{2+}/(Mg^{2+}+Ca^{2+})$ ratio < 0.5 pointing to contribution of Granitic weathering. In the case of Cretaceous aquifer, majority of the samples show $Mg^{2+}/(Mg^{2+}+Ca^{2+})$ ratio > 0.5, however a few samples (C-2, C-13 and C-14) show < 0.5 which also indicate silicate weathering (HCO_3^-/SiO_2 ratio > 10). These samples indicate Granite weathering.

Gypsum/Anhydrite or Pyrite contribution to groundwater is easily assessed using $Ca^{2+}/Ca^{2+}+SO_4^{2-}$ ratio. A ratio of 0.5 indicate Gypsum dissolution, higher values indicate other sources of Ca^{2+} like carbonate or silicate, whereas lower values indicate Ca^{2+} removal either by reverse ion exchange or Calcite precipitation. Quaternary samples show higher values of this ratio (0.5 – 0.9) except in one sample (Q-31) indicating other sources of Calcium in addition to Gypsum. This inference is in good agreement with the inferences obtained from above discussed ionic ratios. In the case of Tertiary aquifer, all the samples show this $Ca^{2+}/Ca^{2+}+SO_4^{2-}$ ratio between 0.66 and 0.93 indicating additional source of Ca^{2+}, which could be Dolomite/Limestone weathering as observed in the case of $Mg^{2+}/(Mg^{2+}+Ca^{2+})$ ratio. An alternate source of high calcium concentrations could result from the Albitization of feldspars at the expense of sodium through the following reaction;

$$CaAl_2Si_2O_8 + 4\ H_4SiO_4 + 2\ Na^+ \leftrightarrow 2\ NaAlSi_3O_8 + Ca^{2+} + 8\ H_2O \qquad (4.2)$$

Cretaceous samples also clearly demonstrate higher values of $Ca^{2+}/Ca^{2+}+SO_4^{2-}$ ratio (0.53 - 0.95) resembling the same behavior of Tertiary aquifer. The availability of additional calcium in solution may result in precipitation of Calcite, Gypsum or Anhydrite. Since the solubility of Calcite is low, kinetically Calcite precipitation is feasible. One sample C-4 shows lesser value indicating Ca^{2+} removal either by ion exchange or precipitation. Gypsum dissolution is further verified using HCO_3^-/sum anions ratio. This ratio greater than 0.8 indicates silicate/carbonate weathering while value < 0.8 indicates Gypsum dissolution. Except a few samples from Cretaceous (C-1, C-9, C-12, & C-16) and one sample from Tertiary formation (T-34), all other samples indicate Gypsum dissolution.

Sources of Na^+ and Cl^- are very important to determine as these ions decide the saline character of groundwater. Na^+/Na^++Cl^- ratio is commonly used to interpret the ion exchange, Albite weathering, seawater contribution. A ratio of > 0.5 indicate Albite weathering or ion exchange, whereas < 0.5 with high TDS (> 500 ppm) indicate reverse softening in addition to seawater. Quaternary samples show Na^+/Na^++Cl^- greater than 0.5 indicating contribution of Albite weathering, except in one sample Q-36 (Mel Parikkalpet) where seawater (backwater) contribution is suggested (section 4.2). Ratios much higher than the seawater value (0.45) can be considered as an evidence for exchange of Na^+ for Ca^{2+} [139]. Evaporated precipitation recharging the system may also cause elevated ratio. In the case of Tertiary and Cretaceous samples, majority of the samples shows Na^+/Na^++Cl^- greater than 0.5 indicating contribution of Albite weathering. Some of the samples (T-11, T-17, T-20, T-27, C-2, C-3, C-5 and C-13) show this ratio < 0.5 and the TDS values are > 500 (except for T-11 and T-17) indicating reverse softening. Ratios < 0.5 may be due to reverse exchange of Ca^{2+} for Na^+ or intrusion of sodium-poor, chloride-rich water [89].

Potassium and chloride are contributed mostly by saline formation water and the ratio of K^+/Cl^- in rainwater is 0.44 whereas in seawater it is 0.02 [11]. The ratio of all the samples is lower than 0.44, indicating that K^+ is being absorbed by the clay layers of the aquifer leading to lower values. A few samples indicate relatively higher K^+/Cl^- ratio (0.1 and above) these are probably originated from dissolution of K^+ bearing minerals, ion exchange (K^+ for Ca^{2+} or Mg^{2+}) or leaching of fertilizers.

4.4 Thermodynamic stability diagrams for silicate systems

Complex aluminosilicate minerals, such as the feldspar minerals, dissolve incongruently and form residual clay minerals. In other words, the ratio of elements which appear in solution differs from that in the dissolving mineral [140]. This is because of the formation of secondary minerals, or weathering residues, such as clays and iron oxides during silicate weathering. The solid phase thermodynamic data for such reactions are not well known and calculated SI values are less reliable predictors of mineral stability [141].

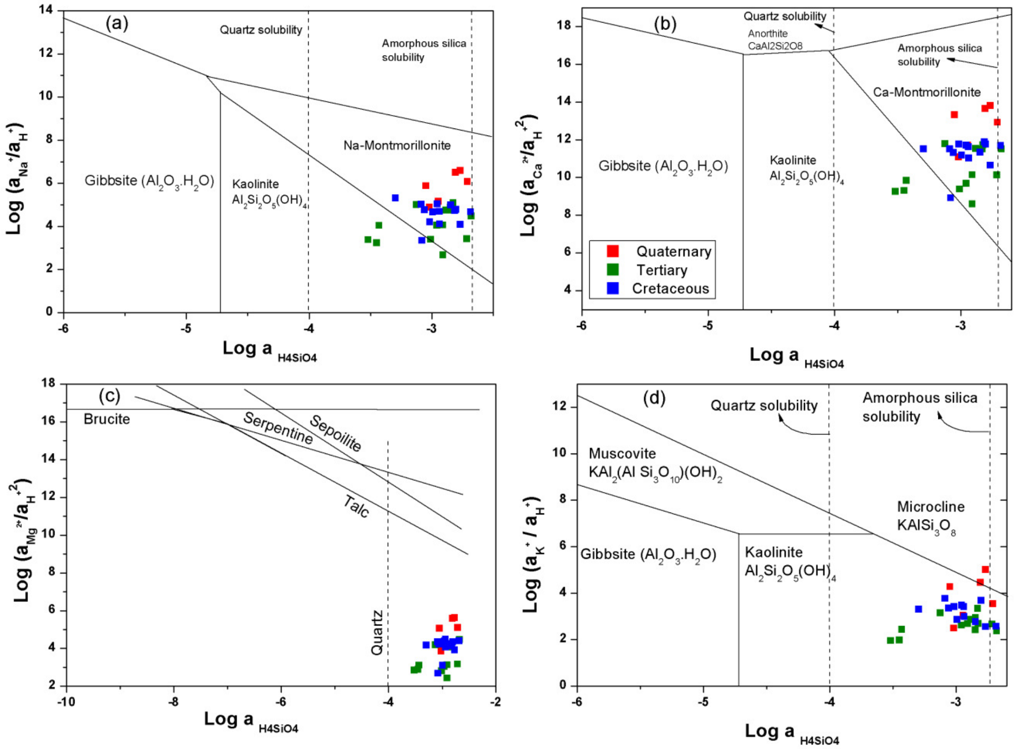

Fig. 4. 5 Stability diagrams of different silicate minerals

In addition, dissolved aluminum concentrations are required for calculating SI values of silicate minerals, and aluminum is difficult to measure in water samples because of its chemical affinity to colloidal material and small concentrations at which it exists.

Assuming equilibrium conditions and that all aluminum is retained in the solid phases, silicate stability diagrams can be used to determine which weathering residues are stable under the conditions indicated by the groundwater. Feldspar is commonly found mineral in sedimentary beds and among feldspars, Plagioclase feldspar is abundant, whereas potash feldspar is found only in unconsolidated material and is limited [142]. In addition, Plagioclase feldspar generally is less stable than potassium feldspar. These observations suggest that plagioclase contributes more to the dissolved load of groundwater than potassium feldspar. As a result incongruent dissolution of Plagioclase feldspar is considered to be the dominant feldspar reaction in sedimentary formations. Water chemistry data for samples from Quaternary, Tertiary and Cretaceous formation aquifer are superimposed on stability diagrams for the sodium, calcium, magnesium and potassium systems (Fig. 4.5 (a-d)). The theoretical controls on the concentration of dissolved silica (SiO_2) in groundwater are the solubilities of Quartz (lower limit) and amorphous silica (upper limit) and plotted on the diagram.

From the thermodynamic diagrams, it can be found that Plagioclase minerals would weather to form dissolved constituents and clay minerals. Incongruent dissolution of Anorthite would produce Ca-montomorillonite and incongruent dissolution of Albite would produce either Na-montomorillonite or kaolinite. A typical incongruent dissolution of sodium silicate (Albite) is shown below;

$$2\ NaAlSi_3O_8 + 2\ CO_2 + 11\ H_2O \leftrightarrow Al_2Si_2O_5(OH)_4 + 2\ Na^+ + HCO_3^- + H_4SiO_4 \qquad (4.3)$$

All the data plot in the Kaolinite or Montomorillonite stability fields, which indicates that Muscovite, Microcline and Gibbsite are unstable solid phases and would react with water to form Kaolinite. In the similar fashion, Ca-silicate diagram indicate that for water associate with Anorthite forms Ca-montomorillonite as the stable solid phase. For Na-silicate system, Kaolinite and Na-montomorillonite are the stable solid phases. Based on the above findings, it seems likely that Ca/Na montomorillonite and kaolinite are the stable products of weathering reaction. These clay minerals form in dry climate and when rapidly dissolving material is available [9, 18].

4.5 Mineral saturation indices

The concentrations of naturally occurring inorganic constituents in groundwater are controlled by the type, abundance and reaction rates of minerals present in the aquifer. Nearly all minerals react with groundwater to some extent. However minerals that react slowly have less effect on the chemical composition of groundwater than minerals that react rapidly [143]. The difference in mineral stability is attributed to changing equilibrium conditions during the formation of the mineral. The abundance of minerals in an aquifer also has an effect on water chemistry. The degree to which a mineral is in equilibrium with water is given by saturation index (SI), which is defined as;

$$SI = Log\ \frac{IAP}{KT} \tag{4.4}$$

where IAP is the ion activity product of the dissolved components in the solution and KT is the solubility product of the solid or gaseous phase at the specified temperature. SI of zero indicates that the water is in equilibrium with the mineral. A negative SI indicates that the water is undersaturated and a positive SI indicates that water is supersaturated.

4.5.1 Carbonate minerals

Saturation index of groundwater for minerals such as Magnesite ($MgCO_3$), Aragonite ($CaCO_3$), Calcite ($CaCO_3$), Dolomite ($CaMg(CO_3)_2$), Strontionite ($SrCO_3$) and Witherite ($BaCO_3$) are given in table 4.2. A saturation index of zero indicates saturation but because of the possibility of CO_2 outgassing and errors in pH and alkalinity, it can be considered that a saturation index of ± 0.2 is indicative of Calcite saturation and ± 0.4 for Dolomite saturation [139]. Based on this criterion, in Quaternary aquifer, samples Q-19, Q-22, Q-23, Q-25 and Q-31 are supersaturated with Calcite while others are saturated. Aragonite is found to be unsaturated to saturated with most of the groundwater from Quaternary aquifer while Dolomite is undersaturated except in Q-19. These observations suggest that all the carbonate minerals tend to dissolve in groundwater except Calcite. Since the Mg^{2+}/Ca^{2+} ratio of these samples is > 1, it is possible that re-precipitated mineral is impure Calcite i.e. Mg-calcite. There were reports on this observation by Drever [10], who proposed that if the Mg^{2+}/Ca^{2+} ratio is near sea water value (5.2), the precipitated calcite can contain up to 20 % Mg-carbonate.

During calcite precipitation, CO_2 is evolved leading to increase in partial pressure, and the equilibrium reaction can be written as follows,

$$Ca^{2+} + HCO_3^{-} \leftrightarrow CaCO_3 + CO_2 + H_2O \qquad (4.5)$$

Table 4. 2 Saturation index of groundwater for carbonate minerals

Sample ID	Magnesite	Dolomite	Calcite	Aragonite	Strontionite	Witherite
	$MgCO_3$	$CaMgCO_3$	$CaCO_3$	$CaCO_3$	$SrCO_3$	$BaCO_3$
			Quaternary aquifer			
Q-7	-0.87	-1.16	-0.09	-0.25	-1.07	
Q-8	-0.62	-1.01	-0.18	-0.35	-0.87	
Q-19	0.31	0.46	0.35	0.19	-0.09	
Q-22	-0.71	-1.18	-0.27	-0.44	-1.00	
Q-23	-0.08	-0.01	0.28	0.12	-0.31	
Q-24	-0.89	-1.00	0.10	-0.07	-1.01	
Q-25	-0.47	-0.42	0.25	0.09	-0.72	
Q-28	-1.05	-1.45	-0.20	-0.36	-1.14	
Q-32	0.19	0.29	0.30	0.14	-0.05	
Q-35	-0.26	-0.26	0.20	0.04	-0.33	
Q-36	-0.55	-0.51	-0.03	-0.17	-2.10	-2.83
Q-39	-0.18	-0.19	0.19	0.03	-0.36	
			Tertiary aquifer			
T-11	-2.30	-3.95	-1.72	-1.86	-3.35	-3.81
T-17	-2.68	-4.76	-2.14	-2.28	-3.50	-5.27
T-20	0.16	0.59	0.37	0.23	-1.17	-2.38
T-21	-1.75	-2.80	-1.12	-1.26	-2.39	-4.52
T-26	-1.55	-2.21	-0.72	-0.86	-1.74	-4.43
T-27	-1.64	-2.52	-0.94	-1.08	-2.00	-4.09
T-29	-0.41	-0.19	0.17	0.03	-1.79	
T-30	-0.44	-0.31	0.08	-0.07	-1.77	
T-31	-0.26	0.03	0.22	0.08	-1.40	-2.91
T-33	-0.26	0.05	0.25	0.11	-1.52	-2.78
T-34	-0.15	0.27	0.36	0.22	-1.69	-2.60
T-37	-0.34	-0.18	0.09	-0.05	-1.89	-3.38
T-38	-1.65	-2.76	-1.18	-1.32	-3.04	-4.21
T-40	-1.89	-3.21	-1.39	-1.53	-3.30	
T-41	-1.94	-3.28	-1.41	-1.55	-3.27	-4.52
			Cretaceous aquifer			
C-1	0.04	0.88	0.77	0.63	-0.74	-2.86
C-2	0.06	0.50	0.37	0.23	-2.30	-3.70
C-3	-0.07	0.22	0.22	0.09	-1.35	-3.32
C-4	-0.17	0.12	0.22	0.08	-1.31	-3.11
C-5	-0.38	-0.26	0.06	-0.08	-1.21	-3.47
C-6	-0.02	0.52	0.47	0.33	-0.90	-3.72
C-9	0.04	0.40	0.29	0.15	-1.31	-3.38
C-10	-0.36	-0.35	-0.05	-0.19	-1.98	-3.81
C-12	-0.02	0.54	0.49	0.35	-1.44	-2.90
C-13	-2.06	-3.23	-1.25	-1.39	-2.43	-4.67
C-14	-1.50	-1.32	0.11	-0.03	-1.72	-4.25
C-15	-0.51	-0.70	-0.26	-0.40	-1.36	-3.87
C-16	0.03	0.46	0.36	0.22	-1.11	-2.87
C-18	-0.20	0.05	0.18	0.04	-1.81	-2.99

In the case of Tertiary aquifers, samples showing undersaturation with respect to Calcite fall in the Northern part of Gingee river (T-11, T-17, T-21, T-26 and T-27) and deep zones of Southeastern part (T-35, T-37 and T-38). These samples show Ca-Mg-HCO_3 facies. Rest of the samples is near saturation to Calcite. Therefore, in these samples Calcite re-precipitation can occur. In Cretaceous aquifer, groundwater samples show supersaturation with respect to Calcite reflecting a good chance of Calcite reprecipitation. These samples also have the Mg^{2+}/Ca^{2+} ratio > 1, indicating formation of Mg-calcite as noticed in the case of Quaternary samples. Only one groundwater sample, C-2 indicates undersaturation. Groundwater in all the three aquifers is found to be undersaturated with respect to Strontionite and Witherite (Table 4.2). The negative values of SI for these minerals suggest that lesser abundance of these minerals.

4.5.2 Sulphate minerals

Gypsum ($CaSO_4$) is a common sulphate mineral present in sedimentary beds and other sulphate minerals are Mirabilite (Na_2SO_4), Epsomite ($MgSO_4$) Celestite ($SrSO_4$) and Barite ($BaSO_4$). The saturation indices of these minerals are shown in table 4.3.

The saturation indices of water samples with respect to Gypsum are under saturated, indicating that it dissolves to form Ca^{2+} and SO_4^{2-} ions. The contribution of this mineral to the dissolved load is limited by its low abundance in Quaternary and in some Tertiary formations. However in the case of Cretaceous formation, it can be observed that SI values indicate less undersaturation which could be due to dissolution of Gypsum/Anhydrite in rocks, which can be represented as follows;

$$CaSO_4 \leftrightarrow Ca^{2+} + SO_4^{2-} \qquad (4.6)$$

Groundwater from all formations shows unsaturation with respect to rest of the sulphate minerals viz., Mirabilite, Epsomite and Celestite. Barite, on the other hand found to be close to saturation in Tertiary and Cretaceous samples. It suggests the presence of Barite in these formations.

Table 4. 3 Saturation index of groundwater for sulphate minerals

Sample ID	Gypsum	Mirabilite	Potash Alum	Epsomite	Celestite	Barite
	$CaSO_4$	Na_2SO_4	$KAl(SO_4)_2$	$MgSO_4$	$SrSO_4$	$BaSO_4$
Quaternary aquifer						
Q-7	-2.86	-7.15	-19.48	-5.16	-2.71	
Q-8	-2.75	-5.75	-17.81	-4.72	-2.31	
Q-19	-3.19	-5.91	-22.56	-4.75	-2.50	
Q-22	-2.97	-6.65	-19.66	-4.93	-2.57	
Q-23	-2.64	-6.02	-20.04	-4.53	-2.11	
Q-24	-1.36	-4.96	-15.68	-3.87	-1.34	
Q-25	-2.39	-6.17	-19.96	-4.64	-2.23	
Q-28	-2.01	-5.63	-16.45	-4.38	-1.82	
Q-32	-2.95	-5.82	-21.84	-4.59	-2.18	
Q-35	-2.06	-5.06	-19.07	-4.04	-1.46	
Q-36	-2.07	-7.12	-18.99	-4.67	-2.84	
Q-39	-2.63	-5.51	-21.13	-4.52	-2.05	
Tertiary aquifer						
T-11	-2.97	-9.31	-16.59	-5.64	-3.29	0.20
T-17	-3.35	-10.38	-15.92	-5.99	-3.41	-1.23
T-20	-2.57	-8.89	-21.57	-4.87	-2.81	-0.06
T-21	-3.32	-10.39	-18.34	-6.05	-3.28	-1.47
T-26	-1.83	-7.60	-15.12	-4.75	-1.55	-0.28
T-27	-2.06	-7.39	-14.79	-4.85	-1.82	0.04
T-29	-2.31	-8.02	-19.70	-4.95	-2.97	
T-30	-2.32	-7.93	-20.11	-4.90	-2.88	
T-31	-2.12	-7.44	-19.35	-4.70	-2.44	0.00
T-33	-2.07	-7.45	-20.31	-4.67	-2.53	0.16
T-34	-2.02	-7.28	-20.69	-4.61	-2.77	0.28
T-37	-2.52	-8.08	-20.83	-5.04	-3.18	-0.74
T-38	-2.68	-8.21	-16.97	-5.25	-3.24	-0.46
T-40	-2.87	-9.54	-16.82	-5.48	-3.47	
T-41	-2.97	-9.26	-16.89	-5.61	-3.53	-0.83
Cretaceous aquifer						
C-1	-2.32	-8.53	-20.48	-5.14	-2.53	-0.69
C-2	-1.77	-7.80	-19.27	-4.17	-3.13	-0.58
C-3	-1.59	-6.98	-19.10	-3.98	-1.85	0.12
C-4	-1.74	-7.32	-18.52	-4.23	-1.96	0.18
C-5	-1.78	-6.43	-19.14	-4.31	-1.74	-0.05
C-6	-2.43	-9.53	-20.84	-5.00	-2.49	-1.36
C-9	-1.69	-6.99	-18.68	-4.06	-1.98	-0.12
C-10	-2.46	-8.99	-19.54	-4.86	-3.10	-0.96
C-12	-1.85	-7.84	-18.11	-4.47	-2.48	0.00
C-13	-1.01	-7.02	-14.40	-3.92	-0.88	0.82
C-14	-0.61	-6.26	-16.31	-4.32	-1.13	0.28
C-15	-2.30	-8.57	-18.12	-4.66	-2.09	-0.67
C-16	-2.34	-8.44	-20.63	-4.75	-2.51	-0.30
C-18	-1.80	-6.92	-19.31	-4.27	-2.48	0.28

4.5.3 Silicate minerals

Silica reactions are more complex and varied even though they appear simple stoichiometrically. The equilibrium reaction can be written as;

$$SiO_2 + H_2O \leftrightarrow H_4SiO_4 \qquad (4.7)$$

The SI data suggests that groundwater from all the three formations are supersaturated with respect to Quartz and Christobalite (Table 4.4), indicating that they are stable solid phases, whereas undersaturated with respect to amorphous silica indicating it is unstable solid phase. In the case of Quaternary samples, silica can precipitate as a result of solution concentration resulting from evaporation in the unsaturated zone [144]. This is further confirmed by enriched isotope composition of the Quaternary samples (section 4.10). However in the case of Tertiary and Cretaceous aquifers, evaporation governed silica precipitation may be unlikely as these aquifers are under semi-confined to confined condition.

4.5.4 Fluoride minerals

Being a common contaminant in groundwater, fluoride minerals are considered important for evaluation. Even though fluoride salts are highly soluble, their low abundance limits the presence of fluoride in groundwater. Fluorite (CaF_2) is a commonly present mineral in sedimentary formations. The SI of this mineral is given in table 4.4. It can be observed that all the three aquifers show undersaturation with this mineral pointing to possibility of further dissolution and increase in dissolved fluoride.

4.6 Statistical Analysis

Factor analysis is used in this thesis to identify statistical association among dissolved constituents and geochemical processes. This method can overcome the limitations of conventional graphical techniques (e.g. Piper’s diagram). As a first step, correlation matrix is generated from a given set of hydrochemical data from each formation to observe nature of correlations among the parameters. In second step, factor analysis is applied to identify the statistical associations or factors. Each factor infers a dominant and distinct chemical reaction or source. Correlations are broadly classified into strong positive correlation (> + 0.7), poor positive correlation (+ 0.5 to + 0.7). Similarly strong inverse correlations for value < -0.7 and moderate < -0.5.

Table 4. 4 Saturation index of groundwater for Silicate, Halite, Fluorite and total ionic strength (IS)

Sample ID	Total IS	Log Pco_2	Halite	Fluorite	Christobalite	Quartz	SiO2 (a)	Albite
			$NaCl$	CaF_2	SiO_2	SiO_2	SiO_2	$NaAlSi_3O_8$
Quaternary aquifer								
Q-7	0.01	-2.68	-6.97	-1.44				
Q-8	0.02	-2.17	-5.88	-2.10				
Q-19	0.01	-3.41	-6.32	-2.25				
Q-22	0.01	-2.80	-6.54	-2.50				
Q-23	0.01	-2.79	-6.19	-2.28				
Q-24	0.02	-1.86	-5.85	-1.30				
Q-25	0.01	-3.12	-6.50	-2.09	0.91	1.33	-0.11	1.70
Q-28	0.01	-1.97	-6.40	-1.44	1.01	1.44	-0.01	2.06
Q-32	0.01	-3.56	-6.38	-2.35	1.19	1.62	0.17	2.72
Q-35	0.02	-2.77	-5.75	-1.82	1.25	1.67	0.23	3.07
Q-36	0.01	-1.49	-6.36	-1.92	0.49	0.88	-0.35	0.33
Q-39	0.02	-3.52	-5.37	-3.27	1.15	1.58	0.13	2.85
Tertiary aquifer								
T-11	0.00	-1.48	-7.53	-4.94	0.50	0.88	-0.35	-0.06
T-17	0.00	-1.11	-8.15		0.59	0.98	-0.25	-0.49
T-20	0.02	-1.52	-6.90	-1.81	0.83	1.22	-0.01	0.33
T-21	0.00	-1.63	-8.28	-3.54	0.78	1.16	-0.06	0.91
T-26	0.01	-1.24	-6.84	-2.75	0.60	0.99	-0.25	1.17
T-27	0.01	-0.99	-6.14	-4.62	0.55	0.94	-0.29	0.93
T-29	0.01	-1.73	-7.00	-2.12	0.65	1.03	-0.21	0.81
T-30	0.01	-1.71	-6.83	-2.25	0.68	1.07	-0.17	0.20
T-31	0.01	-1.66	-6.52	-2.30	0.67	1.06	-0.17	0.76
T-33	0.02	-1.54	-6.39	-2.23	0.66	1.04	-0.19	0.26
T-34	0.01	-1.74	-6.41	-2.27	0.69	1.08	-0.16	0.40
T-37	0.01	-2.08	-7.35	-1.08	0.37	0.75	-0.47	-0.01
T-38	0.01	-1.41	-7.20	-2.39	0.07	0.45	-0.77	-0.88
T-40	0.00	-1.09	-7.94	-2.74	0.04	0.42	-0.80	-1.78
T-41	0.01	-1.05	-7.40	-2.59	-0.03	0.36	-0.87	-1.82
Cretaceous aquifer								
C-1	0.02	-1.49	-7.24	-1.38	0.69	1.07	-0.15	1.06
C-2	0.02	-1.65	-6.43	-2.73	0.56	0.95	-0.28	-0.29
C-3	0.02	-1.85	-7.09	-1.65	0.55	0.93	-0.30	-0.15
C-4	0.02	-1.48	-6.23	-2.53	0.44	0.82	-0.40	-0.45
C-5	0.02	-1.83	-5.70	-2.52	0.21	0.60	-0.63	-0.77
C-6	0.01	-1.67	-7.87	-2.65	0.49	0.88	-0.35	-1.05
C-9	0.02	-1.61	-6.44	-2.57	0.40	0.79	-0.44	-0.52
C-10	0.01	-1.45	-7.84	-2.30	0.58	0.97	-0.27	-0.59
C-12	0.02	-1.66	-6.57	-1.87	0.69	1.08	-0.15	1.56
C-13	0.02	-0.54	-6.48	-2.03	0.41	0.80	-0.43	-2.41
C-14	0.04	-1.45	-6.02	-1.38	0.50	0.89	-0.34	-0.16
C-15	0.01	-1.29	-7.25	-2.51	0.73	1.11	-0.11	0.74
C-16	0.01	-1.71	-7.49	-1.99	0.82	1.21	-0.02	1.16
C-18	0.02	-1.53	-6.27	-2.35	0.66	1.04	-0.19	0.34

4.6.1 Quaternary aquifer

Strong positive correlations are found among Cl^-, Na^+, Mg^{2+} and Sr^{2+}, and also between Ca^{2+} and SO_4^{2-} Moderate positive correlations are observed between ion pairs NO_3^- with Cl^-, Mg^{2+} and F^-. pH also shows good correlations with K^+ and Ca^{2+} (Table 4.5).

Table 4. 5 Correlation matrix of ions in groundwater from Quaternary aquifer

	Cl^-	NO_3^-	SO_4^{2-}	HCO_3^-	Na^+	K^+	Mg^{2*}	Ca^{2+}	Si	pH	F^-	Sr^{2+}
Cl^-	1.00											
NO_3^-	**0.50**	1.00										
SO_4^{2-}	0.17	0.27	1.00									
HCO_3^-	0.26	0.36	**0.56**	1.00								
Na^+	**0.83**	0.17	0.41	0.24	1.00							
K^+	0.09	0.14	**0.50**	0.32	0.04	1.00						
Mg^{2+}	**0.87**	**0.62**	0.27	0.04	**0.82**	0.01	1.00					
Ca^{2+}	0.19	0.07	**0.85**	0.47	0.25	0.48	0.26	1.00				
Si	0.37	0.03	0.14	0.27	0.37	0.14	0.11	0.16	1.00			
pH	0.13	0.24	0.48	**0.55**	0.02	**0.54**	0.07	**0.69**	0.24	1.00		
F^-	**0.64**	**0.60**	0.32	**0.54**	0.31	0.38	**0.58**	0.22	0.09	0.35	1.00	
Sr^{2+}	**0.74**	0.48	0.42	0.00	**0.70**	0.07	**0.88**	0.36	0.24	0.04	0.39	1.00

A total of 3 factors are extracted with eigen values > 1 and the total data variance (TDV) accounted for is 78 % (Table 4.6). Examination of the first factor shows a large portion of covariance (35 %) in the ion chemistry that may be accounted for by the variances of Cl^-, NO_3^-, Na^+, Mg^{2+} and Sr^{2+}. High positive loadings for Mg^{2+}, Sr^{2+}, Na^+ are associated with high positive loadings for Cl^- and NO_3^-. This factor represents backwater or evaporite contribution to the groundwater.

Table 4. 6 Varimax rotated factor loadings – Quaternary aquifer

Component/Factor	1	2	3
Cl^-	**0.92**		
NO_3^-	**0.69**	-0.33	-0.44
SO_4^{2-}		**0.84**	0.34
HCO_3^-		**0.77**	
Na^+	**0.75**		0.49
K^+		**-0.68**	
Mg^{2+}	**0.97**		
Ca^{2+}		**0.86**	
Si			**0.83**
pH		**-0.80**	
F^-	**-0.69**	**0.52**	
Sr^{2+}	**0.87**		

Factor 2 accounts for approximately 30% of TDV. High positive loading of Ca^{2+} is associated with high positive loadings of HCO_3^- and SO_4^{2-}, and negatively with pH and K^+. This factor represents carbonate and sulphate minerals along with K^+ adsorption on clay minerals. There is also an indication of denitrification, since negative loadings of NO_3^- is associated with positive loadings of HCO_3^- [145].

Factor 3 accounts for 12% of TDV and shows that Si varies independently of other constituents in the system. Proposed reactions that explain the silica concentrations could be reversible precipitation of metastable, amorphous aluminosilicates [141]. Dissolution of silicate minerals in the soil may not be important for the silica concentrations in the time scale of this study because these hydrolysis reactions are slow [144]. Moderate positive loading is observed for Na^+ pointing to possibility of Albite weathering, which is also inferred from characteristic ionic ratios (section 4.3)

4.6.2 Tertiary aquifer

Strong correlations are observed between ion pairs Na^+ - Cl^-, Na^+-Ca^-, Na^+ - SO_4^{2-}, Ca^{2+} - Cl^-, Ca^{2+} - SO_4^{2-}, Ca^{2+} - HCO_3^-, Mg^{2+} - HCO_3^-, pH - HCO_3^-, Ca^{2+} - Na^{2+}, Ca^{2+} - Mg^{2+}, Sr^{2+} - K^+. Moderate correlations are observed between ion pairs, Cl^- - SO_4^{2-}, Cl^- - HCO_3^-, Cl^- - Sr^{2+}, Ca^{2+} - SO_4^{2-}, Sr^{2+} - SO_4^{2-}, Na^+ - HCO_3^-, Si - HCO_3^-, pH - Na^+, pH - K^+, Si - Ca^{2+}, Si - Mg^{2+}, pH - Mg^{2+}, pH - Ca^{2+} and pH - F^- (Table 4.7).

Table 4. 7 Correlation matrix of ions in groundwater from Tertiary aquifer

	Cl^-	NO_3^-	SO_4^{2-}	HCO_3^-	Na^+	K^+	Mg^{2*}	Ca^{2+}	Si	pH	F^-	Sr^{2+}
Cl^-	1.00											
NO_3^-	0.25	1.00										
SO_4^{2-}	**0.57**	0.02	1.00									
HCO_3^-	**0.50**	0.14	0.46	1.00								
Na^+	**0.77**	0.07	**0.82**	**0.66**	1.00							
K^+	0.36	0.42	0.26	0.42	0.13	1.00						
Mg^{2+}	0.48	0.13	0.15	**0.85**	0.32	0.39	1.00					
Ca^{2+}	**0.77**	0.13	**0.64**	**0.85**	**0.72**	0.05	**0.77**	1.00				
Si	0.31	0.22	0.15	**0.53**	0.21	0.02	**0.61**	**0.59**	1.00			
pH	0.16	0.14	0.37	**0.83**	**0.54**	**0.51**	**0.56**	**0.53**	0.44	1.00		
F^-	0.21	0.42	0.05	0.30	0.09	0.41	0.15	0.05	0.18	**0.60**	1.00	
Sr^{2+}	**0.63**	0.25	**0.59**	0.03	0.33	**0.70**	0.11	0.49	0.25	0.20	0.28	1.00

A total of three factors were found with a TDV accounting for 80.4 % (Table 4.8). Factor 1 shows high positive loadings of HCO_3^-, Mg^{2+}, Ca^{2+} and Si, which clearly indicates weathering of silicate minerals. During weathering of silicate minerals bicarbonate is released into the system. Common silicate mineral such as Diopside weather as follows;

$CaMgSi_2O_6 + CO_2 + O_2 + H_2O \leftrightarrow Mg^{2+} + Ca^{2+} + HCO_3^- + H_4SiO_4$ (4.8)

Factor 2 accounts for 28.7 % of TDV and shows high loadings of Cl^-, SO_4^{2-}, Na^+ and Sr^{2+} which are common ions present in saline sources such as seawater, backwater or old sea water. Therefore, this factor corresponds to marine source. Factor 3 accounts for 21.7 % of TDV and shows high loadings of NO_3^-, K^+, pH and F^-, which clearly point to contribution of fertilizers and other domestic or industrial effluents.

Table 4. 8 Varimax rotated factor loadings – Tertiary aquifer

Component/Factor	**1**	**2**	**3**
Cl^-	0.38	**0.76**	0.31
NO_3^-			**0.68**
SO_4^{2-}		**0.92**	
HCO_3^-	**0.84**	0.38	0.36
Na^+	0.31	**0.86**	
K^+	0.40	**0.46**	**0.66**
Mg^{2+}	**0.90**		
Ca^{2+}	**0.75**	**0.61**	
Si	**0.80**		0.32
pH	**0.65**		**0.60**
F^-			**0.83**
Sr^{2+}		**0.70**	**0.53**

4.6.3 Cretaceous aquifer

Strong positive correlations are found between Na^+ - Cl^-, Ca^{2+} - SO_4^{2-} and pH - Sr^{2+}. Moderate positive correlations are found between Cl^- - Si; NO_3^- with Si, HCO_3^-, Ca^{2+}, pH, Sr^{2+}; SO_4^{2-} with HCO_3^- and Mg^{2+}; HCO_3^- - pH, Na^+- Si and Mg^{2+} - Ca^{2+} (Table 4.9).

Factor analysis yielded four factors accounting for 81.4% of TDV (Table 4.10). Among which factor 1 represents high positive loadings for HCO_3^- and pH and accounts for 23.6 % of TDV. Bicarbonate is produced by the dissociation of carbonate in the soil and vadose zones, and its contribution to the groundwater depends upon pH and Pco_2. Moderate loading of Sr^{2+} and NO_3^- are also represented by this factor. This indicates contribution of anthropogenic inputs such as fertilizer and other effluents.

Factor 2 accounts to 23.4% of TDV and represents high loadings for Cl^-, Si and Na^+. This is possible provided groundwater is evolved and ion exchange is the dominant process. Cretaceous formation contains abundant clay layers which can also act as good source of Cl^-, and also mediate ion exchange. Factor 3 accounts 20% of TDV and is represented by Ca^{2+} and SO_4^{2-} indicating contribution of Gypsum mineral. There are also moderate loadings of NO_3^- and F^-. Factor 4 accounts 14.5 % of TDV and shows high factor loadings of K^+ and Mg^{2+}, which are macronutrients needed for plant growth and moderate loading of F^-. This factor represents recharge from root zone.

Table 4. 9 Correlation matrix of ions in groundwater from Cretaceous aquifer

	Cl^-	NO_3^-	SO_4^{2-}	HCO_3^-	Na^+	K^+	Mg^{2*}	Ca^{2+}	Si	pH	F^-	Sr^{2+}
Cl^-	1.00											
NO_3^-	0.28	1.00										
SO_4^{2-}	0.48	**0.63**	1.00									
HCO_3^-	0.47	**0.53**	**0.63**	1.00								
Na^+	**0.80**	0.10	0.46	0.32	1.00							
K^+	0.27	0.04	0.05	0.03	0.15	1.00						
Mg^{2+}	0.03	0.15	**0.59**	0.26	0.32	0.39	1.00					
Ca^{2+}	0.40	**0.60**	**0.81**	0.33	0.19	0.01	**0.51**	1.00				
Si	**0.57**	0.18	0.38	0.45	**0.55**	0.43	0.04	0.18	1.00			
pH	0.17	**0.54**	0.48	**0.67**	0.04	0.18	0.22	0.44	0.23	1.00		
F^-	0.32	0.16	0.27	0.18	0.01	0.27	0.47	0.24	0.32	0.16	1.00	
Sr^{2+}	0.10	**0.52**	0.40	0.49	0.02	0.25	0.37	0.45	0.24	**0.84**	0.00	1.00

Table 4. 10 Varimax rotated factor loadings – Cretaceous aquifer

Component/Factor	1	2	3	4
Cl^-		**0.87**		
NO_3^-	**0.53**		**0.67**	
SO_4^{2-}	(0.32)	**0.44**	**0.76**	
HCO_3^-	**0.70**	**0.45**		
Na^+		**0.92**		
K^+		(0.30)		**0.79**
Mg^{2+}			**0.41**	**0.78**
Ca^{2+}	(0.30)		**0.82**	
Si		**0.75**		
pH	**0.94**			
F^-	(0.34)		**0.59**	**0.51**
Sr^{2+}	**0.48**			

Factor analysis sometimes suffers from its inability to separate source influences that are collinear in time or space in certain complex monitoring locations. In other words, multiple processes/sources, which have nearly the same chemical composition may be smeared together into a single, common factor [146].

4.7 Geochemical modeling (inverse modeling approach)

4.7.1 Quaternary aquifer

In Quaternary formations, wells are generally shallow and groundwater flow direction follows the topographic contour. Two flow paths are considered for calculating mole transfer values in this aquifer. The flow lines are shown in Fig 4.6.

Flow path 1: Mannadipet (Q-22) to Thirubhuvanai (Q-23)

In the first instance the constraints and phases chosen are commonly present ions and their associated minerals. Summary of the model parameters are given in table 4.11. Since K-feldspar and Albite are known to be present in this region, they are forced to be present in all the model solutions. First run of these parameters has led to 15 solutions. The phases and constraints are further refined to yield better solutions. Since the facies of both these waters are same that is Na-Mg-HCO_3-Cl, ion exchange can be ignored as this would have changed the facies of the water. Aluminum is a trace ion and present in equal concentration so it was also ignored from the constraints list. Similarly pyrite was ignored as there is no pH change observed between these two wells. Pyrite oxidation leads to decrease in the pH as shown by the following reaction [89];

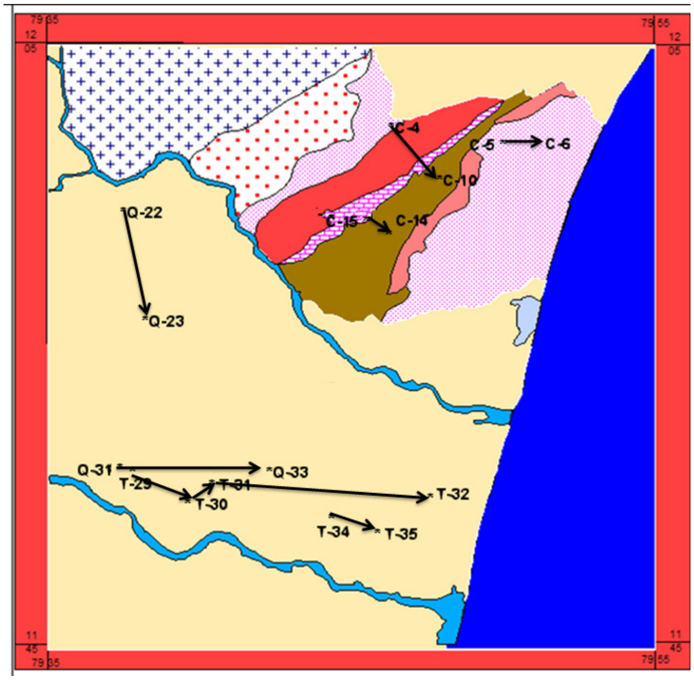

Fig. 4. 6 Flow paths identified for inverse modeling

$FeS_2 + 3.75\ O_2 + 3.5\ H_2O \leftrightarrow Fe(OH)_3 + 2\ SO_4^{2-} + 4\ H^+$ (4.9)

On the other hand, Aragonite was included in the phases as it was noted that Sr^{2+} has increased from 0.9 to 1.7 ppm and there is no phase accounting for this increase. The revised summary is given in Table 4.11 (revised). This has led to 5 solutions and given in Table 4.12.

Table 4. 11 Summary of constraints and phases used for modeling (Quaternary aquifer)

Flow path -1	**Revised**	**Flow path-2**
WELLS	WELLS	WELLS
Initial Well: Mannadipattu (Q-22)	Mannadipattu (Q-22)	Initial Well: Karayanpathur (Q-31)
Final Well : Thirubhuvanai (Q-23)	Thirubhuvanai (Q-23)	Final Well: Kaduvanur (Q-33)
PARAMETERS	**PARAMETERS**	**PARAMETERS**
Mixing: No	Mixing: No	Mixing: No
Evaporation: No	Evaporation: No	Evaporation: No
Rayleigh Calcs: No	Rayleigh Calcs: No	Rayleigh Calcs: No
Exchange: Ca/Na		
CONSTRAINTS (8)	**CONSTRAINTS (7)**	**CONSTRAINTS (7)**
Carbon	Carbon	Carbon
Sulfur	Sulfur	Sulfur
Calcium	Calcium	Calcium
Aluminum	Magnesium	Magnesium
Magnesium	Sodium	Sodium
Sodium	Potassium	Potassium
Potassium	Chloride	Chloride
Chloride		
PHASES (10)	PHASES (9)	PHASES (9)
CALCITE	CALCITE	CALCITE
+K-SPAR	+K-SPAR	+K-SPAR
GYPSUM	CO2 GAS	CO2 GAS
NaCl	DOLOMITE	DOLOMITE
CO2 GAS	Ca-MONT	Ca-MONT
DOLOMITE	+ALBITE	+ALBITE
EXCHANGE	ARAGONIT	ARAGONIT
PYRITE	GYPSUM	GYPSUM
Ca-MONT	NaCl	NaCl
+ALBITE		

Model 1 and 2 can be ignored as there are replicates of model 4 and 5 with only a change of one phase (Calcite instead of Aragonite). Among model 3, 4 and 5, model 3 can be ignored as there is addition of CO_2 shown (+ 0.63) and from the saturation index calculations, there was no change in the Pco_2 values (Table 4.4). Therefore model 3 can be ignored.

Between model 4 and 5, model 4 indicates precipitation of Aragonite which seems improbable as the SI of Aragonite increases from Q-22 to Q-23 (from - 0.44 to + 0.2) which suggests Aragonite dissolution. Therefore model 5 found to be best plausible solution. This is also supported by the fact that increase in Sr^{2+} concentration (0.9 to 1.7 ppm) which is nearly doubled from Q-22 to Q-23.

In most sedimentary aquifers, the strontium levels are primarily controlled by the reaction of groundwater with carbonate or sulphate minerals present. Dissolution of minerals like Aragonite or Gypsum, or evaporite deposits or mixing of meteoric water with the interstitial water are the common sources of strontium [110]. High Sr^{2+} concentration in groundwater (Q-23) can be attributed to recrystallisation of Aragonite. Aragonite dissolves in water and re-precipitates forming stable Calcite form (inversion of crystal structure) releasing Sr^{2+} into groundwater. This happens because Sr^{2+} fits readily in the orthorhombic Aragonite structure but not in rhombohedral Calcite structure [147].

Table 4. 12 NETPATH output for flow path 1 (Quaternary aquifer)

MODEL		**1**	**MODEL**		**2**	**MODEL**		**3**
CALCITE		-0.59	CALCITE		0.64	K-SPAR	+	0.01
K-SPAR	+	0.01	K-SPAR	+	0.01	CO2 GAS		0.64
CO2 GAS		1.22	DOLOMITE		0.68	DOLOMITE		0.68
DOLOMITE		0.68	Ca-MONT		-7.32	Ca-MONT		-3.51
ALBITE	+	1.03	ALBITE	+	1.03	ALBITE	+	1.03
GYPSUM		0.11	GYPSUM		0.11	GYPSUM		0.11
NaCl		1.36	NaCl		1.36	NaCl		1.36
MODEL		**4**	**MODEL**		**5**			
K-SPAR	+	0.01	K-SPAR	+	0.01			
CO2 GAS		1.22	DOLOMITE		0.68			
DOLOMITE		0.68	Ca-MONT		-7.32			
ALBITE	+	1.03	ALBITE	+	1.03			
ARAGONIT		-0.59	ARAGONIT		0.64			
GYPSUM		0.11	GYPSUM		0.11			
NaCl		1.36	NaCl		1.36			

Flow path 2: Karayampathur (Q-31) to Kaduvanur (Q-33)

This flow path considers Karayampathur (Q-31) as recharging water and Kaduvanur (Q-33) discharging water. Even though Mel Parikkalpet falls in the same flow line it was not considered for modeling as the influence of backwater is suggested from the hydrochemical trends as well as from ionic ratios (section 4.2 and 4.3). The model input conditions were maintained similar as shown by table 4.11 (revised). The NETPATH output yielded 5 solutions (Table 4.13). Among the 5 solutions generated, two can be ignored as there is only a difference of one phase (i.e. Calcite and Aragonite). Since Aragonite, Dolomite and Calcite are found to be close to saturation from saturation index calculations (Table 4.2). It is possible that these minerals may precipitate. The

Pco$_2$ has shown substantially decrease in Q-33, which infer addition of CO$_2$. The mole transfer values of K-spar, Dolomite, Gypsum and NaCl remain the same in all the solutions. Based on these observations, models 2, 3 and 5 can be ruled out. Between model 1 and 4, precipitation of Calcite seems probable as the SI value changes from 0.4 to 0.2. So model 1 seems to be the best possible solution. The increase in Sr^{2+} also supports Calcite precipitation rather than Aragonite precipitation. The Sr^{2+} might have derived from Gypsum mineral in this case.

Table 4. 13 NETPATH output for flow path 2 (Quaternary aquifer)

MODEL		1		MODEL		2		MODEL		3	
CALCITE		-0.59		CALCITE		-0.38		K-SPAR	+	-0.14	*
K-SPAR	+	-0.14	*	K-SPAR	+	-0.14	*	CO2 GAS		-0.38	
CO2 GAS		0.21		DOLOMITE		0.68		DOLOMITE		0.68	
DOLOMITE		0.68		Ca-MONT		-1.27		Ca-MONT		-3.55	
ALBITE	+	-0.94	*	ALBITE	+	-0.94	*	ALBITE	+	-0.94	*
GYPSUM		0.53		GYPSUM		0.53		GYPSUM		0.53	
NaCl		4.86		NaCl		4.86		NaCl		4.86	
MODEL		4		MODEL		5					
K-SPAR	+	-0.14	*	K-SPAR	+	-0.14	*				
CO2 GAS		0.21		DOLOMITE		0.68					
DOLOMITE		0.68		Ca-MONT		-1.27					
ALBITE	+	-0.94	*	ALBITE	+	-0.94	*				
ARAGONIT		-0.59		ARAGONIT		-0.38					
GYPSUM		0.53		GYPSUM		0.53					
NaCl		4.86		NaCl		4.86					

(* constraint ignored)

4.7.2 Tertiary aquifer

Among Tertiary aquifer, 4 flow lines are considered for modeling the mineral transfer. Sornavur to Kalinjikuppam (T-29 to T-30), Kalinjikuppam to Karayampathur (T-30 to T-31), Karayampathur to Krishnapuram (T-31 to T-32) and Thirupanampakkam to Bahur (T-34 to T-35). The flow lines are shown in Fig. 4.6. The list of constraints (7 number) and phases (9 numbers) included in model calculations are given in Table 4.14.

Flow path 1: Sornavur to Kalinjikuppam (T-29 to T-30)

From the NETPATH output it can be found that 4 solutions exist for flow path-1, Sornavur to Kalinjikuppam (T-29 to T-30). The mole transfer values for Halite, K-spar, Gypsum and Dolomite are same in all the solutions (Table 4.15). Since the groundwater facies has remained same from T-29 to T-30, the ion exchange can be ignored, hence models 1 and 2 are invalid.

Both models 3 and 4 seem feasible as the Aragonite and Calcite shows precipitation which is in line with the saturation of these minerals (Table 4.2). Between Aragonite and Calcite, Aragonite precipitation seems improbable as Sr^{2+} concentration shows an increase. Therefore model 4 can be best possible solution.

Table 4. 14 Summary of constraints and phases used for modeling (Tertiary aquifer)

Flow Path 1	Flow Path 2	Flow Path 3	Flow Path 4
WELLS	WELLS	WELLS	WELLS
Initial well: Sornavur	Kalinzhikuppam	Karayampathur	Thirupanampakkam
Final well: Kalinzhikuppam	Karayampathur	Krishnapuram	Bahur
PARAMETERS	PARAMETERS	PARAMETERS	PARAMETERS
Mixing: No	Mixing: No	Mixing: No	Mixing: No
Evaporation: No	Evaporation: No	Evaporation: No	Evaporation: No
Rayleigh Calcs: No	Rayleigh Calcs: No	Rayleigh Calcs: No	Rayleigh Calcs: No
Exchange: Ca/Na	Exchange: Ca/Na	Exchange: Ca/Na	Exchange: Ca/Na
CONSTRAINTS (7)	CONSTRAINTS (7)	CONSTRAINTS (7)	CONSTRAINTS (7)
Carbon	Carbon	Carbon	Carbon
Sulfur	Sulfur	Sulfur	Sulfur
Calcium	Calcium	Calcium	Calcium
Magnesium	Magnesium	Magnesium	Magnesium
Sodium	Sodium	Sodium	Sodium
Potassium	Potassium	Potassium	Potassium
Chloride	Chloride	Chloride	Chloride
PHASES (9)	PHASES (9)	PHASES (9)	PHASES (9)
+ALBITE	+ALBITE	+ALBITE	+ALBITE
ARAGONIT	ARAGONIT	ARAGONIT	ARAGONIT
CALCITE	CALCITE	CALCITE	CALCITE
CO2 GAS	CO2 GAS	CO2 GAS	CO2 GAS
DOLOMITE	DOLOMITE	DOLOMITE	DOLOMITE
EXCHANGE	EXCHANGE	EXCHANGE	EXCHANGE
GYPSUM	GYPSUM	GYPSUM	GYPSUM
+K-SPAR	+K-SPAR	+K-SPAR	+K-SPAR
NaCl	NaCl	NaCl	NaCl

Table 4. 15 NETPATH output for flow path 1– Tertiary aquifer

MODEL		1	MODEL		2	MODEL		3	MODEL		4
ALBITE	+	1.08	ALBITE	+	1.08	ARAGONIT		-0.16	CALCITE		-0.16
ARAGONIT		-0.70	CALCITE		-0.70	CO2 GAS		-0.54	CO2 GAS		-0.54
DOLOMITE		0.16	DOLOMITE		0.16	DOLOMITE		0.16	DOLOMITE		0.16
EXCHANGE		-0.58	EXCHANGE		-0.58	EXCHANGE		-0.04	EXCHANGE		-0.04
GYPSUM		-0.01	GYPSUM		-0.01	GYPSUM		-0.01	GYPSUM		-0.01
K-SPAR	+	0.02	K-SPAR	+	0.02	K-SPAR	+	0.02	K-SPAR	+	0.02
NaCl	+	0.47	NaCl	+	0.47	NaCl	+	0.47	NaCl	+	0.47

Flow path 2: Kalinjikuppam to Karayampathur (T-30 to T-31)

In this flow path, the NETPATH output lists five solutions (Table 4.16). The facies of water change from Na-Ca-HCO_3-Cl type to Na-Mg-HCO_3-Cl type indicating increase of Mg^{2+} and decrease of Ca^{2+} along the flow path. This could be possible by ion exchange of Na^{+} with Ca^{2+}. Models 1 and 2 indicate precipitation of Aragonite or Calcite which contradicts the SI values

(Table 4.2). Similarly model 3 indicates addition of CO_2 gas, which would increase Log Pco_2 value significantly. This also doesn't match with the increase in Log Pco_2 value. And also the Sr^{2+} increase is found to be 0.3 to 0.5 ppm. Based on these observations, model 4 seems to be the best possible solution.

Table 4. 24 NETPATH output for flow path 2– Tertiary aquifer

MODEL		1	MODEL		2	MODEL		3	MODEL		4	MODEL		5
ALBITE	+	1.11	ALBITE	+	1.11	ALBITE	+	0.5	ARAGONI		0.2	CALCITE		0.2
ARAGONI		-	CALCITE		-	CO2 GAS		1.1	CO2 GAS		0.8	CO2 GAS		0.8
CO2 GAS		1.38	CO2 GAS		1.38	DOLOMIT		0.0	DOLOMIT		0.0	DOLOMIT		0.0
DOLOMIT		0.01	DOLOMIT		0.01	EXCHANG		0.2	EXCHANG		0.5	EXCHANG		0.5
GYPSUM		0.21	GYPSUM		0.21	GYPSUM		0.2	GYPSUM		0.2	GYPSUM		0.2
K-SPAR	+	0.07	K-SPAR	+	0.07	K-SPAR	+	0.0	K-SPAR	+	0.0	K-SPAR	+	0.0
NaCl	+	0.77	NaCl	+	0.77	NaCl	+	0.7	NaCl	+	0.7	NaCl	+	0.7

Flow path 3: Karayampathur to Krishnapuram (T-31 to T-32)

In flow path Karayampathur to Krishnapuram (T-31 to T-32), only two solutions are found (Table 4.17). These solutions differ in Aragonite and Calcite phases. The hydrochemical facies point to increase in Ca^{2+} compared to Mg^{2+} and decrease in Sr^{2+} concentration. Therefore model 2 seems to be the best possible solution.

Table 4. 17 NETPATH output for flow path 3– Tertiary aquifer

MODEL		1	MODEL		2
ARAGONIT		-0.19	CALCITE		-0.19
CO2 GAS		0.30	CO2 GAS		0.30
DOLOMITE		0.26	DOLOMITE		0.26
EXCHANGE		-0.37	EXCHANGE		-0.37
GYPSUM		-0.03	GYPSUM		-0.03
K-SPAR	+	-0.10 *	K-SPAR	+	-0.10*
NaCl	+	0.92	NaCl	+	0.92

(* constraint ignored)

Flow path 4: Thirupanampakkam to Bahur (T-34 to T-35)

In flow path Thirupanampakkam to Bahur (T-34 to T-35), four solutions are found. Among different phases Halite, K-Spar, Albite and Gypsum show same mole transfer values (Table 4.18).

Table 4. 18 NETPATH output for flow path 4– Tertiary aquifer

MODEL		1	MODEL		2	MODEL		3	MODEL		4
ALBITE	+	0.22	ALBITE	+	0.22	ARAGONIT		-0.33	CALCITE		-0.33
ARAGONIT		-0.43	CALCITE		-0.43	CO2 GAS		-0.11	CO2 GAS		-0.11
DOLOMITE		-0.23	DOLOMITE		-0.23	DOLOMITE		-0.23	DOLOMITE		-0.23
EXCHANGE		-0.51	EXCHANGE		-0.51	EXCHANGE		-0.41	EXCHANGE		-0.41
GYPSUM		-0.05	GYPSUM		-0.05	GYPSUM		-0.05	GYPSUM		-0.05
K-SPAR	+	0.02	K-SPAR	+	0.02	K-SPAR	+	0.02	K-SPAR	+	0.02

Model 2 and 4 are repetitive for minerals Calcite and Aragonite. Model 3 shows removal of CO_2 gas, which would lead to decrease in Log Pco_2 value. This is in contrary to the saturation index (Table 4.4), wherein Log Pco_2 increases from - 2.04 to - 1.41. Based on the above observations, it can be concluded that model 1 is best fit for the observed change in water composition.

4.7.3 Cretaceous aquifer

In Cretaceous aquifer three flow lines are considered for inverse modeling. These flow lines include Ozhindiapattu to Sanjivinagar (C-4 to C-10), Mathur to Kanagachettikulam (C-5 to C-6) and Sedarapet to Karasur (C-15 to C-14). The flow lines are shown in Fig. 4.6. The list of constraints and phases are given in table 4.19.

Flow path 1: Ozhindiapattu (C-4) to Sanjivinagar (C-10)

In flow line Ozhindiapattu to Sanjivinagar (C-4 to C-10), NETPATH calculations yielded nine solutions (Table 4.20). Models 2-4 are repetitive of models 5-7 (interchange of Calcite and Aragonite). Model 3 and 7 can be ignored as the pH is slightly increased and DO is 3.3 ppm which would not allow Pyrite to precipitate. Pyrite oxidizes to change the water pH slightly acidic (equation 4.9). Model 4 and 8 can be ignored as $Ca^{2+}/Ca^{2+}+SO_4^{2-}$ ratio suggests Calcite/Aragonite precipitation (Table 4.1). Saturation index of Aragonite and Calcite suggest that these minerals are added along the flow (Table 4.2), therefore model nos. 1, 2, 5 and 6 can be ignored. The best fit solution is model 9.

Flow path 2: Mathur (C-5) to Kanagachettikulam (C-6)

In flow line Mathur to Kanagachettikulam (C-5 to C-6) NETPATH yielded 16 solutions (Table 4.21). Models 5-8, 12-14, 15 and 16 are repetitive (interchange of Calcite and Aragonite). Model 4 shows precipitation of Gypsum which contradicts the negative value for saturation index of Gypsum (Table 4.4). Therefore model 4 can be ignored. Model nos. 3, 11 and 15 show both Goethite and Pyrite minerals responsible for occurrence of iron in water. The mole transfer values in these models suggest that iron should maintain a constant value along the flow, which is not the case found.

The iron concentration reduces from 58 to 18 ppb indicating precipitation of iron minerals. Therefore models 3, 11 and 15 can be ignored. Models 9 and 10 include Anorthite which doesn't occur commonly in this region, so these models can be ignored. Possibility of pyrite precipitation is not feasible due to the presence of DO in groundwater. Based on these observations, model 2 is found to be best solution.

Table 4. 19 Summary of constraints and phases used for modeling (Cretaceous aquifer)

FLOW PATH 1	FLOW PATH 2	FLOW PATH 3	REVISED
WELLS	WELLS	WELLS	WELLS
Initial well: Ozhindiapattu	Initial well: Mathur	Initial well: Sedarapet	Sedarapet
Final well: Sanjivinagar	Final well: Kanagachettikulam	Final well: Karasur	Karasur
PARAMETERS	PARAMETERS	PARAMETERS	PARAMETERS
Mixing: No	Mixing: No	Mixing: No	Mixing: No
Evaporation: No	Evaporation: No	Evaporation: No	Evaporation: No
Rayleigh Calcs: No	Rayleigh Calcs: No	Rayleigh Calcs: No	Rayleigh Calcs: No
Exchange: Ca/Na	Exchange: Ca/Na	Exchange: Ca/Na	Exchange: Ca/Na
CONSTRAINTS (8)	CONSTRAINTS (8)	CONSTRAINTS (8)	CONSTRAINTS (7)
Carbon	Carbon	Carbon	Carbon
Sulfur	Sulfur	Sulfur	Sulfur
Calcium	Calcium	Calcium	Calcium
Magnesium	Magnesium	Magnesium	Magnesium
Sodium	Sodium	Sodium	Sodium
Potassium	Potassium	Potassium	Potassium
Chloride	Chloride	Chloride	Chloride
Iron	Iron	Iron	
PHASES (12)	PHASES (11)	PHASES (12)	PHASES (10)
+ALBITE	+ALBITE	+ALBITE	+ALBITE
+ANORTH	+ANORTH	+ANORTH	+ANORTH
ARAGONIT	ARAGONIT	ARAGONIT	ARAGONIT
CALCITE	CALCITE	CALCITE	CALCITE
CO2 GAS	DOLOMITE	CO2 GAS	CO2 GAS
DOLOMITE	EXCHANGE	DOLOMITE	DOLOMITE
EXCHANGE	+K-SPAR	EXCHANGE	EXCHANGE
+K-SPAR	NaCl	+K-SPAR	+K-SPAR
NaCl	GYPSUM	NaCl	NaCl
GYPSUM	PYRITE	GYPSUM	GYPSUM
PYRITE	GOETHITE	PYRITE	
GOETHITE		GOETHITE	

Flow path 3: Sedarapet (C-15) to Karasur (C-14)

In flow line Sedarapet to Karasur (C-15 to C-14), based on the given input conditions NETPATH found 27 solutions. Since the outputs are high it is difficult to interpret the probable chemical reaction, hence constraint and phases are modified, given in the table 4.19 (Revised). Iron concentration is nearly constant between these waters (29 and 37 ppb), therefore one constraint (iron) and two associated phases (Goethite and Pyrite) were removed from model parameters.

Table 4. 20 NETPATH output for flow path 1– Cretaceous aquifer

MODEL		1	MODEL		4	MODEL		7
ARAGONIT		-0.21	ARAGONIT		1.08	CALCITE		-0.73
CO2 GAS		1.30	DOLOMITE		0.37	CO2 GAS		1.81
DOLOMITE		0.37	EXCHANGE		-0.55	DOLOMITE		0.37
EXCHANGE		-0.55	K-SPAR	+	0.20	EXCHANGE		-0.55
K-SPAR	+	0.20	NaCl		2.37	K-SPAR	+	0.20
NaCl		2.37	GYPSUM		-1.81	NaCl		2.37
GYPSUM		-0.51	PYRITE		0.65	PYRITE		-0.26
PYRITE		0.0002	GOETHITE		-0.65	GOETHITE		0.26
MODEL		2	MODEL		5	MODEL		8
ARAGONIT		-0.21	CALCITE		-0.21	CALCITE		1.08
CO2 GAS		1.30	CO2 GAS		1.30	DOLOMITE		0.37
DOLOMITE		0.37	DOLOMITE		0.37	EXCHANGE		-0.55
EXCHANGE		-0.55	EXCHANGE		-0.55	K-SPAR	+	0.20
K-SPAR	+	0.20	K-SPAR	+	0.20	NaCl		2.37
NaCl		2.37	NaCl		2.37	GYPSUM		-1.81
GYPSUM		-0.51	GYPSUM		-0.51	PYRITE		0.65
GOETHITE		0.0002	PYRITE		0.0002	GOETHITE		-0.65
MODEL		3	MODEL		6	MODEL		9
ARAGONIT		-0.73	CALCITE		-0.21	CO2 GAS		1.08
CO2 GAS		1.81	CO2 GAS		1.30	DOLOMITE		0.37
DOLOMITE		0.37	DOLOMITE		0.37	EXCHANGE		-0.55
EXCHANGE		-0.55	EXCHANGE		-0.55	K-SPAR	+	0.20
K-SPAR	+	0.20	K-SPAR	+	0.20	NaCl		2.37
NaCl		2.37	NaCl		2.37	GYPSUM		-0.73
PYRITE		-0.26	GYPSUM		-0.51	PYRITE		0.11
GOETHITE		0.26	GOETHITE		0.0002	GOETHITE		-0.11

The revised set of data yielded 8 solutions (Table 4.22). Model 4 and 5 include Anorthite which is not common in this formation, so these models are ignored. The chemical facies changes from Mg –Ca type to Ca-Na type indicating reduction in Mg^{2+} concentration and increase in Na^{+} concentration. This change infers precipitation of Dolomite (section 4.2). Models 2, 5 and 8 are repetitive (interchange of Calcite for Aragonite). From Log Pco_2 values exsolution of CO_2 can be inferred (Table 4.4). Therefore models 3 and 6 can be ignored which shows positive mole transfer values for CO_2 gas. $Na^{+}/Na^{+}+ Cl^{-}$ ratio indicates that Albite weathering is feasible (Table 4.1). Since the Sr^{2+} concentration is nearly same in both the waters (C-15 and C-14), Aragonite dissolution can be minimum. Based on these observations, model 1 is seems to be the best possible solution.

Table 4. 21 NETPATH output for flow path 2– Cretaceous aquifer

MODEL		1	MODEL		5	MODEL		9	MODEL		13
ALBITE	+	1.96	ALBITE	+	1.96	ANORTH	+	0.98	ANORTH	+	0.98
ARAGONIT		0.26	CALCITE		0.26	ARAGONIT		0.26	CALCITE		0.26
DOLOMITE		-1.10	DOLOMITE		-1.10	DOLOMITE		-1.10	DOLOMITE		-1.10
EXCHANGE		0.47	EXCHANGE		0.47	EXCHANGE		1.45	EXCHANGE		1.45
K-SPAR	+	-0.09*	K-SPAR	+	-0.09*	K-SPAR	+	-0.09*	K-SPAR	+	-0.09*
NaCl		3.19	NaCl		3.19	NaCl		3.19	NaCl		3.19
GYPSUM		0.33	GYPSUM		0.33	GYPSUM		0.33	GYPSUM		0.33
PYRITE		0.00	PYRITE		0.00	PYRITE		0.00	GOETHITE		0.00
MODEL		2	MODEL		6	MODEL		10	MODEL		14
ALBITE	+	1.96	ALBITE	+	1.96	ANORTH	+	0.98	ANORTH	+	1.31
ARAGONIT		0.26	CALCITE		0.26	ARAGONIT		0.26	CALCITE		0.26
DOLOMITE		-1.10	DOLOMITE		-1.10	DOLOMITE		-1.10	DOLOMITE		-1.10
EXCHANGE		0.47	EXCHANGE		0.47	EXCHANGE		1.45	EXCHANGE		1.45
K-SPAR	+	-0.09*	K-SPAR	+	-0.09*	K-SPAR	+	-0.09*	K-SPAR	+	-0.09*
NaCl		3.19	NaCl		3.19	NaCl		3.19	NaCl		3.19
GYPSUM		0.33	GYPSUM		0.33	GYPSUM		0.33	PYRITE		0.17
GOETHITE		0.00	GOETHITE		0.00	GOETHITE		0.00	GOETHITE		-0.17
MODEL		3	MODEL		7	MODEL		11	MODEL		15
ALBITE	+	2.62	ALBITE	+	2.62	ANORTH	+	1.31	ARAGONIT		0.26
ARAGONIT		0.26	CALCITE		0.26	ARAGONIT		0.26	DOLOMITE		-1.10
DOLOMITE		-1.10	DOLOMITE		-1.10	DOLOMITE		-1.10	EXCHANGE		1.45
EXCHANGE		0.14	EXCHANGE		0.14	EXCHANGE		1.45	K-SPAR	+	-0.09*
K-SPAR	+	-0.09*	K-SPAR	+	-0.09*	K-SPAR	+	-0.09	NaCl		3.19
NaCl		3.19	NaCl		3.19	NaCl		3.19	GYPSUM		1.31
PYRITE		0.17	PYRITE		0.17	PYRITE		0.17	PYRITE		-0.49
GOETHITE		-0.17	GOETHITE		-0.17	GOETHITE		-0.17	GOETHITE		0.49
MODEL		4	MODEL		8	MODEL		12	MODEL		16
ALBITE	+	2.91	ALBITE	+	2.91	ANORTH	+	0.98	CALCITE		0.26
ARAGONIT		0.26	CALCITE		0.26	CALCITE		0.26	DOLOMITE		-1.10
DOLOMITE		-1.10	DOLOMITE		-1.10	DOLOMITE		-1.10	EXCHANGE		1.45
K-SPAR	+	-0.09*	K-SPAR	+	-0.09*	EXCHANGE		1.45	K-SPAR	+	-0.09*
NaCl		3.19	NaCl		3.19	K-SPAR	+	-0.09*	NaCl		3.19
GYPSUM		-0.14	GYPSUM		-0.14	NaCl		3.19	GYPSUM		1.31
PYRITE		0.24	PYRITE		0.24	GYPSUM		0.33	PYRITE		-0.49
GOETHITE		-0.24	GOETHITE		-0.24	PYRITE		0.00	GOETHITE		0.49

(* constraint ignored)

4.7.4 Distribution of species

Activity coefficients of multivalent ions are most susceptible to ionic strength changes and a similar dependence on charge exists for complex ion stability. It is seen that free Ca^{2+}, Mg^{2+}, SO_4^{2-} and carbonate concentrations are reduced to a variable extent even in relatively dilute groundwater, while monovalent ions are generally unassociated to levels as high as seawater [148]. The most important ion pairs in natural waters are $CaCO_3^0$ and $CaSO_4^0$ which are generally present in significant amounts and $MgSO_4^0$, $MgHCO_3^+$ and $CaHCO_3^+$ in trace or negligible quantities.

Distribution of alkaline earth metals, Mg^{2+} Ca^{2+} and Sr^{2+} is analyzed along the flow path 3, Sedarapet to Karasur (C-15 to C-14) in Cretaceous formation. The calculated speciation percentages by NETPATH are given in table 4.23.

Table 4. 22 NETPATH output for flow path 3– Cretaceous aquifer

MODEL		1	MODEL		2	MODEL		3	MODEL		4
ALBITE	+	1.00	ALBITE	+	1.00	ALBITE	+	2.03	ANORTH	+	0.50
ARAGONIT		0.52	CALCITE		0.52	CO2 GAS		0.52	ARAGONIT		0.52
DOLOMITE		-1.37	DOLOMITE		-1.37	DOLOMITE		-1.37	DOLOMITE		-1.37
EXCHANGE		-0.53	EXCHANGE		-0.53	EXCHANGE		-1.04	EXCHANGE		-0.02
K-SPAR	+	0.06	K-SPAR	+	0.06	K-SPAR	+	0.06	K-SPAR	+	0.06
NaCl		5.62	NaCl		5.62	NaCl		5.62	NaCl		5.62
GYPSUM		5.61	GYPSUM		5.61	GYPSUM		5.61	GYPSUM		5.61
MODEL		5	MODEL		6	MODEL		7	MODEL		8
ANORTH	+	0.50	ANORTH	+	1.02	ARAGONIT		1.02	CALCITE		1.02
CALCITE		0.52	CO2 GAS		0.52	CO2 GAS		-0.50	CO2 GAS		-0.50
DOLOMITE		-1.37	DOLOMITE		-1.37	DOLOMITE		-1.37	DOLOMITE		-1.37
EXCHANGE		-0.02	EXCHANGE		-0.02	EXCHANGE		-0.02	EXCHANGE		-0.02
K-SPAR	+	0.06	K-SPAR	+	0.06	K-SPAR	+	0.06	K-SPAR	+	0.06
NaCl		5.62	NaCl		5.62	NaCl		5.62	NaCl		5.62
GYPSUM		5.61	GYPSUM		5.61	GYPSUM		5.61	GYPSUM		5.61

From these percentage values it is be found that most common species are M^{2+} (dissociated form), $MHCO_3^+$, MCO_3 and MSO_4, (associated forms) which changes their relative proportion depending up on the concentrations of counter anion and pH. Among different species, dissociated form (free ion) is present in highest percentage followed by MSO_4 then $MHCO_3^+$ then MCO_3. The undissociated forms together make up to 30%.

Table 4. 23 Speciation of Mg2+, Ca2+, Sr2+ along flow path 3 (Cretaceous aquifer)

	Location	units	Sedarapet (C-15)	Karasur (C-14)
		Measured values		
	Mg^{2+}	ppm	43	10.2
	Ca^{2+}	ppm	53	264
	Sr^{2+}	ppm	1.6	1.5
	SO_4^{2-}	ppm	32	570
	HCO_3^-	ppm	366	265
		Modeled percentages		
Calcium	M^{2+}	%	93	77.1
	MCO_3	%	0.3	0.1
	$MHCO_3^+$	%	5	2.4
	MSO_4	%	2.1	20.3
Magnesium	M^{2+}	%	93	76.7
	MCO_3	%	0.1	<0.01
	$MHCO_3^+$	%	4.4	2.3
	MSO_4	%	2.8	21
Strontium	M^{2+}	%	91	70.4
	MCO_3	%	0.1	0.05
	$MHCO_3^+$	%	6.8	4.5
	MSO_4	%	2.1	25.5

Among the three alkaline earth metals studied, Sr^{2+} shows the highest percentage of undissociated forms. Strontium forms smaller hydration sphere compared to calcium and magnesium due to low ionic potential. This helps in forming stable ternary surface complexes with carbonate [149]. The low solubility of undissociated forms of strontium facilitates longer migration without being removed from the system by either precipitation or absorption on the aquifer material.

4.8 Possible mechanism for arsenic release into groundwater

Arsenic is found in most of the groundwater of this region in the range 0.5 to 41.9 ppb. In a few groundwater samples the levels are higher than drinking water limit of 10 ppb [150]. One sample from each Quaternary and Tertiary formations and three samples from Cretaceous formation showed higher levels of arsenic (13.7 - 41.9 ppb). The concentration of arsenic is particularly high in Cretaceous formation which is one of the most exploited aquifers of this region. Different mechanisms of arsenic mobilization from rocks and sediments in to groundwater have been proposed by researchers [44, 151, 152], however there are mainly three postulates on arsenic contamination which are commonly referred to, viz.,

1. Displacement of arsenic from sediment by phosphates from chemical fertilizers.
2. Oxidation of arsenopyrite as a consequence of lowering of groundwater levels
3. Reduction of arsenic containing iron oxyhydroxide in the presence of biodegradable organic matter

Impact of chemical fertilizers leads to high amounts of phosphate and nitrates in groundwater. Low concentrations of nitrate and phosphate in groundwater indicate minimum contribution from chemical fertilizers. From the correlation of arsenic with nitrate and phosphate, it can be observed that arsenic is not positively correlated. Based on these observations, first postulate can be ruled out.

Occurrence of Marcasite (a polymorph of Pyrite) is reported in this region [51]. Therefore there is a chance of arsenic resulting from Pyrite oxidation. But, Pyrite oxidation also increases dissolved sulphate concentration and decrease in pH of groundwater. The sulphate levels are less in groundwater (< 60 ppm) except in C-11 (570 ppm), and pH is neutral (6.9 to 7.3) indicating that Pyrite oxidation may not be taking place in the present case. Similar inference is also shown in the case of characteristic ionic ratios (Section 4.3) and geochemical modeling (section 4.7).

In reductive dissolution mechanism, iron oxyhydroxide reduces facilitating the adsorbed arsenic on sediments release in to groundwater. This reduction can be driven by microbial action. Most of the arsenic is found in Cretaceous aquifer, and the groundwater shows low DO (< 2 ppm) indicating reducing environment of the aquifer. Presence of hydrogen sulfide odor at the sampling sites, low dissolved sulfates and presence of Goethite in sediments (Fig. 5.2), infer reductive dissolution of iron oxyhydroxide could be the governing process for the observed increase in arsenic. Prevalence of reduction condition of the aquifer is further supported by presence of SRB in groundwater (section 3.5.2). At the initial stages of sulphate reduction, some of the arsenic released from Goethite by SRB may be co-precipitated as authigenic sulfide, but once sulfide is consumed arsenic starts building up in groundwater. Similar situations of microbial mediated transformations were reported elsewhere by researchers [153, 154].

4.9 Inference from microbial studies

Besides addressing water quality issues, microbial evaluation of groundwater is also useful in understanding the geochemical behavior of the aquifer. Microbes play a significant role in affecting the leaching and transport of toxic elements in deeper subsurface horizons [155]. In particular, SRB facilitates the reduction of heavy metal and metalloids from higher to lower oxidation states and biodegradation of organic pollutants [156]. SRB also plays an important role in remediation of contaminated groundwater and soil.

In the study area it is found that the non-disinfected groundwater has high bacterial loads (TVC: 1.8 X 103 to 3.3 X 104 cfu/mL and presence of E. coli in half of the samples analyzed. No correlation is found between TVC and E. coli amounts indicated that the E. coli are not always present as a component of bacterial load, even when total bacterial numbers were high for a given sample. This would suggest that the observed total bacterial may have originated from environmental sources such as soil/organic debris, and not from direct fecal contamination. High variation in the E. coli could be due to presence of varying amounts of organic content or clayey nature of the sediments or longer residence times of the groundwater which can be envisaged from the highly heterogeneous nature of sediments in this region as mentioned in the geology of the region. There is no strong correlation observed between major ions with presence of bacteria in the groundwater. However, concentration of nutrients such as NO_3^- and PO_4^{3-} are very low in the affected samples, which also confirms that the bacterial proliferation is favored in the groundwater.

The production and proliferation of microbes depend on the favorable conditions prevailing in the surroundings, for e.g. presence of dissolved oxygen [157], water chemistry such as pH, temperature, salt content and organic carbon contents [158]. To evaluate the existing conditions, correlations of microbial content with well depth, DO, TOC are studied. Microbes included are E. coli and SRB, and no aquifer-wise analysis was done.

A decreasing trend is seen in the case of E. coli with well depth whereas no such trend is observed for SRB (Fig. 4.7 a). All the samples tested positive for SRB belong to either Tertiary or Cretaceous sedimentary formations. No sample from Quaternary alluvium showed the presence of SRB. In general it is observed that the diversity and number of microorganisms diminish with depth from the surface of the soil to rock strata below the aquifer. This is because, with depth the environment becomes increasingly hostile for bacterial life [159].

Correlation of E. coli and SRB with DO is shown in Fig. 4.7 b. It can be seen from the figure that in general E. coli shows increasing trend with DO whereas SRB doesn’t show any particular trend with DO. E. coli is also found to be present in low DO groundwater which indicates that these are anaerobic or microaerophilic in nature. Condition of low DO can considerably extend the survival of these microorganisms in water and can act as potential reservoirs for pathogens of faecal origin [160].

Similarly, variation of these bacteria with TOC is shown in Fig.4.8. It can be found that E. coli shows a positive correlation with TOC whereas SRB doesn’t show any particular trend and mostly present in samples with low TOC. Association of coliform contaminants with organic matter is also reported by other researchers [161].

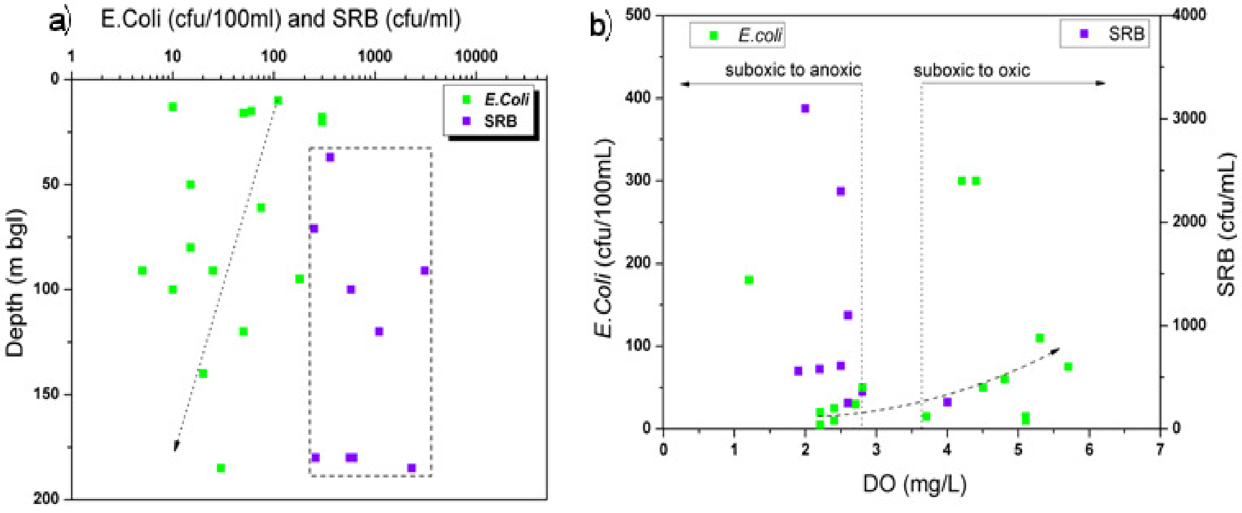

Fig. 4. 7 Correlations of microbial populations with a) well depth and b) DO, dotted lines is eye guide to the data

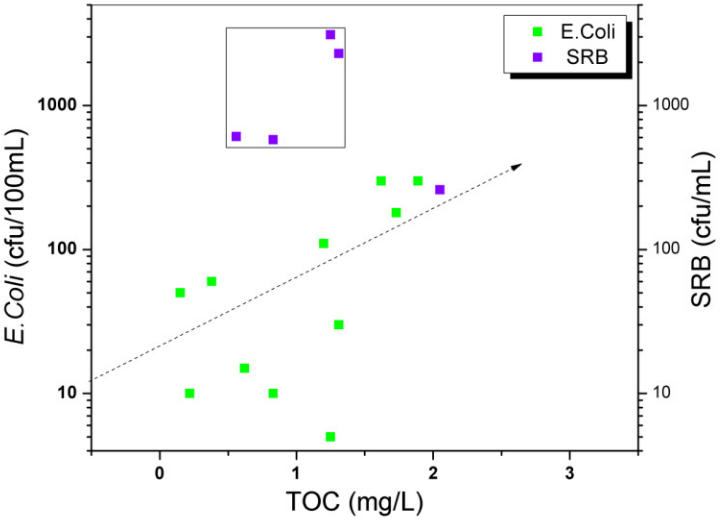

Fig. 4. 8 Correlation between microbial populations and TOC, arrow is eye-guide to E.coli data

4.10 Environmental isotope indicators

Groundwater recharge and dynamics in this region are complex phenomena to understand as the groundwater resources are influenced by the dual monsoon system, contribution of rivers, tanks and agricultural return flows, and proximity to sea. Environmental isotope indicators have been widely used for assessing such factors or processes as each member has its characteristic isotopic signature [27].

4.10.1 Stable isotopes of water (^{2}H & ^{18}O)

Rainwater

Precipitation is the main source for surface and subsurface water. The stable isotope ratios of $^2H/^1H$ and $^{18}O/^{16}O$ in precipitation are affected not only by moisture sources but also by the continental and altitude effects [27]. In this region the altitude difference is about 30 m, and lateral spread from coast is about 25 kms, therefore these factors may not influence isotopic composition of precipitation significantly. However, amount effect and impact of dual monsoon system play a role in controlling the isotopic signature of precipitation.

It is important to isotopically characterize the NEM as much of the precipitation is contributed by this (section 1.9.1). A plot of δ^2H versus $\delta^{18}O$ of precipitation samples from NEM is shown in Fig. 4.10. The best fit equation for the LMWL is found to be,

$$\delta^2 H \ = 7.7\ (\pm 0.93) \times \delta^{18}O + 4.2\ (\pm 5.3)[\mathrm{R}\ =\ 0.87, \mathrm{N} = 22] \qquad (4.10)$$

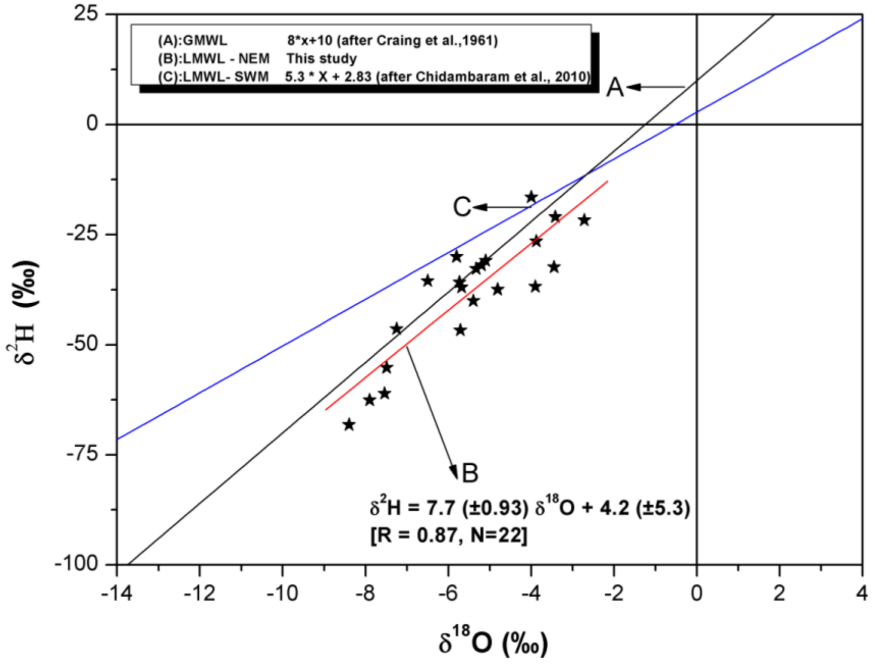

Fig. 4. 9 Plot of δ^2H versus $\delta^{18}O$ precipitation samples from North East Monsoon (NEM), South West Monsoon (SWM) and Global Meteoric Water Line (GMWL)

In general LMWL falls close to the GMWL with slight deviation, which results from differences in climatic factors such as air temperature, secondary evaporation, seasonality of precipitation and moisture source [27, 31]. It can be found from the plot (Fig. 4.9) that the slope of LMWL is close to GMWL, indicating that precipitation is not modified by secondary evaporation significantly.

Lower temperatures prevailing during November – January months in this region might be limiting the secondary evaporation of the rain drop during its descent. Y-intercept is found to be lesser than GMWL value of 10, which signifies contribution of re-circulated water. This region has a large number of tanks and in addition intensive agricultural activities, which contribute significant moisture to the atmosphere. Similar observations were noted by other researchers [162, 163].

Isotope contours (δ^2H and $\delta^{18}O$) for groundwater from three aquifers are shown in Fig. 4.10 (a & b), which demonstrate that variations are similar for both the isotopes. From the contour map it can be visualized that Northeastern parts show depleted isotope values, which can be possible if groundwater is recharged by high amount rains such as storm events. Towards Western parts the isotopic value gets enriched. Also in Southern parts the enrichment is found which is still higher. This can be attributed to the contribution of surface water sources in this region, like backwater, tanks, streams and also agricultural return flows.

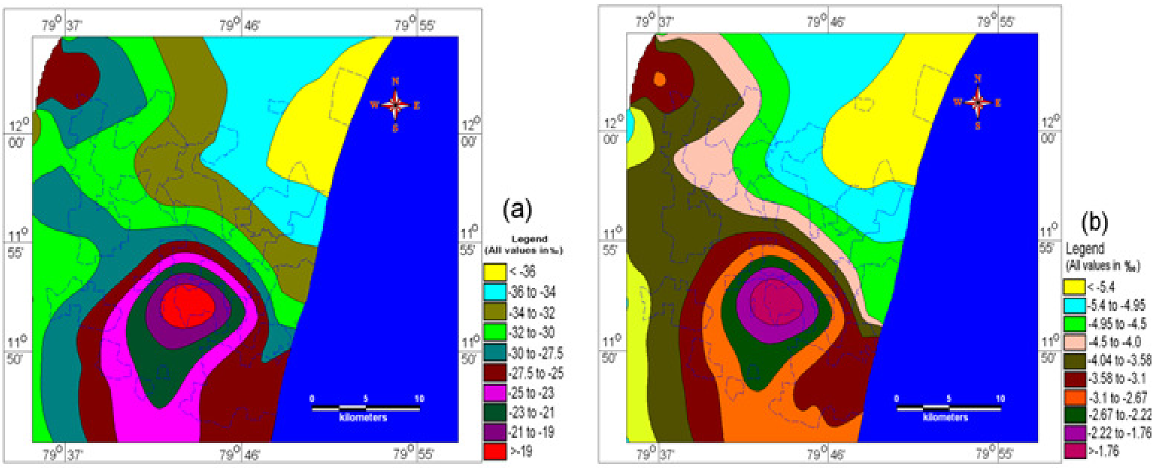

Fig. 4. 10 Contour map of (a) δ^2H and (b) $\delta^{18}O$ of groundwater samples from all aquifers

Quaternary aquifer

Isotopic composition of Quaternary samples range from -5.1 to -1.3‰ for $\delta^{18}O$ and -32.7 to -12.5‰ for δ^2H, which indicate that the groundwater is isotopically enriched. A wide range of isotope data in this aquifer indicates multiple sources of recharge to groundwater. The δ^2H versus $\delta^{18}O$ plot, shown in Fig. 4.11, indicates that all the Quaternary samples fall close to LMWL for NEM as compared to LMWL for SWM, indicating NEM as major contributor of groundwater recharge as compared to SWM. Best fit of the isotope data indicates that the samples are evaporated and fall on a line with a slope of 4.9. The evaporation line is given as;

$$\delta^2H \ = 4.95 \times \delta^{18}O - \ 11 (\mathrm{R} = 0.9, \mathrm{N}=12) \tag{4.11}$$

This suggests that groundwater is getting significant contribution from evaporated sources. The best fit line on extrapolation (dotted line in Fig. 4.11) provided recharging water isotopic composition which is -25.7 ‰ and -3.37 ‰ for δ^2H and δ^{18}O respectively. These values are similar to average isotope values of NEM (appendix 2.6). Broadly two groups of water are seen, group (a) less enriched and group (b) more enriched. This kind of grouping can be possible when the infiltration rates of recharge water are different or/and differential contribution of evaporated surface water.

Tertiary and Cretaceous aquifers

The isotope distribution in Tertiary aquifer ranges from - 6.5 to - 2.9 ‰ for δ^{18}O and - 22.5 to - 43.8 ‰ for δ^2H. This indicates relatively narrow distribution as compared to Quaternary aquifer. From the plot δ^2H versus δ^{18}O plot, shown in Fig. 4.13, it can be seen that sample data spread along the LMWL-NEM indicating predominant recharge from NEM and no significant evaporation during recharge. A few samples demonstrate enriched isotope values (T-9 to T-11) which could be due to surface water contribution at these locations or interconnection with Quaternary aquifer. In the case of Cretaceous aquifer, sample data lie on the LMWL-NEM with a few samples falling between both LMWLs, which show some component of recharge from SWM. Unlike Quaternary and Tertiary samples, Cretaceous samples demonstrate a very narrow spread of isotope data, indicating a common source of recharge.

The source of groundwater is further confirmed by d-excess values. If the d-excess values ranges between 8 and 10, it is assumed to be representative of primary precipitation. The d-excess value in the precipitation can be greater than ten, if the evaporation in the source region takes place under lower humidity [32]. Alternately, significant re-evaporation of local surface waters under low humidity creates vapor mass with high d-excess, if such vapor mixes with atmospheric reservoir and re-condenses, the resultant precipitation will have high d-excess [27]. Lower d-excess values (< 10) signify evaporation of rain water leaving the residual groundwater with lower d-excess values.

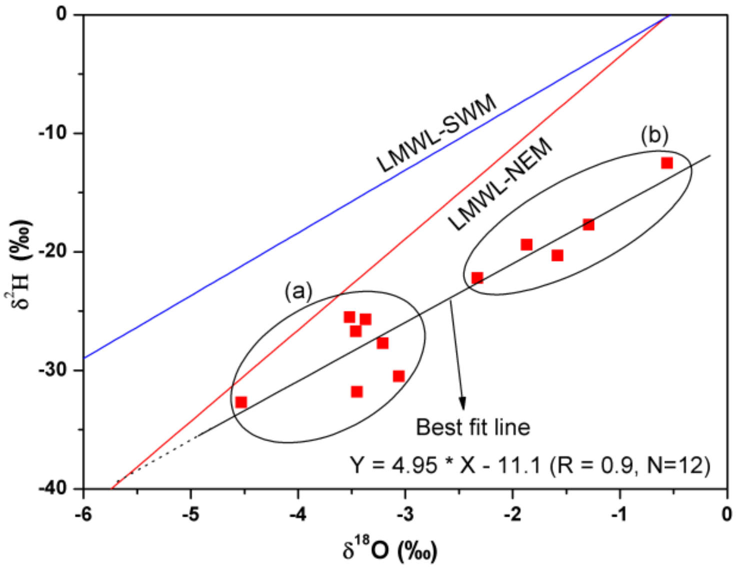

Fig. 4. 11 Plot of δ^2H versus δ^{18}O data of groundwater samples from Quaternary aquifer, (a) less evaporated, (b) more evaporated

Quaternary samples show d-excess values ranging from -8 to 3.5 ‰ (-2.9 ± 4.1‰), which could be attributed to contribution from evaporation of rainwater or surface water bodies. In the case of Tertiary and Cretaceous aquifers, groundwater indicates high d-excess 5.8 ± 2.7‰ and 7.2 ± 2.3‰ respectively. These values of d-excess also indicate limited modification due to evaporation before recharge. A plot of d-excess versus δ^{18}O is given in Fig. 4.13.

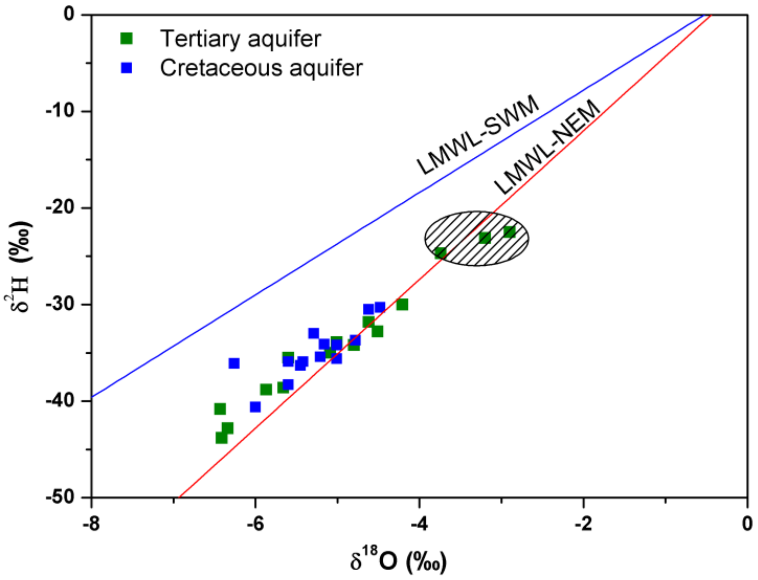

Fig. 4. 12 Plot of δ^2H versus δ^{18}O data of groundwater samples from Tertiary and Cretaceous aquifers, encircled samples show enriched composition

An inverse relation is observed between d-excess and δ^{18}O plot, this inverse trend signifies kinetic evaporation of the water before recharging groundwater. It can be seen from the plot that three Tertiary aquifer samples falling on the enriched part (encircled values) also show lower d-excess, which again point to the contribution of evaporated waters, like Tanks or agricultural return flow. The figure also shows that recharge to Tertiary and Cretaceous aquifer is precipitation dominant, whereas Quaternary aquifer is dominantly recharged by evaporated rainwater/surface waters. At a few places Tertiary and Quaternary aquifers are interconnected and the data fall in mixing zone.

Common processes that govern dissolved salts in groundwater are dissolution of minerals, evaporative enrichment and saline water mixing. These processes can be easily discerned by Cl$^-$ - δ^{18}O correlation. Figure 4.14 (a) represents Cl$^-$ variation with respect to δ^{18}O in Quaternary samples. All the three above said processes are indicated in the figure, samples (Q-1, Q-3, to Q-7 and Q-11) show dissolution dominance, these samples also fall close to the LMWL-NEM in the case of δ^{2}H versus δ^{18}O (Fig. 4. 11). Other samples (Q-2, Q-8, Q-9 and Q-10) show evaporation dominance. One sample, Q-12 show high Cl$^-$ and show moderate enrichment in δ^{18}O indicating

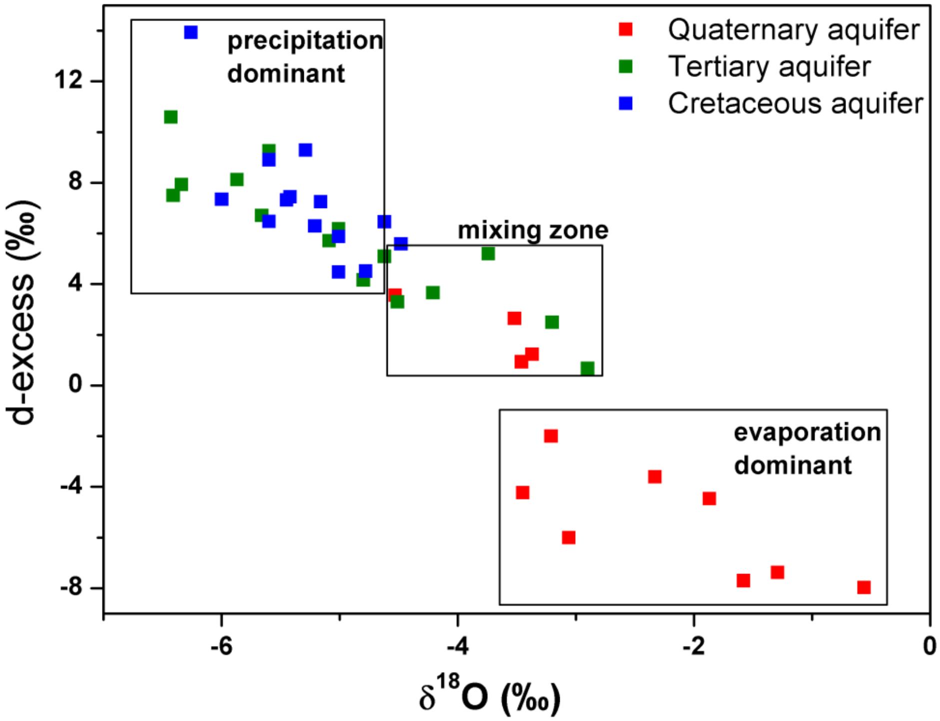

Fig. 4. 13 Plot of d-excess versus δ^{18}O data of groundwater samples from all aquifers with dominant recharge sources identified

contribution of saline and evaporated surface water bodies such as backwater. Tertiary aquifer dominantly represents dissolution processes, except in three samples T-9 to T-11 where Cl^- as well $\delta^{18}O$ found to be higher (Fig. 4.14 b). Cretaceous aquifer on the other hand show increase Cl^- values with relatively constant $\delta^{18}O$ values, indicating dissolution processes is controlling the total dissolved content (Fig. 4.14 c) in this aquifer.

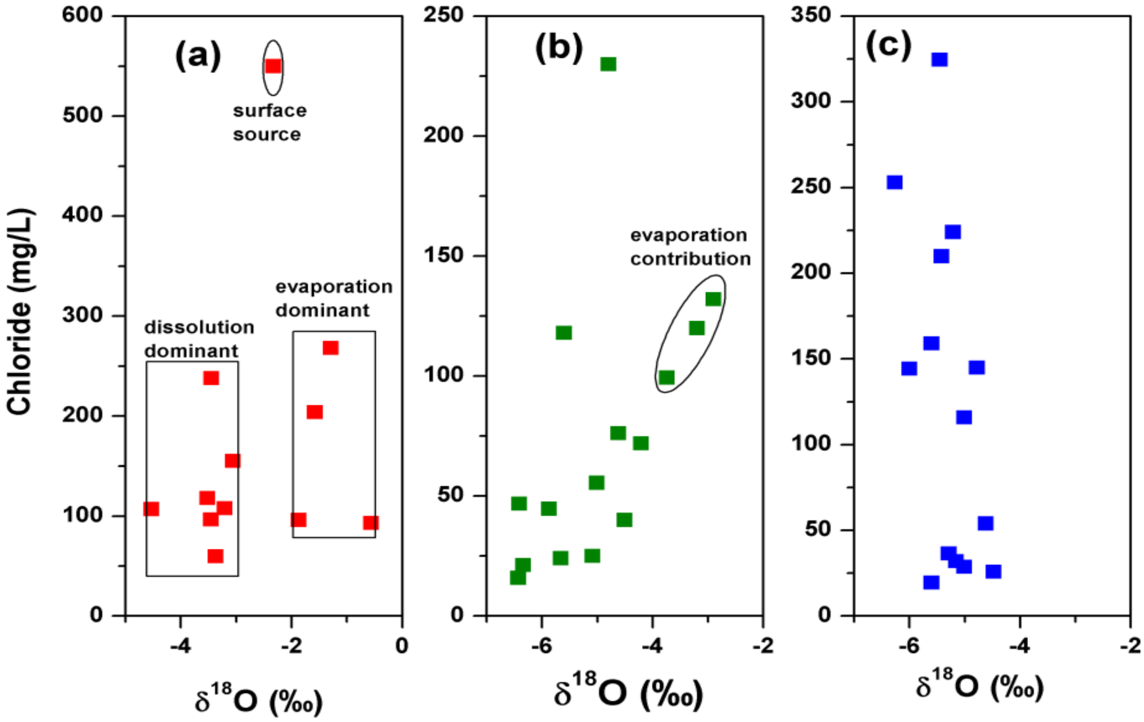

Fig. 4. 14 Plot of chloride versus $\delta^{18}O$ data of groundwater samples from (a) Quaternary, (b) Tertiary and (c) Cretaceous aquifers

4.10.2 Carbon-13 ($\delta^{13}C$)

The contour map of the ^{13}C isotope of groundwater is shown in Fig. 4.15 a. It can be observed that $\delta^{13}C$ values enrich from Northwest to Northeast regions, whereas an opposite trend is noticed in the Southern part of the study area, i.e. $\delta^{13}C$ value depletes from Southwest to Southeast region. In the Northern region, contribution of root zone CO_2 imparts a depleted $\delta^{13}C$ value to the groundwater in the East but as groundwater picks up carbonate from the formation, it becomes enriched towards West.

Aquifer-wise analysis shows that $\delta^{13}C$ composition of the groundwater from Quaternary aquifer displays a value of -19.7 which represents contribution of root zone CO_2. In the case of Tertiary and Cretaceous aquifers the $\delta^{13}C$ composition varies from - 18.2 to - 9.6 ‰ and - 21.8 to - 9 ‰ respectively. These ranges demonstrate progressive enrichment in ^{13}C isotope values which is attributed to carbonate dissolution as predicted by hydrochemical trends, characteristic ionic ratios and modeling studies (Sections 4.2, 4.3 and 4.7). However, Tertiary and Cretaceous aquifers don't display any apparent difference in $\delta^{13}C$ composition.

Recharge at higher elevations with high vegetation cover has more negative $\delta^{13}C$ values because root zone contributes a greater proportion of CO_2 compared to recharge taking place at lower elevations. In addition to depleted $\delta^{13}C$ composition, recharge at higher elevations also contains less total inorganic carbon, because the duration that open system conditions prevail is shorter. At lower elevations a greater proportion of atmospheric CO_2 is incorporated into the infiltrating waters, because of increased atmospheric contact. In addition, dissolution of carbonate minerals leads to higher bicarbonate content and enriched $\delta^{13}C$ composition in groundwater. These processes are visualized in $\delta^{13}C$ and HCO_3^- plot (Fig. 4.15 b). Figure shows that in Tertiary aquifer $\delta^{13}C$ values don't vary with HCO_3^- content (shown by dotted line), whereas Cretaceous samples demonstrate a clear enrichment in $\delta^{13}C$ with increase in HCO_3^-, indicated by a dotted arrow in the Fig. 4.15 b.

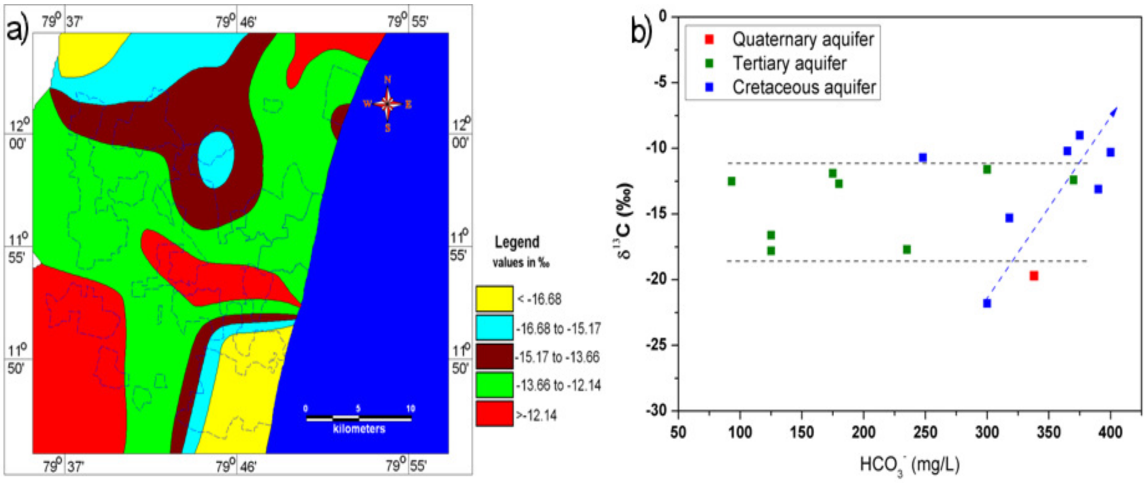

Fig. 4. 15 a) Contour map of $\delta^{13}C$ composition of the groundwater, b) Plot of $\delta^{13}C$ versus HCO_3^-, dotted arrow is eye guide

4.10.3 Environmental tritium

Tritium concentration in most of the samples ranges from 2.5 to 6.5 T.U. indicating present day recharge to these aquifers. A few Cretaceous samples show low tritium (< 2 T.U.) indicating old groundwater recharged prior to 1960's. Cretaceous samples show wide variation in tritium content from 1 to 6 T.U. with a narrow distribution of $\delta^{18}O$ (- 6.26 to - 4.48 ‰) indicating a common source to the groundwater with different travel times. It is interesting to note that inverse trend exist in the case of groundwater from Tertiary formation. The ^{3}H distribution is narrow (3.1 to 5.9 T.U.) while $\delta^{18}O$ distribution is wide ($\delta^{18}O$; - 6.4 to - 2.9 ‰). These trends indicate that groundwater is more or less of the same age while its recharge sources are different, such as different monsoons or contribution from surface waters.

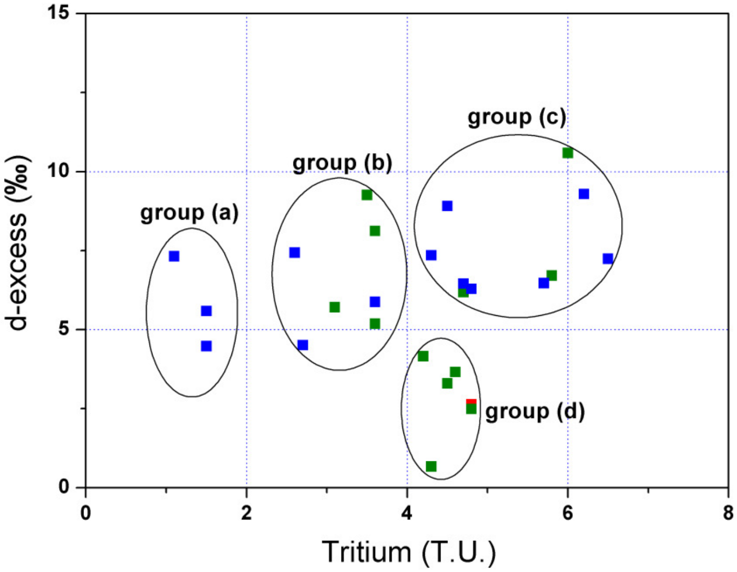

Fig. 4. 16 Plot of d-excess versus ^{3}H content of groundwater delineating probable sources and processes

In order to evaluate the nature of source and recharge dynamics, d-excess is plotted against ^{3}H (Fig. 4.16). Four different groups of groundwater were identified in this plot. Groundwater falling in group (a) belongs to Cretaceous aquifer, this water is old and recharged by monsoonal rains without much contribution from the re-circulated inland waters. Group (b) represents groundwater from Tertiary and Cretaceous aquifers, these waters are sub-modern and with similar d-excess values as that of group (a) and are recharged by monsoon. Group (c) consists of groundwater from Tertiary and Cretaceous formations, which are recently recharged water and the source of recharge is precipitation. Unlike other groups, group (d) displays lower d-excess values (0 - 5‰) and modern tritium which indicates recharge is modern and the recharge source is mostly evaporated water bodies such as agricultural fields, ponds and tanks etc.

4.11 Temporal Variations

Groundwater samples collected from nine locations during pre monsoon are compared to those collected during post monsoon to evaluate seasonal variation in chemistry and stable isotope data. In general there is a shift in hydrochemical trends from mixed facies to Ca-Mg-HCO_3 type facies during pre-monsoon (Fig. 4.17 a & b). Similarly a slight enrichment in isotopic composition is noted during pre-monsoon period in most of the instances. These trends indicate seasonal fluctuations are not very significant, which may be due to dispersion of chemical and isotopic signatures during groundwater travel.

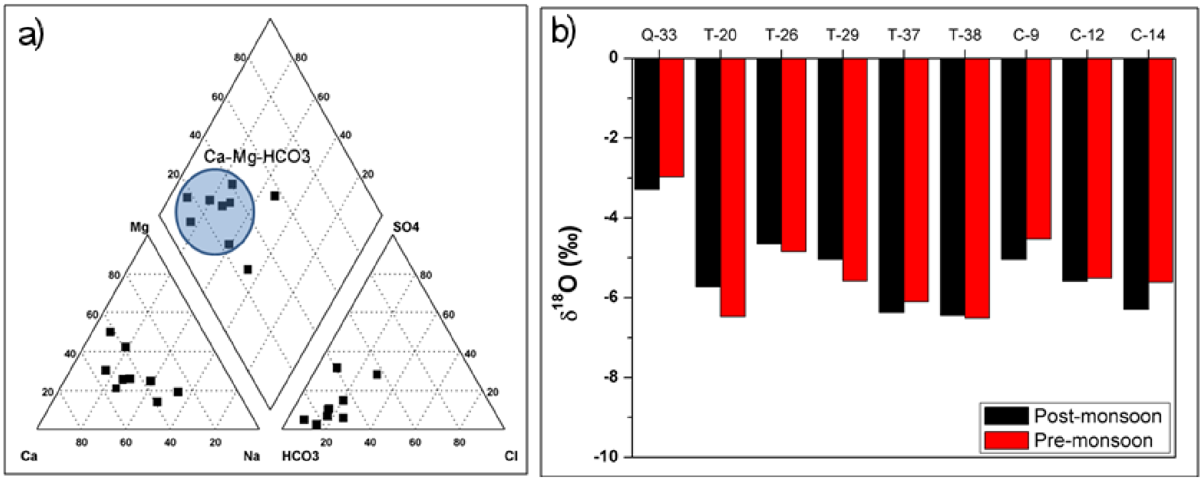

Fig. 4. 17 Seasonal variations in (a) chemistry and (b) $\delta^{18}O$ content of selected groundwater samples

4.12 Conclusions

Quaternary aquifer

Groundwater in Quaternary aquifer is mainly Na-Mg-HCO_3-Cl and Na-Ca-HCO_3-Cl types. Characteristic ionic ratios indicate ion exchange and weathering of carbonate rocks as dominant processes. An increase in EC is observed in Southern part of the study area from West to East with changing facies, which is attributed to contribution from backwater present in the area. Ion versus chloride plots indicated sources like evaporite, Gypsum and processes like ion exchange and dissolution. Silicate stability diagrams indicated that Kaolinite stable solid phase along with K-feldspar, Na or Ca-Montomorillonite phases. This demonstrates that the groundwater is not fully evolved.

Statistical treatment of the chemistry data indicated backwater influence, denitrification, Albite weathering as dominant processes influencing groundwater. Inverse modeling calculations carried out for two flow paths demonstrated that K-spar, Dolomite, Gypsum and Halite are common minerals dissolving in groundwater, whereas Aragonite/Calcite, Albite, Ca-Montomorillonite contribution varies depending upon initial water composition.

An attempt has also been made for the first time to establish LMWL for NEM which is a major contributor of rainfall to this region. Wide distribution in stable isotope composition indicates multiple sources of recharge while correlations between δ^2H and $\delta^{18}O$ demonstrate evaporation effect. Contribution of evaporated surface water is also confirmed using d-excess values. Isotope and Cl^- variations indicate that increasing TDS in the groundwater is due to dissolution, evaporation and mixing with saline water in this aquifer.

Tertiary aquifer

Groundwater mainly belongs to Na-Ca-HCO_3-Cl and Ca-Mg-HCO_3 types. Groundwater collected from North of River Gingee demonstrates silicate weathering from the source rock, whereas carbonate weathering in Southern parts. Characteristic ion ratios indicate processes like Dolomite weathering, Calcite precipitation and cation exchange. Thermodynamic interpretations of silicate minerals reveal that the groundwater is stable with Kaolinite phase indicating the groundwater is geochemically evolved.

Statistical treatment of the chemical data demonstrated contribution of silicate weathering, backwater and fertilizer inputs in to the groundwater. Inverse modeling calculations for four flow paths indicated that positive mole transfer values for Halite, K-spar and Dolomite while negative mole transfer values for Calcite/Aragonite, Exchange, and CO2 gas. Incongruent dissolution of Aragonite is responsible for increased Sr^{2+} concentration in the groundwater.

Isotope composition of Tertiary aquifer demonstrates narrow distribution pointing to common source of recharge. Isotope data of groundwater fall along the LMWL indicating contribution from precipitation without significant evaporation. Isotope variations with Cl^- indicate that dissolution is dominant process contributing to TDS in groundwater. A few samples exhibit interconnection with surface water / Quaternary aquifer. D-excess values also confirm contribution of precipitation as well as interconnections with surface water/Quaternary aquifer. No systematic trend is found between $\delta^{13}C$ and HCO_3^- values pointing to multiple sources of inorganic carbon. Environmental ^{3}H data indicate that the groundwater is sub-modern to modern.

Cretaceous aquifer

In the case of Cretaceous aquifer, the groundwater is dominantly Ca-Mg-HCO_3 type except in some locations near the coast, which show Na-Mg-HCO_3-Cl and Na-Ca-HCO_3-Cl water types. Two geochemical pathways are observed, i) Ca-Mg-HCO_3 type alters to Ca-Mg-HCO3-Cl which attains Ca-Na-SO_4-Cl type and ii) Ca-Mg-HCO_3 type changes to Na-Mg-SO_4-Cl type and to Na-Cl-HCO_3 type. From characteristic ion ratios the basic reactions governing the geochemical reactions were deduced to be dissolution of Calcite followed by cation exchange and leaching from minerals. Silicate stability diagrams indicate evolved nature of groundwater similar to Tertiary aquifer.

The mole transfer values calculated using inverse modeling for three flow paths indicate that in most of the cases chemistry of groundwater is controlled by addition of Albite, K-spar, Halite, Aragonite and Gypsum phases, and removal of Dolomite. Modeling studies indicate that high strontium concentration in final water is due to incongruent dissolution of Aragonite. Speciation calculations for alkaline earth metals were carried out and $MHCO_3^{+}$ is found to be dominant undissociated species followed by MSO_4 and MCO_3. Undissociated forms account for 30% of total species present. Strontium was found to be associated more with undissociated forms than Mg^{2+} and Ca^{2+}. Isotope trends indicate that groundwater is mostly derived from NEM and increase in TDS is due to dissolution process. Enrichment of $\delta^{13}C$ with HCO_3^{-} indicates dissolution of carbonates. Environmental tritium indicates old and modern groundwater both recharged by monsoonal rains. Microbial studies indicate reducing condition of Cretaceous aquifer which is also acting as a driving force for the reductive dissolution of iron oxyhydroxide and resulting in dissolved arsenic. This is further supported by low DO and sulfates with H_2S odor in groundwater.

For majority of the elements it is important to take account of their relative geochemical abundance since this will exert a fundamental control on availability. It is desirable to know the compositional variability of the aquifer rocks and minerals in order to assess the controlling factors for trace metal occurrence in groundwater. For this purpose sediments obtained from a borehole are studied for isotope and geochemical parameters and the results are discussed in the following chapter.

CHAPTER - 5
IDENTIFICATION OF SOURCE, WEATHERING AND DEPOSITION CHARACTERISTICS OF SEDIMENTS

5.1 Introduction

In this chapter major, trace, rare earths element and ^{13}C isotope data of depth-wise sediments collected from Quaternary, Tertiary and Cretaceous formations in a borehole near Pondicherry are presented and their geochemical relevance is brought out. The distribution patterns and inter elemental correlations are used to identify the provenance, weathering and deposition characteristics. The geochemical data of these sediments is compared to sediments of nearby regions with similar geology and the influence of Deccan volcanism is also evaluated. In addition to this, the arsenic distribution and its correlation with other elements are also discussed. The sediment-arsenic data is compared to other arsenic affected regions and the possibility of arsenic leaching in to groundwater is discussed in light of available theories. The utility of $\delta^{13}C$ information to reinforce the geochemical and mineralogical inferences is highlighted.

5.2 Litholog Characterization

5.2.1 Mineralogy and morphology of sediments

The color of the sediments varies widely across the depth. The fine sediments (sand/clay) vary from yellowish brown to greyish brown to dark grey, whereas clay varies from brown to dark grey. Sandstone color changes from off-white to brownish grey to dark grey, whereas claystone varies from brown to dark grey. The various formations when followed down dip are often difficult to identify based on lithological considerations alone. So, for the present study, a schematic lithological section map is constructed based on the in situ nature (color and texture) of the sediments collected and field information (drilling pattern and local geology), and corresponding formations are assigned by extrapolating the fence diagram from the site Madagadipattu (Fig. 1.3 b).

A schematic section of the borehole is shown in Fig. 5.1. A sandstone formation is observed between 128 - 142 m bgl which is confined between clay formations. Since this zone is characterized by black carbonaceous nature of sediments with fine to medium grained sands, it may belong to Ramanathapuram sandstone of Early Cretaceous period. Above this formation, Vanur sandstone is encountered (60 - 93 m bgl) with a thickness of 33 m, which is sandwiched between clay zones with limestone of about 12 m thick. A thin zone of claystone is encountered above sandstone formation with a thickness of 6 m. Sandstone above the claystone have different color and textures as compared to deeper sandstone deposits. No depth showed presence of prominent limestone formation. Top zone is mostly sand with clay intercalations up to a depth of 10 m bgl are underlied by brown clay of about 6m thickness.

The X-ray diffraction analysis of bulk sample has shown peaks pertaining to Quartz, K-feldspar, Goethite, Magnesium calcite and Iron-magnesian silicate minerals. The XRD patterns of sediments from different depths indicated variation in mineralogy (Fig. 5.2), which may arise either due to diverse nature of source rocks or deposition conditions of these sediments or alteration of minerals as a result of post depositional diagenesis. The XRD patterns don't show any REE or arsenic mineral suggesting these elements are contained in minerals that are either X-ray amorphous such as metal oxides or present in minor quantities (typically < 5%).

Morphology of the sediment grain surfaces shows clay texture with striations, fibrous and honeycomb structure (Fig. 5.3). Straight and curved scratches along with medium to large pits can also be seen in the scanned images. The sediments are medium to fine grained, sub-rounded in shape and moderately to well sorted. The EDS of sediment sample is shown in Fig. 5.4. EDS data indicates high Al/Si ratio pointing to presence of Smectite group minerals or Al-rich amphibole (Hornblende). Calcium is also shown in EDS data, which rules out possibility of the mineral Chlorite. High amount of potassium and flaky nature crystals suggest presence of Micaceous minerals [18]. From ESEM and EDS spectra, it can be concluded that Smectite and Mica are present. A small peak at 1.28 KeV (Lα of As) is observed in EDS spectrum suggesting that As might be present as minor species. The EDS analysis showed that besides Al, Si and O which are common constituents of sediments, Mg, Ca, Na and Fe are also present.

5.2.2 Elemental and isotope distributions

The major element (Na, K, Ca and Fe, S, TOC, TC and TIC) and trace element concentrations (As, Co, Sc, Cr, Zn, Hf, Th and U) are given in appendix 2.10.

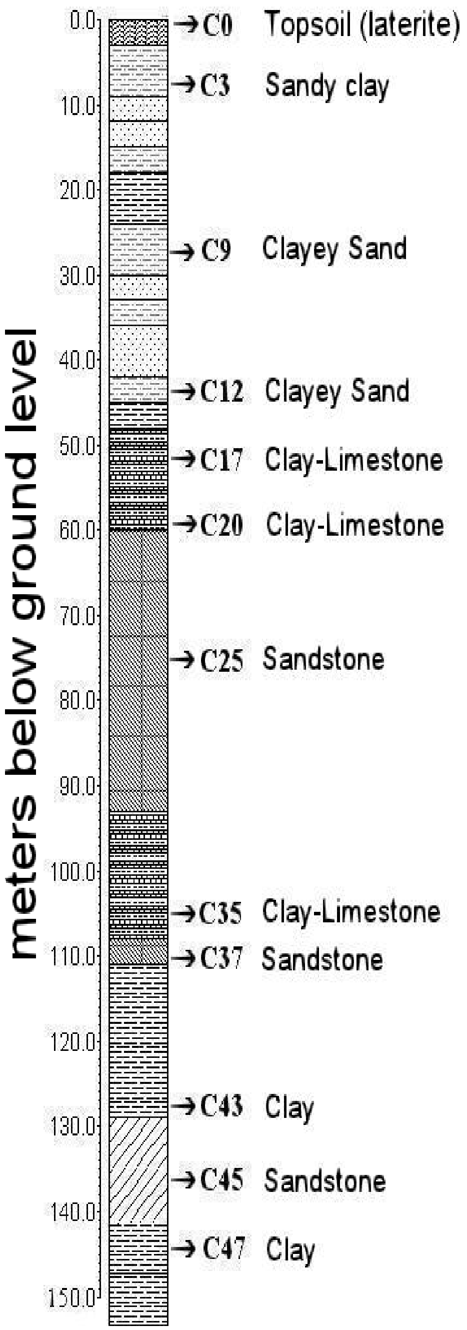

Fig. 5. 1 Schematic map of litho-section at Andiyarpalayam village based on in situ nature of sediments

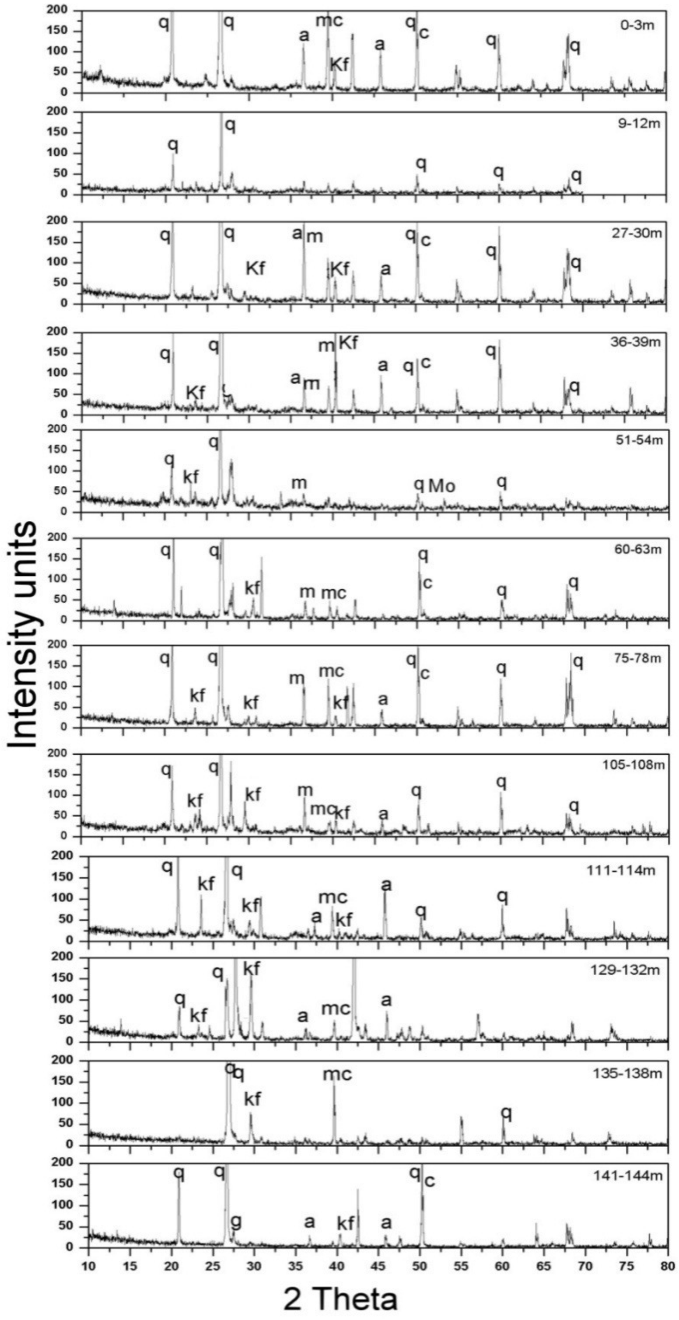

Fig. 5. 2 XRD plots of the bulk sediments at selected depths with major peaks identified (q=quartz, Kf=potash-feldspar, a = aragonite, c=calcite m-mica and Mg-cal = magnesium-calcite)

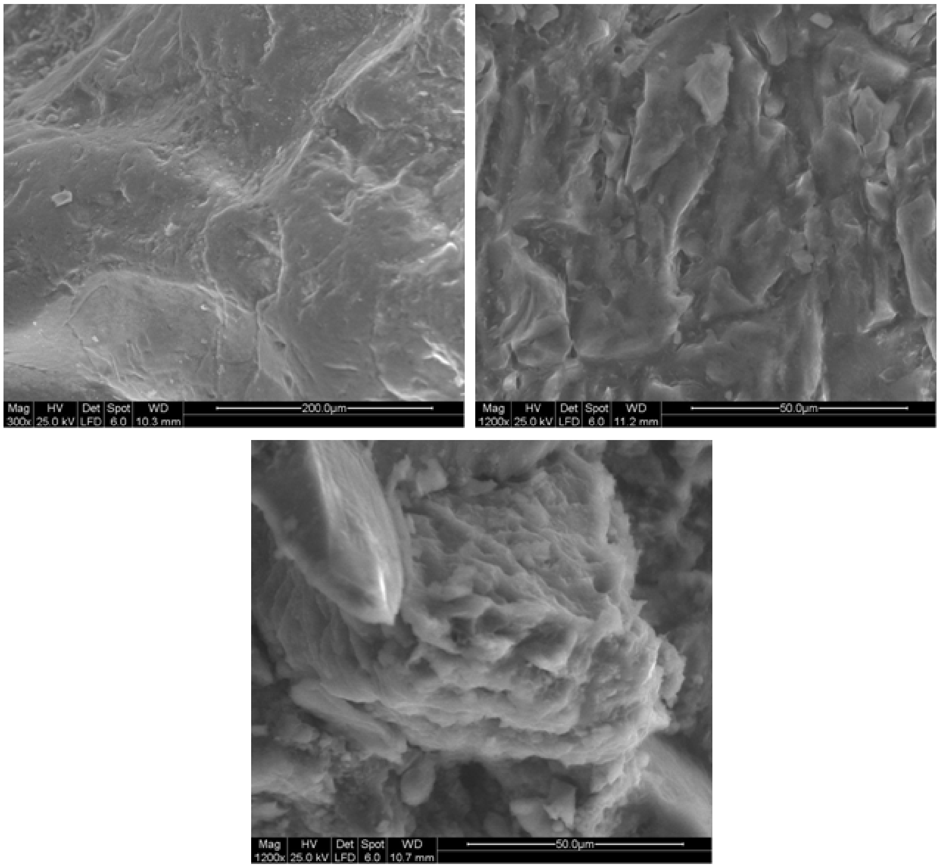

Fig. 5. 3 ESEM scans of grain surfaces showing (a) clay texture with striations, (b) fibrous and (c) honeycomb structure

The REE data (La, Ce, Eu, Yb and Lu) of the sediments is given in appendix 2.10 including the literature values of Chondrite (CI), Post Achaean Australian Shale (PAAS), North American Shale Composite (NASC) and Upper Continental Crust (UCC). Depth profiles of major and trace elements are displayed in Fig. 5.5 (a-d). It is found that vertical profile of major elements show wide distribution with Na and K behaving similarly all through the litho-section (Fig. 5.5 a). Calcium exhibits high variation between 105 – 132 m bgl. Iron content in these samples varies from 0.84 to 3.5 %. High iron contents (2.6 to 3.5 %) are noted in C-17 and samples from deeper formations (C-43, C-46 and C-47). High fluctuations are observed in the iron contents (Fig. 5.5 a).

Trace elements show very similar pattern with U being the least abundant element (BDL to 3 ppm) and Zn being the most abundant (38 to 167 ppm), shown in Fig. 5.5 b. Arsenic content in the sediments range from BDL to 30 ppm. It is observed that among different litho-units arsenic content is maximum in grey clay (30 ppm) while in other cases it ranges from BDL - 17.8 ppm. The sediments belonging to top zone (Quaternary formation) and also sandstone up to a depth of ~35 m bgl show low arsenic content (< 2.5 ppm), whereas slightly increased levels are observed in sandstone, calcareous sandstone, and claystone formations between 35 and 60 m bgl. Deeper formations show slightly increasing trend between 60 and 120 m bgl followed by a spike of As (30 ppm) at 130 m bgl, which declines to 13 ppm with depth (Fig. 5.5 b). The arsenic values in most of the sediment samples are similar to the background value of crustal abundance representing the natural processes of sedimentation. No anomalous sediment-arsenic is observed in any of the litho units at this site.

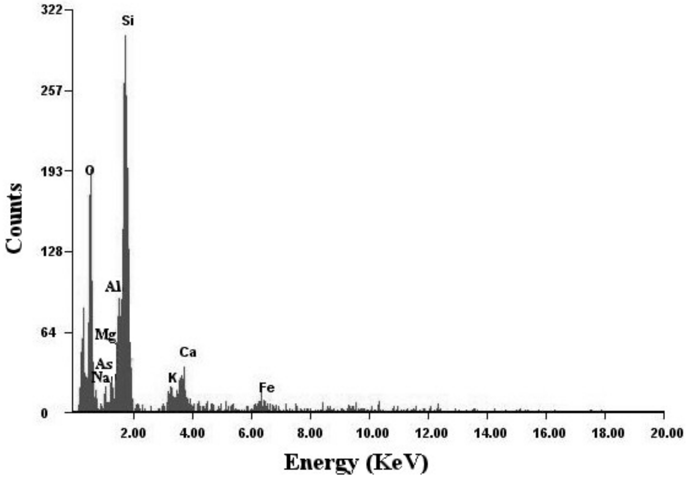

Fig. 5. 4 EDS of sediment (C-43)

Sulfur values range from < 0.01 to 1.4 % and show very similar trends as that of the arsenic. Total carbon (TC) ranges from < 0.001 to 3.9 % and higher value is observed in deeper calcareous sandstone formation (Fig. 5.5 c). TOC is very low in the samples ranging from BDL to 0.2 %. Only samples from deeper zones show marginally higher TOC (0.1 – 0.2 %), where as TOC is very low in all the samples (Fig. 5.5 c). Since the TIC is calculated as the difference between TC and TOC, and TOC being very low, TIC shows similar trend as that of TC (Fig. 5.5 c). Vertical profiles of the REEs are shown in Fig. 5.5 d. It can be observed from the plot that the trends are similar for all the REEs indicating a common source, however it is noted that lighter REE (LREE: La and Ce) have higher concentrations compared to heavier ones (HREE: Yb and Lu).

The ^{13}C isotope values of the inorganic carbon expressed as permil values (‰) against VPDB are given in appendix 2.13. Marine carbonates generally have positive $\delta^{13}C$ values from 0.0 ±3‰ [27], whereas soil gas on the other hand is much lighter isotopically and has $\delta^{13}C$ value of about -26 ± 5‰ in temperate climate [34]. Precipitation of secondary calcite cement leads to $\delta^{13}C$ about of -10 ± 5‰ [164] and very negative values are found when organic compounds are mineralized [164]. It can be seen from the Fig. 5.6 that most of the studied sediments have $\delta^{13}C$ values in the range of -0.1 to -11.4‰ but deep sediments show positive $\delta^{13}C$ values (+1.5‰ and +5‰). The complex geochemical environment of the sediments in this region is clearly reflected in wide range of $\delta^{13}C$ values. Highly enriched $\delta^{13}C$ values indicate marine sources, whereas depleted signatures can be attributed to multiple sources.

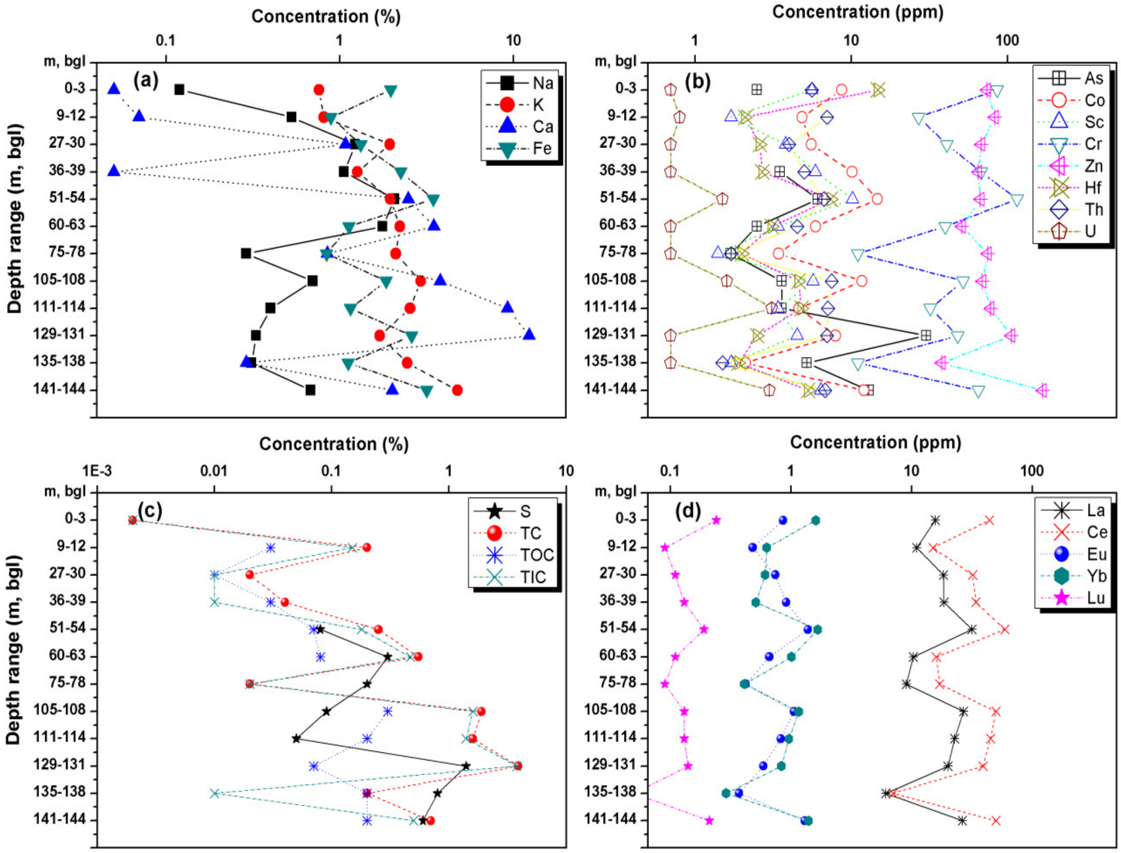

Fig. 5. 5 Depth wise profile of a) major, b) trace, c) S and C and d) REE contents in sediments

5.3 Identification of source rock and weathering characteristics

Chondrite normalized plot of REEs, Fig. 5.7 a, show remarkable uniformity of the sediments with enriched LREEs and depleted HREEs which is a typical pattern of UCC exposed to weathering and erosion. The HREE depletion occurs in source rock, if there is a preferential removal of HREE as carbonate ion complexes during chemical weathering [165] and Granitic feldspars typically show a slight depletion in the HREE [166]. All the sediments in the present study show lesser REE contents compared to UCC, NASC and PAAS. Negative Eu anomalies are often related to a relatively higher concentration of heavy minerals. No pronounced Eu anomaly is noted in the

REE patterns (Fig. 5.7 a), which could be due to absence of heavy minerals in these sediments. NASC is also used for REE normalization especially for sedimentary formations [36]. A plot of NASC normalized REE pattern of the sediments indicates less steep or flat curve with pronounced positive Eu anomaly (Fig. 5.7 b). The positive Eu anomaly reflects the contribution of plagioclase minerals. Although the REEs patterns follow similar trend, the difference in the position of the curves can be attributed to relative contributions of Quartz and clay minerals along the depth.

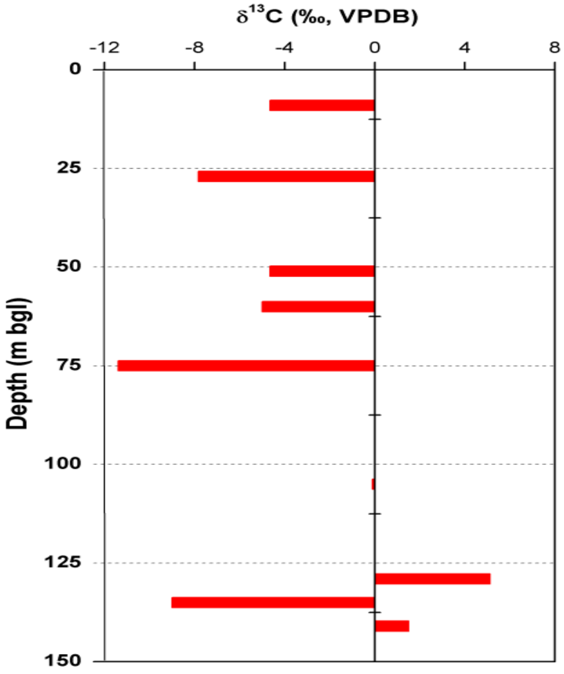

Fig. 5. 6 Depth wise variation of $\delta^{13}C$ in sediments

Elemental ratios (La/Sc, Th/Sc, Th /Cr and Th /Co) have been used in identifying the nature of source rock [167]. The elemental ratios are given in Table 5.1. La and Th are more abundant in felsic rocks than in mafic rocks and the opposite is true for Sc and Co. This is because, Th and La being incompatible elements preferentially gets partitioned into melts and associated with felsic rocks [167]. So, relative enrichments of incompatible over compatible elements indicate a relatively felsic dominated provenance [38]. Typical Th/Sc ratio for post Archean UCC is ~1 while felsic rocks have more than one and mafic rocks show less than one. Most of the analyzed sediments show Th/Sc ratio greater than or equal to unity (1 to 4.14) suggesting felsic rock sources like Granite and Granodiorite (Table 5.1). Some sediment samples also show Th/Sc ratio less than one indicating some contribution from mafic sources. Dominance of felsic source rocks is also demonstrated by scatter plot of Th/Co versus La/Sc [168]. Sediment samples of this study plot near felsic dominance (Fig. 5.8 a). Elemental ratio Th/Cr is also used to differentiate mafic and felsic rock contributions due to redox chemistry [169]. Correlations between La/Th ratio and Hf content are also used to evaluate source rock composition [170]. As illustrated in Fig. 5.8 b, the relatively high Hf contents and low La/Th ratios in these sediments suggest felsic source rocks. It is also noted that sediment data spread towards Andesite type indicating Andesite contribution.

Table 5. 1 Elemental ratios of sediments

Sediment ID	Depth	TREE	La/Sc	Th/Sc	Th/Co	Th/Cr	La/Co	Th/U	La/Th	(La/Lu)cn
	m, bgl									
C0	0-3	62.5	2.8	1	0.65	0.07	1.8	7.67	2.8	6.8
C3	9-12	26.7	6.53	4.14	1.44	0.26	2.28	8.69	1.58	13.1
C9	27-30	51.7	4.86	1.07	0.72	0.1	3.3	5.52	4.55	17.9
C12	36-39	53.8	3.16	0.86	0.5	0.07	1.82	6.88	3.68	15.3
C17	51-54	93.5	3.08	0.66	0.46	0.06	2.14	4.59	4.66	16.8
C20	60-63	27.9	3	1.32	0.76	0.11	1.74	6.19	2.28	9.5
C25	75-78	26.6	6.3	1.19	0.49	0.16	2.62	2.32	5.3	10.1
C35	105-108	79.1	4.7	1.32	0.64	0.14	2.29	4.56	3.57	21.2
C37	111-114	69.5	6.64	2.1	1.54	0.22	4.86	2.31	3.16	17.4
C43	129-131	60.9	4.44	1.56	0.88	0.14	2.51	9.57	2.85	14.4
C45	135-138	13.6	3.53	0.89	0.73	0.14	2.91	2.12	3.96	11.7
C47	141-144	79.5	4.1	1.06	0.57	0.11	2.18	2.28	3.87	13.1
NASC		102.7	2.07	0.82	0.47	0.1	1.19	4.56	2.52	7
UCC		97.4	2.73	0.97	1.07	0.31	3	3.82	2.8	9.7

Felsic and Mafic provenance of sediments can also be differentiated by ternary diagrams such as La-Th-Sc [171] and Th-Hf-Co [41]. The sediments data fall in a Felsic rock dominant region in La-Th-Sc ternary plot (Fig. 5.9 a). But the spread of data points near Andesite is noted as in the case of La/Th versus Hf plot (Fig. 5.8 b). Contribution of Tonalite can be inferred from these observations. Feldspar in these rocks is present as Plagioclase (typically Oligoclase or Andesine) with less alkali Feldspar and more Quartz (> 20%). This is further corroborated by Th-Hf-Co ternary diagram, where the sample data fall along Tonalite and Granitic sources indicating felsic provenance (Fig. 5.9 b).

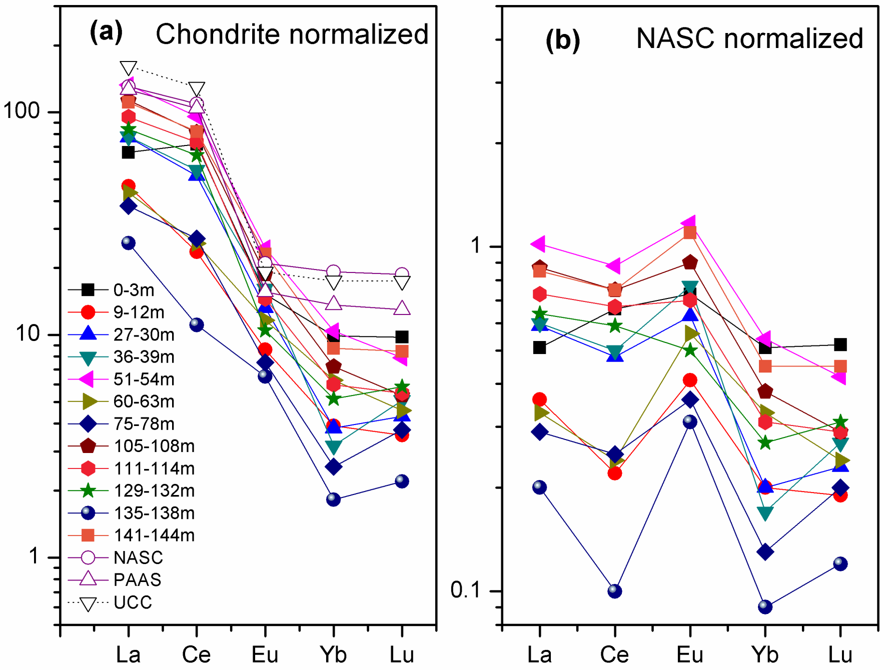

Fig. 5. 7 a) Chondrite normalized rare earth elements plot for the sediments, along with those of NASC, PAAS, UCC and b) NASC normalized REE distributions for sediments demonstrating positive Eu anomaly

Variations in Th/Co and Th/Cr ratios (Table 5.1) are within the felsic source rock ranges and similar to the sediments belonging to nearby regions (Table 5.1). High ratios are noted at 9 - 12 m, 60 - 63 m and 111 - 114 m, which also coincided with the potential aquifer sands of Quaternary, Tertiary and Cretaceous periods. Other elemental ratios of these sediments also show similar ranges as that of sediments from sedimentary formations of nearby regions (Table 5.1). All the ratios indicate felsic nature of source rocks.

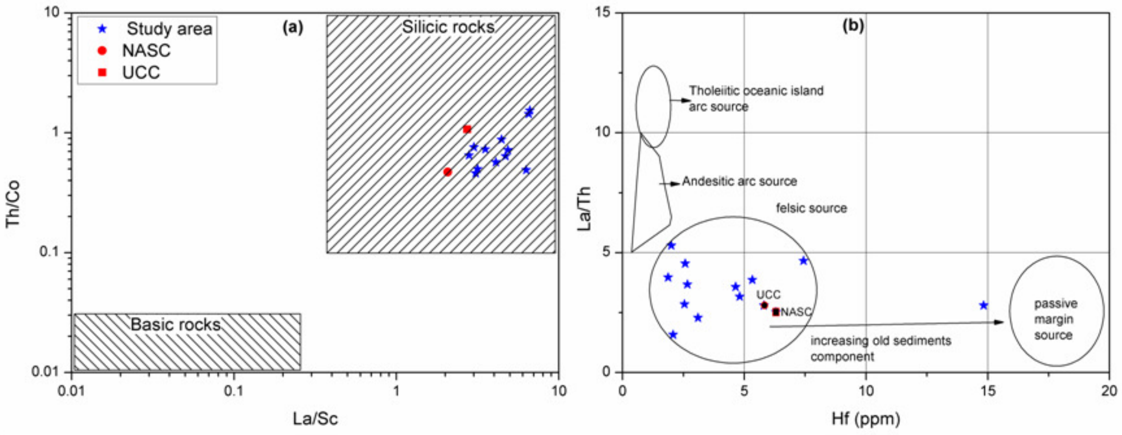

Fig. 5. 8 a) Plot of Th/Co versus La/Sc and b) La/Th versus Hf showing source rock composition for the sediments

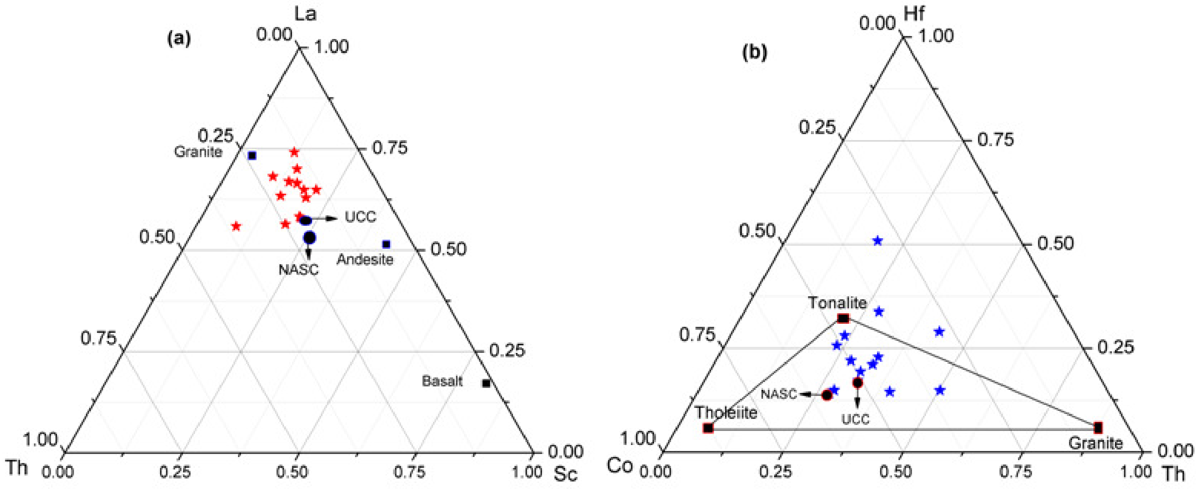

Fig. 5. 9 a) La-Th-Sc and b) Th-Hf-Co ternary diagram for sediments

The total REEs concentration (TREE: summation of La, Ce, Eu, Hf, Lu in ppm) varies with depth and ranges from 13.6 ppm (132 - 135 m) to 93.5 ppm (51 - 54 m) as given in table 5.1. Higher TREE values are noted at 51 - 54 m, 105 - 108 m and 138 - 141 m and lower values at 9 - 12 m, 60 - 75 m and 132 - 135 m. The lower of TREE matches with the potential aquifer sands of different ages; Quaternary, Tertiary and Cretaceous respectively, which is also observed in the case of Th /Cr and Th /Co ratios (Table 5.2). Although the TREE contents are significantly different at different depths, it is interesting to note that the normalized distributions are more or less similar in nature (Fig. 5.7 a&b). Clay and fine sand fractions of the sediments contain high abundance of REEs [172]. Therefore variation in TREE observed in these sediments can be attributed to contribution of variable amounts of clay and fine sand.

The Chondrite normalized values of $(La/Lu)_{cn}$ in the sediments range from 6.8 to 21.2 (Table 5.1) and point to moderate to high degree of weathering. This variation in $(La/Lu)_{cn}$ is ascribed to preferential mobilization of HREE during higher degree of weathering leading to higher $(La/Lu)_{cn}$ ratio [168]. A positive Eu anomaly in NASC normalized REE distribution (Fig. 5.7 b) is indicated in all the sediments, but it is more prevalent in the case of sandstone formation though TREE is lesser compared to other sediments. During the weathering of source rocks, minerals rich in REEs break first and form secondary mineral phases, wherein Eu enriched feldspars and Quartz are preferentially retained leading to positive Eu anomaly. Similar positive Eu anomaly in sediments of Cauvery basin has been reported [76].

Table 5. 2 Trace element and REE ratios of study region and nearby regions

Study Area	La/Sc	Th/Sc	Th/Co	Th/Cr	(La/Lu)cn
Minimum	2.06	0.65	0.46	0.06	6.8
Maximum	6.64	4.13	1.54	0.26	21.2
Average	4.25	1.52	0.79	0.105	13.9
Upper Continental Crustal values [ref. 41]	2.21	0.79	0.63	0.13	9.73
Felsic Rock [ref. 172]	2.5-16.3	0.8-20.5	0.67-19.4	0.13-2.7	3-27
Mafic Rocks [ref. 172]	0.43-0.86	0.05-0.22	0.04-1.4	0.018-0.046	1.1-7
Sediments of Rabanpalli formation	1.1-3.4	1.2-2.7	0.17-0.4	0.12-0.24	4.2-9.7
Sediments from Sillakkudi formation [ref. 77]	1.93-9.36	0.41-6.57	0.14-5.01	0.23-2.94	4.1-23.5

5.4 Evaluation of sediment deposition conditions

The Th/U ratio is often used to present weathering under oxidizing conditions (Mc Lennan et al., 1993) and a value of 3.8 suggests that the sediments are derived from a large homogenized continental provenance. Uranium concentrations in the studied sediments found to vary between BDL and 3ppm, and depths where U is not detected (BDL) coincide with low TREE values. On the other hand, Th concentration in the sediments ranges from 1.5 to 7.5 ppm and high Th concentration is noted in sediments belonging to Late Cretaceous period. Th/U ratio in the sediments ranges from 2.27 to 8.73 indicating non homogeneity in the provenance (Table 5.1). Most of the sediments show high Th/U ratios (4.5 to 9.5) more than UCC reflecting intense weathering of source rocks. It is also noted that recent sediments show higher ratios implying weathering under oxic environments. Lower Th/U ratios in older sediments (less than UCC ratio) reflect anoxic environments.

Detrital Index [DI: detritus (Silicates and Quartz)/Calcite ratio] is used to interpret the deposition conditions. A low DI generally reflects a more distant detrital source, decreased erosion and higher sea-level or deeper water conditions while a high DI indicates more proximal detrital source, increased erosion and lower sea-level or shallower water environment [173]. The XRD patterns (Fig. 5.2) of the sediments from Tertiary and Quaternary formations show presence of Quartz to a greater extent than the Cretaceous formations leading to high DI. It is reasonable to assign this to lower sea level or shallow water environment The calcite is dominant at 27 - 30 m, 60 - 63 m, 75 - 78 m and 135 - 138 m depths rendering a slight decrease in the DI, thus signifying comparatively higher sea-level or deeper water conditions at these depths.

Depleted values of $\delta^{13}C$ are noticed in 27 - 30 m, 75 - 78 m and 135 - 138 m depths, wherein the first depth represents Tertiary and the rest belong to Cretaceous period. Positive $\delta^{13}C$ values are noted at 129 - 132 m and 141 - 144 m of the Cretaceous formation. There is a narrow distribution of $\delta^{13}C$ values in the sediments of Tertiary formations (-1.2 ‰ to -7.5 ‰) compared to extreme variations in Cretaceous formation (-11.4 ‰ to +5.11 ‰). These $\delta^{13}C$ trends suggest 'warm and dry' and 'warm and wet' climatic conditions during Late Cretaceous period. Depths 27 - 30 m and 75 - 78 m comprising permeable sandstone zone show more negative values of $\delta^{13}C$ (-11.4 ‰ and -9 ‰), which could be due to precipitation of carbonates from groundwater. It is observed from the Table 5.1 and appendix 2.13 that depths with negative $\delta^{13}C$ values correspond to low TREE values and these depths belong to higher Quartz bearing formations. It is interesting to note that these values fall in the boundary between Tertiary and Quaternary (27 - 30 m) and between Cretaceous and Tertiary periods (75 - 78 m). The presence of Lignite and Marcasite in these formations supports our finding that reducing conditions prevailed during sediment deposition in Cretaceous period [51, 52].

5.5 Arsenic distribution and its correlations with other elements

In order to understand the source of the arsenic in the sediments, arsenic correlations with other elements are studied. Arsenic data is plotted against iron in sediment samples as shown in Fig. 5.10 a. The linear fit of data indicates a positive correlation between As and Fe (regression coefficient of 0.61). For samples with As content BDL, detection limit of 0.5 ppm is considered for plotting. Deep zone clay sample data (C-43) is not included in linear fit line. Positive correlation indicates that As is associated with iron containing minerals. The molar weight ratios (g/kg) of As to Fe in all the samples range from 0.12 to 0.35 except in one sample where it is 0.87. High As to Fe ratio in sample C-43 could be due to an additional source of As which might be non-ferrous like arsenic sulfides or low ferrous minerals. It is possible that in reducing conditions arsenic can be present as sulfide mineral, such as Orpiment or Realgar [174].

A plot of As versus S content is shown in Fig. 5.10 b. A positive correlation (regression coefficient; 0.84) is observed between arsenic and sulphur contents of sediment samples including C-43. These positive correlations (Fig. 5.10 a 7 b) indicate that iron sulfide (FeS_2; Pyrite / Marcasite) could be the source of As in sediments. In order to confirm the presence of iron sulfide mineral in these sediments, iron content is plotted against corresponding sulfur content as shown in Fig. 5.10 c. Dashed line in the figure represents Pyrite/Marcasite stoichiometric composition. The plot shows that all the samples fall below the line indicating additional source of iron, which is also evident from the presence of Goethite and Ferromagnesian silicates in XRD pattern of the sediment (Fig. 5.2).

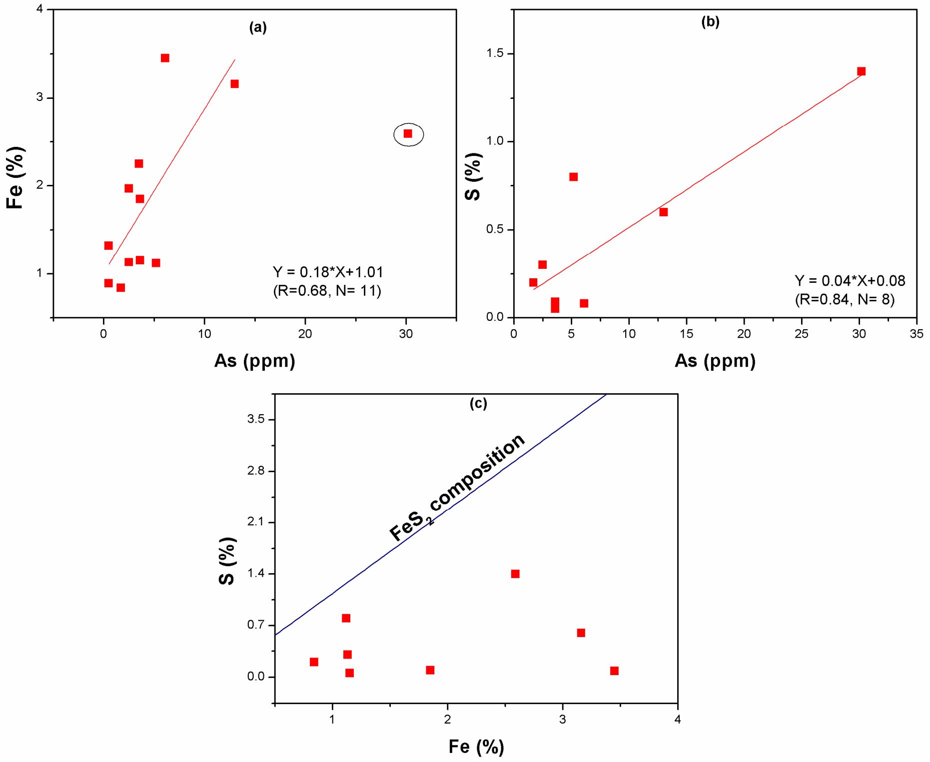

Fig. 5. 10 Correlations among As, Fe and S contents in sediments

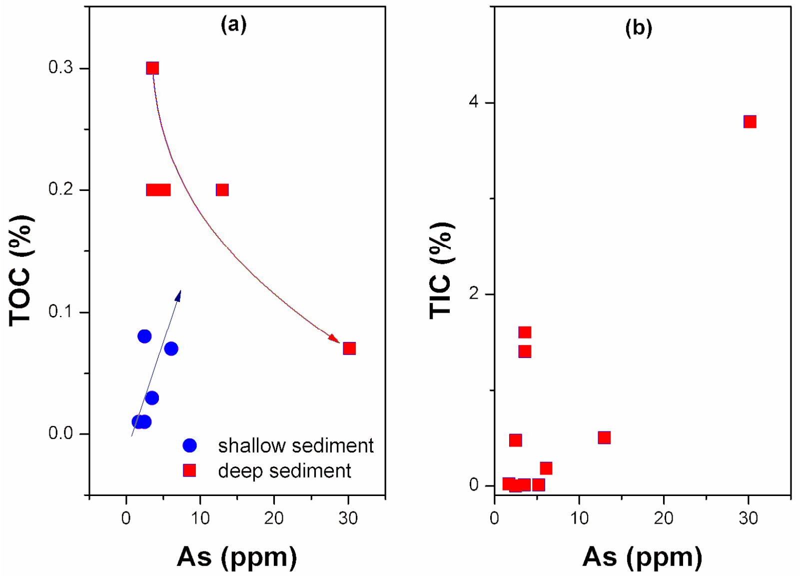

Fig. 5. 11 Arsenic correlations with a) TOC and b) TIC correlations in sediments, arrows are eye guide to data points

In addition to these elements, arsenic is found to be associated with sediments with high organic matter like peat and lignite. Lignite, which is a coal with properties intermediate to those of bituminous coal and peat, is a good source of arsenic. High arsenic content is reported in formations rich in Pyrite, bituminous deposits and organic-rich shale or organic-rich clay [45] and it can be responsible for greater arsenic release into the groundwater [153]. In some sediments of As affected regions 10 - 30% of the arsenic present is associated with the solid organic phase [175]. Since lignite veins are noticed in this region, relation between arsenic abundance and TOC is studied in order to understand the associations in sediment samples.

The correlation between As and TOC contents in these samples is shown in Fig. 5.11 a. Detection limit of 0.005 % is taken for samples having TOC below detection limits. It can be observed that the sediments up to a depth of ~100 m bgl show positive trend between As and TOC, whereas most samples from deeper formations (> 100 m bgl) show inverse trend. The positive trend indicates that upper sediments contain arsenic in association with organic matter. The inverse trend can be possible if the organic matter is consumed by biotic or abiotic processes.

It is observed by some researchers that arsenic can also be contributed from calcareous minerals [176]. In order to verify this hypothesis, TIC content of the sediments is plotted against corresponding arsenic content, as shown in Fig. 5.11 b. Plot shows that there is no clear increasing trend in the As content with increase in TIC. High TIC in C-35 and C-37 is due to the presence of Aragonite. One sample showing high As also shows high TIC (C-43). XRD pattern of this sample shows the presence of Mg - Calcite (Fig. 5.2) and $\delta^{13}C$ value is enriched (+ 5‰

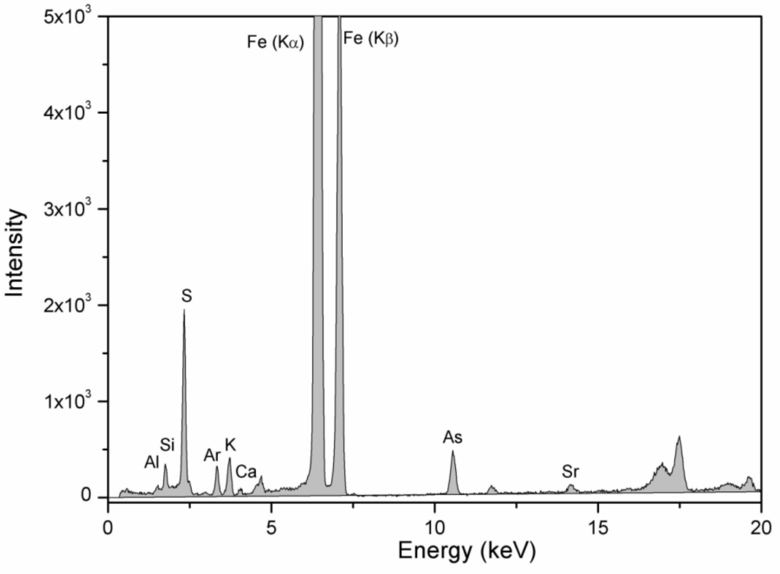

Fig. 5. 12 TXRF scan of sediment from depth 135-138m (C-45)

against VPDB) reflecting its marine origin [27].

Arsenic content in the formations of the affected regions is neither unusually high nor much different from adjacent uncontaminated regions and the range of arsenic concentration is found to be low i.e. 3-12 ppm in some of the affected areas [177]. This confirms the fact that even lean sources can pose a great danger to groundwater contamination. Comparison of the arsenic values of this study with other affected regions (Table 5.3) shows that Quaternary formations have very low arsenic (< 2.5 ppm) therefore these formations may not act as potential sources of arsenic. Tertiary formations have arsenic in the range 0.5 to 6.1 ppm. A positive correlation between As and TOC possibly indicates association of As with organic matter that was co-deposited with the sediments over geologic time. Most of the deeper sediments have shown an inverse trend between As and TOC, this could be due to consumption of organic matter by SRB. Microbiological assay of groundwater samples from some of the Cretaceous aquifers showed the presence of SRB (appendix 2.2). Cretaceous formations show significant arsenic content and fall almost on the higher side of the ranges established in the arsenic affected regions (Table 5.3). These deeper calcareous sandstone formations can act as potential source of As in groundwater, if the aquifer geochemical condition favors the arsenic leaching from the sediments. A few grains of sediment sample of C-45 are analyzed for TXRF for confirming the presence of arsenic. Fig. 5.12 shows the presence of As along with iron sulfide indicating that arsenic is derived from Pyrite or Marcasite.

5.6 Conclusions

Nature of source rock, weathering characteristics and deposition conditions in different sedimentary formations are discussed in this chapter using major, minor, trace, REE and $\delta^{13}C$ isotope data. The mineralogy of the sediments indicates Quartz and Feldspar as the major minerals, whereas Mg-calcite, Aragonite, Calcite and clay minerals as minor ones.

The trace elemental ratios suggest that sediments are mainly derived from felsic source rocks and ternary plots indicate contribution of Tonalites. The major and trace elements show depleted values compared to UCC suggesting that source rocks are weathered and diagenetically altered to remove lithic fragments and increase in the proportion of Quartz relative to source rock. The ratios of redox sensitive elements (Th/U) infer oxic weathering in shallow sediments. Furthermore, REE patterns of all the sediments are almost parallel to each other and characterized by enriched LREE and depleted HREE, which is a typical pattern of UCC exposed to weathering and erosion. These REE patterns are found to be affected by size of the sediment (fine or coarse). Variable ratios of $(La/Lu)_{cn}$ and low TREE suggest moderate to intense weathering of source rocks. The geochemical characteristics of the sediments are found to be similar to that of sediments belonging to similar geology in nearby regions.

The arsenic content in the sediments of this site ranges between BDL to 30 ppm and high arsenic content is found in Cretaceous formation. Arsenic correlates positively with iron and sulfur pointing to contribution of Pyrite or Marcasite mineral, which is further confirmed by TXRF study. Both positive and inverse trends are noted between arsenic and organic matter. A positive correlation observed in shallow sediments indicates that arsenic is present in association with organic source, whereas inverse trend in the case of deep sediments point to bacterial reduction of organic carbon.

Trace metal migration is an important phenomenon in controlling the dynamics of contaminated groundwater. Studies have indicated that particles have a greater contribution in transport of trace metals in groundwater to longer distances than predicted. In the next chapter the role of particles in groundwater is discussed.

CHAPTER - 6
ROLE OF GROUNDWATER PARTICLES IN TRACE METAL MIGRATION

6.1 Introduction

For proper risk assessment the role of colloidal particles in contaminant transport assumes greater importance, for which both size and chemical, and mineralogical aspects of particles need to be characterized and quantified to explain and predict the role played by colloidal particles in groundwater systems.

As many factors affect the particle size during separation it becomes difficult to assign a specific dimension to the particle. These shortcomings in separation of particles by filtration constrained the study of particles with high resolution. Many authors classified and studied the particles as “large” and “small” particles [104, 178]. In this work we have grouped the particles into large particles, those retained by filter circles with pore sizes in the range 0.1 - 10 µm, and small particles, those retained by 500 – 300000 Dalton molecular weight cut-off membrane filters. These molecular weights have nominal diameters in the range of 1 – 14 nm. This classification encompasses a 100-fold difference between the small and large particles. The particle ranges studied in this work are marked in Fig. 2.5.

The general objective of this chapter is to increase the understanding of the role of particles in groundwater studies. To address these aspects, i) nature and abundance of particles, ii) Influence of geology and hydrochemistry on particles iii) Implications on trace metal migration.

6.2 Nature and Abundance of particles

It is found that the total particles are in the range of 4.5×10^5 to 3.3×10^6 per liter (Table 6.1). A systematic decrease in particle number density is observed with increasing particle size. This dependence of particle size distribution (PSD) on diameter has usually been described by a power law distribution [179],

$$\frac{dN}{d\emptyset} = A\emptyset^{-\beta} \quad (6.1)$$

where N = colloid number, ϕ = colloid diameter, A = parameter related to the total colloid concentration and β = the opposite of the power-law slope in a log–log basis. The β value gives an indication of the relative proportion of small and large particles. The PSD patterns, dN/dϕ versus ϕ in log-log plot are shown in Fig.6.1. The particle sizes present are limited up to 10 µm.

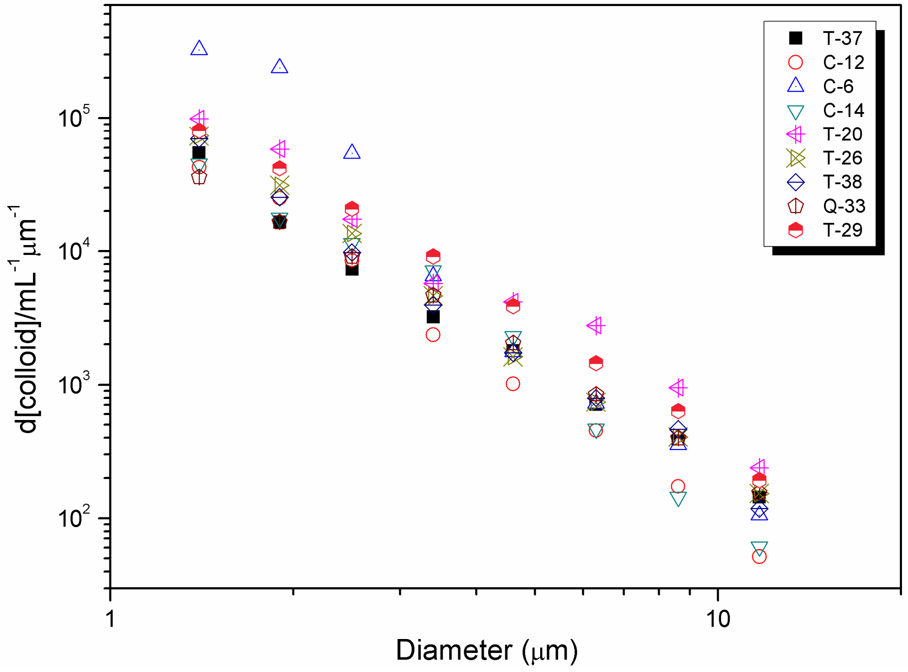

Fig. 6. 1 Particle Size distribution in groundwater

The β value in natural systems usually ranges between 2.5 and 4.5 [179], in the studied groundwater it ranges between 2.54 and 4.03 (Table 6.1). Samples collected from Cretaceous formation show higher values compared to Tertiary formation indicating abundance of smaller particles. Cretaceous formations are particularly abundant in clays which constrain the transport of larger particles by reducing the groundwater movement and enhancing the particle aggregation. The low tritium value (appendix 2.6) also signifies the longer residence time of the groundwater. The lowest β value is found in Q-33 (2.54) indicates abundance of larger particles. Since the sampling depth is 46 m bgl and the formation is mostly alluvium, large particles generated by soil-water interaction might have carried through unsaturated zone and still persisted in the groundwater. In sample T-20 though the well depth is shallower compared to Q-33, the β value is higher (2.69). This is could be possibly because of presence of clay in the unsaturated zone at this site, which assists in particle cohesion and aggregation leading to filtering out of large particles.

Table 6. 1 β value, ionic strength, total particle number density, log PCO2 and TOC data of selected wells

Location	sample	β	Ionic	Particles/100mL	Well depth (m	logPCO	TOC
PeriaKuppam	T-37	2.6	5.3	56600	140	-1.09	-
Katterikuppam	T-12	3.1	11.4	46592	180	-1.45	0.56
Vanur	C-6	4.0	12.7	327620	180	-1.67	2.05
Karasur	C-14	3.1	36.8	54181	185	-1.45	1.3
Pattanur	T-20	2.6	17.6	112400	24	-1.52	3.2
Muthiryapalyam	T-26	2.9	10.6	75938	95	-1.24	1.73
Kannikoil	T-38	2.8	6.2	68668	95	-1.05	
Kaduvanur	Q-33	2.5	18.2	45316	46	-2.63	
Sornavur	T-29	2.8	11.8	96973	61	-1.73	

A systematic decrease in the particle number density is noticed with well depth (Fig. 6.2 a) except in samples from Cretaceous sandstone (C-9 to C-12). This decrease can be attributed to particle aggregation followed by settling as the infiltrated water reaches to deeper depths. However, particle number density versus ionic strength (Fig. 6.2 b) showed scattered trend. Along a flow path mixed patters are found. In Cretaceous formation, the total number of particles decreases along the groundwater flow line (C-9 to C-12) with more or less same ionic strength. This can be due to enhanced stability of particles in groundwater at C-9 due to the presence of organic matter (TOC value 2.5 ppm). In the case of Tertiary formation both increasing and decreasing trends are found. It shows that multiple factors decide the particle number such as organic content, ionic strength etc.

During sequential filtration, it is found that some of the filter circles were ruptured which might be due to clogging or uneven pressure. Therefore, filter circles are grouped and weighed instead of individual circles. The weight of the particles (particle load) collected on various size fractions (0.45 - 1.20 µm, 1.2 - 5µm and 5-8 µm) is shown in Fig. 6.3. Filter circles with pore size < 0.45 µm have particle loads close to minimum measurable weights hence ignored. The average particle load is found to be in the range of 0.64 to 2.6 ppm. Studies on particle concentrations in coastal groundwater system in Tamil Nadu have shown similar values (0.05 - 6 ppm) [87]. In other studies particle concentration in the size range 0.05 - 0.2 µm is found to be up to 1 ppm [180].

It is found that along the flow path from T-29 to T-38, the 0.45 - 1.2 µm fraction increased, whereas 3-5 µm fraction remained relatively constant and heavier fractions 5 -8 µm decreased. This trend can be explained by the difference in settling velocities of particles.

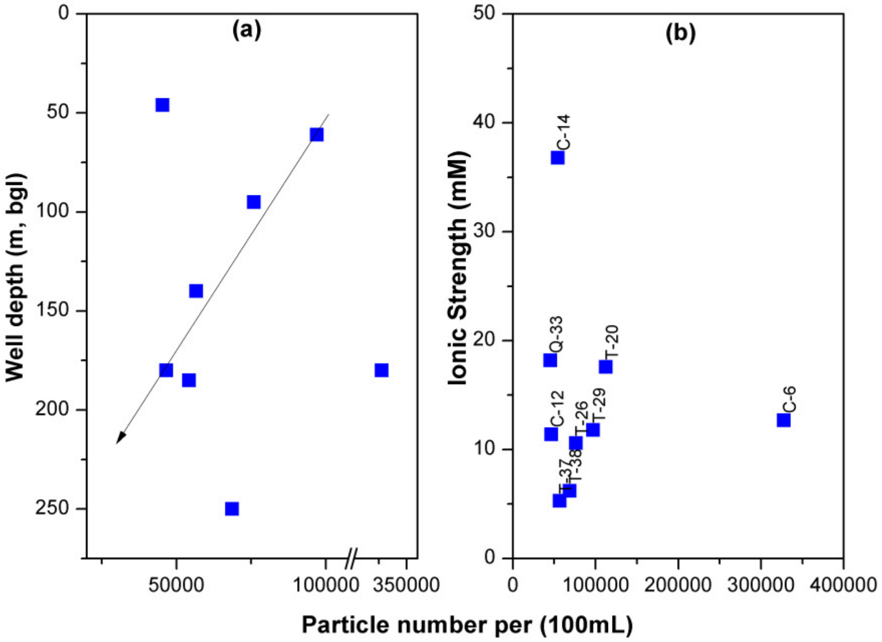

Fig. 6. 3 Particle number density correlations with a) well depth and b) ionic strength

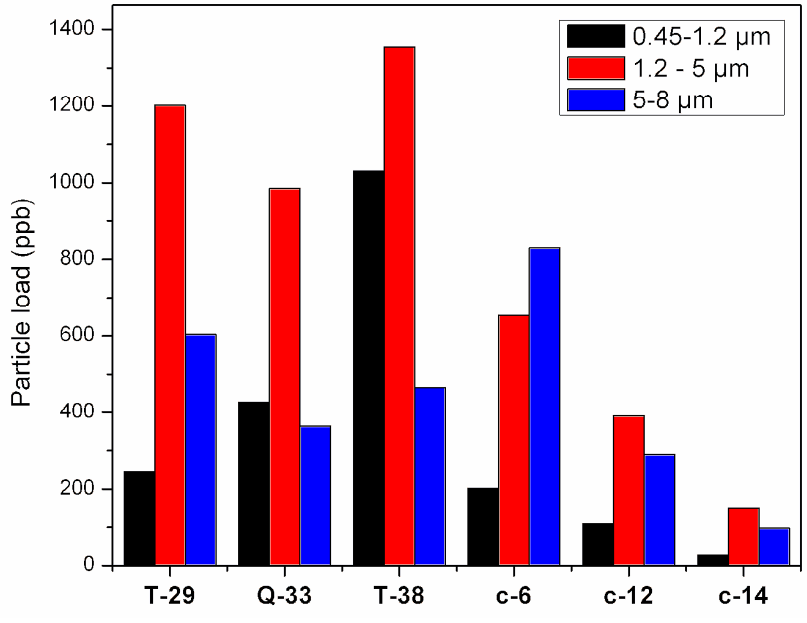

Fig. 6. 2 Particle loads in different size fraction - sequential filtration

There are broadly three main collision mechanisms that govern particles in suspension [181]. The first is particle movement due to random Brownian motion, which is a function of thermal energy (perikinetic coagulation). The second mode of particle collision is fluid shear where particles collide due to spatial velocity gradients in the fluid (orthokinetic coagulation). The third mechanism is collision due to differential settling velocities of particles. The finer particles (0.45 - 1.2 µm fraction) aggregate slowly and are not effectively influenced by gravity, therefore increase along the flow path. But larger particles (5 - 8 µm) are quickly removed by aggregation and sedimentation. But in the case of samples from Cretaceous formation (C-9 to C-12) the particle load decreases along the flow line in all the size fractions, which is in accordance with particle number density (Fig.6.2 b).

SEM scans of the filter circle indicate particles of spherical, elongated and tubular shapes (Fig 6.4). The EDS data suggests clay mineralogy and iron oxide nature. EDXRF study shows that most common elements found on these filter circles are Ca and Fe, with occasional presence of S (appendix 2.15).

Neutron activation analysis (NAA) data of all the filter circles from one site, Kuranpalayam site (C-18) is given in appendix 2.16. The particle load on the filter circles range from 0.07 to 5.13 mg / 10 L water passed that amounts to an average particle load of 7 – 513 µg/L, which is very much within the range found in other samples. A graphical representation of the data is shown in Fig.6.5 (a-f).

The ζ potential of the unfiltered sample indicates a wide variation of ζ potential values from - 50 mV to + 50 mV (Fig. 6.6 a-c). It is generally observed that solution with ζ potential < - 25 mV or > + 25 mV demonstrate stable colloidal solutions. The ultra-filtered aliquots show ζ potential values around - 25 mV (for 0.5 KD and 10 KD fractions) demonstrating that the colloidal fractions are in meta stable condition. From the peak profile of ζ potential it can be observed that the colloids in (unfiltered) original sample don't follow Gaussian distribution (Fig. 6.6 a) due to the possible effect of heterogeneously charged surface sites and steric repulsion forces. However in the case of 0.5 KD fraction, the distribution follows a single Gaussian distribution and demonstrates monodispersity of the solution (Fig. 6.6 b). In the case of 10 KD fraction the both positive and negative ζ potentials are displayed indicating mixture of both positive and negative charged colloids (Fig. 6.6 c) and the solution show bimodal distribution.

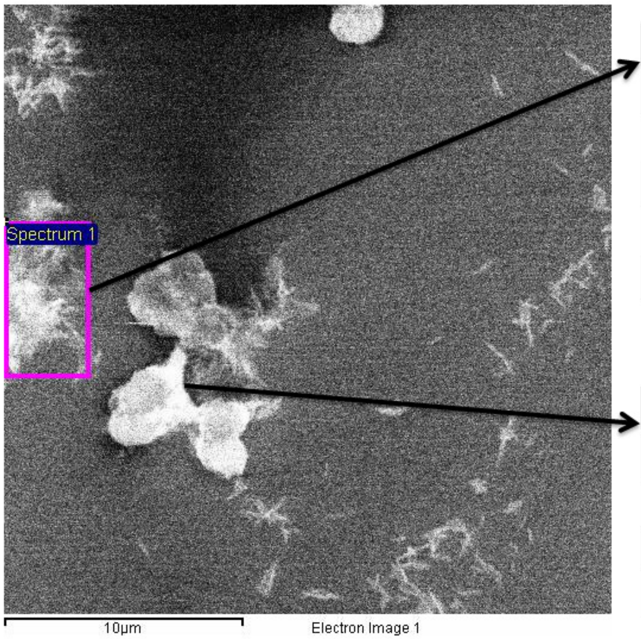

Element	Weight (%)
O	54
Na	9.3
Mg	1.1
Si	33.5
U	2.3

Element	Weight (%)
C	23.6
Fe	6.8
Cu	3.7
O	65.9

Fig. 6. 4 SEM scan of exposed filter circle and EDS of particles

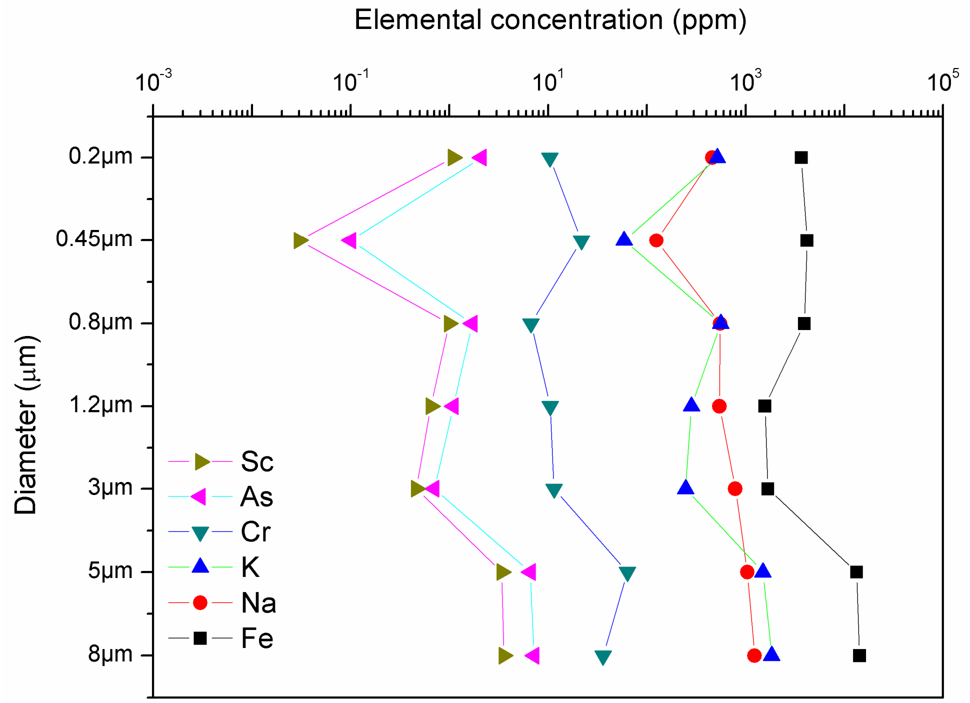

Fig. 6. 5 Elemental concentration versus filter size

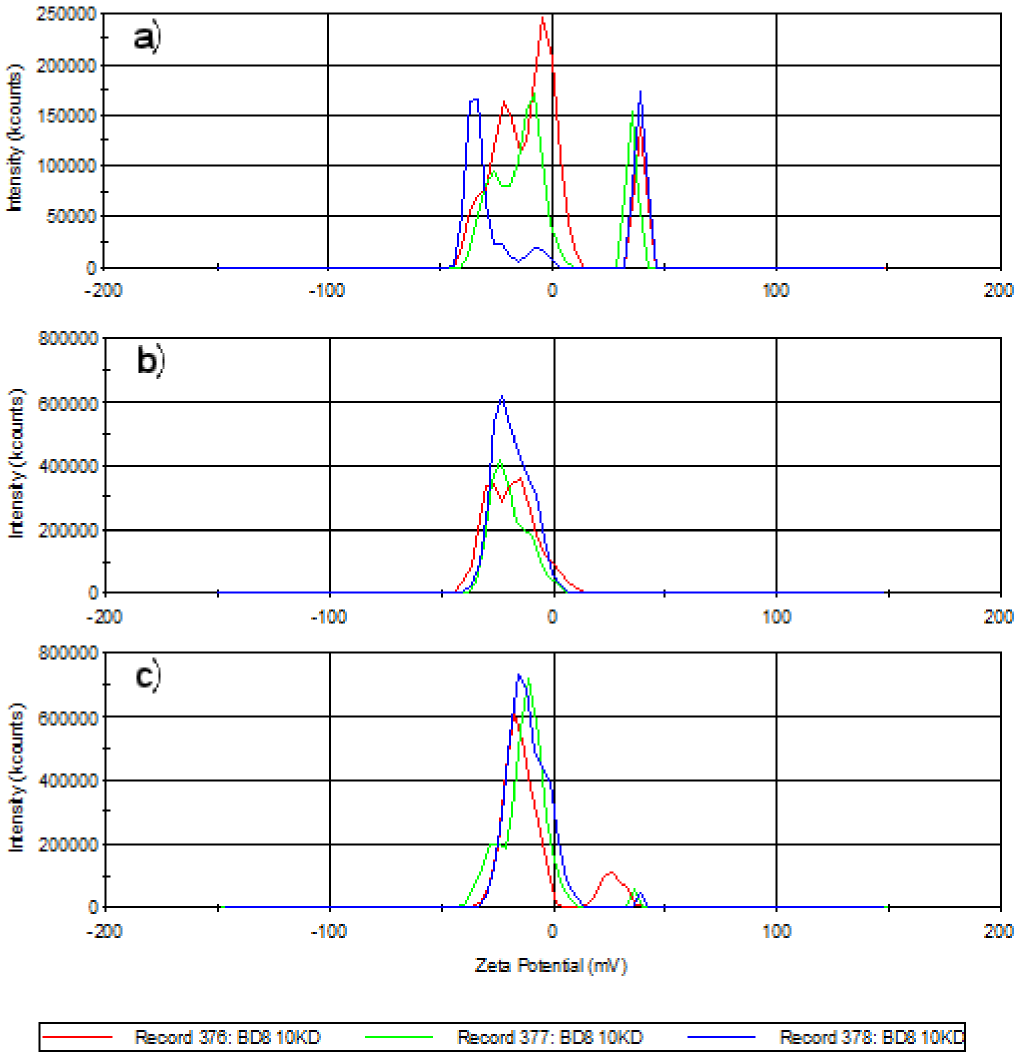

Fig. 6. 6 Zeta potential plots of a) unfiltered, b) 0.5 KD ultra filtered and c) 10 KD ultra filtered aliquots

6.3 Influence of geology and groundwater chemistry on particles

The geology of the formation and particles in water are intimately related as particles originate from the differential breakage of rocks during the erosion according to the intrinsic mineralogical characteristics of the minerals. Mobilization and transport of particles in subsurface media depend on the complex interactions between the formation characteristics and the dynamic properties of groundwater.

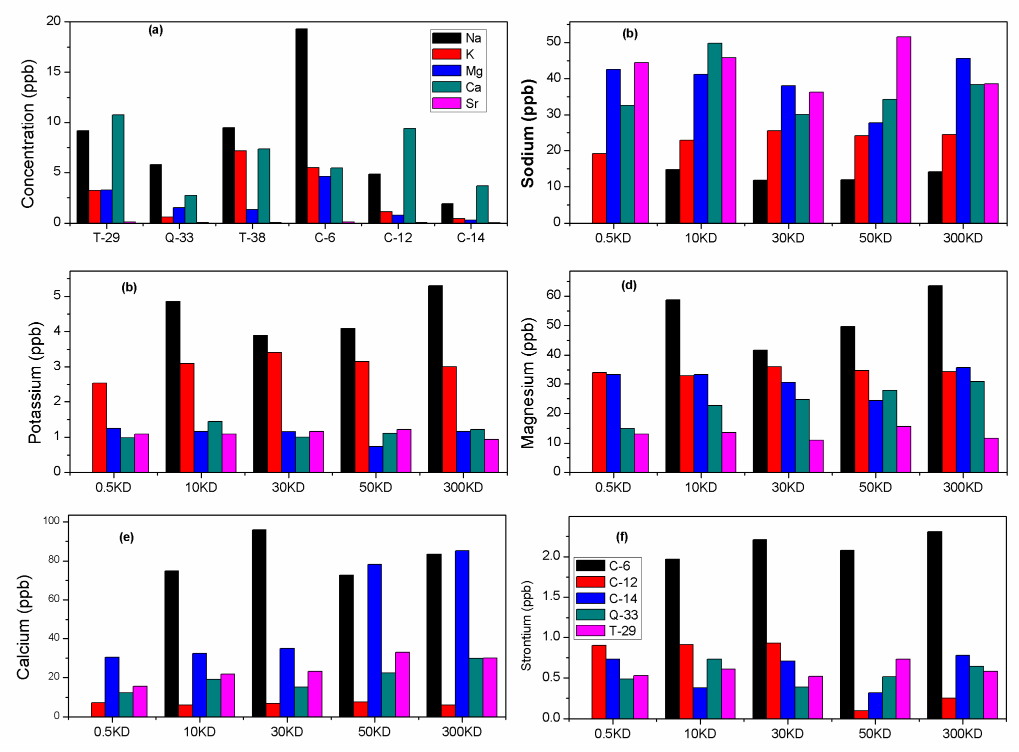

Fig. 6. 7 Chemical concentration of particles a) leachate fractions, and ultrafiltered fractions b) Na$^+$, b) K$^+$, c) Mg^{2+}, d) Ca^{2+} e) Sr^{2+}

Chemical concentration of the particles is measured in order to assess their association with aquifer geology. In the case of Cretaceous aquifer, there is a decrease in ionic concentrations of the leached fractions from recharge to discharge areas, whereas in Tertiary formations the trends are very complex (Fig. 6.7 a). Lowest ionic concentrations are found in C-14 sample collected from limestone formation. Among colloidal fractions, all the fractions mostly indicate more or less same chemical concentrations in a given sample (Fig. 6.7 b-f), but comparison among samples indicates wide variation similar to that of particle chemistry trends (Fig. 6.7 a). It is interesting to note that Ca and Mg show higher values in Karasur in the case of colloidal fractions as compared to other samples which is not the case in particle chemistry.

The samples collected from this region exhibit that particles contain Na, K, Ca, Mg and Fe, which can be cementing material in these sedimentary formations or derived from breakdown of minerals. Alkali metals can be derived from Feldspar (K and Na) or silicate minerals, which have a hardness of 6 - 7 with a mostly blocky & compact structure, whereas other clay minerals range in hardness from 1 to 3 and have a more foliated and lamellar structure [182]. The source of Ca and Mg can be Carbonate minerals in addition to Plagioclase minerals. Fe is a common constituent of Pyrite, Goethite and Ferromagnesian minerals. Distribution of major elements gives no indication that mineral composition of smaller particles is different compared to larger ones.

The mineralogy of the particles is found to be consistent with the make-up of the geological formations. Characterization based on NAA, EDS and EDXRF data indicates that the same chemical types of particles are present in most of the samples and particle size and nature of formation seems to have less impact. The chemical composition of these particles point to the presence of minerals like: Quartz, Calcite, Feldspar, Pyrite etc., which is further supported by the XRD profiles of the sediment samples collected from this region (Fig. 5.2). It is difficult to arrive at the stability behavior of particles due to the existence of a mixture of clay minerals, metal oxides with different surface properties and presence of organic matter. These factors mask the direct importance of mineralogy of the particles on the stability properties.

6.4 Implications on trace metal migration

Understanding the strontium migration in groundwater is of vital significance to nuclear industry as ^{90}Sr ($t_{1/2}$ = 28.8 years) is one of the sizable radioactive contaminant from waste repositories [183]. The Sr^{2+} concentration (0.1 to 3.8 ppm) is found to be high in the groundwater (appendix 2.3). The process governing is found to be incongruent dissolution of Aragonite rather than seawater intrusion, which would have increased chloride concentration proportionally. These results are further verified by inverse modeling studies (section 4.7). It is reported that in most cases the elements like, Al, Fe, Mn, Co, Ni, Cu and Zn are affected by filtration artifacts, whereas elements Sr, Ba, Ca, Mg, Na and SiO_2 are affected by dilution [184]. In order to nullify the dilution effect and to have a better estimate of association of Sr^{2+} with particles, Sr^{2+}/Ca^{2+} (percent ratio) is used in this study so that preferential absorption of Sr^{2+} can be estimated over Ca^{2+} in both size ranges (particulate and colloidal).

Table 6. 2 Sr^{2+}/Ca^{2+} ratio (in %) in particulate and colloidal fractions

Location	Sample Code	Particulate	Colloidal
Vanur	C-6	0.89	2.62
Katterikuppam	C-12	2.47	9.06
Sornavur	C-14	0.80	2.40
Kaduvanur	Q-33	1.99	2.80
Karasur	T-29	0.73	1.12

It can be observed from the table 6.2, that Sr^{2+}/Ca^{2+} ratio ranges between 0.7 to 2.5 % in particulate fraction, whereas in colloidal fraction it is in the range of 1 to 9 %. This clearly demonstrates that Sr^{2+} preferential partitions in to colloidal over particulate matter as compared to Ca^{2+}. The relative increase in Sr-association with colloidal fraction is very clearly evident in the case of Cretaceous samples but the same is not true in the case of other samples. Sample collected from limestone formation (C-14) shows much lower colloidal and particulate associated Sr^{2+} due to high Ca^{2+} by Calcite dissolution.

Degeldre et al. [185] suggested that precipitation of minerals directly from groundwater is also equally important process responsible for particles, in addition to alteration of host rock material by groundwater with subsequent suspension. In order to understand whether Sr-associated colloids are precipitated strontium minerals or other inorganic compounds (clay or oxides) with Sr^{2+} adsorbed on them, saturation of strontium minerals and clay minerals in groundwater is verified (Tables 4.2 to 4.4). From modeling studies, it is found that the source of Sr^{2+} is Aragonite mineral which on dissolution releases Sr^{2+} into groundwater. This released Sr^{2+} partitions into dissolved and colloidal species depending on the groundwater chemistry. The dissolved Sr^{2+} if present in excess quantities precipitates as Celestite or Strontionite in presence of high sulphate or carbonates respectively.

The SI values show undersaturation with respect to Celestite (-3.5 to -2.5) and Strontionite (-3.3 to-0.9), pointing that Sr^{2+} is not associated with mineral precipitates. The SI values of clay mineral (Kaolinite) show super-saturation (2.8 to 4.9) indicating the possibility of Sr^{2+} associated with these clay minerals. The clay particles are generally associated with larger surface areas and therefore likely to result in high Sr^{2+} association.

6.5 Applicability of the results in the present study

The particle concentration in groundwater is usually of the order of the µg/L and thus the contamination risks are obvious during water sampling and particle separation. Particles (colloidal) can be generated as artifacts even during on-line sample preparation. Errors commonly arise from excessively high or low pump rates, contamination from borehole activities, complex hydrological situations, contamination from tubes varying the composition of the groundwater, air contamination (uptake and loss of CO_2), aggregation-coagulation effects, long storage times prior to analyses, analytical errors etc. In this work, a few errors could be avoided by choosing bore wells constructed much before 2 years before sampling, and containing PVC casing. Errors from complex hydrology are addressed by choosing wells tapping the same geological formation. Long storage errors are minimized by separating particles within hours of sampling and analyzing within a month. Analytical errors are minimized by employing suitable calibration standards and participating in inter-comparison exercises. However, errors due to loss of gases and subsequent aggregation, coagulation effects could not be addressed in this study. Some more studies are needed to distinguish the true nature of colloids associated with strontium.

6.6 Conclusions

The particle number density in the groundwater is in the range of 4.5×10^5 to 3.3×10^6 per litre with a maximum particle size of 10 µm. Particle size distribution followed power law distribution and the calculated β value fall within the natural range, 2.5 to 4. A systematic decrease in particle number density is observed with well depth, which can be attributed to particle aggregation and sedimentation. The particle load in the size range 0.45 µm to 8 µm is found to be 0.64 to 2.6 mg/L.

Morphological studies indicate particles of spherical, elongated & tubular shapes, and particle agglomeration is noted on the filter circles. Elemental analysis has indicated the presence of Ca and Fe rich particles in the groundwater and NAA studies on filter circles has showed the presence of As and Cr. Zeta potential experiments have indicated that the particles demonstrate mixture of positive and negative charged colloids in 10 KD fraction with a bimodal distribution, whereas 0.5KD fraction is dominated by negative charged colloids with a single Gaussian distribution.

From the chemical studies it can be concluded that the chemical nature of the particles is consistent with the mineralogy of the aquifer. Among various groundwater chemical parameters, organic matter is found to significantly influence the presence of particles in groundwater. There is no systematic trend noticed along groundwater flow in case of particle number density for most of the groundwater samples.

To understand the migration of Sr^{2+} through particles in groundwater, preferential association of Sr^{2+} over Ca^{2+} in both size fractions is evaluated. It is found that Sr^{2+}/Ca^{2+} ratio is always higher in colloidal fraction compared to particulate fraction. The increase of this ratio is also observed along flow path in the case of older and deeper groundwater of Cretaceous formation as compared to younger and shallower groundwater of other formations. From the saturation indices of the strontium minerals it can be stated that the Sr^{2+} migration takes place by the formation of clay bound colloids in groundwater.

SUMMARY

Hydrochemical analysis of groundwater from major aquifers viz., Quaternary, Tertiary and Cretaceous aquifers has indicated that Ca^{2+}, Na^{+}, HCO_3^{-} and Cl^{-} are dominant ions. Based on TDS classification, 29% of the samples fall under desirable and 61% under permissible categories. No nitrate or fluoride contamination is observed in groundwater, but arsenic concentration up to 40 ppb is observed in some groundwater samples from deep zones. A wide variety of micro-organisms are found in groundwater and half of the samples have shown presence of E. coli bacteria. Therefore microbial decontamination is necessary before using groundwater for potable purpose. Microbial studies also indicate presence of SRB in a few groundwater samples inferring reducing condition of the aquifer. Based on SAR, RSC and Na % indicators that qualify the water for irrigation suitability, most of the groundwater can be classified as 'excellent' or 'permissible' category. In some locations groundwater contains high Na % along with high EC, which reduces the osmotic activity of plants and limits the absorption of water and nutrients from the soil. Hence groundwater at these locations is unfit for irrigation.

Aquifer-wise study has been carried out to unravel the geochemical processes taking in each aquifer. Quaternary aquifer is dominated by $Na\text{-}Mg\text{-}HCO_3\text{-}Cl$ and $Na\text{-}Ca\text{-}HCO_3\text{-}Cl$ facies. Primary reactions involve ion exchange and weathering of carbonates in this aquifer. A significant increase is noticed in salt content towards Eastern direction in Sothern part of the study area. Variation in facies is also observed in the groundwater. These observations suggest influence of backwater at these locations. Statistical treatment of the chemistry data also suggests backwater influence in addition to silicate weathering. Inverse modeling calculations demonstrate that K-spar, Dolomite, Gypsum and Halite are common minerals dissolving in groundwater, whereas Aragonite/Calcite, Albite, Ca- Montomorillonite contribution varies depending initial water composition.

In the case of Tertiary aquifer, groundwater basically belongs to $Na\text{-}Ca\text{-}HCO_3\text{-}Cl$ and $Ca\text{-}Mg\text{-}HCO_3$ facies. Silicate dissolution from the source rock dominates in Northern part of the study area while carbonate weathering dominates in South. Characteristic ion ratios indicate processes like Dolomite weathering, Calcite precipitation and cation exchange. Thermodynamic interpretations of silicate minerals reveal that the groundwater is stable with Kaolinite phase indicating the groundwater are geochemically evolved. Statistical treatment of the chemical data suggests contribution of silicates, backwater and fertilizer inputs in to the groundwater. Inverse modeling calculations indicates that positive mole transfer values for Halite, K-spar and Dolomite while negative mole transfer values for Calcite/Aragonite, Exchange and CO_2 gas. Incongruent dissolution of Aragonite is responsible for increased Sr^{2+} concentration in the groundwater.

Two geochemical pathways are observed in Cretaceous aquifer. One of the pathways indicate dissolution of carbonates followed by Gypsum and leaching from clay layers while other indicated ion exchange followed by dissolution of marine sediments. Characteristic ionic ratios and statistical treatment of the data also confirm these findings. The mole transfer values indicate that in most of the cases chemistry of groundwater is controlled by addition of Albite, K-spar, Halite, Aragonite and Gypsum phases, and removal of Dolomite. Modeling studies also indicate that high strontium concentration in final water is due to incongruent dissolution of Aragonite. Speciation calculations for alkaline earth metals are carried out and $MHCO_3^+$ is found to be dominant undissociated species followed by MSO_4 and MCO_3. Undissociated forms account for 30% of total species present. Strontium is found to be associated more with undissociated forms compared to Mg^{2+} and Ca^{2+}.

An attempt has also been made for the first time to establish LMWL for NEM, which is a major contributor of rainfall to this region. Wide distribution in stable isotope data indicates multiple sources of recharge to the Quaternary aquifer while correlations between δ^2H and $\delta^{18}O$ clearly indicate that the recharge to this aquifer is derived from evaporated sources. This is also confirmed by d-excess values. On the other hand, isotope composition of Tertiary aquifer demonstrates narrow distribution pointing to common source of recharge and it also reflects contribution from precipitation without significant evaporation. A similar behavior in isotope composition is observed in groundwater from Cretaceous groundwater. Environmental tritium indicates both old and modern groundwater in the case of Cretaceous aquifer while Tertiary aquifer consists of sub-modern to modern recharge. Isotope variations with Cl^- indicate that dissolution is dominant process contributing to total salt content in groundwater belonging to Cretaceous and Tertiary aquifers while evaporation and mixing with backwater also play a role in increasing the salt content in the case of groundwater from Quaternary aquifer. At few locations interconnection between Tertiary aquifer and surface water / Quaternary aquifer is observed.

Source rock characteristics, weathering and deposition conditions in different sedimentary formations of the Pondicherry region are evaluated using major, minor, trace, REE and $\delta^{13}C$ isotope data. Sediments consist of Quartz and Feldspar as the major minerals in addition to Calcite, Aragonite, Calcite and clay minerals. Trace elemental ratios suggest that sediments are mainly derived from felsic source rocks, which are weathered and diagenetically altered. The ratios of redox sensitive elements (Th/U) infer oxic weathering in shallow sediments. Furthermore, REE data of the sediments also indicate moderate to intense weathering of source rocks. Positive Eu anomaly is observed in NASC normalized REE patterns, which is coincided with earlier studies carried out in Cauvery basin. The geochemical characteristics of the sediments are found to be similar to that of sediments belonging to similar geology in nearby regions. The arsenic content in the sediments of this site ranges between BDL to 30 ppm and high arsenic content is found in clay zones of Cretaceous formation. Arsenic is positively correlated with iron and sulfur concentrations pointing to contribution of Pyrite or Marcasite mineral, which is further confirmed by TXRF analysis.

The particle load in groundwater is in the range of 0.64 - 2.6 mg/L for size range 0.45 - 8 µm. The particle number density is in the order of 10^5 to 10^6 per litre and maximum particle size found in groundwater is 10 µm. Morphological studies indicate particles of spherical, elongated & tubular shapes. These particles are mainly composed of Ca and Fe. Zeta potential experiments indicate that the particles demonstrate a mixture of positive and negative charged colloids in 10 KD fraction with a bimodal distribution, whereas 0.5 KD fraction is dominated by negative charged colloids with a single Gaussian distribution.

To understand the migration of Sr^{2+} in groundwater, preferential association of Sr^{2+} over Ca^{2+} in colloidal and particulate size fractions is evaluated. It is found that Sr^{2+}/Ca^{2+} ratio is always higher in colloidal fraction compared to particulate fraction. The increase of this ratio is also observed along flow path in the case of older and deeper groundwater of Cretaceous formation as compared to younger and shallower groundwater of other formations. Modeling studies suggest that the strontium migration is mainly through clay bound colloids and undissociated bicarbonate complex.

As far as the future scope of research in groundwater of this region is concerned, early detection of deterioration is necessary to efficiently protect groundwater quality as geogenic contamination once mobilized may take several decades for amelioration. Detailed laboratory experiments are needed to study leaching of arsenic from in situ sediment cores under different pH, Eh, salt content, which would give information on leachable fraction of arsenic that its availability in groundwater. There is an immediate need to study the isotope systematics of groundwater using $^{234}U/^{238}U$activity ratio, ^{34}S and ^{3}H-^{3}He dating techniques that would give a clearer picture on contaminant dynamics and immensely help to the local groundwater authorities to take precautionary remedial measures.

REFERENCES

[1]. Shiklomanov A. and Rodda J. C., Summary of the Monograph 'World Water Resources at the beginning of the 21st Century, prepared in the framework of IHP UNESCO, 2003.

[2]. UNESCO, World Water Assessment Programme, UN World Water Development Report 2: Water: A Shared Responsibility; Paris, UNESCO and New York, Berghahn Books, 2006, p. 279.

[3]. Vaidyanathan A., Indian Journal of Agricultural Economics 51 (1-2): 1996, 184-192.

[4]. Gupta S.K., Deshpande R.D., Current Science, Vol. 86, No. 9 (2004) 1216-1224.

[5]. Athavale R.N., Rengarajan R. and Muralidharan D., Journal of Geological Society of India, 39 (1992) 235-244.

[6]. Matthew Rodell, Isabella Velicogna & James S. Famiglietti, Nature (460)999-1002.

[7]. Herczeg A.L. and Edmunds W., Inorganic ions as tracers. In environmental tracers in subsurface hydrology, (Eds.) P.G. Cook and Herczeg A.L., (1999) 31-77, Boston, Kluwer AP.

[8]. Glynn P.D. and Plummer L.N., Hydrogeol. J., 13(2005) 263-287.

[9]. Hem J.D., Study and Interpretation of the Chemical Characteristics of Natural Water. USGS WSP 2254, 1989.

[10]. Drever J.I., The geochemistry of natural waters, Pretice-Hall Inc., 1988,pp. 437.

[11]. Faure G., Principles and Applications of Inorganic Geochemistry: Macmillan, New York, (1991) 626 pp.

[12]. Chebotarev I.I., Geochimica et cosmochimica Acta. 8 (1955) 22-48.

[13]. Sanchez-Martos F., Pulido-Bosch A., Calaforra J.M., Appl. Geochem. 14 (1999) 735–745.

[14]. de Vriesa J.J., Selaolob E.T. and Beekmanc H.E., Journal of Hydrology 238 (2000) 110–123.

[15]. John Mather, Relationship between rock, soil and groundwater compositions, Geochemical processes, weathering and groundwater recharge in catchments, (Eds.) O.M. Saether and P. de Caritat, 1997, Balkema

[16]. Langmuir D., Aqueous Environemtal Geochemistry, Prentice-Hal, New Jersy, 1997.

[17]. Stumm W, Morgan J, Aquatic Chemistry. 3rd edition. John Wiley and Sons, New York. 1996.

[18]. Worden R.H., Morad S., Clay minerals in sandstones: controls on formation, distribution and evolution. Int. Assoc. Sedimentol. Spec. Publ., 2003, pp. 3-41.

[19]. Bear J. and Bachmat Y., Introduction to modeling of transport phenomena in porous media, Kluwer Academic Publishers Group, 1990.

[20]. Gurunadha Rao V.V.S., Dhar R.L., Jayachand T. and Khoker C.S., Environmental Geol., 39 (2000) 1138-1146.

[21]. Plummer L.N., Busby J.F., Lee R.W. and Hanshaw B.B., , Water Resources Research, 26 (1990) 1981-2014.

[22]. Carl I. Steefela, Donald J. DePaoloa , Peter C. Lichtnerc, Earth and Planetary Science Letters , 240 (2005) 539–558.

[23]. Wenning R.J. and Erickson G.A., Trends in Analytical Chemistry, 13 (1994) 446–457.

[24]. Raghunath R., T.R.S. Murthy, B.R. Raghavan, Water Research, 36 (2002) 2437–2442.

[25]. Swan A.R.H and Sandilands M, Introduction to Geological Data Analysis, Blackwell, Oxford (1995).

[26]. Reyment RA, Joreskog KH. Applied factor analysis in the natural sciences. Cambridge, England; Cambridge University Press, 1993.p. 371.

[27]. Clark, I. D. and Fritz, P., Environmental isotopes in hydrogeology, New York, Lewis Publishers, 1997.

[28]. Sharp Z., Principles of Stable Isotope Geochemistry. Pearson Prentice Hall, NJ 2007.

[29]. Cook P. and Herczeg A., Environmental Tracers in Subsurface Hydrology. Boston, USA, 1999.

[30]. Craig, H., Science, 133 (1961)1702-1703.

[31]. Rozanski K., Araguas L. and Gonfiantini R., Isotopic patterns in modern global precipitation. In: Climate change in continental isotopic records. American Geophysical Union, Geophysical Monograph 78 (1993) 1-36.

[32]. Gat J.R. and Carmi I., J. Geoph. Res.,75 (1970).3039-3048.

[33]. Carothers W.W. and Kharaka Y.K. Geochim. et Cosmochim. Acta. 44 (1980) 323-332.

[34]. Rightmire C.T. and Hanshaw B.B., Water Resour. Res., 9 (1973) 958-967.

[35]. Libby W.F., Phys. Rev. 69 (1946) 671-672.

[36]. Henderson P., Rare Earth Element Geochemistry, Elsevier, Amsterdam, 1984.

[37]. Cullers R.L., Lithos 51 (2000) 181–203.

[38]. McLennan S. M., Hemming S. R., McDaniel D. K., Hanson G. N., Geochemical approaches to sedimentation, provenance and tectonics, in: Johnsson, M. J., Basu, A. (Eds.), Processes Controlling the Composition of Clastic Sediments, Geol. Soc. Am. Spec. Pap. 284 (1993) 21–40.

[39]. Ma J.L., Wei G.J., Xu Y.G., Long W.G.and Sun W.D., Geochim. et Cosmochim. Acta 71 (2007) 3223–3237.

[40]. Francesco Perri, Salvatore Critelli, Giovanni Mongelli and Cullers R. L., Int. J. Earth Sci. (Geol Rundsch), 2010, DOI 10.1007/s00531-010-0602-6.

[41]. Taylor S R, and McLennan S.M., The continental crust: its composition and evolution. Blackwell, Oxford, 1985.

[42]. Sinha S., Islam R., Ghosh S.K., Rohtash Kumar and Sangode S.J., Curr. Sci. 92 (2007) 1103-1113.

[43]. Attendorn, H.G., Bowen, R. N. C., Radioactive and Stable Isotope Geology, Chapman & Hall, London, 1997.

[44]. Smedley, P.L., Kinniburgh, D.G., Appl. Geochem.17 (2002) 517–568.

[45]. Bhumbla D., Keefer R., Arsenic mobilization and bioavailability in soils. In: Nriagu, J.O. (Ed.). Arsenic in the Environment, Part 1: Cycling and Characterization. John Wiley & Sons Inc., 1994, 51–82.

[46]. Ryan J.N. and Elimelech M., Colloids and surfaces A : Physicochemical and Engineering Aspects 107 (1996) 1-56.

[47]. Honeyman J.T. and Santschi P.H.,. The role f particles and colloids in the transport of radionuclides and trace metals in the oceans. In: J. Buffle and H.P. Van Leeuwen (Eds.), Environmental Particles, Lewis, Chelsea, Ml, 1992, 379-423.

[48]. Morel F.M.M. and Gschwend P.M., The role of colloids in the partitioning of solutes in the natural waters. In: W. Stumm (Eds.), Aquatic Surface Chemistry. Wiley, NY, 1987, 405-422.

[49]. Buffle J. and van Leeuwen H.P., Environmental Particles: Volume 1, Lewis Publishers, MI, USA (1992) 554.

[50]. Wen L.S., Santschi P.H., Gill G. and Paternostro C., Environ. Sci. and Technol. 31(1997) 723-731.

[51]. Sukhija B.S., Reddy D.V. and Vasanthakumar Reddy I., Study of groundwater resources of Pondicherry and its environs, National Geophysical Research Institute, Hyderabad, 1987, 1-153.

[52]. CGWB, Groundwater Resources and Development Prospects in Pondicherry Region, Union Territory of Pondicherry, Central Ground Water Board, Ministry of Water Resources, Southern Region, Hyderabad, India, 1993.

[53]. Raghava Rao, K.V., Krupanidhi, K.V.J.R., Balasubramaniyan, G., Subramaniyan, P.R. and Natarajan, P. (1976) Report on groundwater survey and exploration in the Union territory of Pondicherry and its environs, CGWB report, India.

[54]. Somasundaram M. V., Ravindran G.and Tellam J. H., Ground Water, 31(1993) 4-11.

[55]. Nathalie Gassama, Sophie violette, Noemi d'ozouville, Aline Dia and Nathalie Jendrzejewski, Multiple origin of water salinization in a coastal aquifer, Bay of Bengal, Hydrology of the Mediterranean and Semiarid Regions. In proceedings of an international symposium held at Montpellier. IAHS Publ. no. 278 (2003) 471-476.

[56]. Rangarajan R .and Balasubramanian A., J.App.Hydrol. 2 (1990) 15-22.

[57]. Sastri J.C.V. and Lawrence J.F., Geophysical Res Bull 26-1 (1988) 39–44.

[58]. Srinivasamoorthy K., Chidambaram S., Anandhan P. and Vasudevan S., Journal of geochemistry,20 (2005).181-190.

[59]. Pandian K. and Sankar K. Journal Geological Society of India, 69 (2007) 970-982.

[60]. Ramesh R., Shivkumar K., Eswaramoorthy S. and Purvaja G.R., Environ Geol. 25 (1995).126–136.

[61]. CGWB, Groundwater quality in shallow aquifers of India, Central Ground Water Board, Ministry of Water Resources, Government of India, 2010, p. 177.

[62]. Venkateswaran K. and Natarajan R. Indian Journal of Marine Science 16 (1987) 51-53.

[63]. Abhay Kumar V.K. and Dube H.C, Journal of Marine Biology Association of India 37 (1985) 98-101.

[64]. Vaidya S.Y., Vala A.K.and Dube H.C., J. Microbiol.41 (2001) 37–39.

[65]. Anderson Y. and Bohan P. Disease surveillance and water borne outbreaks. In water quality. Guidelines, Standards and Health, (eds.) Fewtrell L. and Bartram J., London, IWA Publishing, 2001.

[66]. Walsh J.A., Estimating the burden of illness of the tropics. In; (eds.) K.S. Warren and A. A. F. Mahoud, Tropical and Geographical medicine (2^{nd} ed.), New York, Mc-Graw Hill, 1990.

[67]. Shivanna K., Tirumalesh K. and Suresh S., Environmental Isotope hydrochemical investigation for characterization of groundwater in Tiruvanmiyur Coastal aquifer, Tamil Nadu, India, In: Taylor and Francis P. Bhattacharya, A.L. Ramanathan, A.B. Mukherjee, J. Bundschuh, D. Chandrasekharam & A.K. Keshari (Eds.) Balkema Book, “Groundwater for

Sustainable development Problems, Perspectives and Challenges", Chapter 18, 2006,pp.183-198.

[68]. Rao S.M., Jain S.K., Navada S.V. and Shivanna K., Isotopic Studies on Sea Water intrusion and interrelations between Water Bodies: Some Field Examples. Isotope techniques in water resources development, Proc. International Symposium, IAEA, Vienna SM-299/76, 1987.403-425.

[69]. Sukhija, BS., Reddy, DV., Nagabushanam, P., Hussain, S. and Giri, VY. (1996) The use of environmental isotopes and Chloride as natural tracers to investigate the effectsof depressurization of a coastal aquifer for lignite mining, India. Hydrol J, v.4 (2), pp. 70 – 87.

[70]. Sukhija B.S., D.V. Reddy and P. Nagabhushaman, Quart. Res.50 (1998) 252-260.

[71]. Saravana Kumar .U, Suman Sharma, S.V. Navada, A.S. Deodhar, J. Hydrol. 364 (2009) 23–39.

[72]. Prasanna M.V, Chidambaram S, Shahul Hameed A and Srinivasamoorthy K. Environ. Monit. Assess. (2009). DOI 10.1007/s 10661-009-1092-5.

[73]. Chidambaram. S., M. V. Prasanna, A. L. Ramanathan, K. Vasu, S. Hameed, U. K Warrier, K. Srinivasamoorthy, R. Manivannan, K. Tirumalesh, P. Anandhan, and G. Johnsonbabu., Hydrol. Process. (2009) DOI: 10.1002/hyp.7300.

[74]. Altrin A. J. S., Lee Y.I., Verma S.P. and Ramasamy S., J. Sediment. Res. 74 (2004) 285-297.

[75]. Madhavaraju J., Ramasamy S., Alastair Ruffell and Mohan S. P., Cret. Res. 23 (2002) 153-163.

[76]. Pramod Singh and Rajamani, V., Geochim.et Cosmochim. Acta 65 (2001) 3093–3108.

[77]. Bakkiaraj D., Nagendra R., Nagarajan R. and Altrin A.J.S., J. Geol. Soc. India 76 (2010) 453-467.

[78]. Madhavaraju J. and Lee Y., Curr. Sci. 98 (2010) 528-537.

[79]. Das D., Samanta G., Mandal B.K., Chowdhury T.R., Chanda C.R. Chowdhury P.P., Basu G.K. and Chakraborti D., Environ. Geochem. Health 18 (1996)5–15.

[80]. Chakraborti D., Biswas B.K., Chowdhury T.R., Basu G.K., Mandal B.K., Chowdhury U.K., Mukherjee S.C., Gupta J.P., Chowdhury S.R., Rathore K.C., Curr. Sci. 77 (1999) 502-504.

[81]. Acharyya S.K., Curr. Sci. 82 (2002) 740-744.

[82]. Subramanian V., J. Geol Soc India 29 (1987) 205-220.

[83]. Singhal R.K., Preetha J., Rupali Kapre, Tirumalesh K., Kumar S.C. and Hegde A.G., Environ. Internat. 32 (2006) 224-228.

[84]. Ayyadurai K. and Krishnaswamy K., Environ. Biol.10 (1989) 165-171.

[85]. Subramanian V., Ramanathan A.L. and Vaithyanathan P., Ibid, 20 (1989) 286-290.

[86]. Stephen-Pichaimani V., Jonathan M.P., Srinivasalu S., Rajeshwara Rao and Mohan S.P., Environ Geol 55 (2008) 1811–1819.

[87]. Deepthi Rani and Sasidhar, Environ Earth Sci 62 (2011)233–243.

[88]. Donaldson E.M., Talanta 28 (1981) 825–831.

[89]. Hounslow A.W., Water quality data - analysis and interpretation, CRC press Inc, 1995.

[90]. Andrew O. Simm, Craig E. Banks, Richard G. Compton, Electroanalysis 17 (2005) 1727–1733.

[91]. Williams S. T., Bergey's manual of systematic bacteriology. Baltimore, 1989.

[92]. APHA, AWWA, WEF., Standards for Examination of Water and Wastewater, 20th ed. American Public Health Association, Washington DC USA, 1999.

[93]. Coplen T.B., Wildman J. and Chen J., Anal. Chem. 63 (1991) 910-912.

[94]. Nair A.R., Possibilities of liquid scintillation counting for tritium and radio carbon measurements in natural water. In, proceedings of the Workshop on Isotope Hydrology, Mumbai,1983,pp 41–56.

[95]. Plummer L.N., Prestemon E.C., and Parkhurst D.L., An Interactive Code (NETPATH) for Modeling Net Geochemical Reactions along a Flow Path Version 2.0: U.S. Geological Survey Water-Resources Investigations Report 94-4169, Reston, Virginia, 1994.

[96]. Truesdell A.H. and Jones B.F., WATEQ, A computer program for calculating chemical equilibria of natural waters, U.S. Geological Survey, 2 (1974) 233-274.

[97]. Ball J.W. and Nordstrom D.K., User's manual forWATEQ4F, with revised thermodynamic data base and test cases for calculating speciation of major, trace, and redox elements in natural waters: U.S. Geological Survey Open-File Report 91-183 (1991) p.189.

[98]. Papatheodorou George, Gerasimoula Demopouloua, Nicolaos Lambrakis, Ecological Modeling 193 (2006) 759–776.

[99]. Lambrakis N., A. Antonakos and G. Panagopoulos, Water Res. 38 (2004) 1862–1872.

[100]. Helena B., Pardo R., Vega M., Barrado E., Fernandez J. and Fernandez L.,. Water Res. 34 (2000) 807–816.

[101]. David Love, Dieter Hallbauer, Amos Amos, Roumiana Hranova, Physics and Chemistry of the Earth 29 (2004) 1135–1143.

[102]. Mitsuru Ebihara and Tsutomu Miura, Geochimica et Cosmochimica Acta, 60 (1996) 5133-5144.

[103]. Walkey A.J. and Black I.A., Soil Science 37 (1934) 29-38.

[104]. McCarthy J, Degueldre C, Sampling and characterization of colloids and particles in groundwater for studying their role in contaminant transport. In, Environmental particles, volume 2, Environmental analytical and physical chemistry series, IUPAC, Lewis Publishers, 1993.

[105]. Chittleborough D.J., Hotchin D.M. and Beckett R., Soil Sci. 153 (1992) 341–348.

[106]. Knollenberg R. G. and Veal D. L., Optical particle monitors, counters, and spectrometers: performance characterization, comparison and use. In, proceedings of the 37th Annual Technical Meeting of the Institute of Environmental Sciences. San Diego, 1991, 750–771.

[107]. Rees T.F., Ranville J.F. Characterization of colloids in the Mississippi River and its major tributaries Water Res. Invest. USGS, 88-4220, 1989, pp. 513–522.

[108]. Lienemann Charles-Philippe, Andreas Heissenberger, Gary Grant Leppard, Didier Perret, Aquatic Microbial Ecology 14 (1998).205-213

[109]. Peavy H. S., Rowe D. R., and Tchobanoglous G. T., Environmental Engineering, McGraw-Hill Inc., New York, 1985, pp. 22–31.

[110]. Brian Hitchon, Perkins, E. H., & Gunter, W. D., Introduction to ground water geochemistry, Geoscience Publishing Ltd., Alberta, 1999.

[111]. Fifield F. W., and Haines P. J., Environmental analytical chemistry (2nd ed.). Oxford, Blackwell, 2000.

[112]. Tyson R.V. and Pearson T H., Modern and ancient continental shelf anoxia: an overview. In, Tyson R V, Pearson TH (eds.) Modern and ancient continental shelf anoxia, Geological Society Special Publication, No. 58, 1991, pp. 1-26.

[113]. Handa B.K., Ground Water 13 (1975) 275–281.

[114]. Tirumalesh K., Shivanna K., and Jalihal A.A., Hydrogeol. J. 15 (2007) 589-598.

[115]. David, M. D., and Gentry, L. E., J. Environ. Qual. 29 (2000) 494-508.

[116]. WHO, Guidelines for drinking water quality, Recommendations (2nd edition) world health organization Geneva, 1993.

[117]. BIS, Indian Standard Specifications for drinking water IS: 10500: 1991, 1-5.

[118]. Chapra S.C., Surface Water Quality Modeling. McGraw-Hill Inc., New York. 1997.

[119]. Davies, S. N., and DeWiest, R. J. M., Hydrogeology. New York: Wiley, 1966.

[120]. Todd D.K., Ground water hydrology, New York: Wiley, 1980.

[121]. Durfor C. N. and Becker E., Public water supplies of the 100 largest cities in the United States, water supply paper No. 1812, 1964, 343-346.

[122]. Richards L. A., Diagnosis and improvement of saline and alkali soils. Washington: US Dept. of Agriculture, Agri. Hand book, 1954.

[123]. Trivedy R. K. and Goel P. K., Chemical and biological methods for water pollution studies. Karad: Environmental Publication, 1984.

[124]. Karanth K. R., Groundwater assessment, development and management. New Delhi, Tata-McGraw- Hill, 1987.

[125]. Wilcox L. V., The quality of water for irrigation use, U.S. Dept. of Agriculture, Tech, Bull, 962, Washington, D. C., 1948, 1–40.

[126]. Ramakrishna, Groundwater handbook, India, 1998.

[127]. Wilcox L. V., Classification and use of irrigation water. U.S. Geological department, Agri Arc. 969. pp. 19, Washington, D. C., 1955.

[128]. Eaton, E. M., Soil Science, 69 (1950) 123–133.

[129]. Lloyd J. W. and Heathcote J. A., Natural inorganic hydrochemistry in relation to groundwater. Clarendon, Oxford, 1985, pp. 294.

[130]. USSL, Diagnosis and improvement of saline and alkaline soils. Washington: United States Salinity Laboratory, U. S. Department of Agriculture, 1954.

[131]. Piper A.M., A graphic procedure in the geochemical interpretation of water analysis, Trans Amer. Geophys union, v.25 (1944) 914–923.

[132]. Garrison Sposito, The chemistry of soils, Oxford University Press Inc. 1989.

[133]. Matthess G, The properties of Groundwater, John Wiley, New York, 1982.

[134]. Ophori D. U. and Toth J., Ground Water 27 (1989) 20–26.

[135]. Whiteman K.J., J.J. Vaccaro J.B. Gonthier and H.H. Bauer., The hydrogeologic framework and geochemistry of the Columbia Plateau aquifer system, Washington, Oregon, and Idaho. Prof. Paper 1413-B. USGS, Washington DC, 1994.

[136]. Choia Byoung-Young, Seong-Taek Yuna, Bernhard Mayerb, So-Young Honga, Kyoung-Ho Kima, Ho-Young Joa, Chem. Geol.306–307 (2012) 103–113.

[137]. Capaccioni B., M. Didero C. Paletta P. Salvadori, J. Hydrol. 253 (2001) 14–26.

[138]. Feth J.H., Chloride in natural continental waters – a review, U.S.Geol. Survey Water – Supply Paper 2176, 1981.

[139]. Sprinkle C.L., Geochemistry of the Floridan aquifer system in Florida and in parts of Georgia, South Carolina, and Alabama, USGS Prof. Paper 1403-1, 1989.

[140]. Appelo C.A.J., Postma D., Geochemistry, Groundwater and Pollution, A A Balkema Publishers, 2005.

[141]. Harry Y. McSween, Steven McAfee Richardson, Maria E. Uhle, Geochemistry: Pathways and Processes, Columbia University Press, 2003.

[142]. Leroy L. Knobel, Roy C. Bartholomay and Brennon R. Orr, Preliminary delineation of natural geochemical reactions, Snake river plain aquifer system, Idaho national engineering laboratory and vicinity, Idaho, Water-Resources investigations report, U.S. Geological Survey, 97-4093, 1997.

[143]. Chappelle F.H., Water Resour. Res. 19 (1983) 545-558.

[144]. White A. F., Chemical Weathering Rates of Silicate Minerals in Soil, in, White, A. F., and Brantley, S. L. (Eds.), Chemical Weathering Rates of Silicate Mineralogy: Mineralogical Society of America Reviews in Mineralogy, v. 31, 1995, p. 407- 461.

[145]. Komor S.C., Anderson H.W., Ground Water 31 (1993) 260–270.

[146]. Olmez I, Beal J.W., Villaume J.F., Water Res. 28(1994) 1095-1101.

[147]. Hanshaw B.B. and Back W., J. Hydrol. 43 (1979) 287-312.

[148]. Deutsch W.J., Groundwater Geochemistry: Fundamentals and Applications to Contamination, Lewis publishers, Washington DC, 1997.

[149]. Sahai N., Carroll S. A., Roberts S., O'Day P. A., J. Colloid Interface Sci. 222 (2000) 198-212.

[150]. WHO, RC-54, Arsenic contamination in groundwater affecting some countries in the Southeast Asia region. The fifty fourth regional committee of Southeast Asia region. Yangon, Myanmar, SEA/RC54/8, 2001.

[151]. Chowdhury T.R., Kumar G., Mandal B.K., Samanta G., Chowdhury U.K., Chandra C.R., Lodh D., Lal Roy S., Saha K.C., Roy S., Kabir S., Quamruzzaman Q., Chakraborti D., Nature 401 (1999) 545-546.

[152]. Nickson R.T., McArthur J.M., Burgess W., Ahmed K.M., Ravenscroft P., Rahman M., Nature 395 (1998) 338.

[153]. McArthur J.M., Banerjee D.M., Hudson-Edwards K.A., Mishra R., Purohit R., Ravenscroft P., Cronin A., Howarth R.J., Chatterjee A., Talkdar T., Lowry D., Houghton S., Chadha D.K., Appl. Geochem. 19 (2004) 1255–1293.

[154]. Macur R.E., Jackson C.R., Botero L.M., Mcdermott T.R., Inskeep W.P., Environ. Sci. Technol. 38 (2004) 104–111.

[155]. Hesham M.B., Mohamed A.E.K., Ahmed E.H., J Cont Hydrol. 108 (2009) 152–167.

[156]. Hao O.L., Metal Effects on Sulfur Cycle Bacteria and Metal Removal by Sulfate-Reducing Bacteria. IWA Publishing, London, 2000.

[157]. Jansons J, Edmunds LW, Speight B, Bucens M.R., Water Research 23 (1989) 301-306.

[158]. Melnick J.L., Gerba C.P., CRC Critical Reviews in Environment Control 10 (1980) 65-93.

[159]. Bitton G, Harvey R.W., Transport of pathogens though soil and aquifers. In: Mitchell R (ed) Environmental Microbiology, Wiley-Liss, New York, 1992, pp. 103-124.

[160]. Roslev P., Bjergbaek L.A., Hesselsoe M., J. App. Microbiol. 96 (2004) 938-945.

[161]. Percival S.L., Walker J.T., Hunter P.R., Microbiological aspects of biofilms and drinking water. CRC Press: Boca Raton, 2000.

[162]. Datta P. S., S. K. Tyagi and H. Chandrasekharan, J. Hydrol. 128 (1991) 223–236.

[163]. Mukherjee T. K. and H. Chandrasekharan, J. Nucl.Agric. Biol. 22 (1993) 34–41.

[164]. Frtiz P., Fontes J. Ch., Frape S.K., Louvat D., Michelot J.L., Balderer W., Geochem. et Cosmochim. Acta 53 (1989) 1765-1775.

[165]. Johannesson K.H., Stetzenbach K.J., Hodge V.F., Lyons W.B., Earth Planet. Sci. Lett. 139 (1996) 305-320.

[166]. Aubert P. Stille Probst A., Geochim. Cosmochim. Acta 65 (2001) 387–406.

[167]. Wronkiewicz D.J., Condie K.C., Geochim. et Cosmochim. Acta 51 (1987) 240-246.

[168]. Cullers R.L., Chem. Geol. 191 (2002) 305-327.

[169]. Feng R., Kerrich R., Geochim. et Cosmochim. Acta 54 (1990) 1061-1081.

[170]. Floyd P.A. and Leveridge B.E., J. Geol. Soc. London 144 (1987) 531-542.

[171]. Cullers R. L., Geochim. et Cosmochim. Acta 58 (1994) 4955-4972.

[172]. Cullers R.L., Basu A., Suttner L.J., Geochim. et Cosmochim. Acta 63 (1988) 275-297.

[173]. Stéphanie Duchamp-Alphonse, Nicolas Fiet, Thierry Adatte, Maurice Pagel, Palaeogeography, Palaeoclimatology, Palaeoecology 302 (2011) 243–254.

[174]. O’Day P.A., Carroll S.A., Waychunas G.A., Environ. Scien. Tech 32 (1998) 943–955.

[175]. Anawar H.M., Akai J., Komaki K, Terao H., J. Geochem. Explor. 77 (2003)109–31.

[176]. Schreiber M.E., Simo J.A., Freiberg P.G., Hydrogeol. J. 8(2000) 161-176.

[177]. Kinniburgh D.G., Smedley P.L., Arsenic contamination of groundwater in Bangladesh. British Geological Survey report. WC/00/19, 2001.

[178]. Buffle J., Complexation reactions in aquatic systems, Ellis Horwood, 1988.

[179]. Filella M., Colloidal properties of submicron particles in natural waters, K.W. Wilkinson, J. Lead (Eds.), Environmental Colloids and Particles: Behaviour, Separation and Characterisation, Wiley, New York, 2007, pp. 17–93

[180]. Hedqvist, Studsvik Nuclear A.B., Granitic groundwater colloids sampling and characterization. Colloids analysis from KLX17A (416.0 to 437.5 m) and KLX15A, Claude Degueldre, Paul Scherrer Institute, Villigen and University of Geneva, Switzerland, 2008.

[181]. Kevin Gardner and Defne S. Apul, Influence of colloids and sediments on water quality, in environmental and ecological chemistry, (Ed. Aleksandar Sabljic), in encyclopedia of life support systems, 2006.

[182]. Klein C., Manual of Mineral Science, 22nd ed. John Wiley and Sons, New York, 2002.

[183]. Gephart R. E. and Hanford A., Conversation about Nuclear Waste and Cleanup; Battelle Press, Columbus, OH, 2003.

[184]. Horowitz A.J., Lum K.R., Garbarino J.R., Hall G.E.M., Lemieux C., and Demas C.R., Environmental Science and Technology, 30 (1996) 954-963.

[185]. Degueldre C, Grauer R, Laube A, Oess A, Silby H, Appl. Geochem. 11 (1996).697–710.

Appendix 2. 1 Geographical coordinates and physical parameters of groundwater

Location name	longitude	latitude	Location code	Well depth	Temp	pH	Eh	DO	E. C.	Alkalinity
Quaternary aquifer										
Suthukkeni	79.6785	12.0149	Q-7	18	ND	7.87	455	ND	508	175
S.Pudukuppam	79.6915	12.021	Q-8	16	ND	7.65	435	ND	1199	600
Sorapet	79.6626	11.955	Q-19	13	ND	8.80	449	ND	922	290
Mannadipattu	79.6361	11.917	Q-22	10	ND	7.97	443	ND	685	168
Thurubhuvanai	79.6434	11.9292	Q-23	20	ND	8.19	435	ND	1035	295
Ariyur	79.6673	11.9117	Q-24	18	ND	7.36	448	ND	1718	375
Gudapakkam	79.729	11.936	Q-25	13	ND	8.30	433	ND	763	173
Embalam	79.7155	11.8736	Q-28	10	ND	7.41	447	ND	1046	318
Karayampathur	79.6525	11.8229	Q-31	15	ND	8.83	433	ND	864	228
Kaduvanur	79.6959	11.8203	Q-33	46	ND	8.12	441	ND	1552	265
Thirupanampakkam	79.7152	11.8115	Q-34	35	30.8	7.12	185	2.6	1120	338
Melperikkal pet	79.7554	11.7924	Q-36	20	ND	8.48	453	ND	1929	113
Tertiary aquifer										
Pillaichavadi	79.8569	12.0063	T-11	130	31.3	6.40	342	3.9	306	62
Kuyilpalayam	79.8353	11.9881	T-17	40	31.5	6.02	ND	2.8	282	60
Pattanur	79.7751	11.9821	T-20	28	30.9	7.24	ND	3.7	1150	430
Murattandichava	79.7898	11.9793	T-21	80	32.1	6.73	321	3.5	256	93
Muthiryapalayam	79.7694	11.9261	T-26	95	31.0	6.59	368	1.0	737	175
Lawspet	79.8167	11.9558	T-27	100	31.1	6.35	ND	5.0	1084	180
Sornavur	79.6277	11.8239	T-29	61	29.5	7.30	369	5.5	798	300
Kalinzhikuppam	79.6459	11.8096	T-30	108	29.3	7.24	389	5.3	853	275
Karayampathur	79.6525	11.8229	T-31	105	31.7	7.30	320	4.1	1053	343
Krishnapuram	79.6854	11.8266	T-32	150	31.2	7.20	313	2.6	1198	370
Kaduvanur	79.6959	11.8203	T-33	55	30.5	7.39	298	3.9	1136	360
Thirupanampakkam	79.7152	11.8115	T-34	50	32.1	7.57	403	3.9	557	235
Bahour	79.7397	11.81	T-35	180	31.7	6.66	ND	1.9	626	135
Periyakanganaku	79.7669	11.78	T-37	140	32.9	6.32	394	2.0	360	125
Kanniyakoil	79.7767	11.8035	T-38	215	32.3	6.27	258	1.6	402	125
Cretaceous aquifer										
Sethanapattu	79.6993	12.0556	C-1	100	31.6	7.32	416	6.2	1240	545
Vinayakapuram	79.7178	12.0504	C-2	80	32.2	5.82	395	3.5	1360	153
Katrambakkam	79.7513	12.0555	C-3	100	31.5	7.26	ND	4.0	1372	335
Ozhindiayapattu	79.7766	12.0498	C-4	100	31.4	7.43	437	3.3	1143	303
Mathur	79.8312	12.0443	C-5	180	31.9	7.10	249	6.9	1540	340
Kanagachettikulam	79.8712	12.0399	C-6	100	31.1	7.31	305	2.2	1731	248
Vanur	79.7357	12.0228	C-9	80	31.1	7.34	ND	4.0	976	375
Sanjivi Nagar	79.7989	12.0211	C-10	165	32.5	7.31	241	2.3	1331	400
Katterikuppam	79.7065	12.0015	C-12	180	30.5	7.05	229	3.5	701	318
Valudhavur	79.7014	11.9793	C-13	110	31.9	7.31	342	4.3	1167	365
Karasur	79.7395	11.983	C-14	185	32.1	6.87	448	2.5	2194	217
Sedarapet	79.7509	11.9875	C-15	180	32.1	6.87	229	3.2	792	300
Thiruchitrambalam	79.775	11.9901	C-16	100	31.0	7.38	258	6.0	851	374
Kurayanpalayam	79.6603	11.9656	C-18	100	31.4	7.22	248	2.0	1245	390

Note: latitude and longitude in degrees; well depth in meters bgl, DO, Alkalinity in ppm, Temp. in °C and Eh in mV

Appendix 2. 2 Chemical and microbial data of groundwater

Code	Cl^-	NO_3^-	SO_4^{2-}	HCO_3^-	Na^+	K^+	Mg^{2+}	Ca^{2+}	Si	CBE	TDS-calc	TVB	E. coli	SRB
Quaternary aquifer														
Q-7	59.7	12.3	8.3	214	58	2.85	21	36	ND	4.8	414	2700	nd	nd
Q-8	204.0	3.2	17.5	427	221	5.61	36.6	28.32	ND	3.7	946	4000	50	nd
Q-19	96.6	1.1	19.2	354	164	2.48	26.3	8.4	ND	4.5	674	21600	10	nd
Q-22	107.0	9.0	11.7	204	87	2.40	26	19.8	ND	1.7	470	18000	nd	nd
Q-23	155.0	34.0	22	360	142	2.76	42.5	27.8	ND	-0.7	789	2400	nd	nd
Q-24	238.0	6.0	141	458	214	1.47	40.7	113	ND	3.1	1216	3650	300	nd
Q-25	108.0	1.6	29.6	210	96	4.09	21	31.8	25.3	3.2	531	22000	nd	nd
Q-28	93.0	7.9	52	387	144	1.84	25.4	50.76	31.8	3.5	798	33000	110	nd
Q-31	96.0	7.0	30	278	143	6.60	23.5	8.8	49.7	4.6	644	3100	60	nd
Q-33	268.0	2.7	80.4	323	233	1.15	39.9	33.24	54.8	1.8	1041	18000	15	nd
Q-34	118.0	0.2	58.0	412	152	1.04	22.6	49.3	26.8	-1.5	841			
Q-36	550.0	31.3	22	137	275	4.28	51.7	34.4	44.3	-1.9	1155	3600	300	nd
Tertiary aquifer														
T-11	44.7	15.8	10.4	76	25	2.80	8.1	20.2	27.4	-2.8	231			
T-17	24.1	10.2	4.5	73	11	4.80	7.8	18.2	34.6	0.0	189	8000	nd	360
T-20	118.0	1.7	14.6	525	44	0.60	70.2	76.0	58.8	-3.2	914	18800	nd	nd
T-21	15.9	4.8	3.8	113	12	3.54	8.6	24.4	54.2	1.6	241	4500	15	nd
T-26	76.2	5.1	72.1	214	75	5.30	13.4	59.5	34.5	1.6	559	3950	180	nd
T-27	230.0	16.0	44.9	220	129	8.20	19.1	63.2	30.9	-3.4	764	9100	nd	nd
T-29	55.5	16.6	27.0	366	72	1.57	22.6	55.2	36.8	-3.8	654	25400	75	nd
T-30	72.0	14.4	26.4	336	81	2.20	26.6	56.7	40.0	1.6	656			
T-31	99.4	5.2	46.6	418	124	4.80	26.8	54.8	41.6	-1.2	823			
T-32	132.0	4.7	43.5	451	128	0.73	33.1	71.2	39.7	-1.0	906	4800	nd	250
T-33	120.0	0.2	54.0	439	132	0.87	29.3	62.5	41.9	-1.8	882			
T-34	25.1	0.3	28.6	287	69	1.60	15.1	27.0	21.1	-3.2	477	5600	50	1100
T-35	40.0	0.0	24.0	165	60	2.50	9.6	19.2	10.4	1.1	332	3760	nd	560
T-37	21.3	0.3	11.2	153	20	1.90	11.8	25.4	10.0	-2.8	256	1800	20	nd
T-38	46.8	0.0	8.2	153	32	2.05	12.5	28.6	8.5	-1.1	292	10800	nd	nd
Cretaceous aquifer														
C-1	36.5	4.7	16	665	66	1.55	35.0	127	43.1	-0.8	999	24600	10	580
C-2	159.0	28.3	308	186	90	3.40	36.0	151	23.2	0.3	990			
C-3	224.0	7.6	80	409	71	6.40	72.6	97	32.2	-2.5	1002			
C-4	32.0	18.0	190	369	104	5.00	40.3	52	31.1	-2.9	843			
C-5	210.0	35.0	83	415	121	8.10	58.8	97	24.5	0.5	1055			
C-6	324.7	0.6	115	302	261	4.45	32.2	58	14.2	1.5	1114	4300	25	nd
C-9	28.7	2.3	16	458	19	5.27	39.1	80	27.0	-3.2	679	30000	nd	260
C-10	116.0	0.1	141	488	133	12.80	49.3	60	23.0	-3.8	1025	8000	nd	nd
C-12	19.6	0.2	20	387	29	3.70	40.1	55	32.5	0.5	589	17600	nd	610
C-13	144.3	2.7	57	445	78	10.50	45.5	101	44.2	-0.7	930			
C-14	253.0	31.7	570	265	170	4.60	10.2	264	28.3	-5.1	1600	4500	30	2300
C-15	54.0	12.5	32	366	42	2.10	43.4	53	47.9	-1.9	655			
C-16	25.8	10.2	27	456	50	0.67	40.4	57	58.2	-3.2	727			
C-18	145.0	0.3	105	476	155	1.60	36.7	59	39.9	-5.0	1021	2800	5	3100

Note: all concentrations in ppm, except CBE in %, TVB, SRB in cfu/mL and E.coli in cfu/100mL

Appendix 2. 3 Minor and trace ions data

Sample Code	F	Br	PO_4^{3-}	Li	Sr	Al	B	TOC	Fe	As	Mn	Zn	Ba	Cu	Ni
	ppm	ppm	ppm	ppm	ppm	ppm	ppm	ppm	ppb	ppb	ppb	ppb	ppb	ppb	ppb
Quaternary aquifer															
Q-7	0.54	BDL	BDL	0.01	0.90	0.01	ND	0.73	ND	ND	ND	ND	ND	ND	ND
Q-8	0.32	0.60	BDL	BDL	1.40	0.01	ND	0.15	ND	ND	ND	ND	ND	ND	ND
Q-19	0.48	0.34	BDL	0.02	0.70	0.01	ND	0.22	ND	ND	ND	ND	ND	ND	ND
Q-22	0.22	BDL	BDL	0.02	0.90	0.01	ND	1.03	ND	ND	ND	ND	ND	ND	ND
Q-23	0.26	BDL	BDL	0.01	1.70	0.01	ND	0.86	ND	ND	ND	ND	ND	ND	ND
Q-24	0.44	BDL	BDL	BDL	2.10	0.01	ND	1.62	ND	ND	ND	ND	ND	ND	ND
Q-25	0.28	0.30	BDL	0.04	0.80	0.01	0.05	1.37	ND	ND	ND	ND	ND	ND	ND
Q-28	0.50	0.40	BDL	0.01	1.40	0.01	0.08	1.20	ND	ND	ND	ND	ND	ND	ND
Q-31	0.41	0.20	BDL	0.01	0.90	0.01	0.08	0.38	ND	ND	ND	ND	ND	ND	ND
Q-33	0.42	0.60	BDL	0.02	2.30	0.01	0.09	0.62	ND	ND	ND	ND	ND	ND	ND
Q-34	0.50	BDL	BDL	BDL	0.16	0.03	0.12	BDL	18.4	17.8	102.7	26.0	244.2	2.2	BDL
Q-36	0.08	BDL	BDL	0.01	2.30	0.01	0.07	1.89	ND	ND	ND	ND	ND	ND	ND
Tertiary aquifer															
T-11	0.02	BDL	0.06	0.01	0.18	0.1	0.07	BDL	24.0	0.5	4.6	52.7	514.8	9.7	BDL
T-17	BDL	BLD	BDL	0.01	0.30	0.1	0.07	BDL	28.0	0.5	2.8	89.0	42.1	BDL	BDL
T-20	0.50	0.26	BDL	BDL	0.84	0.01	0.18	3.24	20.0	14.1	1	22.0	424.2	2.0	BDL
T-21	0.09	BDL	BDL	0.01	0.50	0.21	0.12	BDL	14.3	0.5	1	18.6	31.1	5.6	BDL
T-26	0.17	BDL	BDL	0.02	2.14	0.24	0.02	1.73	8.0	0.5	33.7	44.0	36.4	4.6	BDL
T-27	0.02	0.40	BDL	0.02	2.10	0.15	0.07	BDL	23.3	0.7	1	24.0	140.4	17.0	BDL
T-29	0.35	BDL	BDL	BDL	0.23	0.06	0.07	BDL	30.3	BDL	BDL	13.9	BDL	3.7	BDL
T-30	0.30	0.22	0.40	BDL	0.30	0.01	0.09	BDL	32.0	BDL	BDL	8.6	BDL	3.7	6.4
T-31	0.31	0.63	BDL	BDL	0.50	0.03	0.08	BDL	22.5	1.2	2.1	25.5	128.7	5.2	2.5
T-32	0.30	BDL	BDL	BDL	0.47	0.01	0.17	BDL	22.6	1	3.4	61.1	210.4	3.8	BDL
T-33	0.30	0.70	BDL	BDL	0.21	0.01	0.05	BDL	15.1	7.6	53.9	24.0	212.9	3.0	BDL
T-34	1.62	BDL	0.06	0.01	0.11	0.07	0.11	ND	55.3	0.5	5.6	12.1	28.8	6.2	3.8
T-35	0.41	0.12	BDL	0.01	0.10	0.1	0.11	BDL	24.0	0.5	20.5	33.0	55.8	7.0	BDL
T-37	0.25	BDL	BDL	BDL	0.12	0.08	0.06	BDL	22.0	7	BDL	17.7	BDL	5.5	BDL
T-38	0.30	0.15	BDL	BDL	0.15	0.09	0.11	BDL	25.0	0.8	24	18.0	71.3	4.0	BDL
Cretaceous aquifer															
C-1	0.62	0.11	1.00	0.05	1.50	0.1	0.14	0.83	18.0	0.5	1	16.5	93.6	2.3	12.0
C-2	0.30	BD	0.20	0.02	3.80	0.01	0.13	0.43	18.6	2.4	2.6	29.8	181	4.7	BDL
C-3	0.16	1.30	BDL	0.01	0.08	0.01	0.08	BDL	35.0	1.7	4	12.0	26.4	BDL	BDL
C-4	0.71	BDL	0.08	0.02	0.53	0.01	0.06	BDL	12.9	9.7	2.9	10.0	45.7	23.6	21.3
C-5	0.20	BDL	BDL	0.02	1.10	0.01	0.54	BDL	58.2	2.1	4.4	13.0	146.3	5.4	BDL
C-6	0.25	BDL	BDL	0.04	1.20	0.01	0.07	BDL	18.9	1.8	7.2	18.6	55	BDL	24.3
C-9	0.17	BDL	BDL	0.01	1.30	0.01	0.06	2.05	13.8	41.9	3.7	24.6	16.2	3.9	BDL
C-10	0.24	0.83	BDL	0.03	0.58	0.01	0.08	BDL	19.5	5.3	2.6	15.0	40.3	3.9	BDL
C-12	0.30	BDL	0.07	0.01	0.24	0.01	0.05	0.56	21.5	1.6	2.9	BDL	29.2	28.7	51.9
C-13	0.40	BDL	0.15	0.02	0.45	0.26	0.03	0.84	59.0	0.5	13.3	12.9	129.4	9.6	BDL
C-14	0.50	BDL	BDL	0.04	1.50	0.01	0.11	1.31	29.4	21.6	3.5	44.4	36.5	3.2	BDL
C-15	0.25	BDL	BDL	BDL	1.60	0.06	0.15	0.38	36.9	1	3.1	8.2	40.3	8.1	BDL
C-16	0.43	BDL	BDL	0.01	0.74	0.06	0.03	BDL	13.4	1	1	81.9	106.2	2.7	BDL
C-18	0.30	BDL	BDL	0.02	0.23	0.01	0.06	1.25	20.9	13.7	95.5	180.0	122.9	19.0	BDL

Appendix 2. 4 Optimized parameters for arsenite determination by ASDPV

Initial Potential	-0.5 V
Final Potential	0.3 V
Increment	0.005 V
Amplitude	0.05 V
Pulse Width	0.05 Sec
Sample Width	0.025 Sec
Pulse Period	0.2 Sec
Deposition Potential	-0.6 V
Deposition Time	210 sec
Preconditioning	0.15 V
Preconditioning time	60 Sec
Quiet Time	5 Sec
Sensitivity (A/V)	1e-04 A/V

Appendix 2. 5 Total arsenic and arsenite concentration in selected groundwater

Location	As(total)	As(III)±3σ
	ICPMS (µg/l)	(µg/l)
Karasur	21.6	3.3±0.59
Vanur	41.9	5.25±0.75
Kuranpalayam	13.7	2.7±0.58
Thirupanampakkam	17.8	2.4±0.59

Appendix 2. 6 Environmental isotope data of groundwater (post-monsoon) and rainwater

Sample Code	δ^2H	$\delta^{18}O$	$\delta^{13}C$	^3H	d-excess	Precipitation samples		
Quaternary aquifer						**Location**	$\delta^{18}O$	δ^2H
Q-7	-25.7	-3.37	ND	ND	1.24			
Q-8	-20.3	-1.58	ND	ND	-7.71	SIPCOT (Jan)	-5.68	-36.9
Q-19	-26.7	-3.46	ND	ND	0.93	Pondicherry (Jan)	-7.25	-46.4
Q-22	-32.7	-4.53	ND	ND	3.56	Annamalai Nagar (Jan)	-5.73	-35.8
Q-23	-30.5	-3.06	ND	ND	-6.00	Bahour (Nov)	-0.21	-3.1
Q-24	-31.8	-3.45	ND	ND	-4.23	Puduthurai (Nov)	0.71	12.6
Q-25	-27.7	-3.21	ND	ND	-2.00	Pillaichavadi (Dec)	-3.42	-21.0
Q-28	-12.5	-0.56	ND	ND	-7.97	Annamalai Nagar (Feb)	-7.90	-62.6
Q-31	-19.4	-1.87	ND	ND	-4.47	Pondicherry (Dec)	-3.45	-32.3
Q-33	-17.7	-1.29	ND	ND	-7.37	Portnova (Dec)	-2.72	-21.7
Q-34	-25.5	-3.52	-19.70	4.8	2.64	Kollidam (Dec)	-2.20	-6.4
Q-36	-22.2	-2.33	ND	ND	-3.61	Sirkali (Jan)	-5.20	-31.9
Tertiary aquifer								
T-11	-38.8	-5.87	-18.2	3.6	8.12			
T-17	-38.6	-5.66	-9.6	5.8	6.71			
T-20	-35.5	-5.60	-15.3	3.5	9.26			
T-21	-40.8	-6.43	-12.5	6.0	10.60			
T-26	-31.8	-4.62	-11.9	ND	5.09			
T-27	-34.2	-4.80	-12.7	4.2	4.16			
T-29	-33.9	-5.01	-11.6	4.7	6.18			
T-30	-30.0	-4.21	ND	4.6	3.66			
T-31	-24.7	-3.74	ND	3.6	5.19			
T-32	-22.5	-2.90	-12.4	4.3	0.67			
T-33	-23.1	-3.20	ND	4.8	2.49			
T-34	-35.0	-5.09	-17.7	3.1	5.71			
T-35	-32.8	-4.51	ND	4.5	3.30			
T-37	-42.8	-6.34	-16.6	ND	7.92			
T-38	-43.8	-6.41	-17.8	ND	7.50			
Cretaceous aquifer								
C-1	-33.0	-5.29	-17.5	6.2	9.29			
C-2	-35.9	-5.60	-15.5	4.5	8.91			
C-3	-35.4	-5.21	-17.6	4.8	6.29			
C-4	-34.1	-5.16	ND	6.5	7.24			
C-5	-35.9	-5.42	ND	2.6	7.44			
C-6	-36.3	-5.45	-10.7	1.1	7.32			
C-9	-34.2	-5.01	-9.0	3.9	5.88			
C-10	-35.6	-5.01	-10.3	1.5	4.48			
C-12	-38.3	-5.60	-15.3	5.7	6.47			
C-13	-40.6	-6.00	-10.2	4.3	7.35			
C-14	-36.1	-6.26	ND	ND	13.93			
C-15	-30.5	-4.62	-21.8	4.7	6.46			
C-16	-30.3	-4.48	ND	1.5	5.59			
C-18	-33.7	-4.78	-13.1	2.7	4.51			

Note: δ^2H, $\delta^{18}O$, $\delta^{13}C$, d-excess in ‰ vs. VSMOW, 3H in T.U.

Appendix 2. 7 Chemical and isotope data of groundwater (pre-monsoon)

Sample Id	E.C.	F^-	Cl^-	NO_3^-	SO_4^{2-}	HCO_3^-	Na^+	K^+	Mg^{2+}	Ca^{2+}	$\delta^{18}O$	δ^2H
Q-33	1136	0.30	120.0	0.2	54	439.2	132.0	0.87	29.3	62.5	-25.6	-2.97
T-20	1150	0.5	118	1.7	14.6	525	44.1	0.6	70.2	76	-40.1	-6.47
T-26	737	0.17	76.2	5.1	72	213.5	75.0	5.30	13.4	59.5	-31.6	-4.84
T-29	798	0.35	55.5	16.6	27	366.0	71.9	1.57	22.6	55.2	-39.5	-5.58
T-37	360	0.25	21.3	0.3	11	153.0	20.2	1.90	11.8	25.4	-40.0	-6.1
T-38	402	0.30	46.8	0.0	8	152.5	32.1	2.05	12.5	28.6	-43.3	-6.51
C-9	976	0.17	28.7	2.3	16	458.0	18.8	5.27	39.1	79.7	-23.8	-4.53
C-12	722	0.3	23.1	2.4	21.8	476	36	3.1	37.5	110	-34.9	-5.51
C-14	2194	0.50	253.0	31.7	570	265.0	170.0	4.60	10.2	264.0	-35.2	-5.61

Appendix 2. 8 Details of target nuclei for neutron activation analysis

S.No.	Radionuclide	Half life (hrs)	Gamma Energy (KeV)	Detection Limit (ppm)
1	^{24}Na	14.96	1368.55	54.9
2	^{42}K	12.36	1524.7	5178
3	^{59}Fe	1068	1099	1032
4	^{60}Co	26934.8	1173	0.75
5	^{46}Sc	2011.92	889	0.09
6	^{51}Cr	664.8	320	5.15
7	^{65}Zn	5863.2	1115	14.6
9	^{76}As	26.3	1099	0.50
8	^{141}Ce	780.24	145.45	3.52
9	^{233}Pa (Th)	647.28	312	0.53
10	^{239}Np (U)	56.568	277	0.73
11	^{140}La	40.272	487.03	0.48
12	^{177}Lu	161.52	208.36	0.04
13	^{175}Yb	100.44	396.32	0.3
14	^{152}Eu	116508	344.3	0.13
15	^{181}Hf	1017.26	482.16	0.47

Appendix 2. 9 Deviation of measured values from the recommended values

S. No.	Element	This work (mg/Kg), (with 2σ error)	Recommended values
1	Na	2431, 77	2400
2	K	13529, 5655	12100
3	Fe	27103, 688	25700
4	Co	9, 0.8	8.9
5	Sc	8.3, 0.13	8.3
6	Cr	60, 5	60
7	Zn	129, 14	104
8	Ce	64, 3.2	61
9	As	12.4, 1.1	13.4
9	Th	8, 0.49	8.2
10	U	2, 0.8	2.6
11	La	29, 0.56	28
12	Lu	0.33, 0.03	0.3
13	Yb	2.34, 0.19	2.4
14	Eu	1, 0.12	1
15	Hf	5.4, 0.48	5.1

Appendix 2. 10 Major, TC and TOC data of sediments

Sediment ID	Depth range	Na	K	Ca	Fe	S	TC	TOC	TIC
	m, bgl	%	%	%	%	%	%	%	%
C0	0-3	0.12	0.76	0.05	1.97	<0.001	0.002	BDL	0.002
C3	9-12	0.53	0.81	0.07	0.89	<0.001	0.2	0.03	0.15
C9	27-30	1.23	1.94	1.08	1.32	<0.001	0.02	0.01	0.01
C12	36-39	1.06	1.26	0.05	2.25	<0.001	0.04	0.03	0.01
C17	51-54	2.07	1.96	2.48	3.45	0.08	0.25	0.07	0.18
C20	60-63	1.77	2.22	3.48	1.13	0.30	0.55	0.08	0.47
C25	75-78	0.29	2.10	0.85	0.84	0.20	0.02	<0.01	0.02
C35	105-108	0.70	2.92	3.78	1.85	0.09	1.90	0.30	1.60
C37	111-114	0.40	2.54	9.26	1.15	0.05	1.60	0.20	1.40
C43	129-131	0.33	1.70	12.34	2.59	1.40	3.90	0.07	3.80
C45	135-138	0.31	2.45	0.29	1.12	0.80	0.20	0.20	0.01
C47	141-144	0.68	4.75	2.01	3.16	0.60	0.70	0.20	0.50
UCC		1.22	1.16	2.56	1.76				

2.10 (cont.) Minor and trace element data of sediments

Sediment ID	Depth range	As	Co	Sc	Cr	Zn	Hf	Th	U
	m, bgl	ppm	ppm	ppm	ppm	ppm	ppm	ppm	ppm
C0	0-3	2.5	8.69	5.6	86	74	14.8	5.6	0.7
C3	9-12	BDL	4.85	1.7	27	83	2.1	7.0	0.8
C9	27-30	BDL	5.57	3.8	41	68	2.6	4.0	0.7
C12	36-39	3.5	10.14	5.9	68	65	2.7	5.0	0.7
C17	51-54	6.1	14.72	10.2	115	67	7.4	6.7	1.5
C20	60-63	2.5	5.92	3.4	40	51	3.1	4.5	0.7
C25	75-78	1.7	3.43	1.4	11	75	2.0	1.7	0.7
C35	105-108	3.6	11.73	5.7	52	69	4.6	7.5	1.6
C37	111-114	3.6	4.64	3.4	32	78	4.8	7.1	3.1
C43	129-131	30.2	7.94	4.5	48	106	2.5	7.0	0.7
C45	135-138	5.2	2.11	1.7	11	38	1.9	1.5	0.7
C47	141-144	13	12.04	6.4	65	168	5.3	6.8	3.0
UCC			17.3	14	92	67	5.3	10.5	2.7

2.10 (cont.) Carbon-13 and REE data of sediments

Sediment ID	Depth	$\delta^{13}C$	La	Ce	Eu	Yb	Lu
	m, bgl	**‰ VPDB**	**ppm**	**ppm**	**ppm**	**ppm**	**ppm**
C0	0-3	nd	15.7	44	0.86	1.60	0.24
C3	9-12	-4.65	11.0	15	0.48	0.63	0.09
C9	27-30	-7.83	18.3	32	0.74	0.61	0.11
C12	36-39	nd	18.5	34	0.91	0.51	0.13
C17	51-54	-4.65	31.5	59	1.38	1.67	0.19
C20	60-63	-5.00	10.3	16	0.66	1.01	0.11
C25	75-78	-11.40	9.0	17	0.42	0.41	0.09
C35	105-108	-0.10	26.8	50	1.06	1.16	0.13
C37	111-114	nd	22.6	45	0.82	0.96	0.13
C43	129-131	5.12	19.9	39	0.59	0.83	0.14
C45	135-138	-9.00	6.1	7	0.37	0.29	0.05
C47	141-144	1.50	26.3	50	1.30	1.40	0.21
NASC			31.0	67	1.18	3.10	0.46
UCC			30	64	0.88	2.2	0.32
PAAS			38.2	80	1.08	2.82	0.43
Chondrite-CI			0.24	0.61	0.06	0.16	0.02

Appendix 2. 11 Details of membrane filters used for ultrafiltration

Type	Nominal Pore Size	Nominal molecular weight cut-off (Dalton)	Material
Amicon XM300	14nm	300,000	PAN/PVC copolymer
Amicon XM50	3.1nm	50,000	PAN/PVC copolymer
Amicon PM-30	2.2nm	30,000	Polyester sulphone
Amicon PM-10	1.6nm	10,000	Polyester sulphone
Amicon YC05	1.1nm	500	cellulose acetate

Appendix 2. 11 Particle size distribution in groundwater

Particle Size	Milli-Q	T-37	C-12	C-9	C-14	T-20	T-26	T-38	Q-33	T-29
1	275	1379	7068	36106	9520	1505	1364	1343	7328	1340
1.4	435	2193	1705	12980	1811	3965	2938	2792	1440	3216
1.9	645	8276	1250	11877	8897	2922	1561	1271	8296	2095
2.5	784	4382	5126	32446	6917	1048	8166	5878	5464	1250
3.4	588	2892	2130	5832	6415	5134	4158	3544	4180	8244
4.6	492	2152	1220	2116	2760	4988	1944	2078	2452	4632
6.3	328	1204	768	1224	791	4700	1256	1350	1436	2464
8.6	276	866	398	818	331	2186	930	1062	912	1454
11.7	148	446	160	328	189	740	474	366	480	596
15.9	132	268	74	106	132	168	254	202	232	298
21.5	156	176	36	24	79	48	80	64	92	114
29.3	96	96	30	8	20	20	16	34	28	58
39.8	76	56	14	14	8	0	12	10	8	36
54.1	45	32	2	10	4	0	2	6	0	26
73.6	18	12	6	0	0	0	0	0	0	8
100	12	8	2	4	1	0	2	2	0	7

Appendix 2. 13 EDXRF data (counts) of some exposed filter circles

Sample Location	Filter circle	Fe	Ca	S
C-12	**0.45 µm**	2387	6139	
C-12	**1.2 µm**	2362	4846	
C-12	**3 µm**	2172	7348	2529
C-12	**5 µm**	2999	5355	
T-38	**0.45 µm**	1013	1566	
T-38	**1.2 µm**		5093	
T-38	**3 µm**	688	2049	
T-38	**5 µm**	982	6171	
T-29	**0.45 µm**	2318	5655	
T-29	**1.2 µm**	2804	4778	
T-29	**3 µm**	2534	4305	2017
T-29	**5 µm**		4470	

Appendix 2. 14 NAA data of exposed filter circles (C-18)

	dry weight	Fe	Na	K	Cr	Br	As	Sc
	mg	ppm	ppm	ppm	ppm	ppm	ppm	ppm
0.2µm	0.07	3668	460	518	10.4	1.3	2.1	1.09
0.45µm	0.95	4201	125	59	21.7	0.8	0.2	0.05
0.8µm	1.14	3945	552	559	6.7	0.9	1.7	0.99
1.2µm	2.93	1571	544	284	10.5	2.1	1.1	0.65
3µm	4.93	1686	786	247	11.5	2	0.7	0.46
5µm	2.35	13346	1043	1503	63.5	2.5	6.6	3.4
8µm	5.13	14240	1238	1837	36	3	7	4

LIST OF PUBLICATIONS FORMING PART OF THE THESIS

Part of the work being submitted for the award of the degree of Doctor of Philosophy has been published / communicated.

International Journals

1. Rare earth elements distribution in clay zones of sedimentary formation, Pondicherry, South India, K. Tirumalesh, K. L. Ramakumar, S. Chidambaram, S. Pethaperumal and Gursharan Singh, Journal of Radioanalytical and Nuclear Chemistry (**10.1007/s10967-011-1606-9**).
2. An over view on NETPATH geochemical modeling- a case study from coastal aquifer of Pondicherry, K. Tirumalesh, K. L. Ramakumar, K. Shivanna, S. Chidambaram, Groundwater Monitoring and Management through Hydrogeochemical Modeling Approach, IK International Publishing House, New Delhi, march 2010, pp.33-47.
3. Occurrence of arsenic and its distribution in different sedimentary formations of coastal Pondicherry, India, K. Tirumalesh, K. L. Ramakumar, S. Chidambaram, Gursharan Singh and Pethaperumal, Applied Geochemistry (under review).
4. Microbial evaluation of groundwater from major sedimentary aquifers of Pondicherry region – insights into redox condition of the aquifer system, K. Tirumalesh, K. L. Ramakumar, S. Chidambaram, S. Pethaperumal, Gursharan Singh, D. Prakash, N. Nawani and M.V. Prasanna, Environmental Monitoring Assessment (under review).
5. A study on evolution of sedimentary deposits from coastal Pondicherry region using geochemical and isotope tools, K. Tirumalesh, S. Chidambaram, K. L. Ramakumar, U.P. Kulkarni, S. Pethaperumal, Gursharan Singh, Sedimentology (under review).
6. Evaluation of groundwater quality and its suitability for drinking and agricultural use in Pondicherry and its environs, South India, K. Tirumalesh, S. Chidambaram, K. L. Ramakumar, S. Pethaperumal, Gursharan Singh, Environmental Monitoring Assessment (under review).
7. Environmental isotopic constraints for the origin and residence time of groundwater from sedimentary aquifers of Pondicherry region (under preparation).
8. A study on evolution of groundwater geochemistry in coastal aquifers of Pondicherry region using statistical and geochemical modeling techniques (under preparation).

9. Role of colloidal particles in migration of strontium in deep groundwater – a case study from Pondicherry region (under preparation).

International Conference / Symposium

1. K.Tirumalesh, K. L. Ramakumar, Gursharan Singh, S. Chidambaram, K. K. Swain, "Arsenic distribution in sedimentary formations of coastal Pondicherry, India – a case study", I2SM 2012.
2. K.Tirumalesh, K. L. Ramakumar, U.P. Kulkarni, Gursharan Singh, S. Chidambaram, "Source rock identification of sediments using trace element ratios and 13C isotope data – a case study from Pondicherry region", I2SM 2012. **(Best Poster Award)**
3. K.Tirumalesh, K. L. Ramakumar, Gursharan Singh, S. Chidambaram, R.K. Singhal, Manisha Venkatesh, "Strontium association with particulate matter in coastal groundwaters of Pondicherry, India", I2SM 2012.
4. K.Tirumalesh, Manoj Sharma, K.Shivanna and K.L. Ramakumar, Determination of arsenite at nanogram level in natural waters by anodic stripping differential pulse Voltammetry", 2nd International conference on Application of Radiotracers in Chemical, Environmental and Biological Sciences (ARCEBS-10), held in Kolkata during 7-13, November 2010., pp. 292-294.
5. K.Tirumalesh, K. Shivanna, K. L. Ramakumar, S. Chidambaram, "Implication of positive Eu anomaly in clay zones of sedimentary formation, Pondicherry, South India", Fourth International Symposium on Nuclear Analytical Chemistry (NAC-IV), held in Mumbai during 15-19, Nov., 2010, pp. 277.